UNIVERSITÀ
DEGLI STUDI
DI PADOVA

Sede Amministrativa: Università degli Studi di Padova

Centro di Ateneo di Studi ed Attività Spaziali "Giuseppe Colombo" (CISAS)

CORSO DI DOTTORATO DI RICERCA IN: SCIENZE TECNOLOGIE E MISURE SPAZIALI

INDIRIZZO: MISURE MECCANICHE PER L'INGEGNERIA E LO SPAZIO

CICLO XXIX

DEVELOPMENT AND TESTING OF HARDWARE SIMULATOR FOR SATELLITE PROXIMITY MANEUVERS AND FORMATION FLYING

Direttore del Corso: Ch.mo Prof. Giampiero Naletto

Coordinatore di Indirizzo: Ch.mo Prof. Stefano Debei

Supervisore: Ch.mo Prof. Enrico Lorenzini

Dottorando: Sergio Tronco

ABSTRACT

Satellite Formation Flying (SFF) and Proximity Operations are applications that have increasingly gained interest over the years. These applications foresee the substitution of a single spacecraft with a system of multiple satellites that perform coordinated position and attitude control maneuvers, which in turn results in higher accuracy of payload measurement, higher flexibility, robustness to failure, and reduction of development costs. These systems present however higher difficulties in their design since they have not only absolute but also relative state requirements, which make them also liable to higher control action expense with respect to (wrt) the single satellite systems. Moreover, applications like Automated Rendez-Vous and Docking (RVD) and in general close proximity maneuvers present a high risk of impact between the satellites, which must be treated with an appropriate design of the on board Guidance Navigation and Control (GNC) system. These aspects justify the development and employment of a ground hardware simulator representative of two or more satellites performing coordinate maneuvers, allowing the investigation of these problems with an easily accessible system.

The aim of my Ph.D. Activities has consisted in the development and testing of the cooperating SPAcecRaft Testbed for Autonomous proximity operatioNs experimentS (SPARTANS) hardware simulator, which is under development since 2010 at the Center of Studies and Activities for Space (CISAS) of the University of Padova. This ground simulator presents robotic units that allow the reproduction of the relative position and attitude motions of satellites in proximity or in formation, and can be therefore employed for the extensive study of control algorithms and strategies for these types of applications, allowing dedicated hardware in the loop to be tested in a controlled environment. At the beginning of my Ph.D., the testbed consisted in the first prototype of Attitude Module (AM), a platform with three rotational Degrees of Freedom (DOF) of Yaw, Pitch and Roll, controllable through a GNC system based on incremental encoders and air thrusters. A small contribution was initially given in support of the execution of a series of 3 DOF attitude control maneuvers tests with the AM. Subsequently, the first activity consisted in the design and development of the air suspension system that enables a low friction translational motion of the a whole Unit of the testbed over the test table, with the characterization of air skids available in laboratory. The subsequent activity consisted in the design and development of the Translation Module (TM), the lower section of the whole Unit, as modular structure supporting the air suspension system, the AM, and the on board localization system. After this activity the on board localization system for position and Azimuth estimation, based on Optical Flow Sensors (OFS), was developed and tested. The system was installed on a TM base prototype and it was calibrated and

tested with the imposition of known motions through rotational and translational motorized stages wich were used in conjunction, presenting max deviations at the level of 0.1° for a total rotational range of 40°, and max deviations of 1 mm for a total translational range of 100 mm. Combined maneuvers, i.e. translational and rotational motions imposed in sequence, were subsequently performed, showing a drift trend, up to approximately 1 cm for a 90° rotation. Subsequently the OFS system was assembled in the TM and integrated with an external vision system, under development in parallel in the context of the SPARTANS project. Results showed a good general concordance between the two systems, but combined maneuvers with extended rotational range showed again a drift trend in the OFS system solution, not only in position but also in Azimuth.
A parallel activity consisted in the design and development of the levellable test table for the Units with a modular structure. Another activity consisted in the development of a Matlab Software Simulator for Units tests planning. A series of preliminary standard and optimal control maneuvers were planned with the software simulator.
The last activity of my Ph.D. consisted in the analysis of an inspection scenario for satellite removal purposes, with the goal of reproducing the relative dynamics in scale with the SPARTANS simulator. The chosen scenario foresaw the inspection, through a vision system on board an inspection satellite, of the currently freely tumbling Envisat spacecraft . The analysis performed with a Matlab software simulator was focused on the acquisition and maintainance of a circular relative orbit at close range starting from a flyaround orbit, through the employment of Model Predictive Control (MPC) and Linear Quadratic Regulator (LQR) optimal controllers. Simulations results showed a lower tracking error in position with the MPC controller wrt to the LQR controller, but with a higher control action expense: for a 6 hours inspection on a 41 m radius circular relative orbit, the max total delta-v component resulted of 3.3 m/s for MPC, while it resulted of 0.7 m/s for LQR.
In the present configuration the SPARTANS testbed presents a first complete Unit and test table to be assembled in the immediate future for the execution of the first position and attitude control maneuvers. The final configuration of the testbed will present a minimum of two Units allowing to perform coordinate control maneuvers for the investigation and study of problems and strategies related to SFF, Automated Rendez-Vous and Docking, and in general proximity manevuers.

SOMMARIO

Il volo in formazione e le manovre di prossimità tra satelliti sono applicazioni che hanno progressivamente acquisito interesse negli ultimi anni. Queste applicazioni prevedono la sostituzione di un singolo satellite con sistemi formati da più satelliti che eseguono manovre coordinate di controllo di posizione e assetto, il che comporta un aumento di accuratezza delle misure dei payload distribuiti, maggior flessibilità, robustezza alle avarie, e riduzione dei costi di sviluppo. Ciònonostante questi sistemi presentano difficoltà maggiori nella loro progettazione, in quanto hanno requisiti di stato non solo assoluti ma anche relativi, il che li rende anche portati a maggiore spesa di azione di controllo rispetto ai sistemi satellitari singoli. Inoltre applicazioni come Automated Rendez-Vous and Docking (RVD) ed in generale manovre di prossimità presentano un alto rischio di impatto tra satelliti, che va trattato con una progettazione appropriata del sistema di Guida Navigazione e Controllo (GNC) di bordo. Questi aspetti giustificano lo sviluppo e l'utilizzo di un simulatore hardware a terra, rappresentativo di due o più satelliti che eseguono manovre coordinate, permettendo l'investigazione e lo studio di queste problematiche con un sistema facilmente accessibile.

Lo scopo delle mie attività di dottorato è consistito nello sviluppo e collaudo del simulatore hardware cooperating SPAcecRaft Testbed for Autonomous proximity operatioNs experimentS (SPARTANS), in sviluppo dal 2010 presso il Centro di Ateneo di Studi e Attività Spaziali (CISAS) dell'Università degli Padova. Questo simulatore di terra presenta Unità robotiche che permettono la riproduzione dei moti relativi di assetto e posizione di satelliti in formazione o in prossimità, e può quindi essere utilizzato per studi estensivi di algoritmi e strategie di controllo per questo tipo di applicazioni, con hardware in the loop collaudabile in un ambiente controllato. All'inizio del mio dottorato, il testbed consisteva nel primo prototipo del Modulo di Assetto (AM), una piattaforma con tre Gradi di Libertà (GdL) rotazionali di Yaw, Pitch, Roll, controllabili con un sistema di GNC basato su encoders incrementali e razzetti ad aria. Un contributo limitato è stato inizialmente dato in supporto all'esecuzione di una serie di manovre di controllo di asseto a 3 GdL con il solo AM. Successivamente la prima attività è consistita nella progettazione e sviluppo del sistema di sospensione ad aria che permette un moto traslazionale a basso attrito dell'Unità intera sul tavolo di collaudo, con la caratterizzazione dei pattini ad aria disponibili in laboratorio. L'attività successiva è consistita nella progettazione e sviluppo del Modulo di Traslazione (TM), la sezione inferiore di un' Unità intera, nella forma di una struttura modulare che supporta il sistema di sospensione ad aria, AM, e il sistema di localizzazione di bordo. In seguito a questa attività è stato sviluppato e testato il sistema di localizzazione di bordo per la stima di posizione e Azimuth basato su sensori Optical

Flow Sensors (OFS) di tipo mouse installati a bordo del TM. Il sistema è stato installato su un prototipo della base del TM ed è stato calibrato e testato con imposizione di moti noti tramite slitte rotazionali e traslazionali usate in congiunzione, presentando deviazioni massime al livello di 0.1° per un range rotazionale totale di 40°, e deviazioni massime al livello di 1 mm per un range traslazionale totale di 100 mm. Manovre combinate, i.e. moti traslazionali e rotazionali effettuati in sequenza, sono state successivamente effettuate, mostrando un trend di drift in posizione, fino a circa 1 cm per una rotazione di 90°. Successivamente il sistema OFS è stato assemblato nel TM ed è stato integrato con un sistema di visione esterno in sviluppo in parallelo nel contesto del progetto SPARTANS. I risultati hanno mostrato una buona concordanza generale tra i due sistemi, ma manovre combinate con range rotazionale esteso hanno mostrato ancora un trend di drift nella soluzione del sistema OFS, non solo in posizione ma anche in Azimuth.
Un' attività parallela è consistita nella progettazione e sviluppo del tavolo livellabile di collaudo delle Unità con una strutta modulare. Un'altra attività è consistita nello sviluppo di un Simulatore Software in Matlab per la pianificazione di test con le Unità. Una serie di manovre preliminari di controllo standard e controllo ottimo sono state pianificate con il simulatore software.
L'attività finale del mio dottorato è consistita nell'analisi di uno scenario di ispezione per operazioni di rimozione di satelliti, con lo scopo di riprodurre la dinamica relativa in scala tramite il simulatore SPARTANS. Lo scenario scelto ha previsto l'ispezione tramite sistema di visione di bordo, del satellite Envisat, attualmente in tumbling libero in orbita. L'analisi, effettuata con un simulatore software in Matlab, è stata concentrata sull'acquisizione e mantenimento di un'orbita relativa circolare a distanza ravvicinata, partendo da un'orbita di flyaround, con l'utilizo di controllori ottimi Model Predictive Control (MPC) e Linear Quadratic Regulator (LQR). I risultati della simulazione di ispezione hanno dimostrato un minore errore di tracking di posizione con il controllore MPC rispetto al controllore LQR, ma con spesa maggiore di azione di controllo: per un'ispezione di 6 ore su un'orbita relativa di raggio 41 m la massima componente di delta-v totale è risultata di 3.3 m/s per MPC, mentre per LQR è risultata pari a 0.7 m/s.
Nella configurazione attuale il simulatore SPARTANS presenta una prima Unità completa ed il tavolo di collaudo che saranno assemblati in modo definitivo nell'immediato futuro, per l'esecuzione delle prime manovre di controllo di posizione insieme ad assetto. Nella configurazione finale il testbed presenterà un minimo di due Unità, permettendo l'esecuzione di manovre di controllo coordinato per l'investigazione e lo studio di problematiche e strategie legate a volo in formazione, Automated Rendez-Vous and Docking, ed in generale manovre di prossimità.

CONTENTS

LIST OF ACRONYMS

AM Attitude Module

ARPO Automated Rendez Vous and Proximity Operations

ARVD Automated Rendez Vous and Docking

DOF Degrees of Freedom

DSS Distributed Satellite System

FCC Formation Flying Control

GNC Guidance Navigation and Control

HCW Hill Clohessy Wiltshire

IMU Inertial Measurement Unit

LEO Low Earth Orbit

LF Leader Follower

LQR Linear Quadratic Regulator

LTI Linear Time Invariant

LTV Linear Time Variant

LVLH Local Vertical Local Horizontal

MIMO Multiple Input Multiple Output

MPC Model Predictive Control

NL Non-Linear

OFS Optical Flow Sensor

OOP Object Oriented Programming

PID Proportional Integral Derivative

PWM Pulse Width Modulation

RHC Reciding Horizon Control

SAR Synthetic Aperture Radar

SFF Satellite Formation Flying

TM Translation Module

INTRODUCTION

The concepts of Spacecraft Formation Flying (SFF) and proximity maneuvers have origins from the work of W. Clohessy and R. Wiltshire during the 1960's, when they employed for the first time Hill's equations for the solution of the rendez-vous and docking problem of two satellites, which resulted in the derivation of the Hill-Clohessy-Wiltshire (HCW) equations of relative motion between two orbiting vehicles.

During the 1990's the idea of implementing new types of satellite systems, for formation flying and proximity manuevers, started to gain increasing popularity in the international community.

The development and implementation of these type of systems finds its justification in a wide range of reasons, depending on the particular application.

Spacecraft formation flying implies a payload that is distributed among several space vehicles which are able to perform coordinated orbital and attitude maneuvers in order to maintain configurations that allow the satisfaction of certain requirements in terms of payload performances. This allows increased measurement accuracy, flexibility, redundance, and reduction of development costs; in turn, these advantages make this type of systems very attractive for applications such as interferometry, Earth gravitational field mapping, imaging, data relay, orbital replenishment.

In the case of spacecraft proximity maneuvers, applications such as rendez-vous and docking or capture with cooperative and non cooperative spacecraft allow automatic repairs in case of failures, mainteinance, insertion of new instrumentation, and also the deorbit of inactive satellites, a relevant application due to the growing concern for the proliferation of space debris in low orbits over the years.

Ground testbeds have been since the beginning of space exploration one of the mostly employed mean of validation of space systems which, once in orbit, cannot generally be either modified or repaired, and for this reason must respond adequately to certain reliability and safety criteria during the design and test phases.

Nowadays in the international community there exist already a number of testbeds that allow the study and investigation of problems related to spacecraft formation flying and proximity manuevers. Ground testbeds allow the study of these problems with a system that is easily controllable, accessible, maintainable, economical, and can be used for different purposes with low modifications, while at the same time providing a good reproduction of the relative attitude and orbital motions of the satellites in close formation and proximity maneuver.

Testbeds for spacecraft formation flying are present in the forms of ground robotic systems, parabolic flight systems and orbital systems, such as the Synchronized Position Hold Engage and

Reorient Experimental Satellite (SPHERES) on board the International Space Station (ISS), and the PRISMA satellites developed by OHB Sweden, in Earth orbit. Under the perspective of the test environment, the parabolic flight and orbital systems represent the ideal type of testbed. They are however characterized by the problems that generally concern every space system, i.e. high development costs and the impossibility of having direct interaction with the hardware modules. This last aspect strongly limits the ability to perform extensive test sessions with varying operative conditions. On the other hand, even though ground simulators represent only to a certain extent the real system operative environment, they compensate the disadvantages of the flight testbeds since they allow costs reduction and continuous interaction with the system units in order to intervene in case of failures, and in order to introduce new components and systems in the units of the simulator.
As already pointed out, systems with two or more cooperating satellites are advantageous especially in terms of measurement accuracy, flexibility, redundance and the ability to carry on a certain mission task even in the eventuality of a whole satellite failure.
However, these systems present a series of disadvantages with respect to (wrt) the classical single satellite systems. In fact when two or more satellites are performing cooperative control maneuvers, either in orbital position or in attitude, the control for each satellite must be carried out in accordance to both absolute and relative requirements, which implies increased complexity of the on board Guidance Navigation and Control (GNC) system and the necessity of having communication links bewteen the spacecrafts. Moreover, the presence of both absolute and relative position and attitude control requirements implies increased propellant consumption for a certain mission duration. Also, while in Earth orbit formations the normally employed sensors for single satellite missions, e.g. GPS receivers, can still be employed for the relative state estimation, for certain missions such as deep space missions, different sensors need to be employed for the direct sensing of relative distance and orientation, and therefore additional development and testing of new technologies is needed in such cases.
The disadvantageous aspects related to cooperating spacecraft systems, represent at the same time on of the main justifications to the design and development of hardware simulators that allow extensive test sessions for the evaluation of representative control and communication systems, with the aim of determining optimal solutions in terms of components, systems and on-board control algorithms.

1.1 Distributed Satellite Systems

The concept of Distributed Satellite System (DSS) represents the general idea of a group of satellites in orbit which have a certain degree of cooperativeness in terms of the tasks carried out through their payloads and in terms of the GNC and communication systems. This level of cooperativeness is in turn related to several mission parameters and drivers: number of satellites, ground coverage, visibility, fuel consumption, payload performances, system reliability and survivability, etc.

A well known type of DSS is the satellite constellation. Satellite constellations are distributed spacecraft systems that are mostly identified by the fact that they present coordinated ground coverage extended over large Earth areas. This is accomplished by distributing satellites over different orbital slots which are maintained through the central ground control, shared by all the satellites, and by the individual satellite control. Generally, spacecrafts in constellation do not have a relative orbital and attitude control system allowing them to perform cooperative maneuvers one with each other. Some constellations, such as the Iridium constellation, share however with the satellite formations the characteristic of having inter-satellite communication links, though for different purposes, in the former case for ground data relay, in the latter for position and attitude estimation data transmission.

Satellite constellations are usually designed so that satellites have similar eccentricity and inclination, in this way individual perturbations acting on each spacecraft produce similar effects, and therefore the constellation geometry can be preserved with a limited amount of station-keeping, with reduced fuel consumption and increased life of the satellites. Also, in the constellation design, another important parameter is the phasing of each spacecraft in an orbital plane, which should ensure that sufficient separation is maintained so that collisions at orbit planes intersections are avoided. Satellite formations on the other hand are not generally characterized by large coverage requirements when flying in Earth orbits. The satellites of a formation are generally distributed over almost identical orbits, with relative distances that vary from the order of km down to few meters.

1.2 Satellite Formation Flying

Satellite Formation Flying (SFF) is a type of DSS in which two or more satellites have cooperative GNC systems and the same type of payload, in this way the resulting payload is formed by several measurement instruments, and is the equivalent of a single, larger measurement instrument.

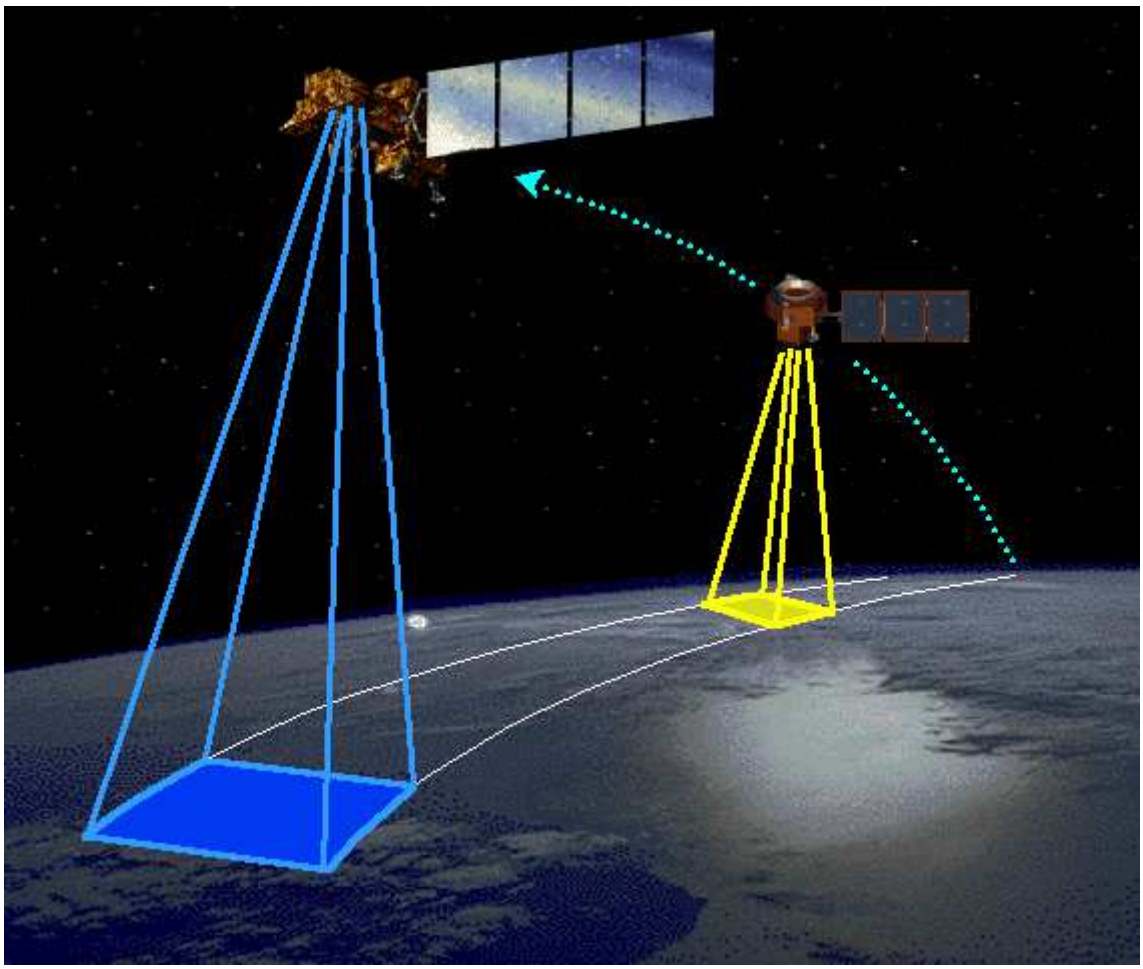

Figure 1 – Landsat-7 and EO-1 satellites in traling formation (NASA)

The cooperativeness of the GNC system on board the satellites is enabled by communication crosslinks that allow continuous transmission of the relative and absolute states estimations performed by each satellite's Attitude and Position Determination system.

Since the control requirements are both absolute and relative, spacecrafts in formation present an increased complexity in terms of the on board GNC system, and can possibly need, for the relative position and orientation assessment, new types of sensors that have not been considered and employed on board satellites up to date.

Another important factor in the overall performance evaluation of these systems lies in the fact that the presence of both absolute and relative requirements implies an increase in propellant consumption, which grows all the more as much as it is needed to compensate orbital perturbations that produce a more or less rapid dispersion of the formation, through long-period differential effects.

In terms of advantages, satellite formations allow firstly the improvement of the performances of the measurement instruments, since the higher dimensions of the payload can result either in

increased measurement area or in increased measurement resolution, or both, wrt single satellite systems performances on the same type of tasks. Moreover, the formation has a certain degree of flexibility since the individual GNC system on board each satellite allows to reach and maintain different configurations, which implies that with this type of satellite system, different kinds of tasks can be carried out.

The presence of two or more satellites instead of one implies a certain degree of redundance and robustness to failure. In case of single satellites partial or total failure, the mission tasks can be still carried out with decreased performances, whereas if replacement satellites are available, the tasks execution can be resumed with the nominal performances specifications. In both cases, there is no need to perform a new launch with a replacement satellite so that the execution of the mission tasks can restart.

One further advantage of cooperative satellites systems is that they result in spacecrafts being more cost effective, since they are smaller and generally require less development and testing effort in terms of safety and reliability, being failure probability requirements somewhat relaxed by the redundance of the system. This implies also reduction of costs associated to the launch system, since smaller satellites can find more easily accomodation in the fairings of launchers.

One of the main scientific applications for which satellite formation flying systems are intended to be developed and employed, are interferometric applications. This type of scientific missions can have the goal of detecting the presence of extrasolar planets that are similar to the Earth, and with satellites in formation, the detectors can be distributed over large baselines, allowing high accuracies in the measurements of interferometric fringes. Also, spacecraft formations for interferometry can be employed for gravitational waves detection in deep space.

Other applications of interest which can be enabled by SFF are Earth missions such as gravitational field mapping, magnetic field mapping, missions for fundamental physics, Earth imaging through Synthetic Aperture Radar (SAR), and also military applications, which benefit from the generally improved and expanded capabilities for communication and imaging tasks.

Nowadays there is already a number of SFF missions that have been successfully operative in orbit. Others are currently under development for launch in the next years.

The TanDEM-X mission of the DLR, the German Aerospace Agency, consists in two satellites in formation, each equipped with radar remote sensing instrumentation, with the goal of acquiring a global Digital Elevation Model (DEM) with unprecedented accuracy, i.e. 12 m in horizontal resolution and 2 m in relative heighy accuracy, as a new reference for commercial and scientific applications. The two satellites were launched and started acquisitions in 2010, and successfully performed the intended mission tasks over the subsequent years.

Another successful formation flight mission with two satellites was the GRACE (Gravity Recovery and Climate Experiment) mission, which derived from a joint partnership between DLR and NASA. The mission launch was in 2002, with two twin spacecrafts being inserted in the same quasi-polar orbit at approximately 500 km altitude, with a varying relative distance along the orbital track, up to 200 km. The GRACE satellites have on board laser ranging equipment, accelerometers and GPS receivers in order to assess precisely their relative position. In this way, precise measurements of Earth's gravity field anomalies can be performed, which allows to determine important information for oceanography, geology and climate evolution.

The PRISMA (Prototype Research Instruments and Space Mission technology Advancement) mission was designed and developed by the Swedish Space Corporation (SSC) in order to demonstrate formation flight and rendez-vous technologies for orbital servicing. The two PRISMA satellites were launched in 2010 in a Sun-synchronous, dawn-dusk orbit, and successfully completed within the end of 2011 all the nominal mission tasks related to autonomous formation flying, rendez-vous, precision proximity operations, final approach and recede maneuvers.

The Evolved Laser Interferometer Space Antenna (eLISA) is a ESA mission under development for the next years for the detection and accurate measurement of gravitational waves. In the eLISA concept there are three spacecrafts in heliocentric orbit, forming a high precision Michelson interferometer with a baseline of one million kilometers. The distance between each satellite and another is monitored in order to detect a gravitational wave. In the eLISA constellation concept the three spacecrafts are orbiting the Sun, trailing 20 degrees behind the Earth. The spacecrafts can be kept at approximately costant distance from the Earth, or they can be allowed to drift as far away as 70 million km, the maximum distance at which the eLISA communication link with the ground station can be maintained.

The Tecnhology Satellite of the 21st Century (TechSat 21) was a demonstration mission developed by the U.S. Air Force Research Laboratory's Space Vehicles Directorate, which foresaw three microsatellites flying in a configurable formation for military purposes such as radio frequency sparse aperture imaging, precision geolocation, ground moving target indication (GMTI), single-pass digital terrain elevation data (DTED), electronic protection, single-pass interferometric synthetic aperture radar (IF-SAR), and high data-rate, secure communications. However, the mission never flew since it was canceled in 2003 due to cost overruns.

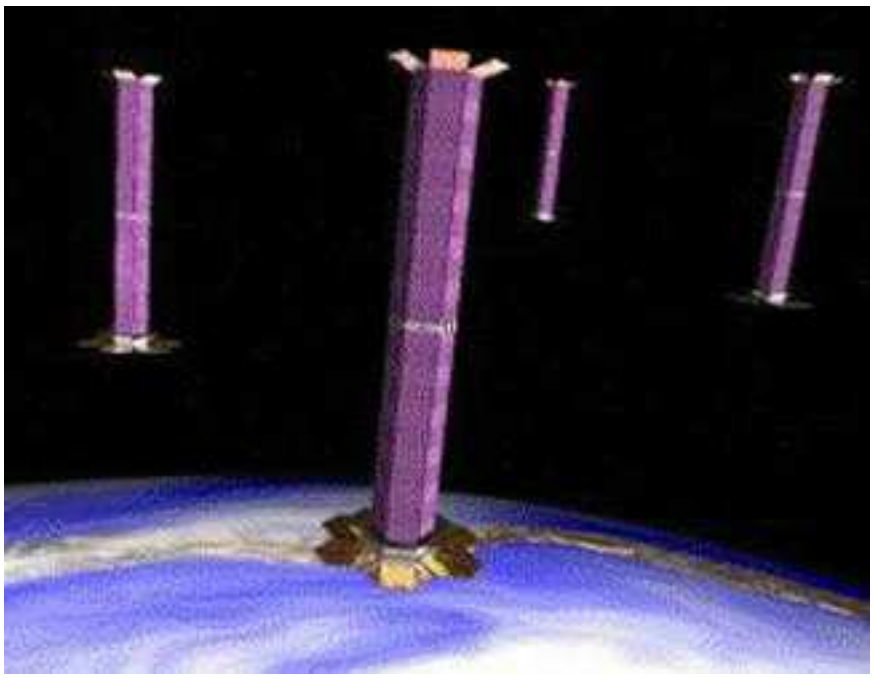

Figure 2 – Cluster Formation for the proposed TechSat-21 Mission

1.3 Satellite Proximity Maneuvers

The concept of spacecraft proximity maneuvers deals with the planning and management of those maneuvers, in particular in the final phases, that have the goal of bringing one satellite to dock with the other by means of complementary interfaces. This type of maneuver is generally referred to as Rendez-Vous and Docking (RVD). Usually, in these maneuvers one spacecraft acts as a chaser, therefore its GNC system implements a guidance and control law in which the other spacecraft is the target, and as such its dynamic state serves as reference for the chaser. In particular, in the final phase of the RVD maneuver there is the relevant risk that the two space vehicles impact one on each other, therefore in this phase the control system must have a highly reliable ability to respect a certain set of conditions and constraints with adequate margin. This aspect becomes even more relevant when the target spacecraft is not cooperative. In this case, since it generally happens when a no more functioning satellite has to be removed from its orbit through the chaser, the maneuver, and therefore the control system, is complicated by the fact that the target satellite has an uncontrolled, freely tumbling motion that has to be estimated through a dedicated measurement system on board the chaser, and possibly because the target does not present a complementary interface for the docking with the chaser, and therefore it must be captured by the chaser through a robotic arm with an end effector grasping one appendix of the target, or through other systems.

Up to date, Rendez-Vous and Docking/Capture in currently operative missions is performed as a non-autonomous maneuver through in the loop intervention of mission operators. In the case of Autonomous Rendez-vous and Proximity Operations (ARPO) between two spacecrafts, the relative GNC system must respond to robustness requisites, with the implementation of reliable collision avoidance and fault management functions. During the last years, a number of missions with demonstrative purposes have been successful in the on orbit execution of ARPO related experiments.

The Engineering Test Satellite 7 (ETS-7) of the JAXA, the Japanese Aerospace eXploration Agency, was a mission launched in 1997 consisting of a target spacecraft and a chaser spacecraft, the latter being the world's first satellite equipped with a robotic arm. The RVD experiments that were planned to be carried out with the two satellites were successfully completed by the first months of 1999.

Figure 3 – Engineering Test Satellite 7 (JAXA)

The eXperimental Small Satellite 10 (XSS-10) of the U.S. Air Force Research Laboratory was a low cost microsatellite launched at the beginning of 2003 with demonstrative purposes for tasks of inspection, rendez-vous and docking, and close-up maneuvering between satellites. The microsatellite was launched as a secondary payload together with a Global Positioning System (GPS) satellite on board a Delta II launch vehicle. After launch and ejection from the upper stage, the XSS-10 spacecraft successfully performed a proximity inspection sequence of the launch vehicle upper stage from which it had been ejected.

The Orbital Express was a mission of the U.S. Defense Advanced Research Projects Agency

(DARPA) and NASA, developed for the demonstration of technologies for rendez-vous, proximity operations, station keeping, capture, docking, fluid transfer and installation of replaceable units. The mission consisted in two satellites, a servicing spacecraft with a robotic carrying a vision system-based navigation system, and a serviceable satellite. The two spacecrafts were launched in 2007, and in the same year they successfully carried out a RVD experiment, which was followed by an operation of replacement of the on board computer of the target satellite.
Moreover, in recent years the Front-end Robotics Enabling Near-term Demonstration (FREND) ground simulator has been developed by DARPA, and successfully tested for the study and investigation of ARPO tecnhologies and strategies applied to non cooperative targets, e.g. satellites needing some kind of servicing, but that were built in previous years and were not therefore equipped with the necessary systems and interfaces for cooperative RVD.

1.4 Original Contributions

Since 2010, the cooperating SPAcecRaft Testbed for Autonomous proximity operatioNs experimentS (SPARTANS) project is under development and testing at the Center of Studies and Activities for Space (CISAS) "G. Colombo" of the University of Padova. The goal of the project is the development and testing of a hardware simulator consisting in two or more units that are representative of two or more satellites flying in formation or performing a proximity maneuver. Each Unit of the simulator is made of two main parts. The lower part is the Translation Module (TM), and it consists in an aluminium structure supporting a suspension system based on air skids, allowing a low friction motion on a glass surface, and a navigation system which allows position and Azimuth estimation. The upper part, connected to the TM, is the Attitude Module (AM), which consists in a 3-axes joint structure, which supports and provides Yaw, Pitch and Roll Degrees of Freedom (DOF) to an aluminium structure. The aluminium structure of the AM carries an Attitude Determination System, and a Guidance Navigation and Control System. All Units of the simulator carry moreover in the AM a Communication System, which allows inter-units crosslinks, and communications with the external control station, consisting of a laptop through which commands can be sent and telemetry data can be received. In the final configuration, the simulator can be employed for extensive studies and investigations of a variety of problems related to SFF, ARPO, cooperative and non-cooperative Rendez-Vous and Capture. One important aspect of the simulator is its high level of modularity, allowing fast replacement of equipment for the substitution of no more functioning components, and also for the installation of systems and sensors, which allows

perfomances comparison between different types of hardware on the same tasks.
The SPARTANS project is supervised and directed by Prof. Enrico Lorenzini (CISAS, Department of Industrial Engineering, University of Padova) and it is carried on by Post doctoral students, Ph.D. students in Space Sciences Technologies and Measurements, and Master's Degree students in Aerospace Engineering, with the collaboration of CISAS researchers.
The main contributions of my Ph.D. to the SPARTANS project have been addressed to the design and development of the TM, to the development and testing of the Optical Flow Sensor (OFS) navigation system on board the TM for position and Azimuth estimation, to the design and assembly of the levellable Units test table, to the preliminary planning of position and attitude PID and optimal control maneuvers through a MATLAB software simulator for the SPARTANS testbed, and to the software analysis of a satellite inspection scenario for reproduction of relative dynamics in scale through the SPARTANS simulator.

1.5 Thesis Outline

Chapter 2 presents and describes the SPARTANS simulator and the related development activities. The subsystems of the AM are described, and subsequently the TM is presented in its main characteristics and subsystems. Subsequently, a description of the main experimental activities related to the simulator is provided, concerning the activities addressed to the characterization, development and testing of the unit's air suspension system, to the design and testing of the simulator test table, and to development, calibration and testing of the OFS navigation system. Moreover, the Section presents additional experimental activities that have to be performed, related to the control thrust force and unit's inertia properties estimation through the torsional wire system of the Measurements Laboratory.
Chapter 3 presents the preliminary activities related to the integration of the OFS navigation system with an external Vision-based navigation system, developed in parallel by other Researchers and PhD students in the context of the SPARTANS project.
Chapter 4 provides firstly a brief description of spacecraft relative motion models, which are essential in the design and implementation of GNC systems applied to SFF and ARPO problems. Following the introduction to relative motion models, a description of the Guidance, Navigation and Control functions is provided, and subsequently different types of control strategies that can be employed in SFF and/or ARPO problems are presented: Proportional-Integral-Derivative (PID) control, Linear Quadratic Regulator (LQR), and Model Predictive Control (MPC), of which an

explicit solution is presented. After that, a series of position and attitude control maneuvers planned with the Matlab Software Simulator of the SPARTANS testbed with standard and optimal control algorithms are presented.

Chapter 5 presents the investigation and related results of a scenario of inspection of a non cooperative satellite in Low Earth Orbit (LEO), through a spacecraft that has to be inserted in a Passive Relative Orbit in order to perform the inspection of the non cooperative target. The results of numerical simulations of the acquisition and maintainance of the inspection orbit are presented, for the cases of manuevers performed through LQR and MPC optimal controllers.

2 SATELLITE PROXIMITY MANEUVERS AND FORMATION FLIGHT HARDWARE SIMULATOR

In this section the spacecraft hardware simulator called SPARTANS under development at the CISAS of the University of Padova, is presented in all its main features and functionalities, with a comprehensive overview of both already developed, and still to be developed components, and related activities. The simulator is composed by a minimum of two Units, which are robotic platforms that allow to a certain extent the reproduction of a spacecraft attitude and position motion, allowing in this way the study and investigation of strategies and problems related to spacecraft formation flight, Rendez-Vous and Docking (RVD), proximity maneuvers, with hardware-in-the-loop implementation of Guidance Navigation and Control (GNC) schemes and algorithms.

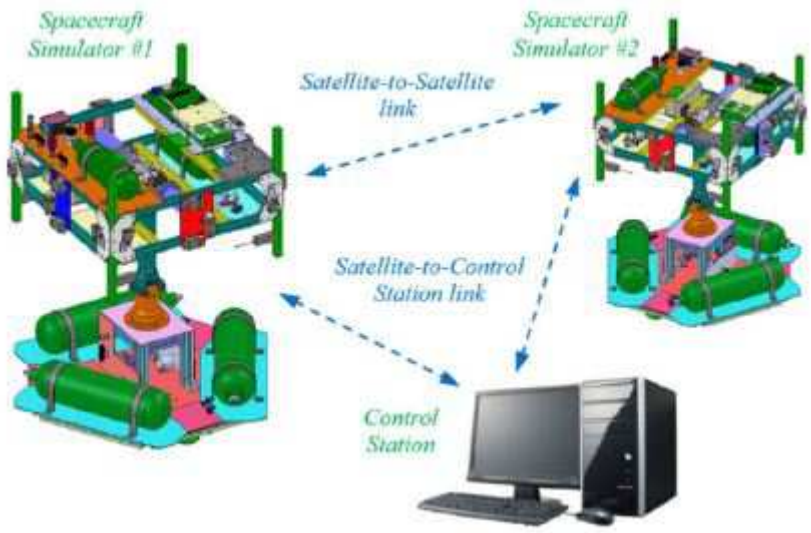

Figure 4 – The SPARTANS cooperating spacecraft testbed

Each Unit of the SPARTANS Simulator is composed of two main elements: the upper section, called Attitude Module (AM), consists of a platform with 3 rotational Degrees of Freedom (DOF) that are enabled by a custom 3-axes joints structure, comprising the Yaw, the Pitch and the Roll joints. Connected to the AM yaw joint there is the lower section called Translation Module (TM), which consists in a platform with 2 planar translational DOF that are enabled by a skids-based air suspension system.

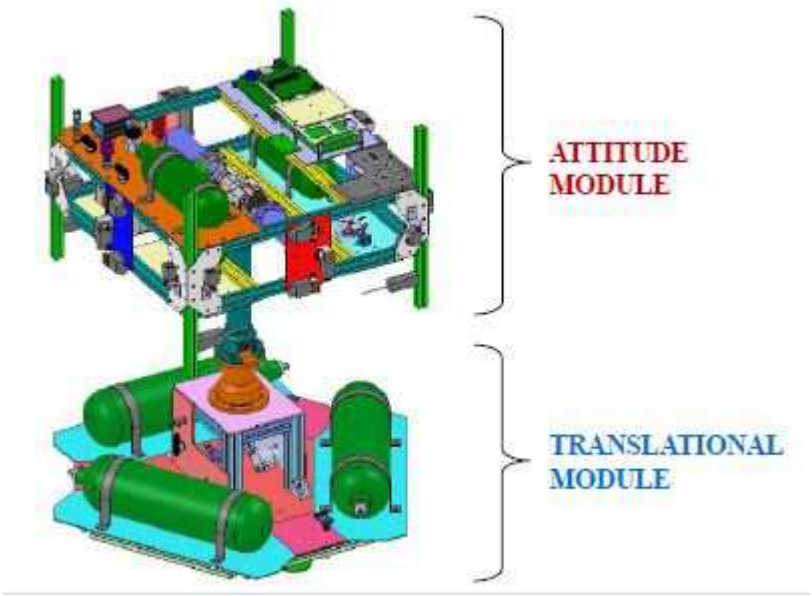

Figure 5 – The Attitude Module (AM) and the Translation Module (TM)

At the moment of the writing of this thesis the SPARTANS project is at the following stage of development: a single AM, with only attitude control enabled, has been completed and tested in a series of attitude control maneuvers up to 3 DOF, with navigation system based on encoders installed in the joints, and IMU installed onboard the structural components of the module. A single TM has been developed, completed at the structural level, and its air suspension system tested in free motion on a glass layer supported by a test table. An incremental and an absolute localization system for the TM motion estimation (position and Azimuth) have been developed and tested. A single preliminary Unit has been assembled with the two developed modules, and its free motion tested on a glass layer supported by a test table.

2.1 Review of Spacecraft Simulators

Testbeds of different types have been used since the beginning of space exploration in order to validate representative hardware and software together. Table (1) reports the characteristics in terms of advantages and disadvantages for different types of testbeds.

TESTBEDS	ADVANTAGES	DISADVANTAGES
On-orbit Testbeds	Fully representative of operative conditions	Very expensive
Parabolic Flights	Good to fair microgravity simulation Fairly easy interaction with payload	Expensive Microgravity lasts about 20 s Not possible to test payload in vacuum or to study thermal cycles effects
Water Tanks	Fair microgravity simulation Long lasting microgravity conditions	High viscous forces / torques Need for a water resistant payload
Spacecraft Simulators	Good microgravity simulation Very easy interaction with the payload	Disturbance forces / torques to be mitigated Partial freedom of motion

Table 1 – Advantages and disadvantages of different types of spacecraft testbeds

Three main categories for spacecraft ground simulators are provided by Schwarz et al. in [6], consisting in planar systems, rotational systems and combined systems. Air bearings are employed in both planar and rotational system, with pressurized air that, passing through the bearing exit channels, create a thin air film which supports the moving sections and moreover reduces the friction that is present between the sections, so that in proper conditions, both the planar and rotational motions result free from disturbance accelerations.

Planar testbeds have two translational and one rotational DOF, with the rotational DOF around the axis orhtogonal to the planar motion plane. These systems can be used to plan and verify GNC strategies for RVD with two simulator units, and for formation flight applications with more than two units. The most renown planar system in the international community is the SPHERES (Synchronized Position Hold, Engage, and Reorient Experimental Satellites) testbed, which has been developed in two different configurations, one as a 3 DOF ground based planar system, and the other as a 6 DOF system which is maintained as a flight testbed on board the International Space Station. Other examples of planar testbeds are the ground facilities developed by the Stanford University's Aerospace Robotics Laboratory in order to study on-orbit assembly, servicing, and repair applications and formation flight maneuvers, and a planar air bearing system with a single robotic arm developed by the University of Victoria.

In the case of rotational systems, only 3 DOF attitude motion is enabled, with limitations on the consented angular range of each rotational axis. As it can be seen from the configurations in Figure

(6), unconstrained Yaw can be more easily obtained, as in the case of the Tabletop and Umbrella configurations developed by NASA, Georgia Tech and Utah State University, but Pitch and Roll angles are constrained to less than 90 deg usually. Contrary to the Tabletop and Umbrella configurations, the Dumbbell configuration, developed by Virginia Tech and University of Michigan, provides unconstrained Roll and Yaw motions by employing two opposite arms with the mounting area separated from the rotation center.

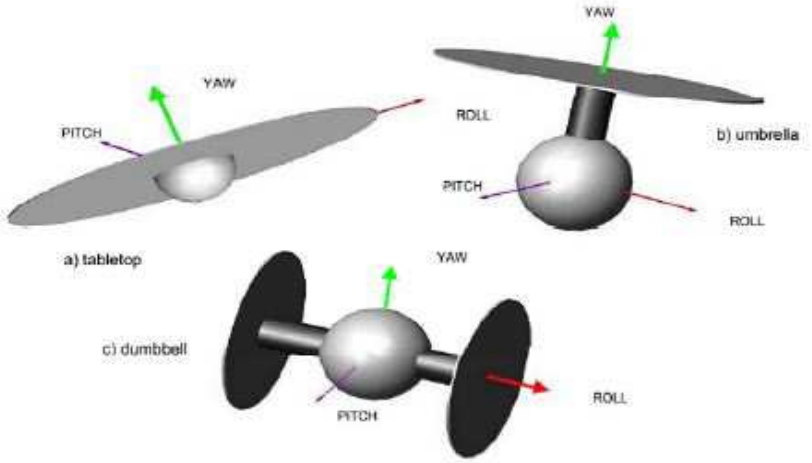

Figure 6 – Tabletop (a), Umbrella (b) and Dumbbell (c) configurations

Combined systems employ both planar and rotational air bearings in order to obtain up to six unconstrained DOF. The Formation Control Testbed is a combined system developed by JPL-Caltech with goal of performing precise autonomous maneuvers for proximity operations and formation flying.

Figure 7 – The Formation Control Testbed (Caltech/JPL)

2.2 The SPARTANS Hardware Simulator

The cooperating SPAcecRaft Testbed for Autonomous proximity operatioNs experimentS (SPARTANS) project consists in a combined planar spacecraft testbed with a minimum of two robotic Units, each with 5 DOF, 3 rotational DOF with unconstrained Yaw and constrained Roll and Pitch, and 2 translational DOF. As already pointed out in the first paragraph of this chapter, each Unit is composed of two fundamental sections, the Translation Module (TM), and the Attitude Module (AM).

The AM is composed at the structural level by a 3-axes Joint structure, which enables the rotational DOF and hosts the encoders employed as fiducial reference for the attitude determination, and by a support structure connected to the outer sections of the 3-axes Joint structure. The support structure hosts the GNC components of the AM, including on board processors, additional attitude navigation sensors, i.e. Inertial Measurement Unit (IMU), and all the components of the air-thrusters based attitude and position control system. The TM, connected in its upper section to the Yaw joint, has the main functions of supporting the AM, supporting the air suspension system which enables the planar DOF, and supporting the incremental navigation system providing estimates of the planar position and Azimuth of the platform. Each Unit carries in the AM a communication system which provides links between each unit, needed for the execution of coordinated maneuvers, and a link with the external control station, consisting in a laptop for commands and telemetry. For the absolute position and attitude determination an external vision based navigation system is employed. .

Figure 8 – First prototype of the complete Unit of the SPARTANS testbed

In the final configuration comprising a minimum of two Units, the SPARTANS testbed is designed to allow the planning, testing and verification of algorithms and strategies for spacecraft proximity maneuvers, formation flight and inspection maneuvers, automated Rendez-Vous and Docking and Rendez-Vous and Capture maneuvers. One of the relevant characteristics of the testbed consists in the modularity of the Unit design, allowing faster and easier replacement of different types of equipment in case of failures, damage, but also in order to assess performance comparisons and carry out different types of maneuvers, as it is for instance the case of Rendez-Vous and Docking or Capture in which either a robotic arm or an interface has to be installed in order to perform the docking or capture between two Units.

2.3 Attitude Module on board Subsystems

The AM is composed of 5 main subsystems, described in sections 2.3.1 to 2.3.6 : the Structural Subsystem, the Propulsion Subsystem, the Attitude and Position Determination and Control Subsystem, the Electric and Power Subsystem, the Communication and Data Handling Subsystem. The AM employs a microcontroller in order to elaborate the sensors measurements and in this way determine the control torque which must be executed by the actuators in order to perform the requested attitude control maneuver. The AM has two main communication links, one with other Units in order to perform coordinated maneuvers, the other with the external Control Station for house keeping and telemetry.

2.3.1 Structural Subsystem

The structure of the AM is composed of the following main elements:

- The Three-Joints System which supports the outer support structure of the AM, and which enables the Yaw, Pitch and Roll DOF,
- An aluminium framework with 20 mm x 20 mm profile beams with lateral T-grooves, joined one to each other with stainless quick connectors,
- rectangular plates in the upper and lower sections of the main structure, in order to support the components of the AM,

- reinforcing plates
- support brackets for air-thrust actuators

The Three-Joints System is composed of three consecutive rotational cylindrical joints with axes that are orthogonal and intersect each other in correspondence of the rotational center. In this system, the design is such that the first joint allows a rotation about the Yaw axis, which coincides with the vertical axis, the second joint allows a rotation about the Pitch axis, and the third joint allows a rotation about the Roll axis. In this system, the Yaw axis rotation is unconstrained, while Pitch and Roll rotations are constrained to the range of [-40°, +40°].

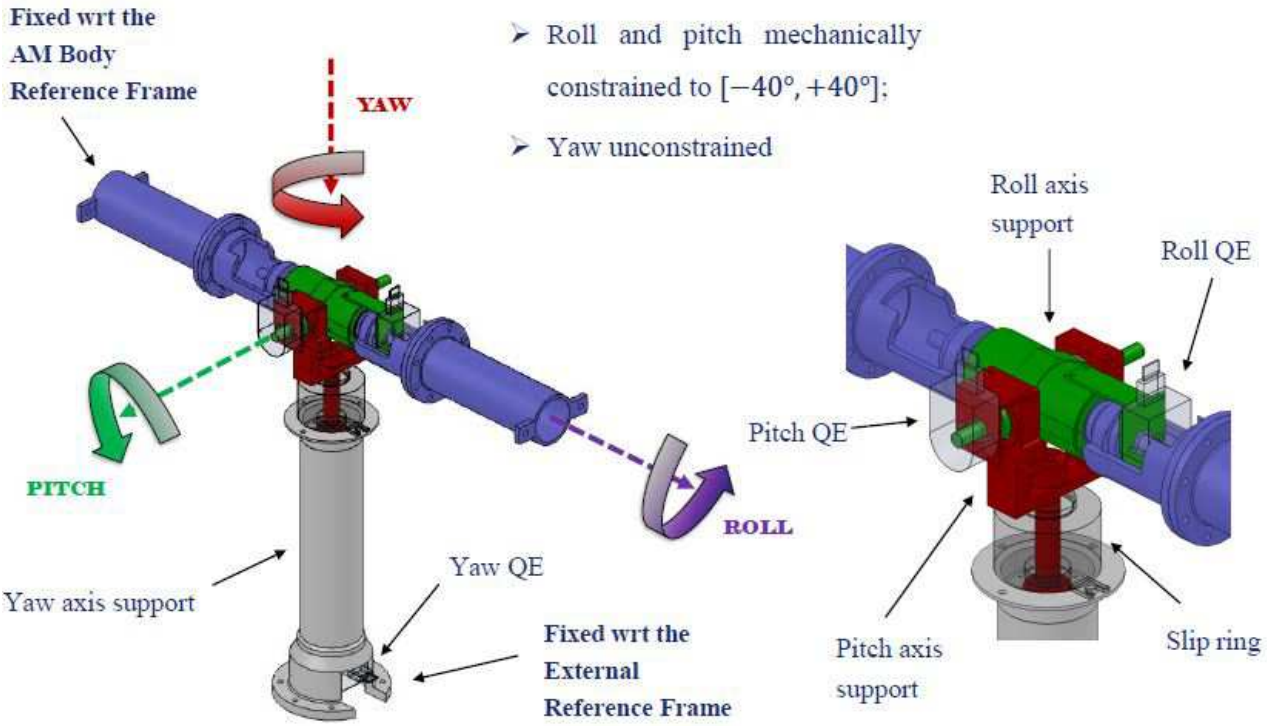

Figure 9 – The Three-Joints System of the AM

In ideal conditions, i.e. absent friction between the joints sections and with AM balanced in weight distribution wrt to its rotation center, the center of mass of the AM coincides with the rotational center of the Three Joints System, in this way the attitude platform presents a dynamic behaviour that is not dependent on gravity-induced torques, but on control torques only.

2.3.2 Propulsion Subsystem

The on board Propulsion Subsystem of the AM consists of two main sections: the high pressure section at a maximum of 200 bar, and the low pressure section at 10 bar. The updated version of the AM, to which this section refers to, is equipped with the components of the propulsion subsystem for both attitude and position control. The previous version included components for attitude control only.

The main components of the high pressure section consist in:

- four Luxfer tanks in composite material with 4 Lt. total capacity for air storage at a maximum of 200 bar
- a fill and vent system for loading the hydraulic circuit, consisting in a quick connector and two ball valves
- a pressure regulator that reduces the air pressure from a a maximum of 200 bar of the high pressure section, to the operative level of the air thrust actuator's nozzle, i.e. 10 bar,
- steel pipe fittings for the connection of the components of the high pressure section

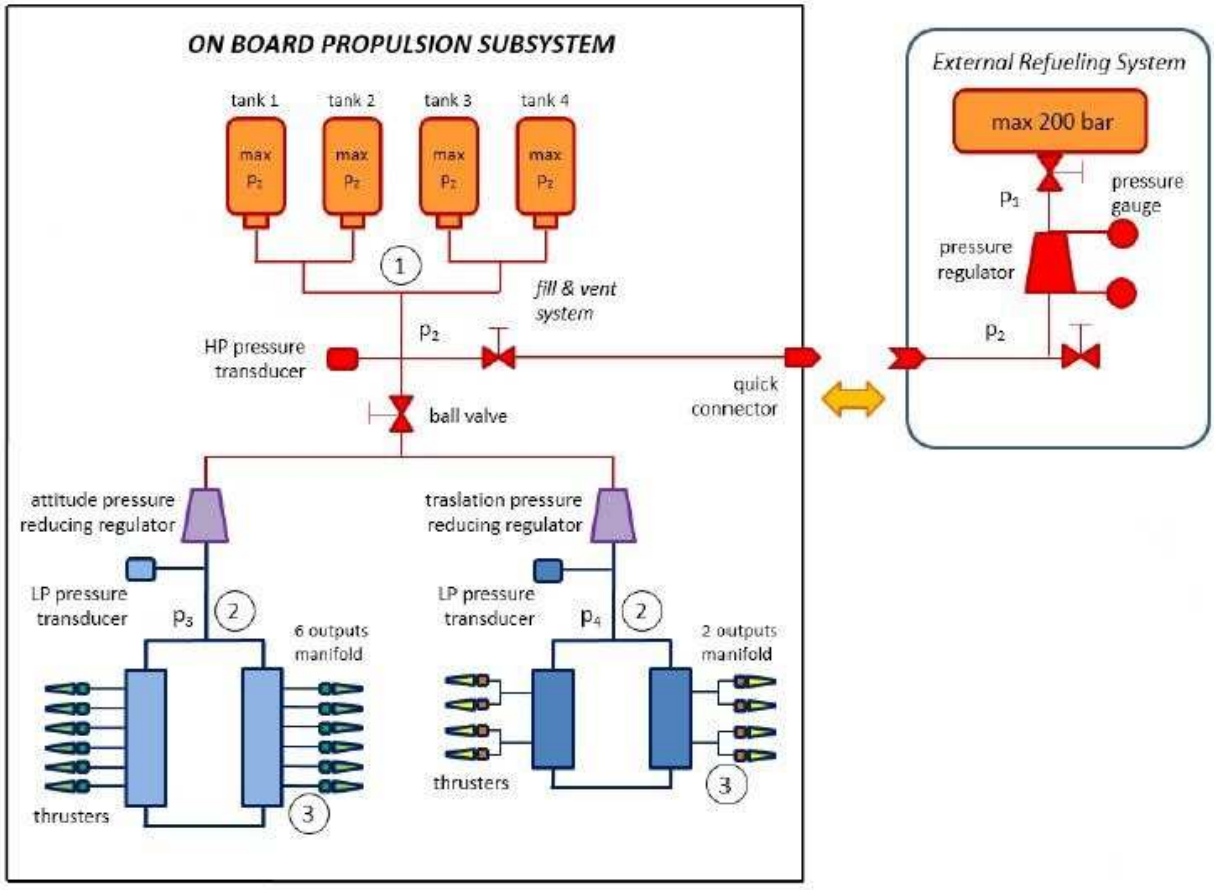

Figure 10 – current AM hydraulic circuit of the Propulsion System

The low pressure section of the AM presents:

- four 6-ways and two 2 double ways manifolds that supply air to the thrusters by distributing the air flow from the pressure regulator
- 20 air thrusters, 12 for the execution of the command attitude control torques, and 8 for the execution of the command position control forces
- plastic pipes for the connection of the elements of the low pressure section of the hydraulic circuit

Each air-thrust actuator is composed by two fundamental elements: an electro-valve and a converging nozzle. The electro-valve is a solenoid valve which opens upon turning on of its power supply, and lets the air flow pass to the converging nozzle, while the nozzle consists in a M5 screw with a central hole of 0.75 mm of diameter.
The actuation axes of the thrusters for both the attitude/position control are disposed so that by using the four appropriate thrusters for each axis, it is possibile to activate only a positive or negative torque/force, to be actuated around/along the designed AM Body axis.

2.3.3 Attitude and Position Determination and Control Subsystem

The Attitude and Position Determination and Control Subsystem is composed by the sensors whose measurements are employed in order to provide an estimation of the AM orientation and planar position wrt to a Local Vertical Local Horizontal (LVLH) External Frame of Reference, and by the electronic boards that are in charge of elaborating the sensors measurements in order to compute the required control action and make it execute by the Propulsion Subsystem.
Each AM carries on board two different types of attitude sensors:

- 3 rotational, incremental optical Quadrature Encoders (QE) which are used to measure the joints rotation with a 0.09° resolution, providing in this way direct measurements of Yaw, Pitch and Roll angles
- an Inertial Measurement Unit (IMU) providing AM attitude and attitude rate estimations wrt to the External Frame of Reference

Because of their higher accuracy wrt to the IMU measurements, QE angular measurements are used as fiducial reference in order to evaluate the IMU measurements drift and bias.
Attitude and position measurements wrt to the External Frame of Reference are moreover performed by a vision system that is installed outside of the test table, and integrated with the AM attitude measurements and the TM incremental position measurements.
In the updated version of the AM, the GNC functions are performed by the microcontroller implemented in a ODROID XU3 single board computer that is installed on board.

2.3.4 Electric and Power Subsystem

The electrical power in the AM is provided by rechargeable batteries connected in series and parallel, and in power distribution DC/DC converters are employed to regulate the battery voltage level to the operative levels required by the other subsystems. Figure (11) shows the current proposed architecture of the on board Electric and Power Subsystem.

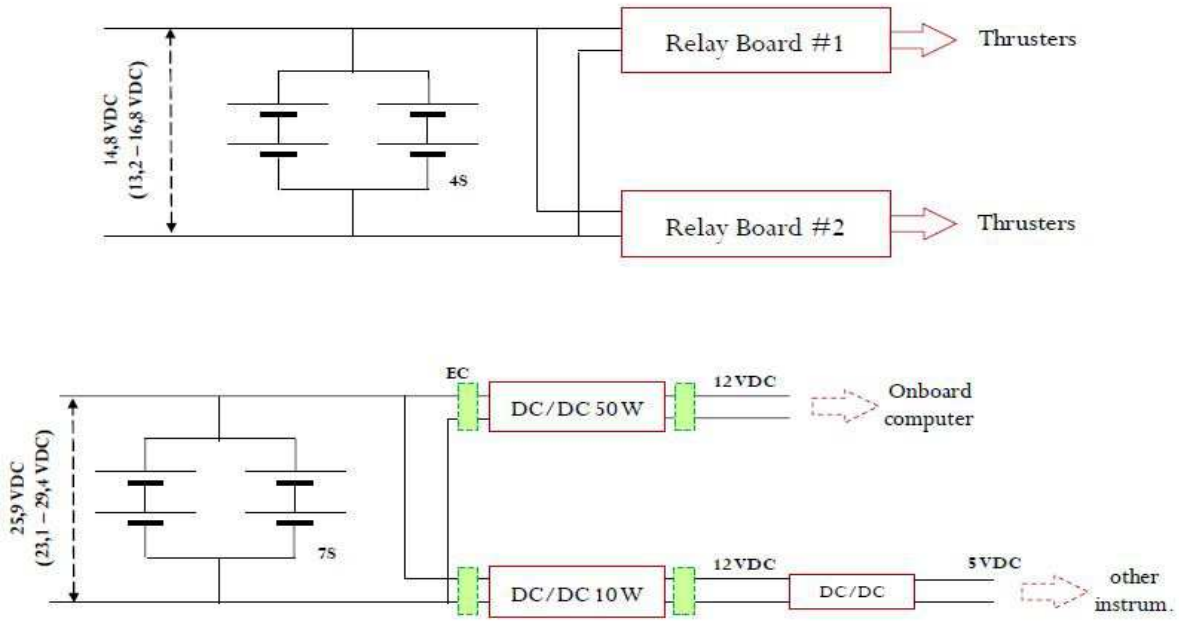

Figure 11 – Current Architecture of the AM Electric and Power Subsystem

2.3.5 Communication and Data Handling Subsystem

In the final configuration of the SPARTANS testbed, the Units and the external Control Station (laptop) use a specific module which allows inter-communication links bewteen Units. For the final configuration of the testbed, two separate channels are foreseen: a first channel links each Unit to each other allowing different types of coordinated maneuvers to be carried out, while the second channel links each Unit to the Control Station, and is allocated to commands and telemetry data transmission, from the Control Station to Unit and vice-versa, respectively.
The communication protocol consists in variable size packets composed of a header with a predetermined number of byte, a n-byte data message, and a checksum with a predetermined number of byte.
The header reports the ID of the transmitting Unit, the ID of the receiving Unit, and the ID associated to that message. The final checksum in employed for error detection in the transmitted data.
Units of the simulator can exchange messages that can be grouped in 5 fundamental types:

- Initiate Link Message, used to initialize communications between Units
- Acknowledge Messages, used to verify that commands from the Control Station are received and executed in synchrony between multiple Units
- Data Request Messages, used by the Control Station to request single or multiple transmission of telemetry or housekeeping data from the Units
- Data Messages, used by the Units to trasmit telemetry, housekeeping and GNC data
- Command Messages, used to command the execution of a specific operation

2.3.6 On Board and Control Station Software

The on board software in the AM on board computer is organized in 6 main libraries, each with a main on board process: the Sensors library, the Position and Attitude Determination System (PADS) library, the Controller (CTRL) library, the Propulsion (PROP) library, the Communication (COMM) library, the Housekeeping (HKP) library. Each library includes moreover two types of functions: the Initialization Functions, used for data structures and variables initialization, or re-initialization, and the Update Functions, used to update the library variables, such as current dynamic state updating and control action computation
The microcontroller implemented in the onboard computer implements two types of processes.

Periodic Interrupt Processes execute actions that are repetitive and time-dependent, e.g. GNC related operations. Event-driven background and GNC tasks on the other hand are employed in the implementation of non time-dependent operations, e.g. software initialization, formation flight scheme change, activation of collosion avoidance schemes, etc. GNC operations that are periodic need to be synchronized since control actions must be computed and above all executed when sensors data are updated.

Figure 12 – The ODROID computer employed on board the AM

On board operations are divided in three hierarchical levels: programs, tests and maneuvers. Each program is associated to a particular executable file, corresponding to one or more tests, each of which corresponds to linear or non-linear sequence of maneuvers, as a convenient way to divide a complex motion in a simpler sequence of maneuvers.

2.4 Development of the Translation Module (TM)

The Translation Module (TM) of the Units of the SPARTANS hardware simulator has been developed after the first prototype of the AM had already been designed, assembled and tested in the execution of attitude control maneuvers. The TM must fulfill three essential functions: supporting the AM, supporting the air-suspension system needed for the activation of the planar DOF, and supporting an incremental navigation system for Unit 2D position and TM Azimuth estimation. The TM has been developed following a modular design which allows easy and rapid modifications, in case of substitution of damaged components, and also in the case of insertion of other components with different functions, e.g. measurement systems, interfaces for capture, etc.

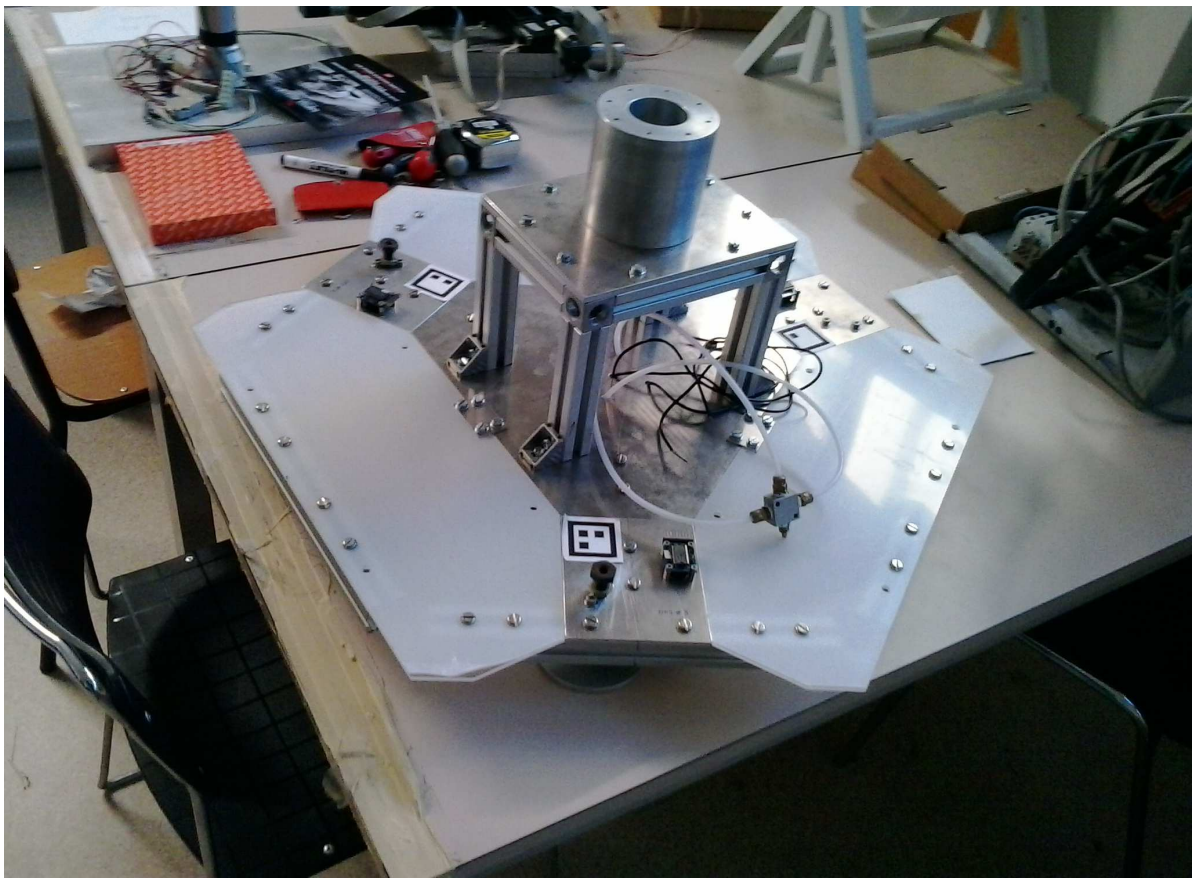

Figure 13 – First prototype of the TM of the SPARTANS testbed

2.4.1 Translation Module On Board Subsystem

The TM is composed of 5 main subsystems that are described in Sections 2.4.1.1 to 2.4.1.4 : the Structural Subsystem, the Air Suspension Subsystem, the Position and Azimuth Determination Subsystem, the Electric and Power Subsystem, the Communication and Data Handling Subsystem. On board the TM a microcontroller is employed in order to elaborate the measurements of the incremental navigation system and save the measurements from the pressure transducers which measures the air pressure at the inlet of the air skids from the hydraulic circuit.

2.4.1.1 Structural Subsystem

The structure of the TM is composed of the following main elements:

- two aluminium hexagonal plates connected in a sandwich configuration with three radial

aluminium profile beams, with the function of supporting the AM interface structure, and the hydraulic circuit of the air suspension system

- three aluminium plates disposed at the outer sections of the TM, with the functions of supporting the air skids of the air suspension system and the mouse sensors of the incremental navigation system
- three plexiglas plates disposed at the outer sections of the TM with the function of supporting the air tanks of the air suspension system
- one central structure, above the hexagonal plates, made of a vertical and horizontal aluminium profile beams supporting un upper aluminium plate, which in turns supports an aluminium cylinder which is connected directly to the AM
- lateral aluminium profile beams disposed in the outer sections of the TM for the structure stiffening and reinforcement

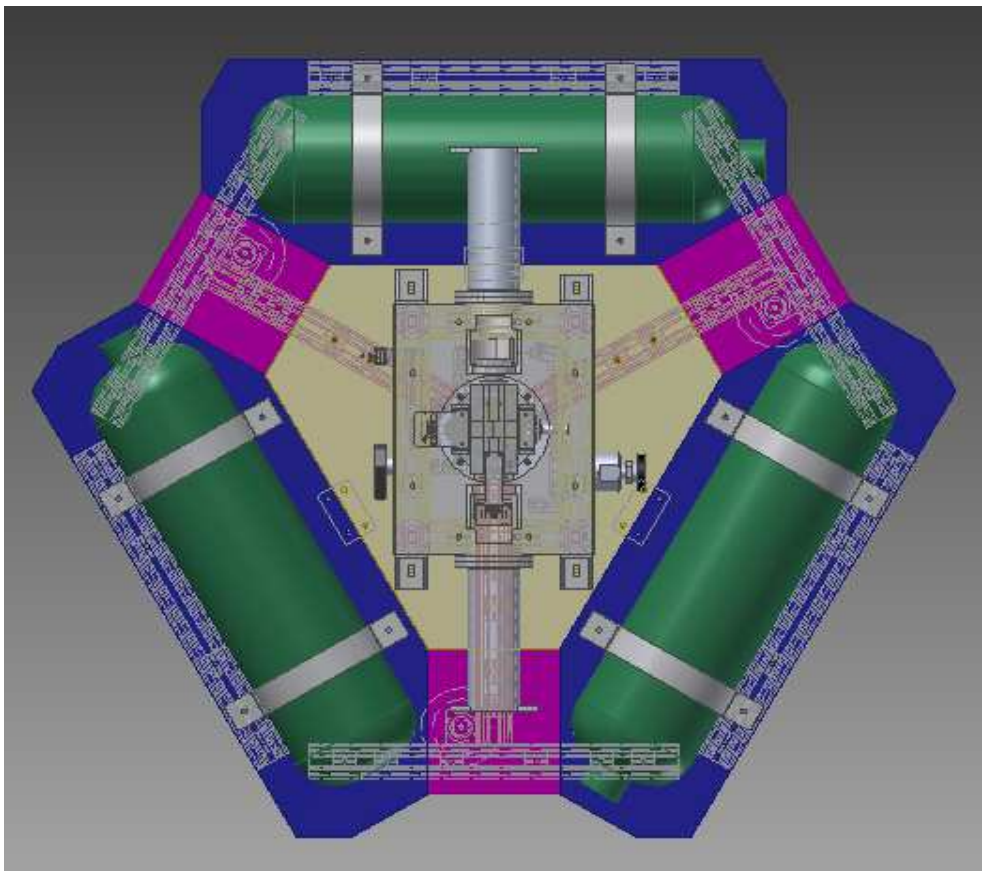

Figure 14 – 3D model of the TM wih AM Three-Joints system, upper view

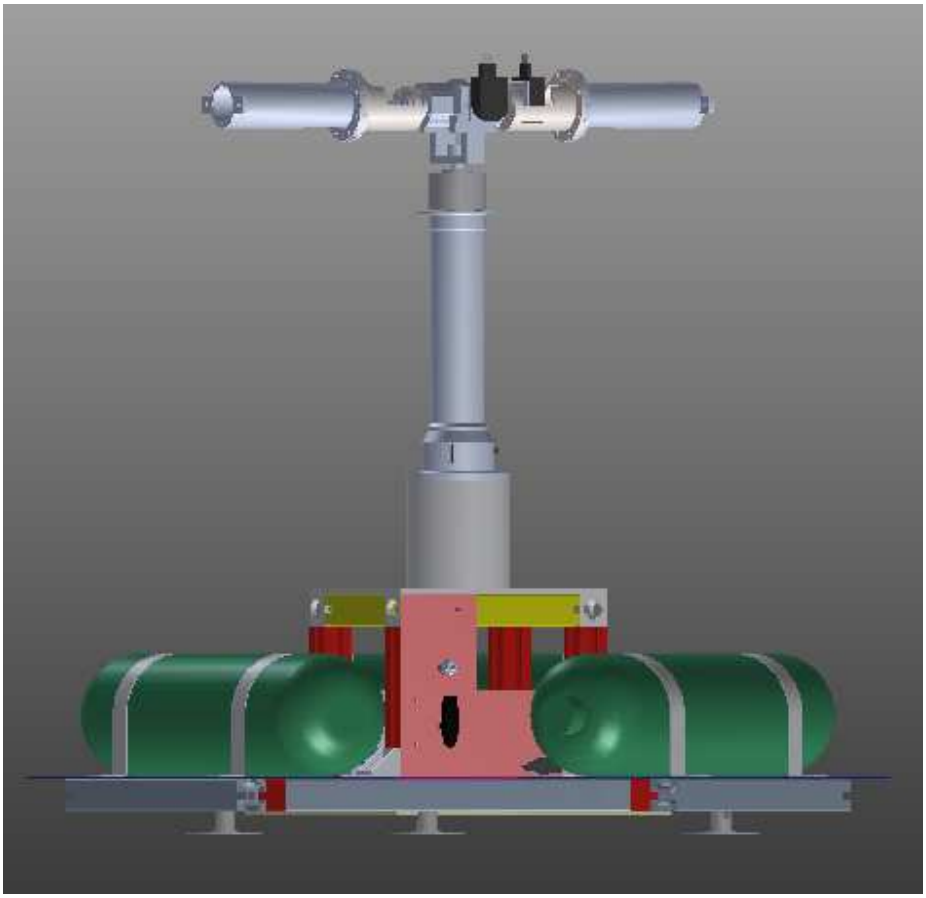

Figure 15 – 3D model of the TM wih AM Three-Joints system, lateral view

This structure has been designed so that the distance from outer vertical section of outer plates to the other at the opposing end of the TM, is of approximately 650 mm, while the distance from the air outlet sections plane of the air skids to the plane of the upper section of the AM support cylinder is of approximately 330 mm.

The TM structure has been designed in order to allow for different configurations in terms of activated DOF. An additional element has been designed for the interface between the TM and the AM, consisting of an aluminium plate which allows the connection of the AM support upper cylinder to the profile beams structure of the AM. In this way two different configurations can be obtained for a single Unit in terms of available DOF. When the interface is mounted in place of the AM Yaw axis support, the Unit presents 3 DOF, 2 planar and 1 rotational DOF as the Azimuth of the whole Unit which moves as a rigid body. When the Yaw axis support is connected instead to the TM, the Unit presents 5 DOF, 2 planar and the 3 rotational DOF provided by the AM joints structure. The AM support cylinder has been dimensioned in order to allow the full range of [-40°, +40°] to the Pitch and Roll DOF of the AM, when the AM axis support is mounted on the TM. Since the Yaw axis support presents a slip ring connection at the bottom, there is a relative rotation

between the AM Yaw axis and the TM. In terms of the control system, the presence of this additional interface results in three different configuration. With the interface plate mounted and the the Yaw axis support removed, the Unit can be controlled either only in 2D position, or both in 2D position and Azimuth, while the configuration with the Yaw axis support installed is employed in order to control all the 5 available DOF. Figure (16) shows the 3D model with Yaw axis support removed and the AM blocked with the additional interface

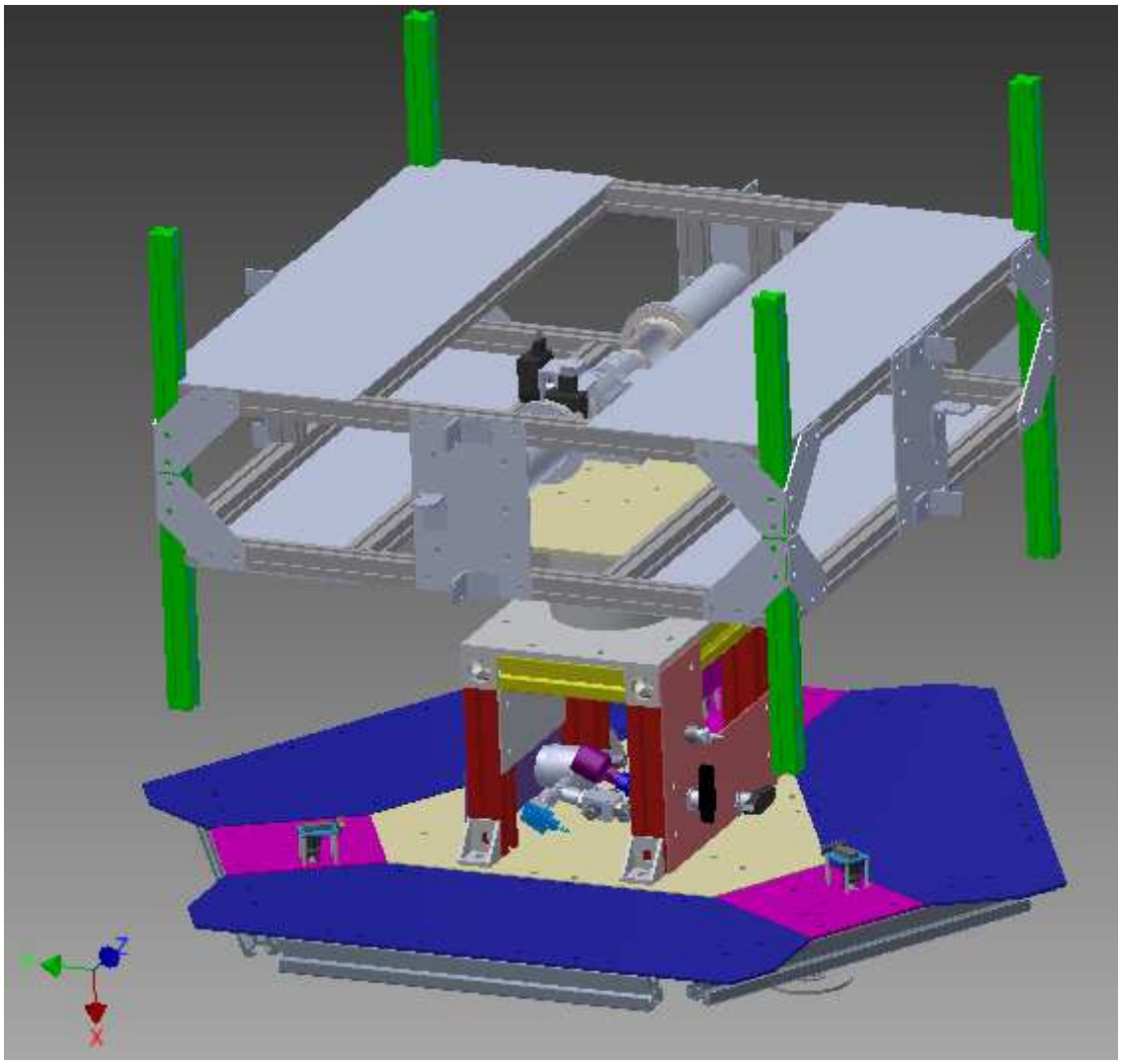

Figure 16 – 3D model of the Unit with blocked AM

During the TM design phase, a series of structural and vibration analyses have been performed in order to assess the behaviour of the structure in presence of static and dynamic loads.
Finite Element Analyses (FEA) have been performed in Inventor on the final 3D model of the TM in order to evaluate the deformation level in the structure as it is likely to be induced by the static loads acting on it, which are given mainly by the weight of the AM corresponding to approximately

23 kg, and a maximum of approximately 8 kg given by the air tanks in full air charge. Figures (17), (18) show the results of the FEA executed with this loads applied on the corresponding locations, with the load corresponding to the AM increased to 50 kg from a measured value of 23 kg, and the total weight of the air-filled tanks increased to 12 kg from an estimated value of 8 kg. As it can be seen from Figure (17), the maximum displacement with this loading conditions results of 0.15 mm, while the minimum safety factor is of 15 (Figure (18)).

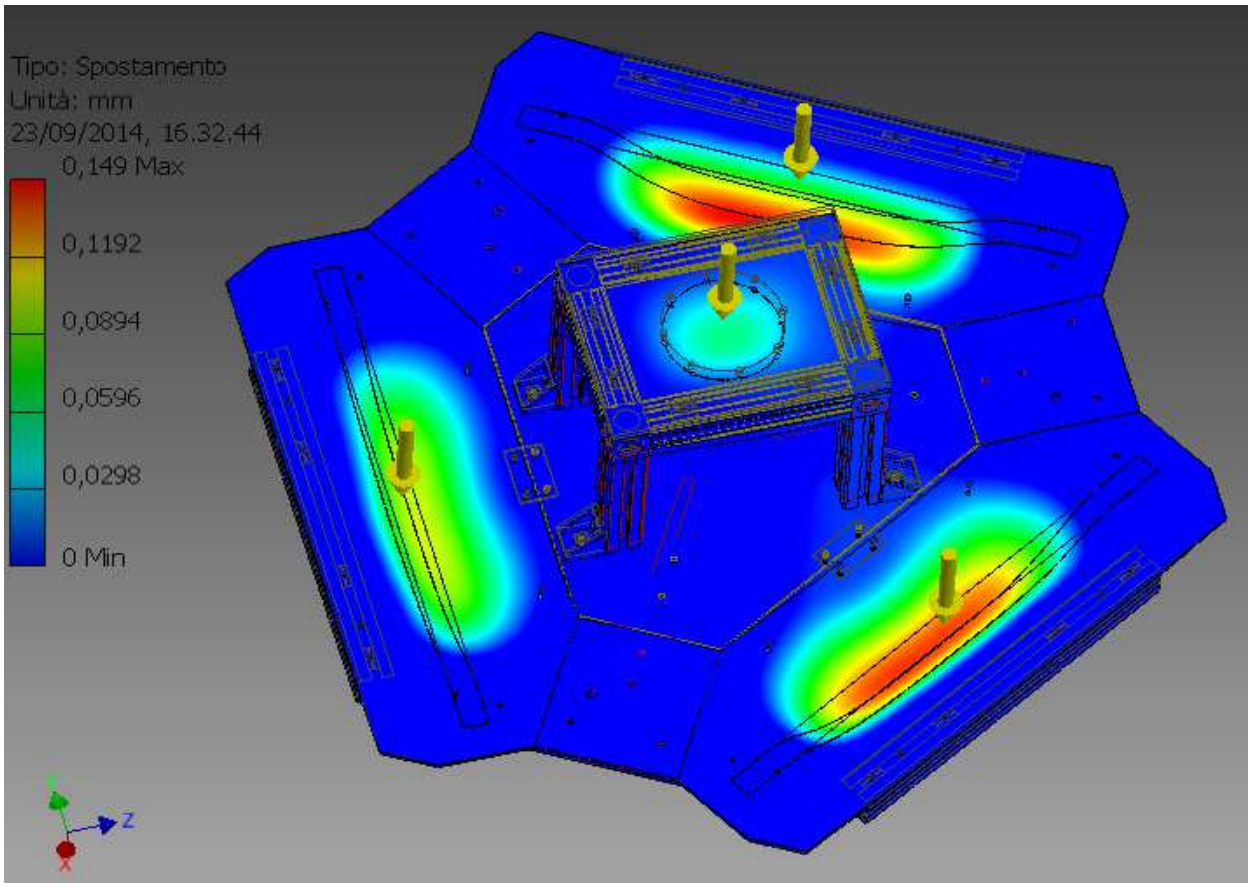

Figure 17 – FEA displacement results on the 3D model of TM with static loads due to AM and air tanks

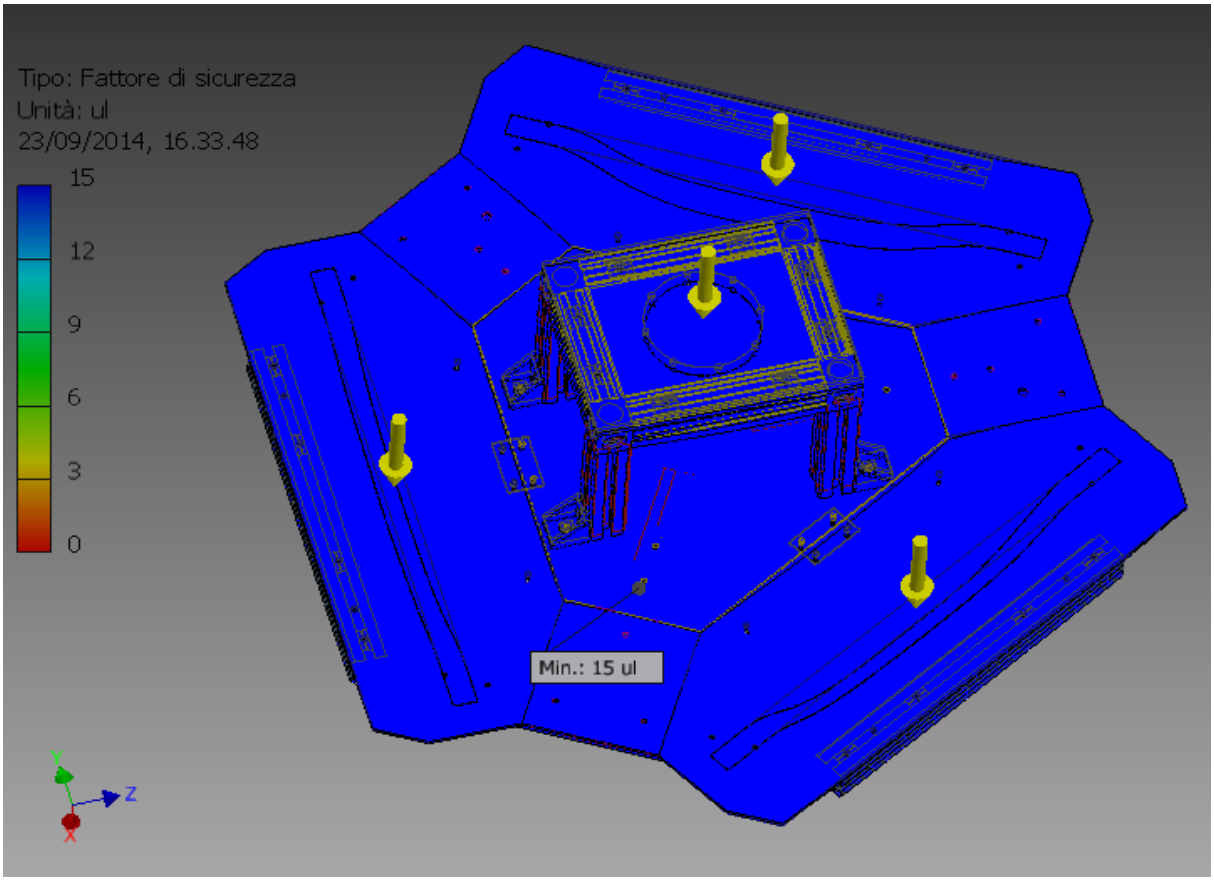

Figure 18 – FEA yield safety factor results on the 3D model of TM with static loads due to AM and air tanks

Vibrational analyses have been moreover performed on the final model of the whole Unit, in this case in order to assess the effects of the position control actuation in terms of the flexular oscillation level it produces, since the position control action is directed towards the structure of the AM, producing in this way a torque wrt to the to center of mass of the whole Unit. Considering the axes in the horizontal directions, orthogonal to the position actuation directions, and considering as a simplification only one actuation direction, the equation of the oscillation produced by the torque that is induced by the position control actuation is given by:

$$I\ddot{\theta}+c\dot{\theta}+k\theta=\tau \qquad (1)$$

with θ the Unit oscillation, I the moment of inertia of the Unit around the axis in the horizontal plane, passing through the Unit center of mass and orthogonal to the direction of the position control actuation, c the damping coefficient, k the flexional stiffness of the Unit, and τ the torque induced by the position control actuation.

The moment of inertia I is a given estimated quantity from the 3D model of the whole Unit, resulting of approximately 9 kg m^2 for the orthogonal horizontal axes passing throught the Unit

center of mass. The flexional stiffness of the Unit has been estimated from a set of FEA simulations on the whole Unit, resulting in an approximate value of 168000 Nm/rad.
The damping coefficient has been estimated as:

$$c = 2\zeta\sqrt{k\,I} \tag{2}$$

with ζ the damping factor of the Unit, which was conservatively taken with a value of 0.5e-4, corresponding to aluminium, as the prevalent material of the Unit.
With parameters estimated, the system response to the impulsive step of a position control actuation was evaluated, resulting in an estimated oscillation within ± 0.1 deg.

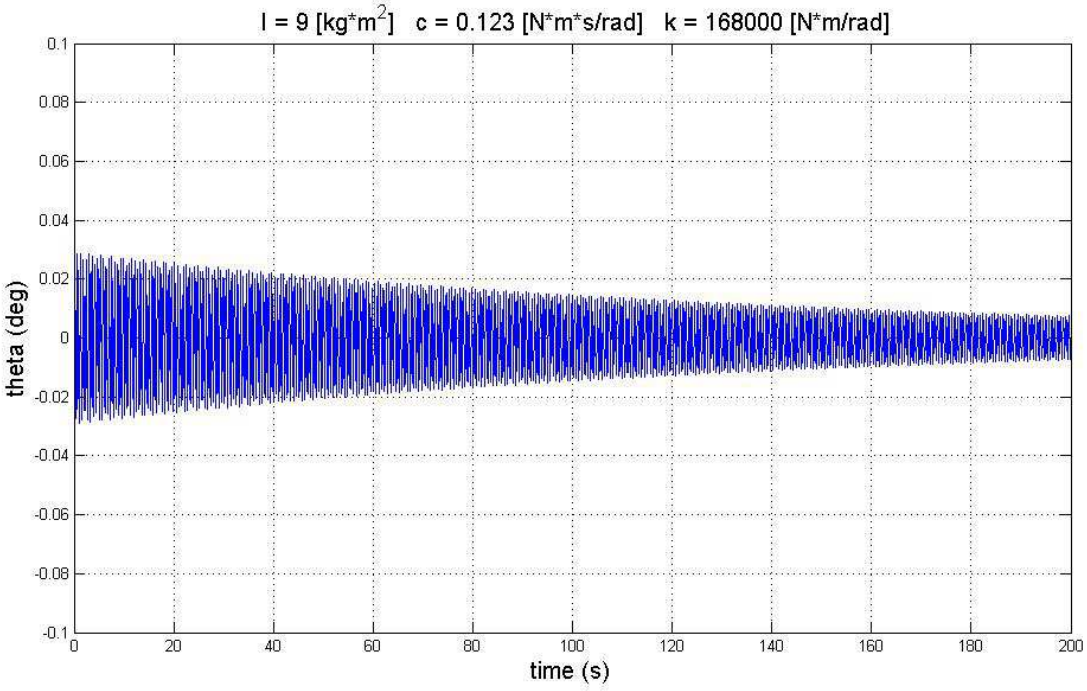

Figure 19 – Estimated Unit oscillation response to impulse input due to position control actuation

2.4.1.2 Air Suspension Subsystem

The Air Suspension Subsystem on board the TM is composed of two fundamental elements: 3 air skids which provide the air film needed to make the Unit slide on the test table with as much as possibile low friction, and the hydraulic circuit, consisting in 3 Luxfer air tanks with 3 lt. capacity each providing the air supply during the tests, and all the components needed to let the air flow

from the tanks to the air skids holes at the operative pressure, and to recharge the air tanks after the tests are over.

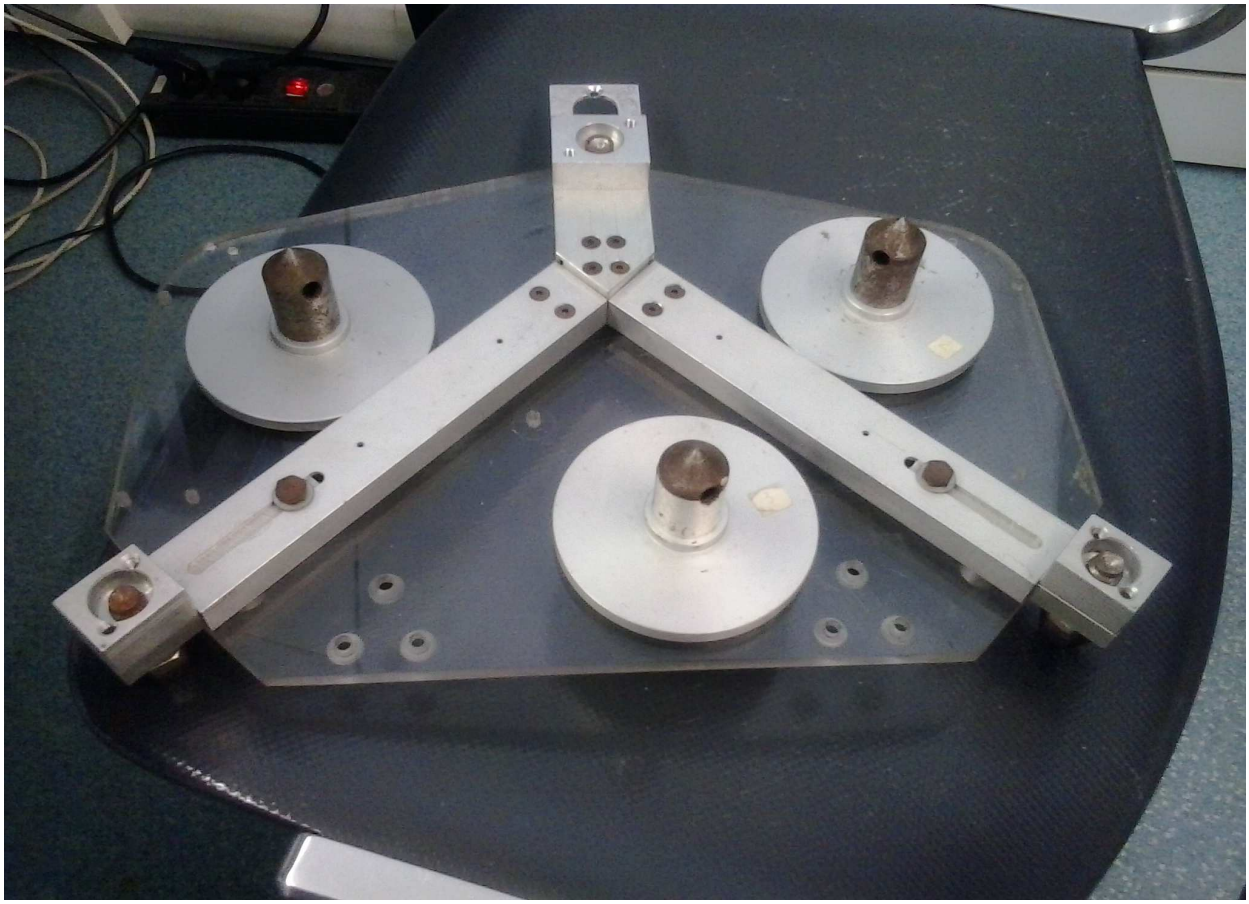

Figure 20 – Air skids of the TM suspension system

The hydraulic circuit, as in the case of the AM is composed of two main sections. The high pressure section comprises all the hydraulic section in which the air from the external supply tanks at 200 bar maximum is transferred to the tanks on board the TM, after the air pressure has been reduced by the on board pressure regulator to the operative level. The other section comprises the part of the circuit which lets the air flow from the on board tanks to skids outlet. Figure (21) shows the hydraulic circuit of the suspension system on board the TM

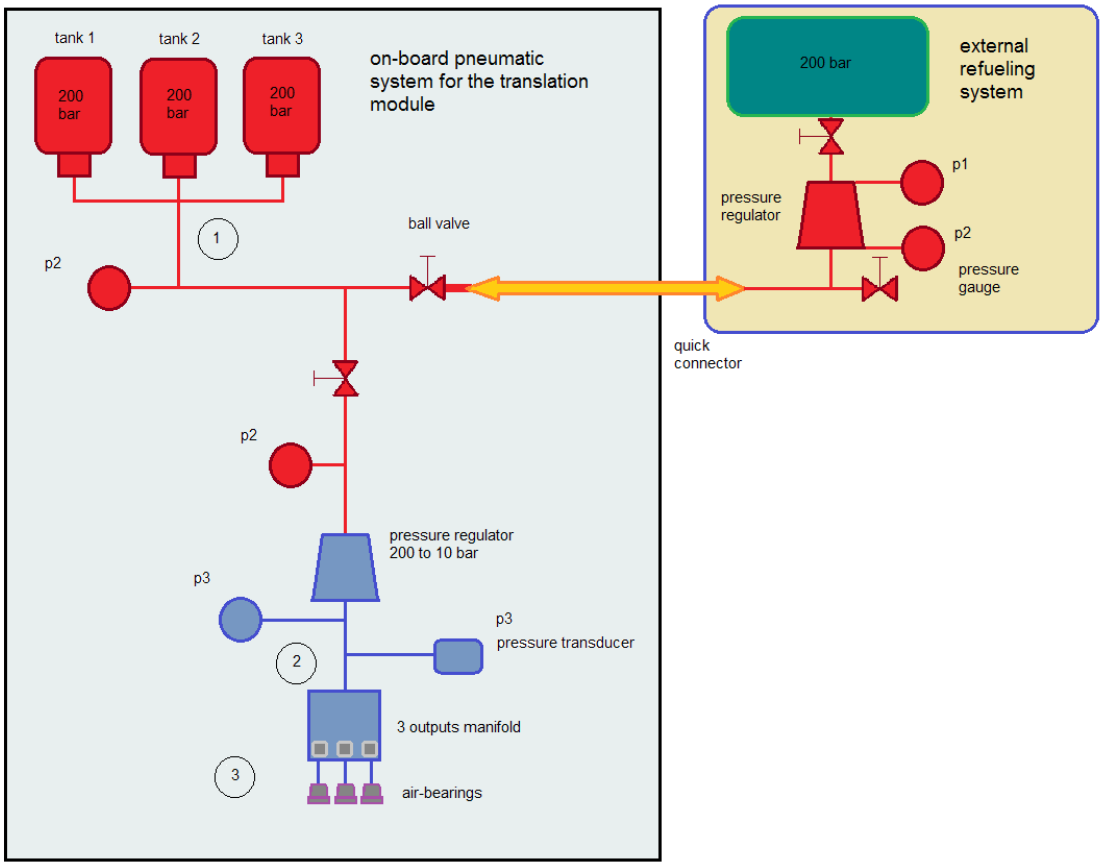

Figure 21 – Hydraulic scheme of the TM Air Suspension Subsystem

The air skids operative pressure level is defined according to the weight level which has to be beared by the air film. A characterization of the air skids has been performed as a preliminary activity before the design of the air suspension system, and is presented in Section (2.6.2.1).

2.4.1.3 Position and Azimuth Determination Subsystem

The Position and Azimuth Determination Subsystem is composed by the mouse sensors whose measurements are employed in order to provide an estimation of the Unit 2D position on the test table and of the TM Azimuth wrt to a Body centered Frame of Reference defined at the first acquisition of the measurement system, and by electronic boards in charge of elaborating the sensors measurements in order to compute and store in memory the position and Azimuth estimations.

For the 2D position and Azimuth estimation the TM carries on board three Optical Flow Sensor (OFS) mouse-like sensors which are used through their incremental counts to estimate the 2D

displacement and azimuthal rotation of the platform on which they are installed. A minimum of two sensors is required to obtain both 2D position and azimuth, which are expressed in the frame of reference corresponding to the orientation of the platform at the first step of acquisition.
OFS measurements and state estimations are provided at high frequency, and since they are referred to the initial Body Frame of Reference they need to be transmitted to the on board computer of the AM in order to be expressed in the External Frame of Reference common to all Units. Section (2.6.3) presents the procedures and activities of calibration and tests of the OFS navigation system, and related results.

Figure 22 – The OFS Sensor

2.4.1.4 Other Subsystems of the TM

The electric power on board the TM is provided by rechargeable batteries which feed the OFS sensors and the pressure transducer which monitors the pressure level at the sections in which the airflow enters in the air skids.
The Communication and Data Handling Subsystem on board the TM is composed by a single channel between the TM electronic board in which the OFS position and Azimuth estimates are saved, and the on board computer of the AM. The communication link is provided by a slip ring connection inserted in the Yaw axis support, and foresees request messages sent from the AM computer to the TM electronic board, and navigation data transmission from the TM electronic board to the AM computer.
The on board software in the TM processor is implemented in an Arduino microcontroller, which converts and saves the data from the pressure transducer for the skids air pressure monitoring, and performs the computation of the TM position and azimuth from the available OFS and saves the estimates.

2.5 Matlab Software Simulator

A Matlab Software Simulator has been developed in order to simulate and plan tests of attitude and position control maneuvers with the SPARTANS testbed. The Simulator has been originally developed with the employment of Object Oriented Programming (OOP), a choice motivated by convenient features like modularity, extensibility and re-usability.
At the moment of the writing of this thesis, the Matlab Software Simulator in its updated version allows 3DOF attitude control maneuvers for the case in which the AM is employed without the TM, planar position control maneuvers, for the case in which the whole Unit is employed with blocked AM and no Azimuth control 2D planar position and Azimuth control maneuvers with AM blocked, and 2D planar position and 3D attitude control maneuvers. Figure (23) reports the software architecture for both attitude and translational control.

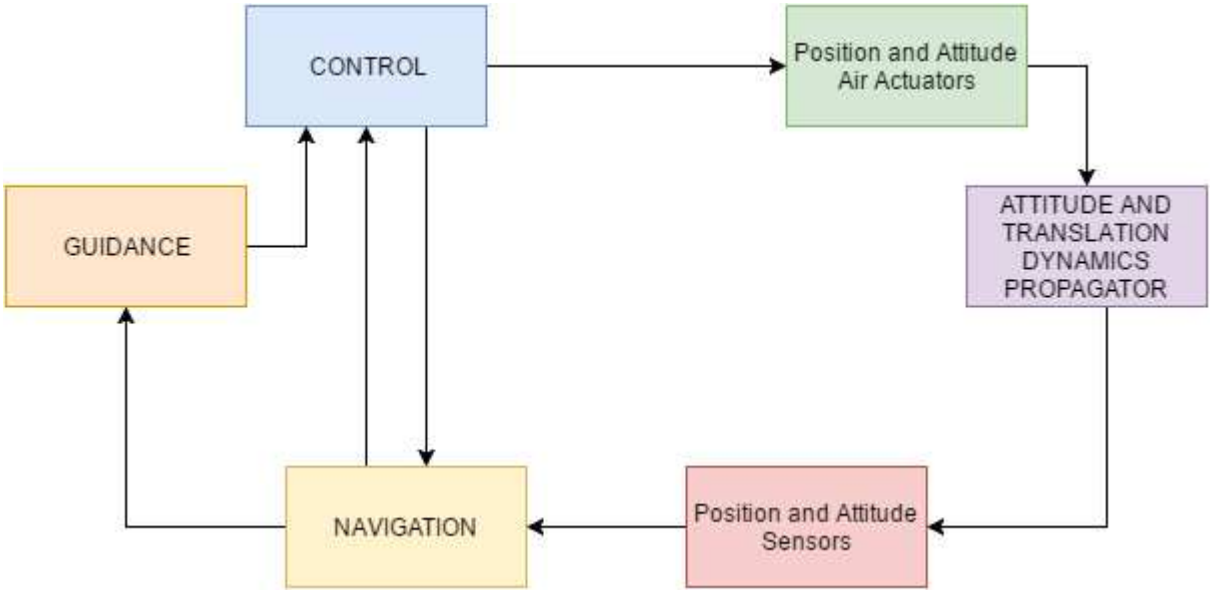

Figure 23 – Software architecture for the attitude and translation dynamics of the Matlab Software Simulator for the SPARTANS cooperating spacecraft testbed

The output of the Control section is given by the command torques and forces, which are imparted to the Air Actuators section. The Air Actuators section provides the actually executed control torques and forces which are included in the Dynamics Propagator, in order to estimate the resulting attitude and position motion. The output of the Dyamics Propagator section is therefore employed to simulate sensors measurements through the Sensors section, and the resulting quantites are employed to derive through the Navigation section the Unit state, which are used to close the loop

with the determination of the Control command actions and the state reference from the Guidance section.
The Simulator features implementation of two fundamental types of controllers, Standard and Optimal controllers. For standard control, a Proportional Derivative Integral (PID) controller for both Attitude and Position is implemented with a proportional and derivative kick avoidance scheme and anti-reset windup scheme, (see Section 4.2.3.1 for details on PID formulation). The PID controller is implemented in both continuous and discretized formulations.
With regards to optimal controllers, Model Predictive Control (MPC) and Linear Quadratic Regulator (LQR) have been implemented for both Attitude and Position control maneuvers. The MPC controller is implemented in both implicit and explicit formulation (see Sections 4.2.3.2 and 4.2.3.3 for details on LQR and MPC formulations, respectively). A series of simulated control maneuvers performed with the Software Simulator are presented in Chapter 4.
The Guidance module is able to implent pseudospectral optimal control methods for attitude and position reference trajectories. Pseudospectral methods solve optimal control problems through approximation of state and control variables as weighted sum of Legendre or Chebyshev polynomial basis, resulting in a set of algebraic equations given by the discretization of differential equations and constraints of the optimal control problem over a grid of orthogonal collocation nodes, and integration in the cost functional approximated by Gauss quadrature rules. The original optimal control problem is therefore transformed into a linear programming problem which is solved numerically through a sparse nonlinear programming solver. Pseudospectral methods are characterized by a exponential (spectral) rate of convergence, faster than any polynomial rate, and good accuracy achievable over coarse grids.

2.6 Experimental and other activites related to the development of the SPARTANS testbed

This Sections presents a series of experimental and additional activities that have been performed for the development of the SPARTANS cooperating spacecraft testbed. As already pointed out in the Thesis Outline, the main contributions of my PhD in terms of these activities consisted in the Air suspension system and test table development, and in the development and testing of the Optical Flow Sensor (OFS) navigation system. Activities related to Thrust force estimation and Inertia properties determination through the Torque Wire system of the Measurements Laboratory are briefly presented as a small contribution at the beginning of the PhD with the first prototype of the AM, and as planned to be performed for the characterization of the first prototype of the complete

Unit.

2.6.1 The Torque Wire System and related experimental activities

This section presents the preparatory experimental activities performed through the Torque Wire System of the Measurements Laboratory, that have been already carried out on the first prototype of the AM, and that have to be carried out on in the next months on the first prototype of the complete Unit. These activites consist in the characterization of the force profiles of the Unit position and attitude air actuators, and in the estimation of the Unit inertia tensor.
In order to perform these activities, a system based on a torsional or torque wire is employed, as the elastic torsional spring of a rotational measurement setup, with some different characteristcs, according to the type of activity: in the the case of thrusters force profile estimation a Torque Balance system is employed, while in the case of Inertia tensor determination a Torque Pendulum system is employed.
In order for both systems to be employed, the wire rotational stiffness has first of all to be estimated. This initial activity is performed with a Torque Pendulum system with known moment of inertia I_w about the wire axis. If the Pendulum system is made to oscillate about the equilibrium condition, and measurements of its free oscillation period T are taken, then the wire rotational stiffness can be estimated as:

$$k_w = 4\pi^2 \frac{I_w}{T^2} \tag{3}$$

Oscillation period measurements are performed by means of a photo-resistance acquisition system, consisting of a laser installed in the Torque Pendulum system, and an external photo-resistance, connected to an acquisition circuit and board, and placed in a fixed position so that when it is hit by the passing laser ray during the oscillations, its resistance decreases, which results in turn in the measured voltage peaking, thereby allowing estimation of the oscillation period. Figure (24) shows the experimental setup employed for the estimation of the wire torsional stiffness.

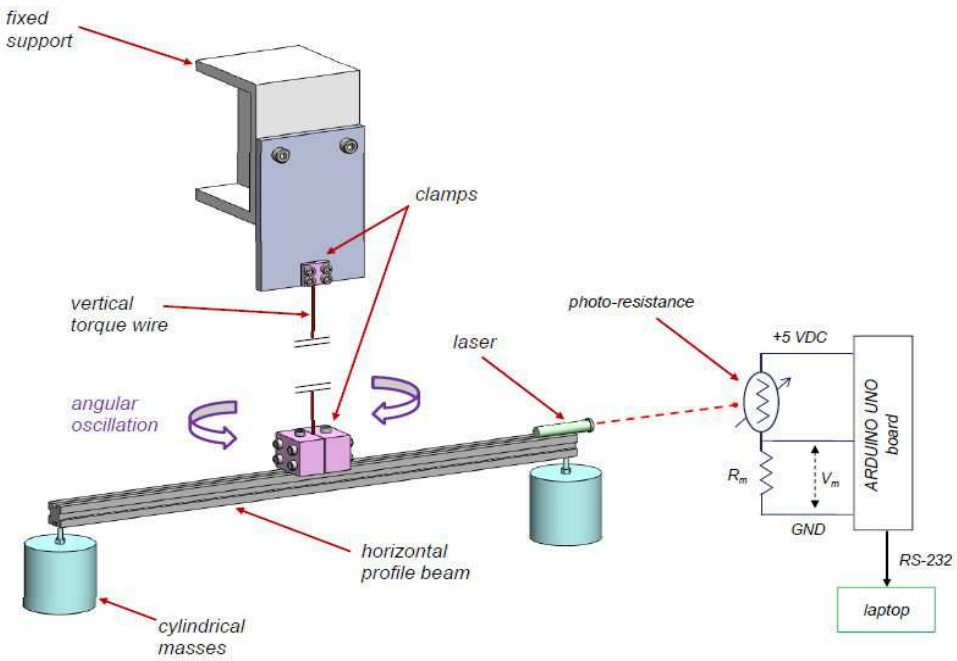

Figure 24 – Experimental setup for Torque Wire torsional stiffness estimation

During characterization of the AM, the photo-resistance system was validated with a secondary method based on a vision system. An external camera was employed in order to acquire sequential images of the experimental setup, and a marker was point on a white background behind the torque wire characterization setup, in order to have a reference for the laser ray passage. With the acquired images at known time instants, the laser ray passages could be retrieved in the images showing the marker on the wall being hit by the laser ray, and therefore the oscillation period could be estimated. This system showed good concordance with the photo-resistance acquisition system, which was then employed for the characterization of the AM.

During the activities of the characterization of the AM, the estimated rotational stiffness uncertainty has been computed through the Kline-Mc-Clintock formula, resulting in:

$$i_{k_w} = 4\pi^2 \frac{I_w}{T^2} \sqrt{\left(\frac{i_{I_w}}{I_w}\right)^2 + 4\left(\frac{i_T}{T}\right)^2} \tag{4}$$

with i_{I_w} and I_T the uncertainties associated to the estimates of I_w and T, respectively. For future actitivities with the Torque Wire Systems updated standards of uncertainty evaluation will be employed (ISO GUIDE 98/3).

2.6.1.1 Thrust Force Estimation

The estimation of the Air actuators force profiles is performed through a Torque Balance system, consisting in the vertical steel wire with known rotational stiffness supporting at its lower end a horizontal profile beam structure with a pair of thrusters attached at the same distance $b/2$ from the wire axis. Under the setup, a goniometer with 0.5° resolution is disposed with its center along the wire axis. When the thrusters are activated, they produce a torque of magnitude $\tau_{thr} = S\,b$, with S the single thruster force. At the equilibrium condition, this torque is balanced by the elastic torque of the wire, $\tau_w = k\,\theta_{eq}$, with θ_{eq} the equilibrium angle of the wire. This angle can be measured by observing the value on the goniometer which is hit by the laser ray, when the equilibrium condition is reached during thrusters activation. With known values of k_w and b , the thruster force can be estimated as:

$$S = k\,\frac{\theta_{eq}}{b} \tag{5}$$

2.6.1.2 Inertia Tensor Determination

The determination of the inertia tensor of the Unit is performed through a Torque Pendulum setup, consisting in the toqrue wire in vertical position, and at its lower end an horizontal profile beam with two lasers at the opposite ends pointing towards the ground. The horizontal beam is connected to a lower structure made of profile beams which supports the Unit and keeps it fixed in the required direction of inertia moment estimation, with the wire axis aligned to the Unit center of mass. Estimation of the oscillation period is performed with the same type of system employed for the estimation of the wire rotational stiffness, with the lasers hitting a photo-resistance connected to an acquisition system, at fixed location on the ground. When the oscillation period T has been estimated, the moment of inertia $I_{m,i}$ of the Unit about the rotation axis can be derived from:

$$I_{m,i,tot} = I_{m,i} + I_{m,i,frame} = k_w\,\frac{T^2}{4\,\pi^2} \tag{6}$$

with $I_{m,i,frame}$ the moment of inertia of the supporting frame with known value, and $I_{m,i,tot}$ the moment of inertia of the overall system, evaluated through the estimation of the oscillation period

of the Torque Pendulum.

The vector of 6 independent components $\boldsymbol{x} = \left[J_{xx}, J_{xy}, J_{xz}, J_{yy}, J_{yz}, J_{zz} \right]^T$ of the inertia tensor referenced to the Body frame, is related to the measurements vector of the inertia moment $\boldsymbol{I}_m$ through the linear equation system $\boldsymbol{A}\,\boldsymbol{x} = \boldsymbol{I}_m$, with matrix $\boldsymbol{A}$ having components dependent on the measurements directions. The 6 components of the inertia tensor can therefore be estimated as $\boldsymbol{x} = \left(\boldsymbol{A}^T \boldsymbol{A} \right)^{-1} \boldsymbol{A}^T \boldsymbol{I}_m$.

2.6.2 Development and testing of the Unit Air Suspension System and of the Simulator Test Table

This section presents the activities related to the development of the skids-based air suspension system enabling the planar translation motion of the Units of the Simulator, and the development of a levelable table supporting the Units of the Simulator and allowing a low friction and balanced translation motion through the air suspension system.

2.6.2.1 Development and testing of the Unit Air Suspension System

In order to provide 2 translational DOF to the Unit of the simulator, a suspension system based on air skids has been developed and tested. For the first prototype of the Simulator Unit, the skids available in the Measurements Laboratory have been tested and employed in the design of the TM. The modular design of the TM allows an easy replacement of the sections supporting the air suspension system in case of substitution of the skids for the first prototype of the Unit, or in case of different skids design for the other Unit/Units that will be developed and assembled.

The main activity related to the development of the air suspension system consisted in the characterization of the skids installed on a platform that allowed insertion of additional loads on it. The skids were fed through an external compressor with 50 Lt capacity, providing air at a maximum of 8 bar, and decreasing in time during the fillout of the compressor tank.

Two main aspects have been studied through the laboratory tests. The first aspect is related to the motion smoothness according to a certain pressure with which the air is provided to the skids in order to create the film that allows the suspension of the platform and consequently enables the planar motion on the test table. This aspect was evaluated empirically, varying the air pressure level

in the range allowed by the regulator of the compressor, and moving manually the platform in order to perceive directly the smoothness of the motion on a glass layer as the upper side of the test table. This allowed the selection, for each load level which was carried by the platform, of the most convenient pressure level for the skids.

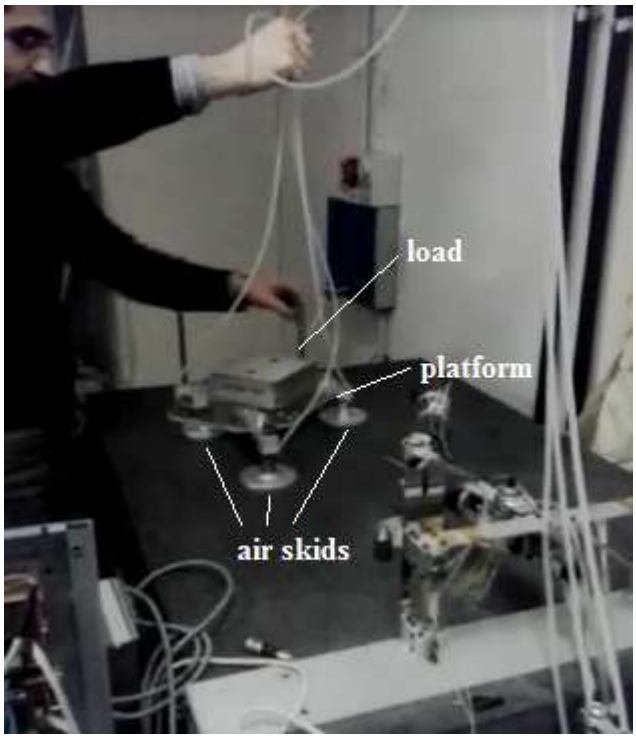

Figure 25 – Test setup for air skids characterization

The second aspect which was evaluated is related to the estimation of the autonomy levels provided by the suspension system, resulting from a certain supported load and selected pressure level at the skids. This aspect was evaluated through tests in which the platform had varying load, and for each load level, the compressor regulator was set to the pressure level which resulted as more appropriate from the previous type of tests. Then, when air was allowed to feed the skids, the time of discharge from the initial pressure in the compressor tank of 8 bar to a pressure of 6 bar was measured with a chronometer. Table (2) reports the results from the tests performed in laboratory.

TEST #1: 20.4 kg tot. - 6.8 kg per skid	
Air pressure provided by regulator	Time of transition of compressor tank pressure from 8 bar to 6 bar
3.5 bar	66 s ± 1 s
3.5 bar	65 s ± 1 s

3.5 bar	64 s ± 1 s
TEST #2: 31.4 kg tot. - 10.5 kg per skid	
Air pressure provided by regulator	Time of transition of compressor tank pressure from 8 bar to 6 bar
4 bar	58 s ± 1 s
5 bar	48 s ± 1 s
5 bar	48 s ± 1 s
TEST #3: 37.4 kg tot. - 12.5 kg per skid	
Air pressure provided by regulator	Time of transition of compressor tank pressure from 8 bar to 6 bar
4 bar	55 s ± 1 s
4 bar	57 s ± 1 s
5 bar	46 s ± 1 s
5 bar	48 s ± 1 s
TEST #4: 43.4 kg tot. - 14.5 kg per skid	
Air pressure provided by regulator	Time of transition of compressor tank pressure from 8 bar to 6 bar
4.5 bar	54 s ± 1 s
4.5 bar	54 s ± 1 s
6 bar	42 s ± 1 s
6 bar	44 s ± 1 s
TEST #5: 49.4 kg tot. - 16.5 kg per skid	
Air pressure provided by regulator	Time of transition of compressor tank pressure from 8 bar to 6 bar
4.5 bar	52 s ± 1 s
4.5 bar	52 s ± 1 s
5 bar	50 s ± 1 s
5 bar	50 s ± 1 s
6 bar	44 s ± 1 s
6 bar	45 s ± 1 s

Table 2 – Air skids characterization test results

It can be noticed from the results how in certain in cases the time of discharge of the compressor air tanks remains constant at the level of seconds with fixed load and skids air pressure, while in others it varies in the order of few seconds. It is likely that if the pressure level provided by the regulator is optimal for the motion smoothness, the air mass flow should present better steadiness wrt to the

case in which the pressure level is not optimal, since higher friction (in the case of too low pressure level) or too high film height (in the case of too high pressure level) are likely to induce irregularieties that alter the air mass flow stability at the skids outlet sections.
The data obtained from this last type of tests were therefore employed in order to estimate parametric curves to be employed in the design of the suspension system of the TM. The curves were determined assuming that the air tanks employed on board the TM have a pressure level that varies from a minimum of approximately 100 bar to a maximum of approximately 200 bar. For this two ends of the initial pressure, the curves of autonomy level and initial air mass in the tanks were determined for each pair of load per skid and air skid pressure levels. This was done by firstly estimating the air mass flow for each configuration reported in Table (2). Considering the ideal gas law, the total air mass in the tank can be estimated as:

$$M = \frac{p\,V\,m}{R_0\,T} \tag{7}$$

in which p is the pressure in the tank, V is the volume of the tank, m is the air molecolar mass with mean value $28.96\,g/mol$, $R_0 = 8.31\,J/mol/K$ is the air molar constant, and T is the temperature in Kelvin. The temperature value was estimated by using a thermometer placed at the external surface of the compressor tank during the tests. In this way, the initial and final air mass for each test were estimated, and considering for each pair of load per skid and skid pressure level the mean value of discharge time from 8 bar to 6 bar in the compressor, a reference value of air mass flow could be therfore evaluated. With the air mass flow estimated, the autonomy levels were then assessed for the cases of 100 bar and 200 bar of initial pressure in air tanks, taking 11 bar as the final pressure level in the tanks, with the total tanks volume as independent variable and the load per skid and skid air pressure as curves parameters. Figures (26), (27) report the curves obtained for the two cases. Moreover, the total initial air mass in the tanks was estimated for the two cases, in order to evaluated its contribution to the total load for a single Unit (See Figures (28), (29)).

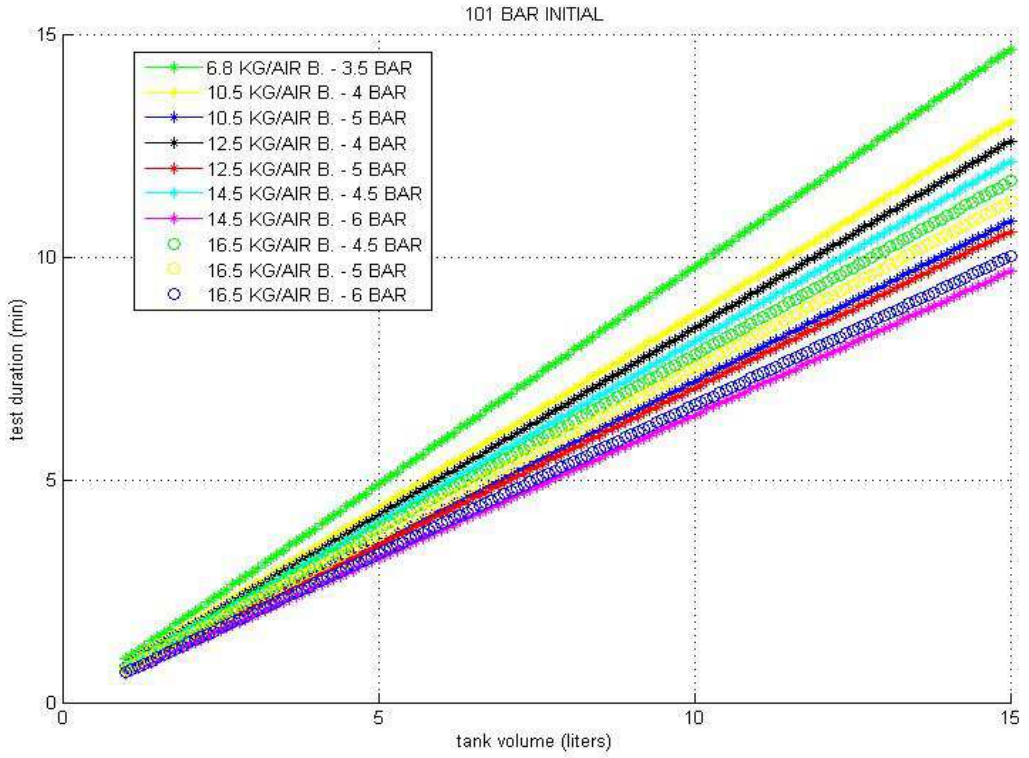

Figure 26 – Autonomy levels curves for Air skids, tanks at initial pressure 100 bar

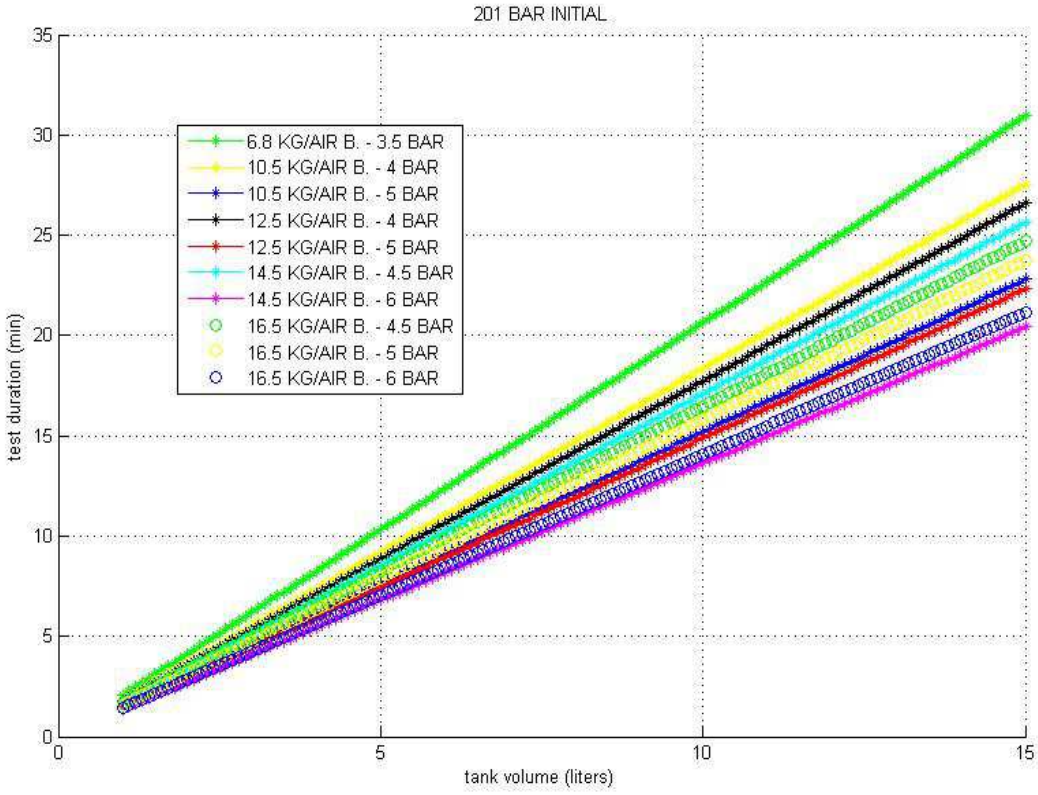

Figure 27 – Autonomy levels curves for Air skids, tanks at initial pressure 200 bar

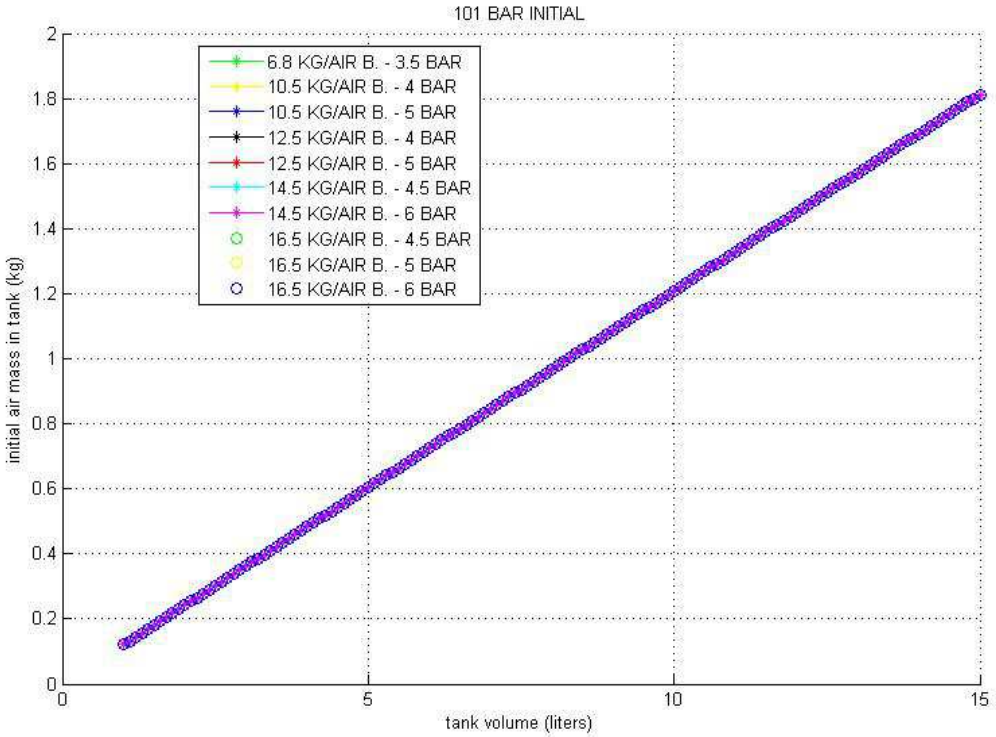

Figure 28 – Initial air mass curves for Air skids, tanks at initial pressure 100 bar

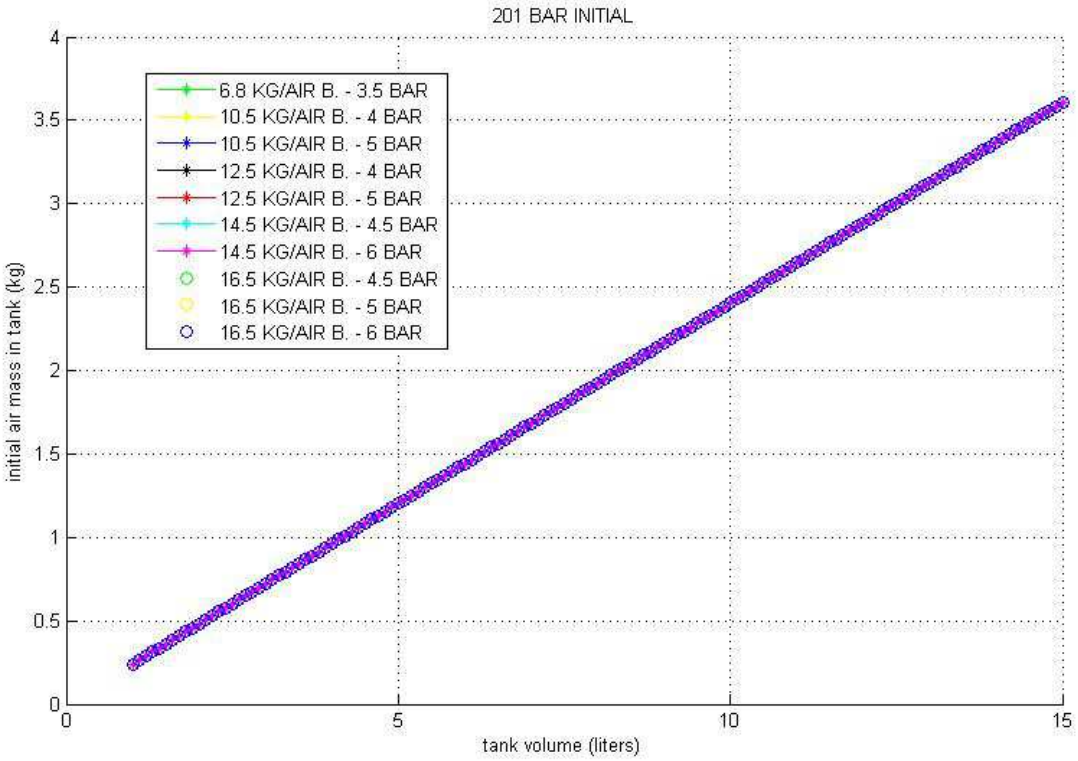

Figure 29 – Initial air mass curves for Air skids, tanks at initial pressure 200 bar

2.6.2.2 Development of the Simulator Test Table

For the Simulator Test Table which supports the Units a series of different solutions were studied and evaluated. A first solution consisted in the employment of a modular lower structure composed of aluminium profile beams disposed horizontally and vertically, with the function of supporting upper layers of aluminium, rubber and glass, in order of disposition. However this solution was eventually avoided since the connections of the profile beams of the lower structure, consisting of mobile joints fastened with screws, resulted likely to generate instabilities and to not provide a sufficient stiffness to the structure. Moreover this configuration required the additional insertion on the structure of a levelling system, which however from a preliminary analysis resulted not implementable with the available instrumentation and systems in the laboratory. A second solution consisted in the employment of granite tables, available in the market with an already built-in leveling system, of the type already present in the Measurements Laboratory, which had already been employed for the air skids characterization tests and had already proven a good leveling capability. However, this solution was avoided because of the high weight of the tables, making their manipulation in the Laboratory difficult with an additional wheel system necessary for moving them, and above all because for the Simulator a minimum test area of 2 x 3 m was considered, which implied, according to the dimensions of the available solutions, a minimum of three granite tables that had therefore to be put together and aligned at the borders, with high probability of having discontinuities in terms of inclination and height level, in the passage from one table of another.

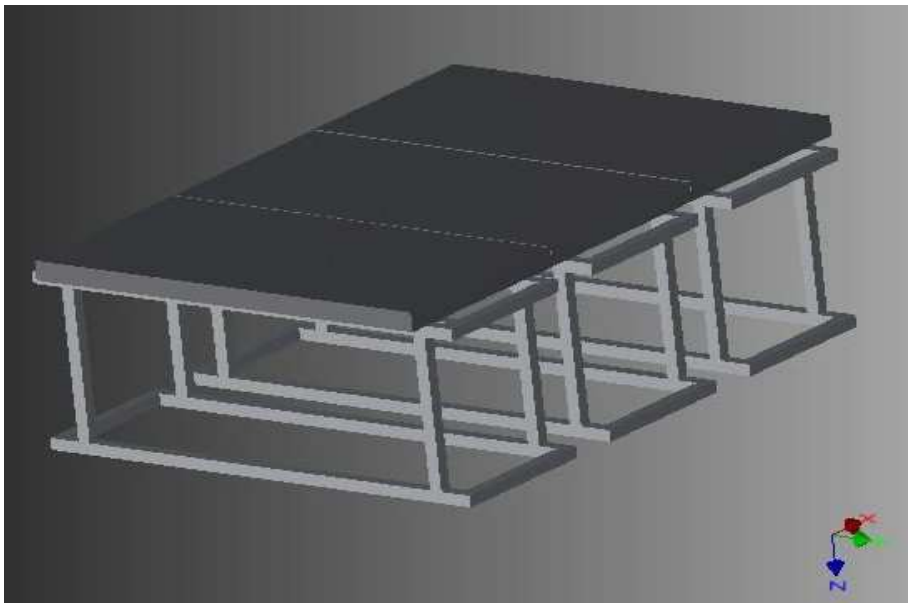

Figure 30 – 3D model of test table with three granite levelable tables aligned at borders

A last configuration, shown in Figure (31) was eventually selected and the moment of the writing of this Thesis, the related components have been ordered and are currently expected for delivery within the next weeks. The configuration is based on two separate separate set of levelable steel legs, and on upper layers of honeycomb aluminium, rubber and glass, to be disposed on the legs set, providing an upper area of 2 x 3 m, as the minimum area for two Units to be tested with sufficient maneuver margin.

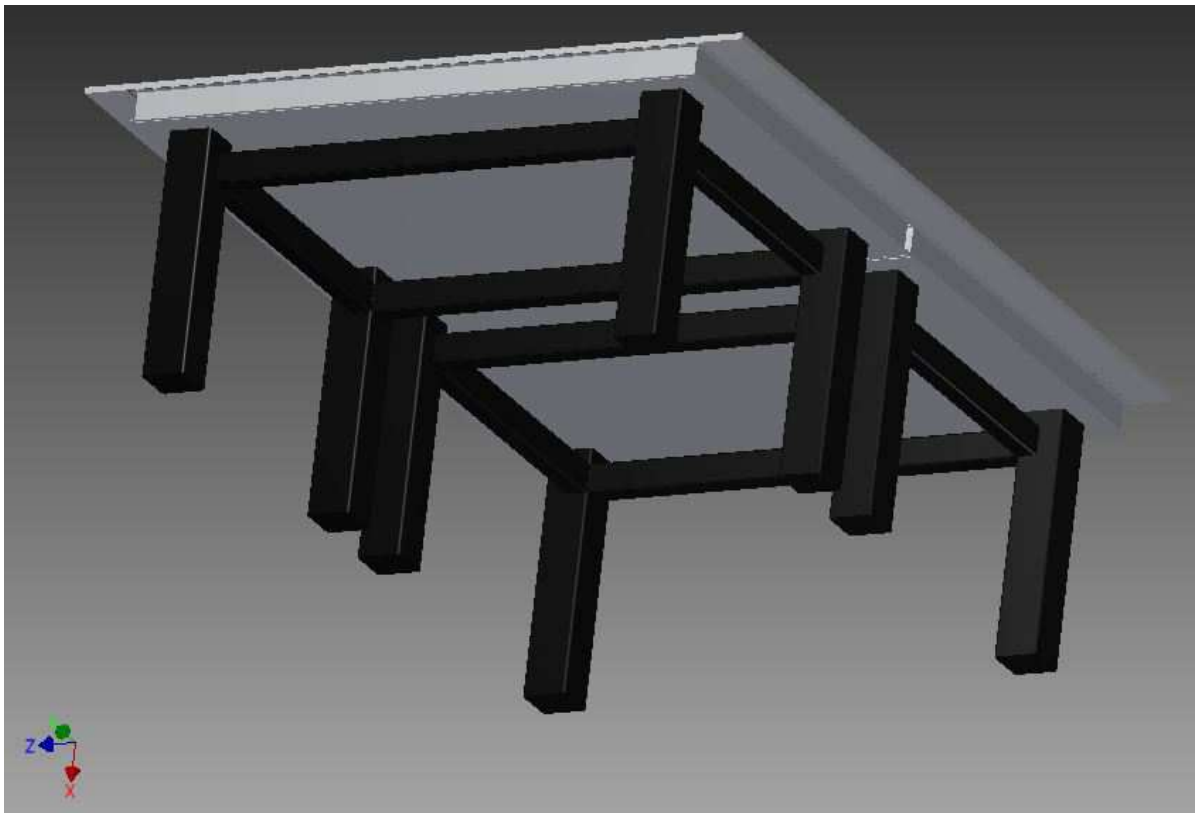

Figure 31 – 3D model of test table with separate levelable steel legs and upper layers of honeycomb aluminium, rubber and glass

For this configuration a series of Finite Element Analyses was performed in order to assess the deformations level of the upper surface due to the loads of the Units weight, and therefore the disturbance force level in the horizontal direction, which can be estimated as:

$$F_d = F_{U,w} \sin \alpha = F_{U,w} \frac{s}{b} \tag{8}$$

With $F_{U,w}$ the load due to the Unit weight , s the vertical elastic displacement between one support point and the other given by the air skids , α the angle between the horizontal plane and

the line passing through two support points, and b the distance between two support points. Two different representative configurations were considered for the simulations, a first configuration with two Units very close to each other, as it can be the case of a Docking maneuver, and a second configuration with each Unit disposed in central location wrt to the two separate levelable legs assemblies. Results of the simulations in terms of elastic displacements of the upper surface of the test table are shown in Figures (32), (33). Considering an estimated weight for each Unit of 45 kg, the first simulation set resulted in a maximum estimated disturbance force at the level 0.0007 N, while the second simulation set resulted in a maximum estimated disturbance force at the level of 0.001 N. The maximum planarity deflection level was obtained from the first configuration of approximately 1 μm over 30 cm, resulting compatible with the planarity requirements for maintainance of the air film provided by the on board suspension system.

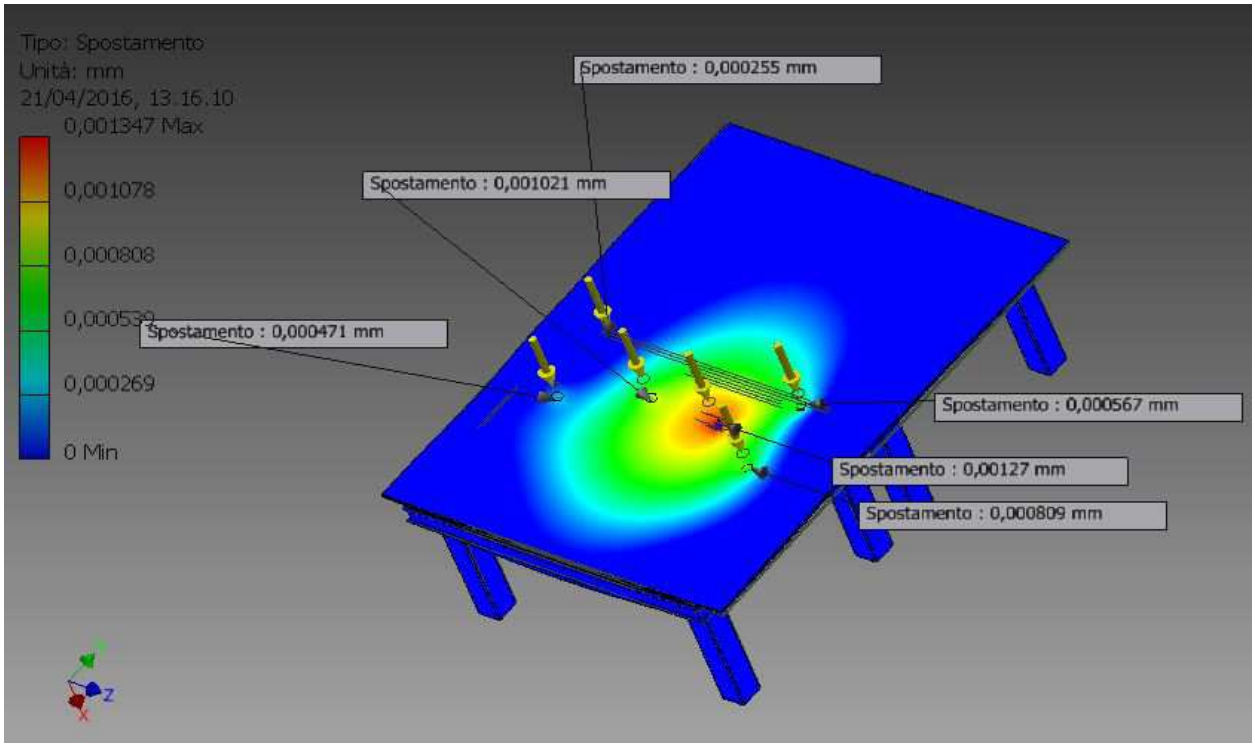

Figure 32 – FEA displacement results on the 3D model of test table with static loads due to the Units weight, configuration 1)

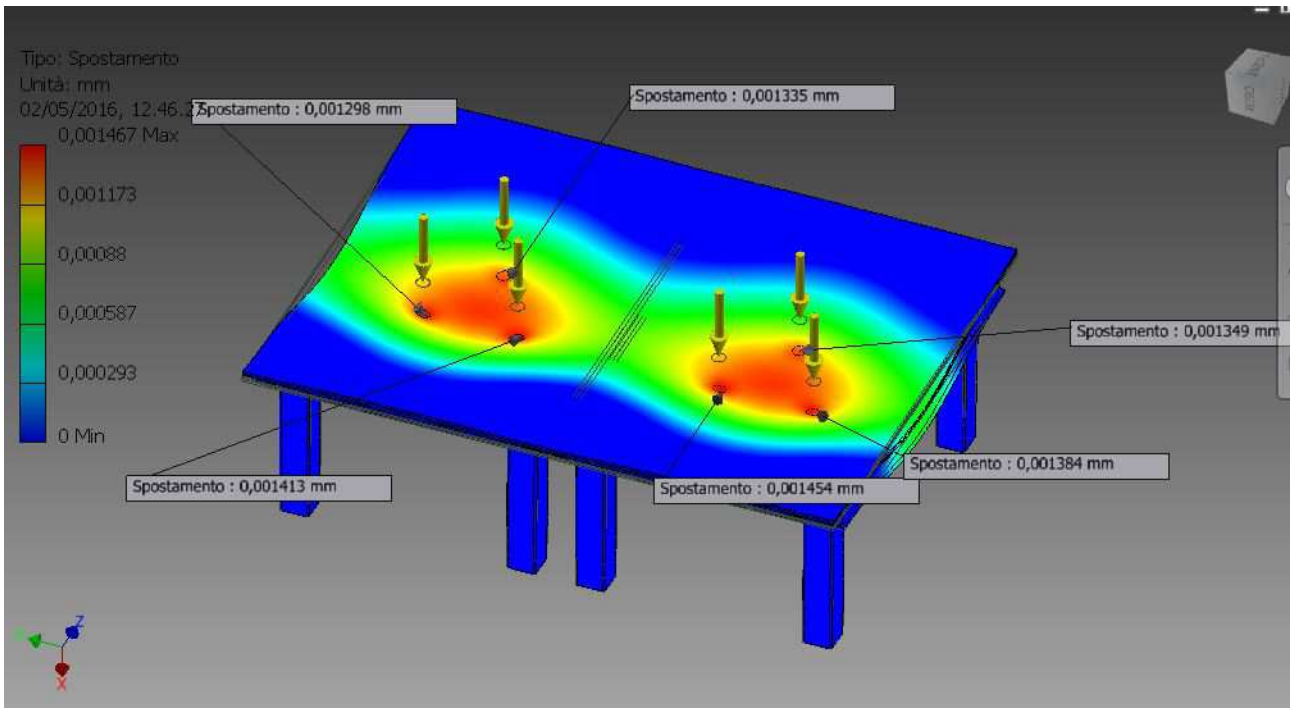

Figure 33 – FEA displacement results on the 3D model of test table with static loads due to the Units weight, configuration 2)

2.6.3 Development, calibration and testing of the Optical Flow Sensor (OFS) based navigation system

This section presents the activities and related results for the development, calibration and testing of an incremental navigation system providing position and Azimuth estimates of the platform on which it is installed, based on mouse-like Optical Flow Sensors (OFS). The sensors acquire continuosly images of the ground and output at each time step the number of counts indicating the sensors displacement wrt to its own Frame of Reference, and therefore without the integration with an external, absolute navigation system, the OFS based navigation system can provide only an incremental state estimation, referred to the Body frame of reference attached to the hosting platform and dependent on the orientation and position of the OFS sensors wrt to the Body frame. For this reason, measurements of the OFS navigation system have to be referred to an absolute frame of reference common to all Units of the testbed, through an external absolute navigation system.

For the OFS system calibration and testing an initial test setup was developed in the Measurements Laboratory, based on a prototype of the TM base, reproducing approximately the relative positions and orientation of the sensors with one to each other and wrt to the TM Body frame, and the

approximate distances of the sensors lenses from the ground.

A single OFS is able to detect the translational motion of the platform in two directions, therefore a minimum of 2 OFS have to be used to estimate the 3 DOF pose of the TM, with the pose consisting in the state formed by the 2D position on the table and the azimuthal angle, i.e. the angle about the vertical axis. With 3 OFS, redundancy is provided to the navigation system. Figure (34) shows the test setup for OFS system calibration and testing.

For the test setup, an aluminium plate, with three profile beams attached on it at 120° one to each other, has been employed to reproduce the central structure of the TM supporting the outer plates on which the OFS are mounted. In order to impart rotational, translational motions to the TM base prototype for the OFS system calibration, the TM base prototype was installed on an assembly composed of one motorized rotational stage with 0.02° declared accuracy, and a translational double stage with 2 planar orthogonal axes and declared accuracy of 5 μm, mounted on the rotational stage. The TM base prototype was installed on the motorized stages assembly so that its geometric center was aligned along the vertical axis to the center of rotation of the rotation stage, so that without having imposed any translational motion, a rotation of the motorized stage did not result in any translational motion, to the extent of the precision with which the geometric center of the TM base prototype and the center of rotation of the rotation stage were aligned.

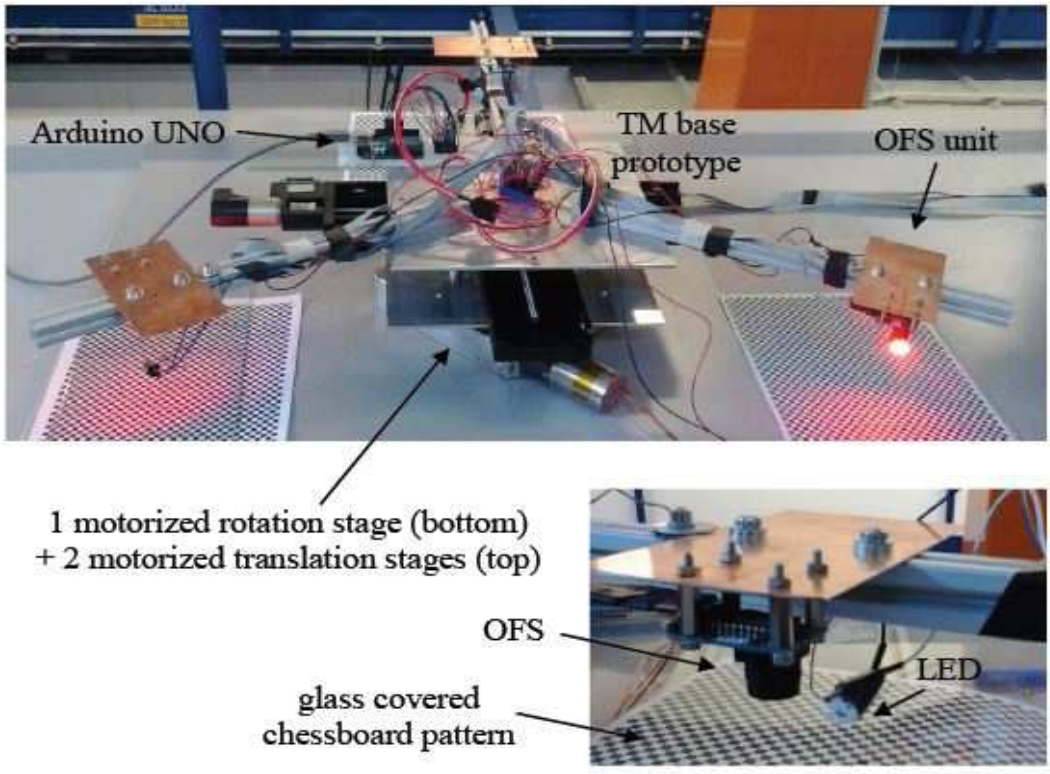

Figure 34 – Test setup for the OFS navigation system with sensors installed in the TM base prototype

The test setup of the OFS navigation system, employed for its calibration and testing, consisted in the following main elements:

- three OFS sensors each with an optical mouse chip Avago Technology ADNS3080, a PCB, a lens mount, and a lens
- a lighting system with three LEDs, one for each sensor
- an Arduino Uno micro-controller

Both in the design of the TM and in the assembly of the test setup, it was decided to place the OFS near the edge of the TM, since for a given pure rotation a higher distance of the sensor from the rotation center implies a higher number of counts and therefore for the same rotation a higher accuracy in the motion estimation.
This system presents the following series of advantages:

- it is a contactless system and therefore it does not interfere in any way with the TM translational motion provided by the suspension system
- each sensors is able to detect motion in two directions at high sample rate and with good resolution
- the available sensors in the market are small, cheap and feature a SPI interface, allowing therefore a compact and low-cost solution which can be easily interfaced with any microcontroller
- the OFS featuring a lens placed above its chip allows manual adjustment of the focus and therefore the mitigation of stringent requirements regarding the distance between the sensor and the ground to which the sensor is pointed, resulting in higher flexibility of the system

An important parameter in this navigation system is related to the quality of the surface to which the sensors are pointed in order to provide the readings. Employment of surfaces with bad quality results in missed readings from the sensors. The surface quality in terms of the OFS navigation system performance is related to two main aspects: the surface pattern and lighting conditions. In order to allow a preliminary selection of a convenient surface pattern, and appropriate lighting conditions, the OFS sensors provide an output parameter called SQUAL, i.e. Surface Quality, which is a percentual value giving an estimation of the ability of the surface to provide as correct as possible measurements. Preliminary tests showed that a chessboard pattern lighted by red light

LEDs fed at 0.4 W and placed near the sensors, presents a SQUAL above 80 % as shown in Figure (35), while typical SQUAL values for a white paper are in the range of 45-50 %.

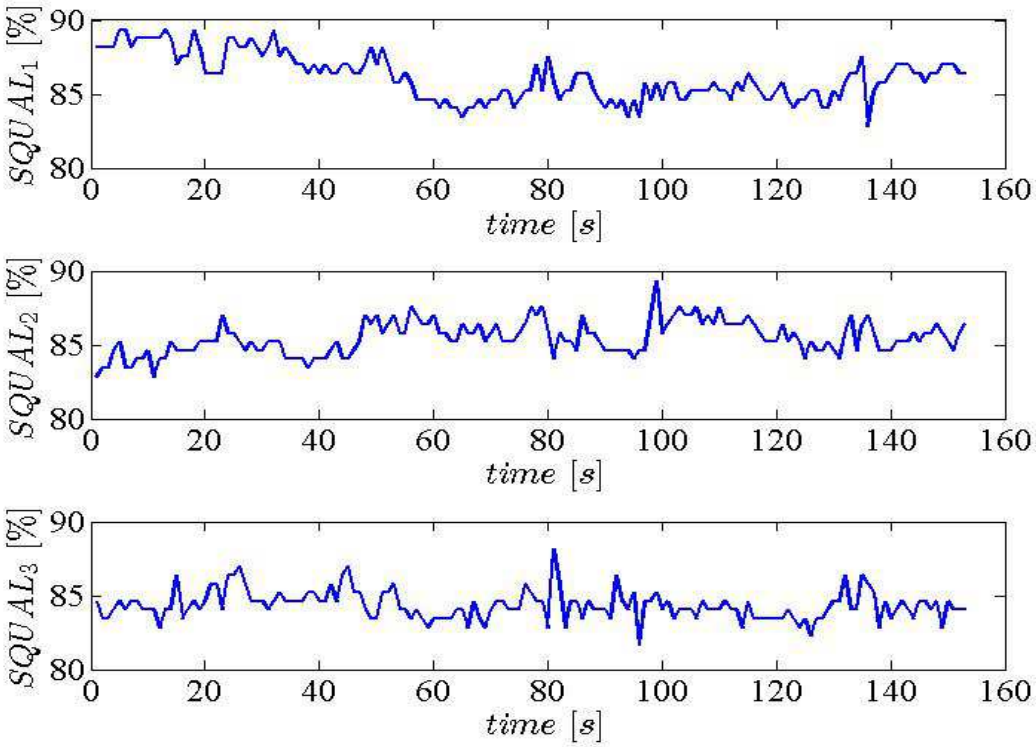

Figure 35 – SQUAL values output by OFS with chessboard pattern

For the motion estimation through the OFS navigation system three Frames of Reference are defined. The first one is the external Global Frame of Reference with axes X^G and Y^G, the second is the TM Body Frame of Reference with axes X and Y, and the third is the sensor intrinsic Frame of Reference given by the OFS measurements directions with axes x_i and y_i, with $i=1,2,3$.

Each OFS has a position, wrt the TM Body Frame of Reference, defined by polar coordinates r_i and θ_i, with r_i the distance between the origin of the sensor frame of reference and the origin of the TM frame of reference, and θ_i the angle between r_i and X, taken positive in counterclockwise direction. The orientation of each OFS wrt to the TM Body frame is given by angle τ_i between $r_{\perp,i}$ and y_i, taken positive in clockwise direction, with $r_{\perp,i}$ the direction orthogonal to r_i passing through the sensor frame of reference origin, and by angle σ_i between Y and y_i, taken positive in clockwise direction. (See Figure (36)).

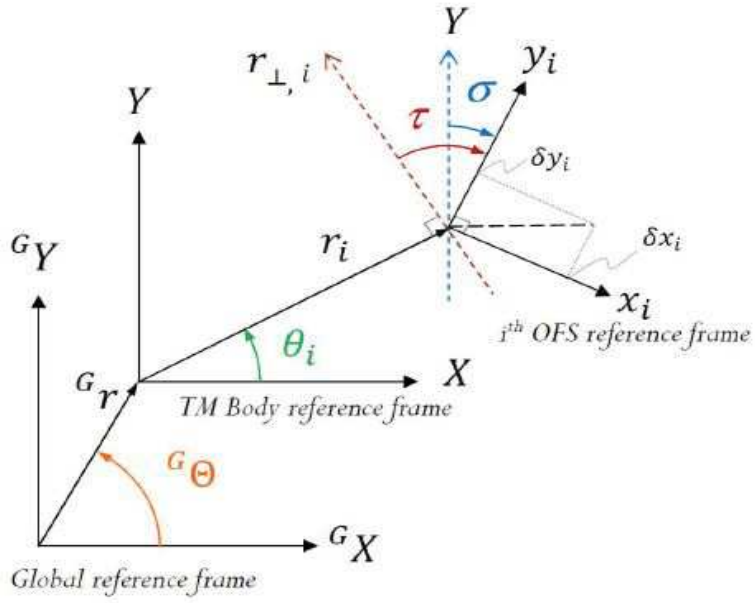

Figure 36 – Frames of Reference definition in the OFS navigation system

Each OFS provides, through an internal algorithm which employs two images of the surface on the ground at two subsequent time instants separated by time interval Δt_k , measurements δx_i and δy_i of the displacement ocurred during time interval Δt_k along its Frame of Reference. Defining $\Delta z = \left[\delta x_1, \delta y_1, \delta x_2, \delta y_2, \delta x_3, \delta y_3\right]^T$ as the incremental measurements vector in the OFS frames of reference, and $\Delta S = \left[\Delta X, \Delta Y, \Delta\Theta\right]^T$ as the TM incremental kinematic state vector in the TM Body frame of reference, at each time step the latter can be computed as:

$$\Delta S = A^+ \Delta z \tag{9}$$

With A^+ the pseudo-inverse of matrix A , which is defined as:

$$A = \begin{bmatrix} \cos\sigma_1 & -\sin\sigma_1 & -r_1\sin\tau_1 \\ \sin\sigma_1 & \cos\sigma_1 & r_1\cos\tau_1 \\ \cos\sigma_2 & -\sin\sigma_2 & -r_2\sin\tau_2 \\ \sin\sigma_2 & \cos\sigma_2 & r_2\cos\tau_2 \\ \cos\sigma_3 & -\sin\sigma_3 & -r_3\sin\tau_3 \\ \sin\sigma_3 & \cos\sigma_3 & r_3\cos\tau_3 \end{bmatrix} \tag{10}$$

The TM pose $\left[X^G, Y^G, \Theta^G\right]$ at time t_k expressed in the Global frame of reference can therefore

be computed through the TM pose at the previous time step t_{k-1} and the incremental kinematic state vector $\left[\Delta X_k, \Delta Y_k, \Delta \Theta_k\right]$ as follows:

$$X_k^G = X_{k-1}^G + \Delta X_k \cos\left(\Theta_{k-1}\right) - \Delta Y_k \sin\left(\Theta_{k-1}\right) \tag{11}$$

$$Y_k^G = Y_{k-1}^G + \Delta X_k \sin\left(\Theta_{k-1}\right) + \Delta Y_k \cos\left(\Theta_{k-1}\right) \tag{12}$$

$$\Theta_k^G = \Theta_{k-1}^G + \Delta \Theta_k \tag{13}$$

With an initial estimate of the TM pose provided, the TM position and orientation can be updated at each time step t_k through the OFS measurements and equations (11), (12), (13). For the real time TM motion estimation, these equations are implemented in the microcontroller on board the platform.

2.6.3.1 Calbration of the OFS navigation system

The estimation of the TM pose through the OFS measurements implies the need to know in advance the values for each sensor of the parameters contained in matrix A, i.e. the position parameters r_i, θ_i, the orientation parameters τ_i, σ_i and the sensitivity k_i of each OFS wrt to the TM Body frame of reference. These parameters have been estimated through the OFS system calibration performed in accordance to the procedure proposed by Bonarini et al. in [13]. In order to reduce systematic errors, a refinement calibration based on an optimization procedure with the available data was subsequently performed.

The calibration is performed through the imposition to the TM prototype of known translational and rotational motions, through the motorized stages assembly described in the previous section. The calibration consists in two main phases: a first translational phase, and a second rotational phase. The translational phase foresees the imposition on the TM of several predetermined linear displacements ΔX, ΔY, simultaneously recording the three OFS raw displacements (counts) $\delta \tilde{x}$, $\delta \tilde{y}$ that are output by the sensor during the motion. For each imposed translational displacement, the sensor sensitivity k_i, i.e. the ratio between metric and raw displacement, and the sensor orientation σ_i are estimated respectively as:

$$k_i = \frac{\sqrt{\Delta X^2 + \Delta Y^2}}{\sqrt{\delta \tilde{x}_i^2 + \delta \tilde{y}_i^2}} \tag{14}$$

$$\sigma_i = \tan^{-1}\left(\frac{\Delta X}{\Delta Y}\right) - \tan^{-1}\left(\frac{\delta \tilde{x}_i}{\delta \tilde{y}_i}\right) \tag{15}$$

For the translational calibration phase, Table (3) reports the imposed translational motions, while Figures (37), (38) report the results in terms of sensitivity k and orientation angle σ. Table (4) reports the mean values of k_i and σ_i for all OFS over the 22 performed tests, taken as best estimations of the parameters.

For the rotational calibration phase, a series of known rotations $\Delta\Theta$ about the TM z axis of the Body frame of reference are imposed with simultaneous acquisition of the sensors measurements, providing the raw readings $\delta \tilde{x}_{i,j}$, $\delta \tilde{y}_{i,j}$ for each rotation step at each j^{th} sampling instant. In this way the distance r_i and orientation τ_i can be computed as:

$$r_i = \overline{k}_i \frac{\sum_j \delta l_{i,j}}{\Delta\Theta} = \overline{k}_i \frac{\sum_j \sqrt{\delta \tilde{x}_{i,j}^2 + \delta \tilde{y}_{i,j}^2}}{\Delta\Theta} \tag{16}$$

$$\tau_i = \tan^{-1}\left(\frac{\delta \tilde{x}_i}{\delta \tilde{y}_i}\right) \tag{17}$$

Imposed rotational motions during the calibration phase are reported in Table (3), Figures (39), (40) report the results of distance and orientation, while Table (4) reports their mean values together with the estimated value for $\overline{\theta}_i = \overline{\tau}_i - \overline{\sigma}_i$.

Test number	Translational phase		Rotational phase
	$\Delta X\,[mm]$	$\Delta Y\,[mm]$	$\Delta\Theta\,[deg]$
1	0	20	2
2	0	10	2
3	-20	0	2
4	0	-10	2
5	0	10	2

6	30	0	2
7	0	-10	-20
8	0	20	-5
9	-30	0	5
10	0	-20	5
11	0	-10	5
12	10	30	5
13	0	-10	5
14	0	-10	5
15	0	-10	-25
16	0	-10	1
17	0	-15	-10
18	10	30	-
19	10	30	-
20	0	-15	-
21	0	-5	-
22	0	-5	-

Table 3 – Imposed translational and rotational motions for the OFS navigation system calibration

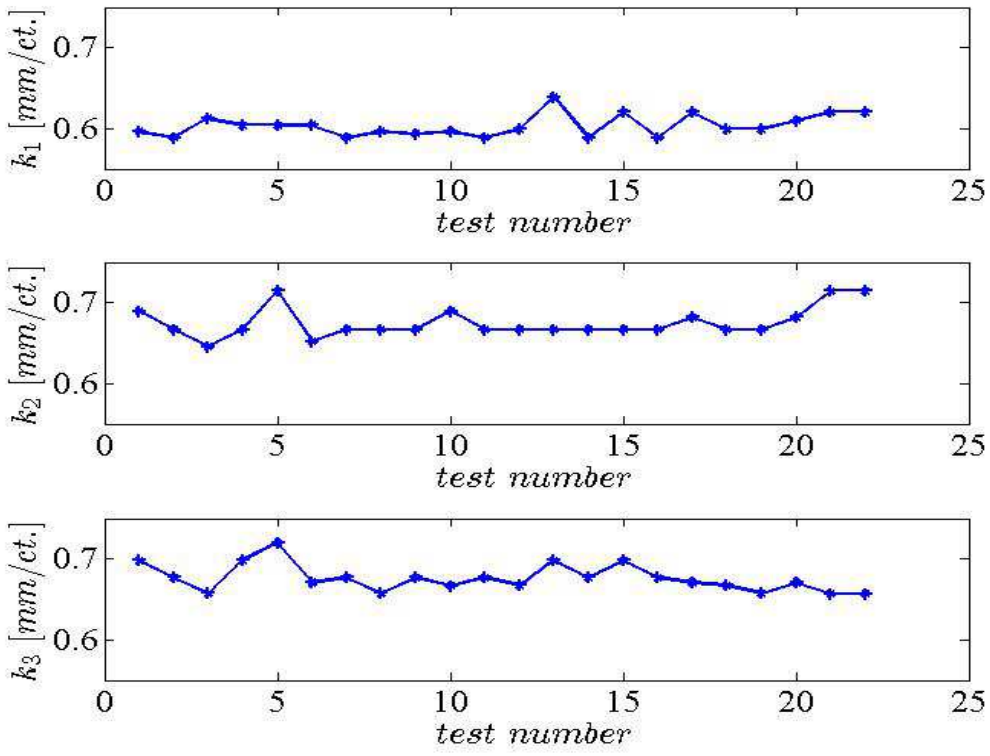

Figure 37 – Resolution values for the OFS from the translational calibration phase

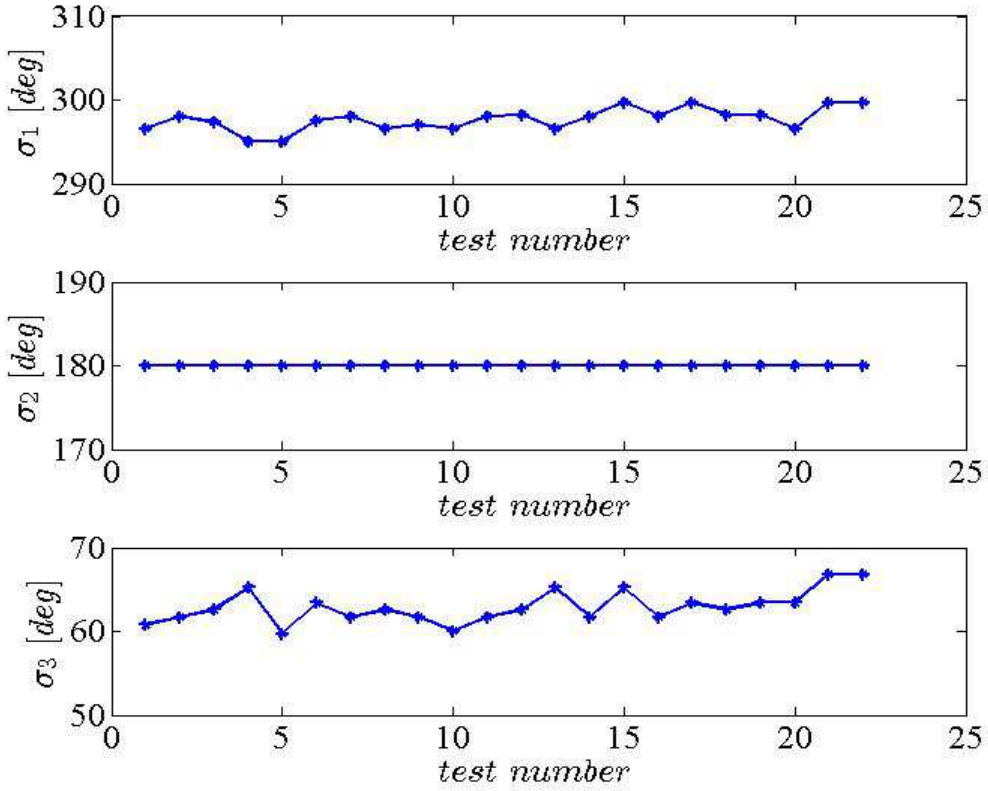

Figure 38 – Orientation values for the OFS from the translational calibration phase

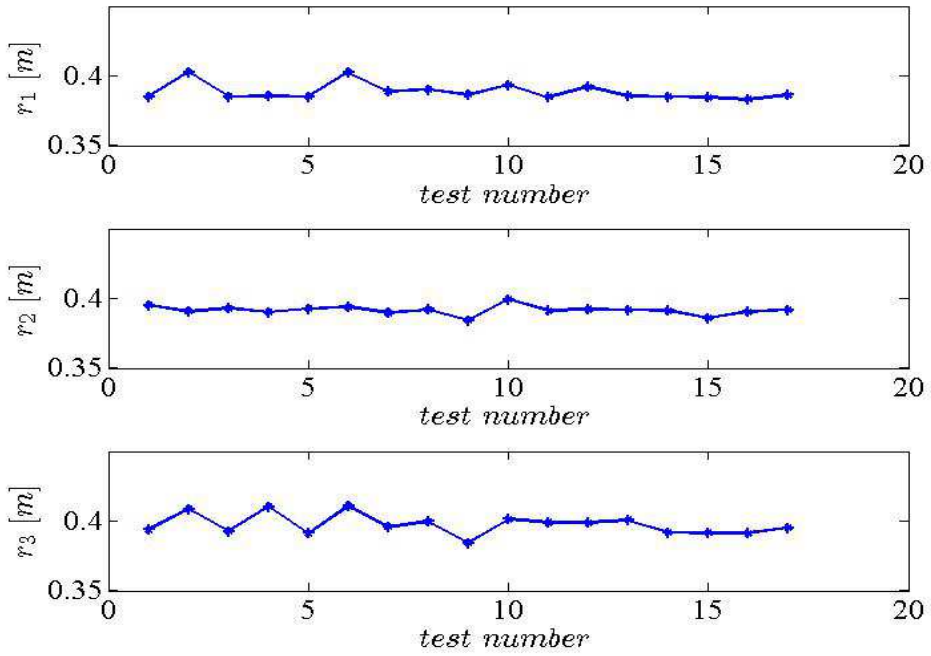

Figure 39 – Radius values for the OFS from the translational calibration phase

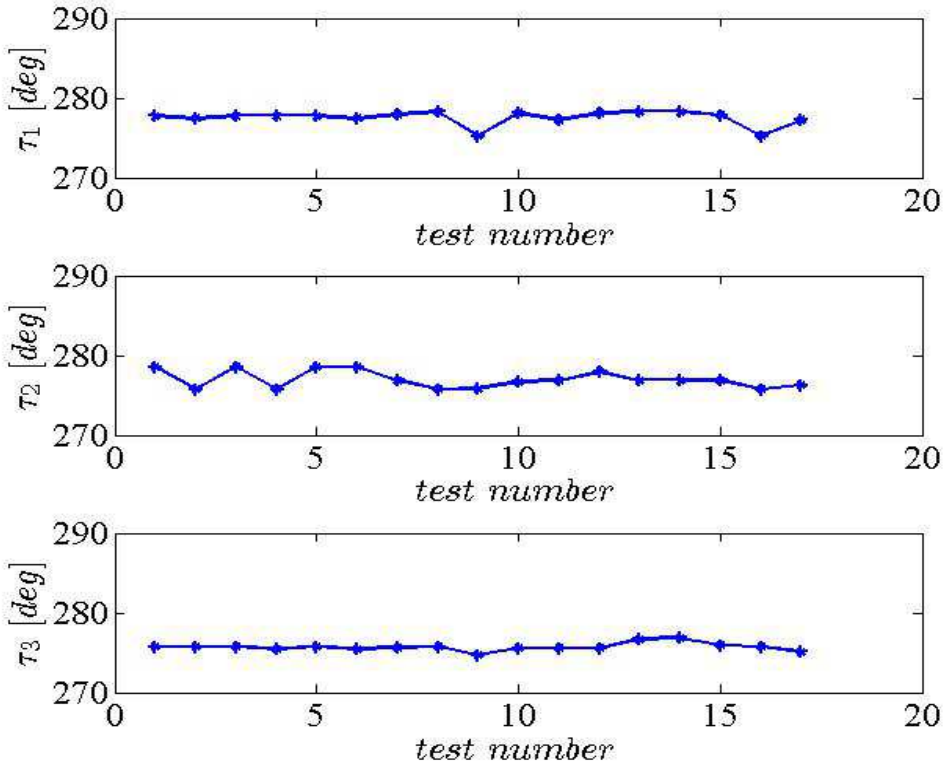

Figure 40 – Orientation values for the OFS from the translational calibration phase

i	Translational phase		Rotational phase		
	$\overline{k_i}[mm/ct.]$	$\overline{\sigma_i}[deg]$	$\overline{r_i}[mm]$	$\overline{\tau_i}[deg]$	$\overline{\theta_i}[deg]$
1	0.60 ± 0.01	298 ± 1	389 ± 6	262.5 ± 0.9	-35.2 ± 1.7
2	0.68 ± 0.02	180 ± 1	392 ± 3	263 ± 1.1	83.1 ± 1.5
3	0.68 ± 0.02	63 ± 2	397 ± 7	264.3 ± 0.5	201.4 ± 2

Table 4 – mean values of OFS system calibration parameters with uncertainties computed as RMS values

The estimates obtained from the calibration procedure have resulted consistent with the approximate values that were expected for the sensors positions and orientations wrt to the TM Body frame, resulting from the design of the TM base prototype. Maximum uncertainties have been estimated as 7 mm for the distance between the OFS frame origins and the TM Body frame origin, and as 2 deg for the angular parameters. Each OFS presents moreover close resolution values of approximately 0.7 mm per count.

This calibration phase performed through translational and rotational maneuvers with the motorized stages was followed by a refinement phase, consisting in an offline software optimization with the goal of finding sensors intrinsic parameters estimates with higher accuracy, through the minimization of the mean square error between the acquired OFS measurements from the calibration tests, and the corresponding measurements reconstructed from the known imposed motion.

Considering the imposed incremental kinematic state vector ΔS_k, the incremental raw measurement vector $\Delta \tilde{z}_k$, with index k of the imposed motion, and the vector of intrinsic parameters that must be optimized $x=\left[k_{1,}\sigma_{1,}r_{1,}\theta_{1,}k_{2,}\sigma_{2,}r_{2,}\theta_{2,}k_{3,}\sigma_{3,}r_{3,}\theta_{3}\right]$, the reconstructed measurements vector $\Delta\tilde{\xi}_k$ can be computed from the predetermined imposed motion as:

$$\Delta\tilde{\xi}_k=\tilde{A}(x)\Delta S_k \tag{18}$$

with matrix $\tilde{A}$ computed as:

$$\tilde{A}=\begin{bmatrix} \cos\sigma_1/k_1 & -\sin\sigma_1/k_1 & -r_1\sin\tau_1/k_1 \\ \sin\sigma_1/k_1 & \cos\sigma_1/k_1 & r_1\cos\tau_1/k_1 \\ \cos\sigma_2/k_2 & -\sin\sigma_2/k_2 & -r_2\sin\tau_2/k_2 \\ \sin\sigma_2/k_2 & \cos\sigma_2/k_2 & r_2\cos\tau_2/k_2 \\ \cos\sigma_3/k_3 & -\sin\sigma_3/k_3 & -r_3\sin\tau_3/k_3 \\ \sin\sigma_3/k_3 & \cos\sigma_3/k_3 & r_3\cos\tau_3/k_3 \end{bmatrix} \tag{19}$$

The objective function that must be minimized is given by:

$$f(x)=\sum_k \| \Delta\tilde{\xi}_k(x)-\delta\tilde{z}_k\|_2^2=\sum_k \| \tilde{A}(x)\Delta S_k-\delta\tilde{z}_k\|_2^2 \tag{20}$$

This minimization problem presents a nonlinear multivariable function. It was solved in Matlab through the function fmincon and through an interior point algorithm, for which the intrinsic parameters vector obtained from the calibration procedure was used as initial values. Table (5) reports the results of the offline optimization.

OFS #	parameter	Estimate before refinement	Estimate after refinement	Difference
1	$k_1[mm/ct.]$	0.604	0.599	0.005
	$\sigma_1[deg]$	297.68	297.9	0.22
	$r_1[mm]$	388.6	383.6	5
	$\theta_1[deg]$	-35.15	-35.64	0.49
2	$k_2[mm/ct.]$	0.675	0.666	0.009
	$\sigma_2[deg]$	180	179.99	0.01
	$r_2[mm]$	391.5	383.1	8
	$\theta_2[deg]$	83.06	83.23	0.17
3	$k_3[mm/ct.]$	0.6762	0.666	0.01
	$\sigma_3[deg]$	62.91	62.74	0.17
	$r_3[mm]$	397.5	386.5	11
	$\theta_3[deg]$	201.39	201.77	0.38

Table 5 – OFS system calibration parameters optimization results

Results of the optimization show that the higher variations occur for the values of r_i and θ_i . Through the offline optimization the initial value of the objective function, i.e. The mean square error between reconstructed and acquired measurements, is reduced by 8.6 %.

2.6.3.2 OFS navigation system tests of motion reconstruction maneuvers

With sensors intrinsic parameters estimates available, a series of motion reconstruction tests were performed with the OFS navigation system in order to assess its level of accuracy.
Three types of maneuvers were performed as motion reconstruction tests: translational only, rotational only, and combined maneuvers (i.e. sequential translations and rotations). Translational maneuvers were performed through the TM base prototype with the OFS navigation system, mounted on the motorized stages assembly, and only the double translational motorized stage turned on in sequential translation steps. Rotational maneuvers were performed with only the rotation stage turned on for continuous rotations, or divided in steps. Combined maneuvers were performed through subsequent translational and rotational displacements. Generally, these type of maneuvers were performed by firstly imposing the translational motion, secondly through the imposition of the rotation, so that the resulting motion was curvilinear, since the geometric centre of the TM base was not anymore aligned to the rotation center of the motorized stage, along the vertical axis. Table (6) reports a sequence of translational, rotational and combined maneuvers tests and relative results, while graphic results of some of the listed tests are reported in Figures (41), (42), (43).

TEST. N.	Type	Maneuver	Final difference between imposed motion and OFS system estimates – non optimized calibration parameters	Final difference between imposed and estimated motion – optimized calibration parameters
1	rotational	+ 20° counterclockwise	$\Delta\Theta = 0.1\,^\circ$	$\Delta\Theta = -\,0.08\,^\circ$
2	rotational	+ 30° counterclockwise	$\Delta\Theta = 0.15\,^\circ$	$\Delta\Theta = 0.13\,^\circ$
3	rotational	- 20° clockwise	$\Delta\Theta = 0.17\,^\circ$	$\Delta\Theta = 0.17\,^\circ$
4	rotational	- 30°	$\Delta\Theta = 0.2\,^\circ$	$\Delta\Theta = 0.08\,^\circ$

		clockwise		
5	translational	+ 3 cm Y + 2 cm X	$\Delta X = 0.3\,mm$ $\Delta Y = 0.5\,mm$	$\Delta X = 0.06\,mm$ $\Delta Y = 0.1\,mm$
6	translational	- 3 cm Y - 2 cm X	$\Delta X = 0.3\,mm$ $\Delta Y = 0.9\,mm$	$\Delta X = 0.08\,mm$ $\Delta Y = 0.5\,mm$
7	combined	+ 3 cm Y + 2 cm X + 10° counterclockwise	$\Delta X = 0.7\,mm$ $\Delta Y = 2\,mm$ $\Delta\Theta = 0.05\,°$	$\Delta X = 0.3\,mm$ $\Delta Y = 1.6\,mm$ $\Delta\Theta = 0.05\,°$
8	combined	- 3 cm Y - 2 cm X - 10° clockwise	$\Delta X = 3\,mm$ $\Delta Y = 1\,mm$ $\Delta\Theta = 0.2\,°$	$\Delta X = 2.5\,mm$ $\Delta Y = 0.7\,mm$ $\Delta\Theta = 0.1\,°$

Table 6 – OFS system motion reconstruction tests results

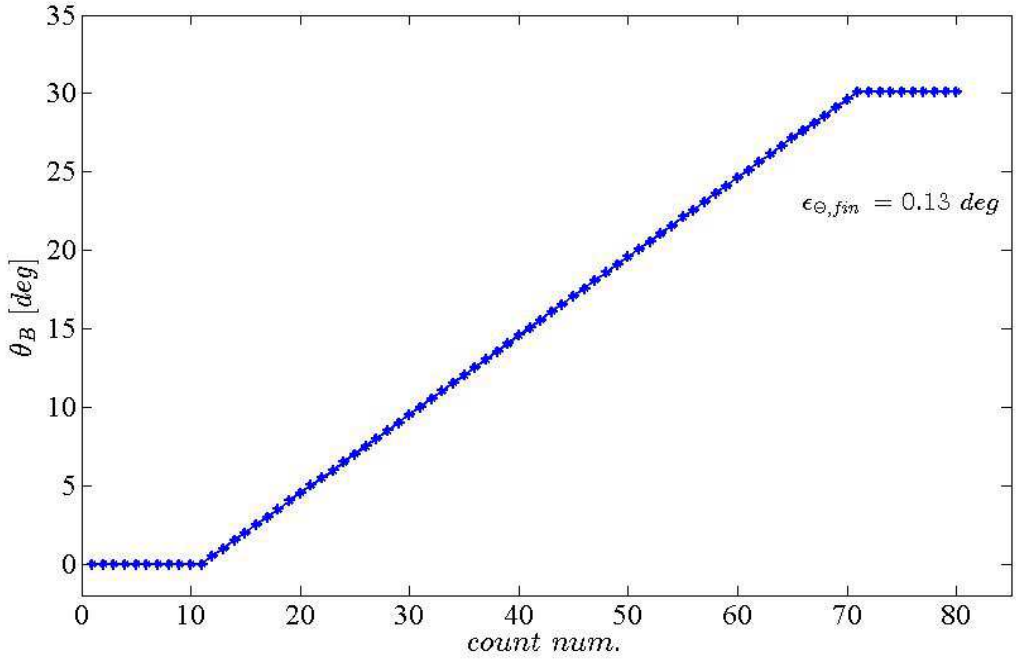

Figure 41 – OFS system rotational motion reconstruction tests results with optimized calibration parameters, Test 2) (see Table (6))

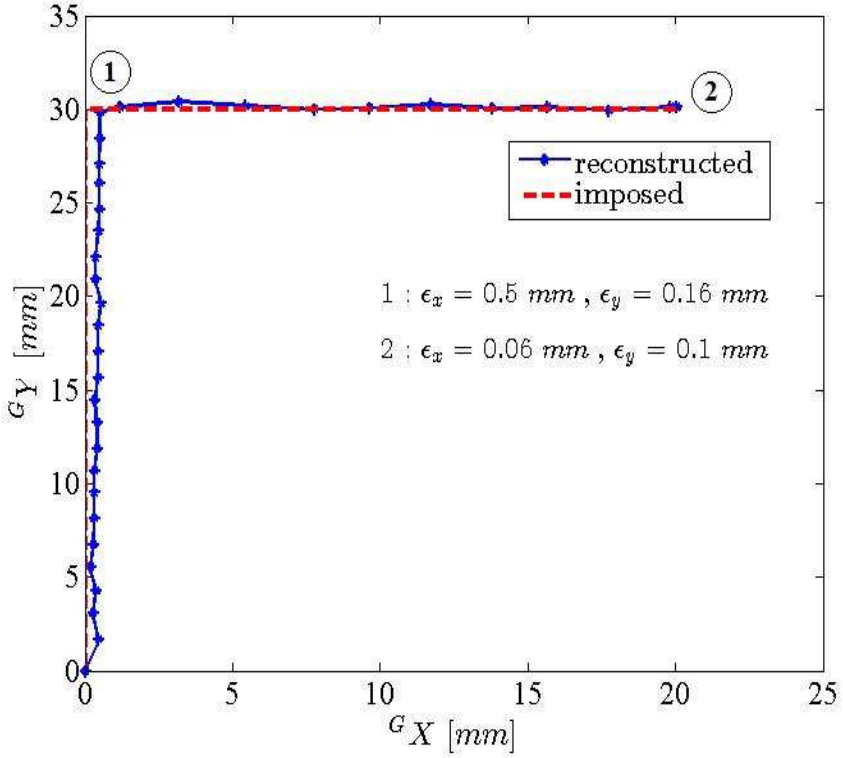

Figure 42 – OFS system translational motion reconstruction tests results with optimized calibration parameters, Test 5) (see Table (6))

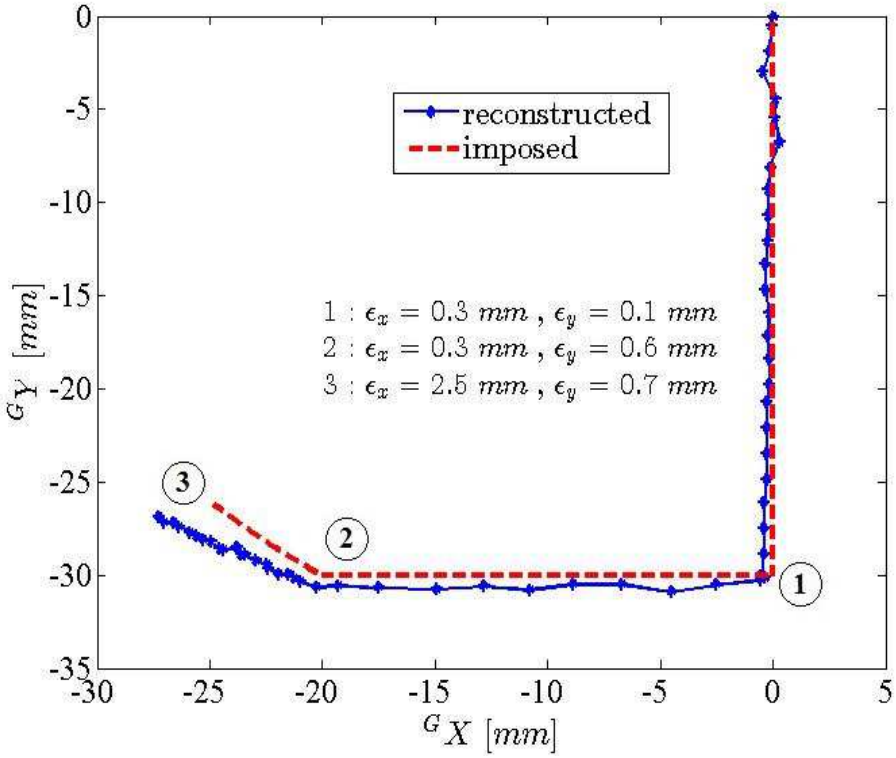

Figure 43 – OFS system combined motion reconstruction tests results with optimized calibration parameters, Test 8) (see Table (6))

As it can be seen from the results, in all types maneuvers the employment of optimized calibration for OFS motion estimation results in a slightly higher accuracy.

A relevant observation regards combined maneuvers. It can be seen from the results that at the end of the rotational phase, which, given the previous translations, consists in a curvilinear trajectory imposed to the TM base prototype, the final differences between the estimated and predetermined motions in terms of 2D position are higher wrt to purely translational maneuvers. From Figure (43) it can moreover be noticed how in the final phase of the combined maneuver the reconstructed motion has a drift trend wrt to the imposed motion.

Further tests were performed for combined maneuvers motion reconstruction, with a first translational phase followed by a rotation, and then the same maneuvers repeated in opposite directions in order to return to the origin. Results reported in Figures (44), (45) are related to a combined maneuver consisting in a translation of 5 cm in the negative Y direction, and a counterclockwise rotation of 20 °, followed by 20° clockwise rotation and 5 cm translation in the positive Y direction in order to bring the TM base protoype back to the original position and orientation.

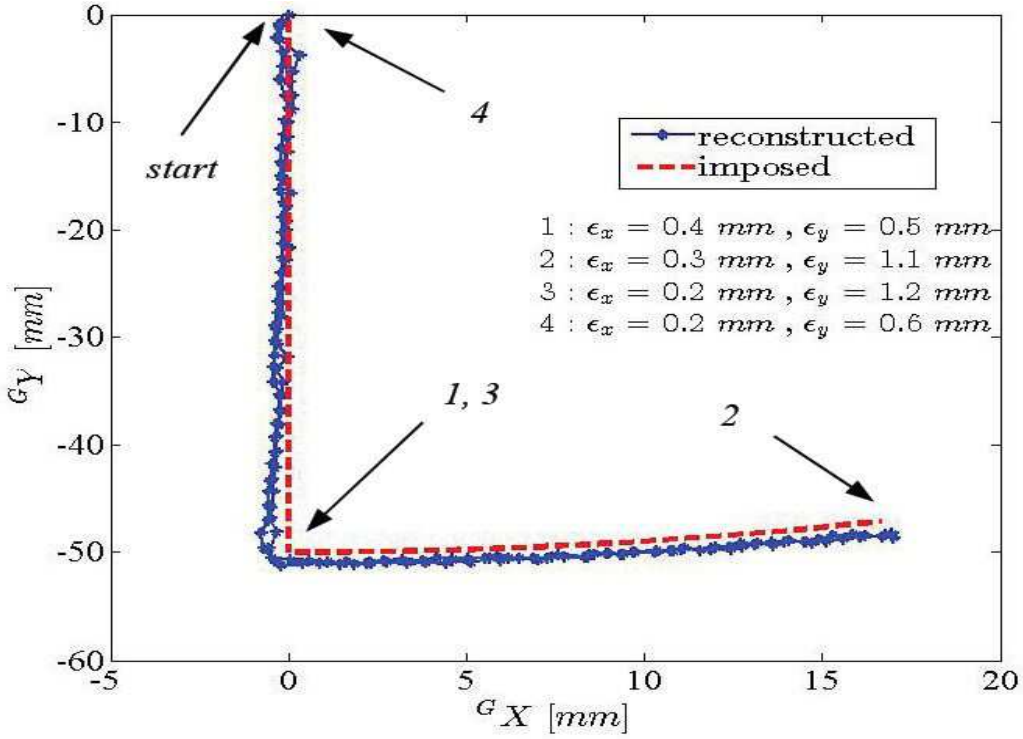

Figure 44 – OFS system combined motion reconstruction test results, translation

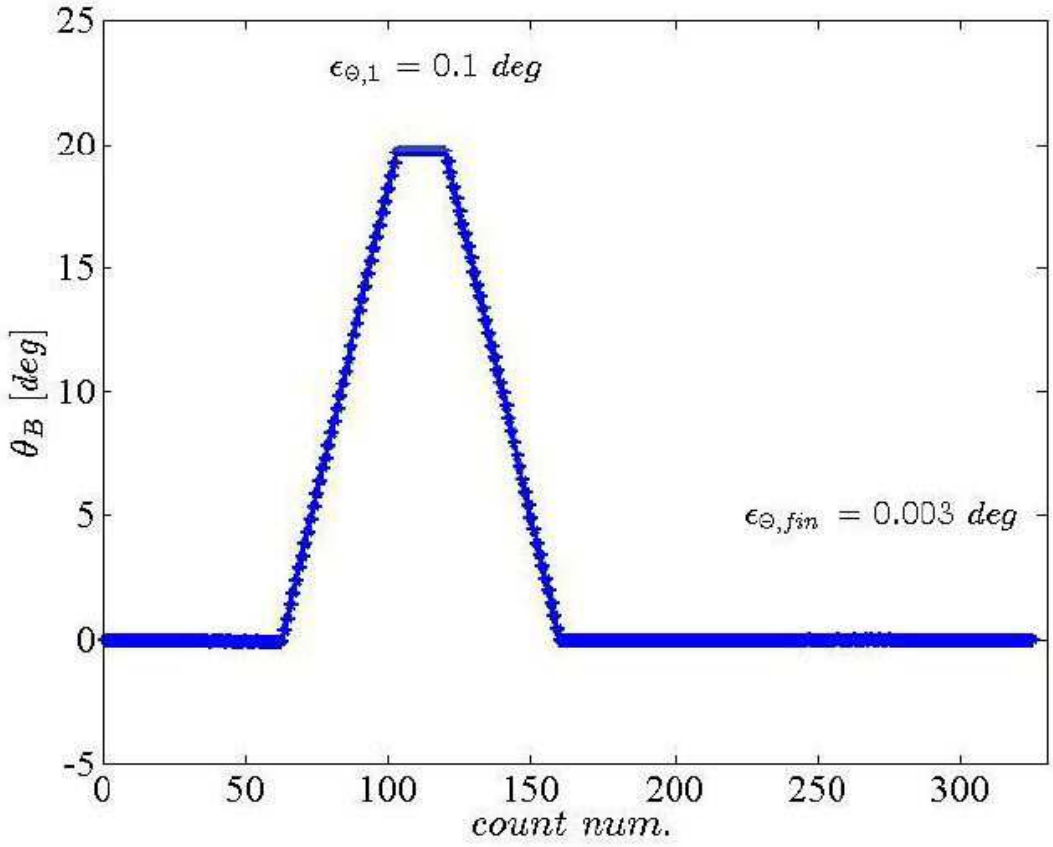

Figure 45 – OFS system combined motion reconstruction test results, rotation

As it can be seen from the results, in this case at the end of the combined maneuver phase (point #2 in Figure (44)) the difference in position between the imposed motion and the OFS system estimate results slightly higher wrt the purely translational phase, but the drift trend of the previous tests results does not appear in the planar position plot reporting both imposed and reconstructed trajectories. As for the previous tests, the rotation at the end of the combined phase presents instead a difference between imposed and reconstructed motions that is at a similar level of the translational phase. It can also be noticed that when the last two motions, opposed to the first two, are imposed in order to bring the TM base prototype to the initial position, the difference in position decreases to levels similar to the initial ones.

To further study combined maneuvers, a slight modification was introduced in the original test setup by replacing the chessboard pattern sheets in A4 format, placed with their central areas as much as possible underneath each OFS (See Figure (34)), with a chessboard patter sheet in A0 format with a central square hole for the TM base prototype and motorized stages assembly, in order to allow virtually unlimited rotations, while with the original setup rotations could not be performed beyond approximately 30°. Figure (46) shows the modified test setup. Also in this case however rotations were eventually limited, to the range of approximately 90°, since the power cables of the

motorized stages created a constraint to the rotations because of their limited length.

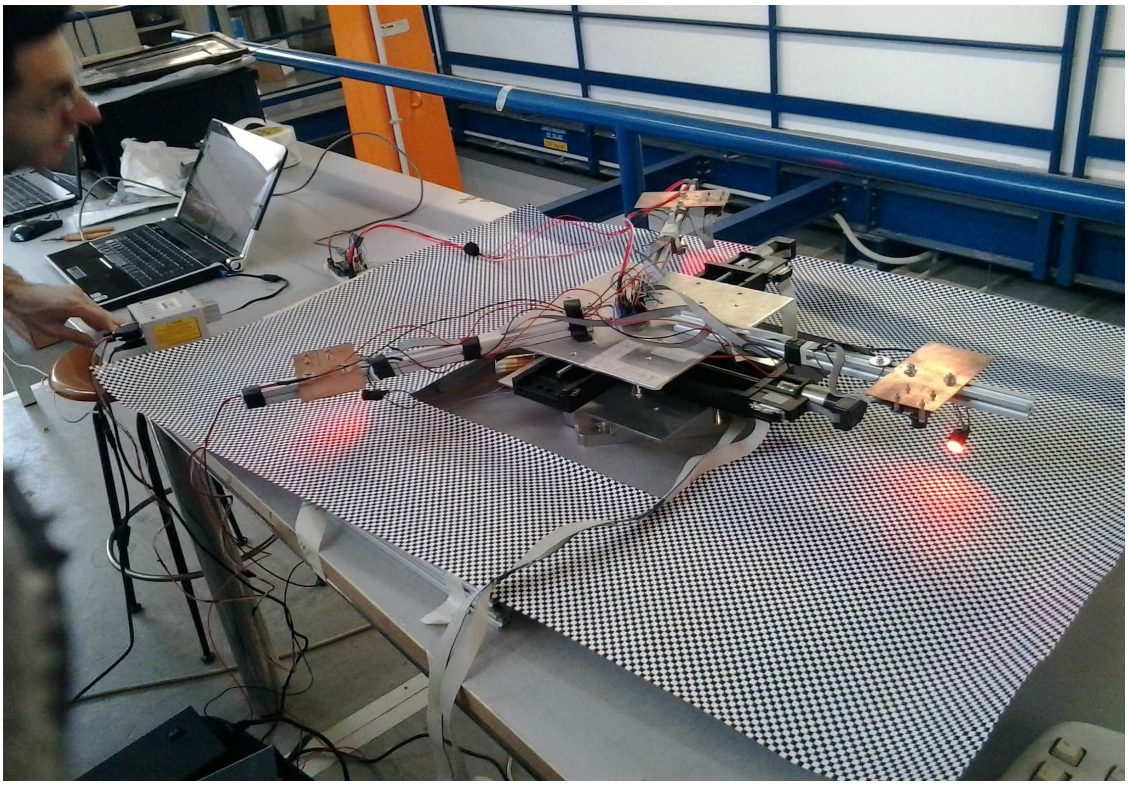

Figure 46 – Test setup for the OFS navigation system with chessboard pattern A0 sheet

With this setup, after some preliminary tests in order to check the system performances with the chessboard patter A0 sheet, a series of repeated maneuver tests were performed, consisting in a translation of 5 cm in the negative Y direction, followed by a clockwise rotation of 90° about the vertical axis. Results are reported in Figure (47).

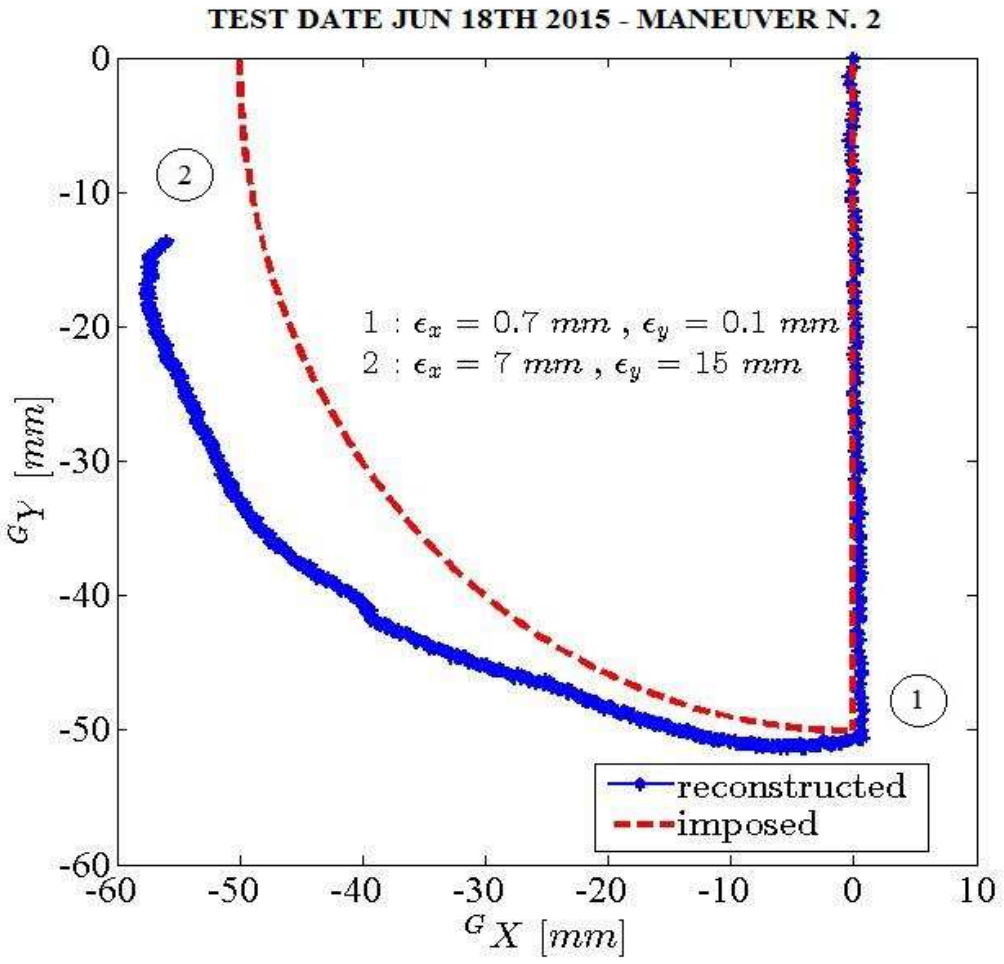

Figure 47 – OFS system motion reconstruction test results, rotation for combined maneuver with extended rotational range

As it can be seen from the results, drift in the position trajectory in this case is evident, with the difference between imposed and reconstructed motions growing from the submillimiter level at the end of the translation phase to the 1-2 cm level, at the end of the combined phase. As it is showed in the next Chapter, also rotation presents a drift trend in the case of curvilinear maneuvers with extended range. In this case, no evident drift behaviour appears in Azimuth rotation.
The drift effect in the OFS system is likely due to the accumulation of missed readings along the OFS axis with lower displacement, and must be compensated through the external navigation system, consisting in a optical camera based vision system with measurements performed at lower frequency wrt to the OFS system.

3 INTEGRATION OF THE OFS NAVIGATION SYSTEM WITH THE VISION SYSTEM

This chapter presents the preliminary activities performed for the integration of the Optical Flow Sensor (OFS) incremental navigation system with the vision based absolute navigation system for the pose (planar position and Azimuth) estimation of a 3DOF Unit.

3.1 Integration of the OFS and Vision based Navigation Systems

For the pose estimation of the TM base, the OFS navigation system has been integrated with a vision based navigation system in order to refer the OFS estimations to an external absolute Frame of Reference common to all Units, and correct them periodically when their accuracy decreases as in the cases of curvilinear trajectories, as seen from the results shown in Section 2.6.3.2 in the previous Chapter. At the moment of the writing of this thesis, the vision system has been employed for the estimation of the pose of the TM only, but in the next few months with the first complete Unit assembled, it will be employed also for the estimation of the 3 DOF attitude of the AM, together with the 2 DOF position of the TM. The final navigation system consists in the vision based navigation system adopted for low frequency position and attitude estimation in an external Absolute navigation system, and on board OFS system for high frequency incremental localization. Morevoer, the vision based navigation system is employed for OFS drift compensation.
The integration of the two navigation systems has been performed with the OFS sensors installed in the nominal configuration in the TM base, with the TM base preliminary assembled in its main central structure, as shown in Figure (48), with the OFS sensors at the right distance from the ground, with styrofoam blocks in order to put the pattern sheets at the right distance. The calibration procedure presented in section 2.6.3.1 has been repeated in this nominal configuration and related results are reported in Table (7).

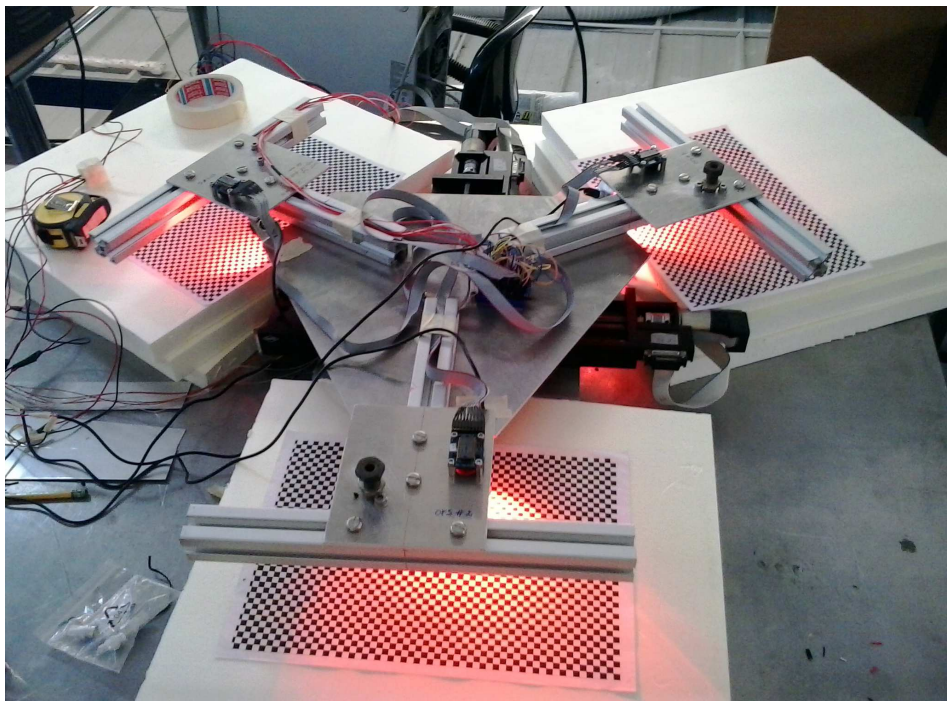

Figure 48 – TM base with OFS system in nominal configuration

	k [m/count]	σ [deg]	r [m]	τ [deg]	θ [deg]	φ [deg]	α [deg]
OFS 1	5.77e-4	28	0.2499	260.8	251.1	170.7	61.9
OFS 2	5.47e-4	269.5	0.2569	263.5	7	173.4	180.4
OFS 3	5.64e-4	150.7	0.2514	263.4	125.6	173.6	299.2

Table 7 – OFS calibration parameters in nominal configuration on board the TM

Additionaly, a series of motion reconstruction maneuvers tests have been performed in the same way reported in Section 2.6.3.2, and results have shown that the OFS system solutions in nominal configuration present levels of deviations from the imposed trajectories similar to those obtained from the tests performed with the TM base prototype.

The vision based localization system employs a camera which acquires images of the test platform, which carries visible on board markers, at known locations in its Body frame. An external computer performs through an algorithm the recognition of the markers and consequently computes the 2D position and Azimuth of the test platform wrt to the camera frame of reference. The pose estimate is computed through an explicit solution of the Perspective from Three Points (P3P) problem. The test setup including the TM base with the OFS mouse sensors installed and the vision based system is shown in Figure (49), while Figure (50) shows the TM with the fiducial markers applied on it for the computation of the vision system solution.

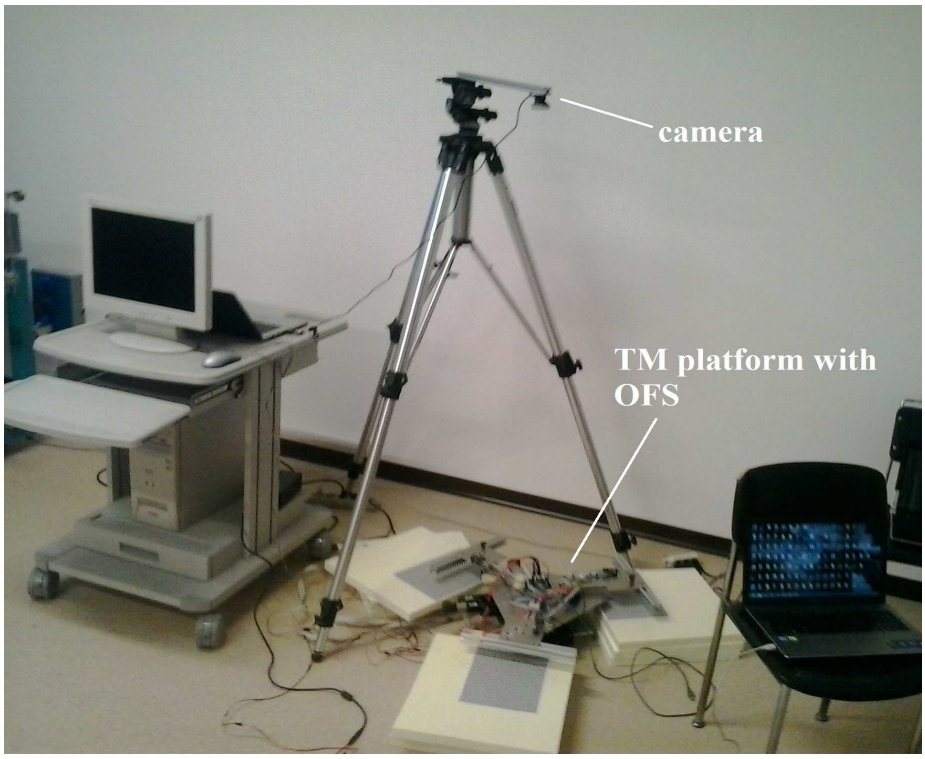

Figure 49 – Test setup for the integration of the OFS navigation system with the vision system

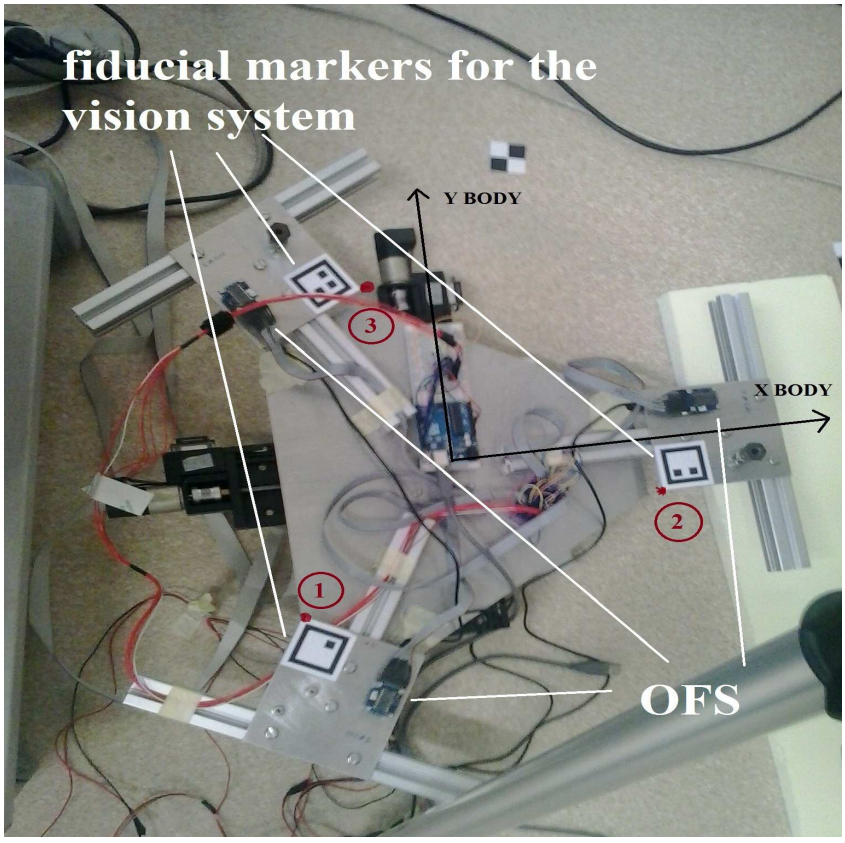

Figure 50 – TM platform with OFS system and fiducial markers for P3P based vision system

3.1.1 The Vision based Localization System

In the Vision based localization system a camera, which periodically acquires images of the test platform with opportune markers on it, is employed as the primary sensor which allows the resolution of the general problem known as Structure From Motion (SFM), which consists in recovering relative camera poses and 3D structure from a set of camera images. The SFM problem includes the problem of 3D reconstruction of the observed structure, and also the estimation of the relative position and orientation of the camera wrt to the observed scene.
For the application which is presented in this section, this type of system is employed for the solution of a particular case of the SFM problem. The camera is aimed towards the test platform, the TM base, which translates and rotates along predetermined trajectories with 3 DOF, two in planar position and one in rotation (Azimuth), by means of the motorized translation and rotation stages. Subsequently, a software in an external computer employs the acquired images in order to evaluate the pose, i.e. the relative position and orientation of the camera wrt to the test platform. This information can then be used to find in turn the relative pose of the test platform wrt the camera, i.e. the position and orientation of the TM base expressed in a Frame of Reference attached to the camera.
For the solution of this problem, the test platform must be set so that it presents a set of points with known 3D positions in its own frame of reference. If the set of points is within the field of view of the camera, then also the projections of the 3D points on the acquired images, i.e. the corresponding 2D points on the image plane, are known, and the problem can be solved. This problem is known for an arbitrary number of points as the Perspective from n Points (PnP) problem, and it presents many different known solutions, given the following general statement: given a set of m control points with 3D coordinates, known in a certain coordinate frame, and given an image in which some subset of the m control points is visible with the camera, determine the location relative to the coordinate system of the control points from which the image was obtained. In the PnP problem, the minimum number of points that can be theoretically used to find a solution is three, resulting in what is known as the P3P problem. It was however found that the employment of three points leads to determining four equivalent solutions and for this reason a fourth point is necessary for the elimination of the ambiguity. Neverthless, P3P is an attractive version of the PnP for two main reasons. Firstly, it presents many direct solutions and secondly its solution can be conveniently embedded into a RANdom Sample Consensus (RANSAC) scheme, which is an algorithm that limits the number of outliers, i.e. erroneous associations of the 2D points in the acquired image plane to 3D control points known in the platform frame of reference.

3.1.1.1 The Perspective from Three Points Problem

The P3P problem, as already pointed out, is solved by determining the position and orientation of the camera wrt the position of the observed platform, from three 2D-3D known points correspondences. The position and orientation of the camera can also be determined in an external World Reference Frame.

A closed-form solution to this problem has been proposed in 2011 by Kneip, Scaramuzza and Siegwart in [30]. In this formulation, the aligning transformation between the position of the points in the camera frame of reference and the position and orientation of the camera is computed in one single stage, in contrast to previous proposed solutions which involve an intermediate derivation of the control points in the camera frame of reference. This is implemented through the introduction of Intermediate Camera and World Reference frames of reference, and through the expression of their relative positions and orientations by means of two parameters only. The projection of a world point into the parametrized camera pose leads to a quartic equation, allowing to find up to four solutions of the parameter pair, and a subsequent backsubstitution leads finally to the corresponding camera pose, i.e. the position C and orientation matrix R of the camera wrt to the World Frame , under the condition that the 3D coordinates of three observed control point fixed to the platform, $P_{1,}P_{2,}P_{3}$, are given, and therefore also the corresponding unitary vectors $\vec{f}_{1,}\vec{f}_{2,}\vec{f}_{3}$ pointing towards the three control points from the camera frame of reference origin, are known in the camera frame of reference (See Figure (51)).

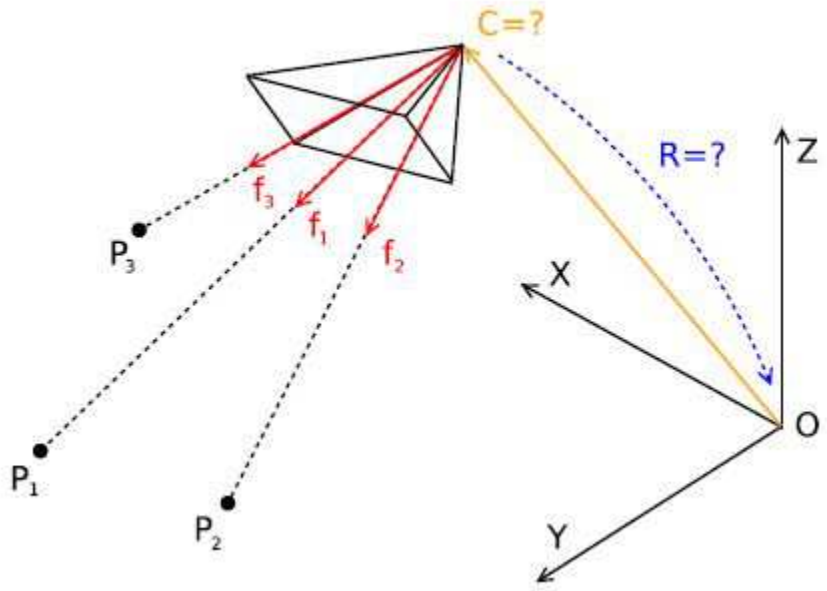

Figure 51 – The P3P problem

The frame of reference fixed to the camera is denoted as ν. An Intermediate Camera frame of reference $\tau=\left(C,\vec{t}_x,\vec{t}_y,\vec{t}_z\right)$ is defined with:

$$\vec{t}_x=\vec{f}_1 \tag{21}$$

$$\vec{t}_z=\frac{\vec{f}_1\times\vec{f}_2}{\|\vec{f}_1\times\vec{f}_2\|} \tag{22}$$

$$\vec{t}_y=\vec{t}_z\times\vec{t}_x \tag{23}$$

From this definition follows that control points vectors can be transformed from frame of reference ν to frame of reference τ through the transformation matrix $T=\left[\vec{t}_x,\vec{t}_y,\vec{t}_z\right]^T$. Also, if the orientation of τ is known in the World Reference Frame, then also the orientation of ν is known through T.

An intermediate World Frame $\eta=\left(P_{1,}\vec{n}_{1,}\vec{n}_{2,}\vec{n}_3\right)^T$ is defined through points $P_{1,}P_{2,}P_3$ with the condition that they are not collinear, with:

$$\vec{n}_x=\frac{\vec{P_1P_2}}{\|\vec{P_1P_2}\|} \tag{24}$$

$$\vec{n}_z=\frac{\vec{n}_x\times\vec{P_1P_3}}{\|\vec{n}_x\times\vec{P_1P_3}\|} \tag{25}$$

$$\vec{n}_y=\vec{n}_z\times\vec{n}_x \tag{26}$$

The world points can therefore be expressed into η by applying the transformation matrix $N=\left[\vec{n}_{1,}\vec{n}_{2,}\vec{n}_3\right]^T$, after having referred them to P_1. A semi-plane Π is defined, containing points $P_{1,}P_2$ and C and therefore also the unitary vectors $\vec{n}_x,\vec{t}_x,\vec{t}_y,\vec{f}_1$ and $\vec{f}_2$. Points $P_{1,}P_2$ and C of which the distance d_{12} between P_1 and P_2, and the angle β between $\vec{f}_1$ and $\vec{f}_2$ are known, since $\cos\beta=\vec{f}_1\cdot\vec{f}_2$. Parameter α is defined as the angle $\overline{P_2P_1C}$.

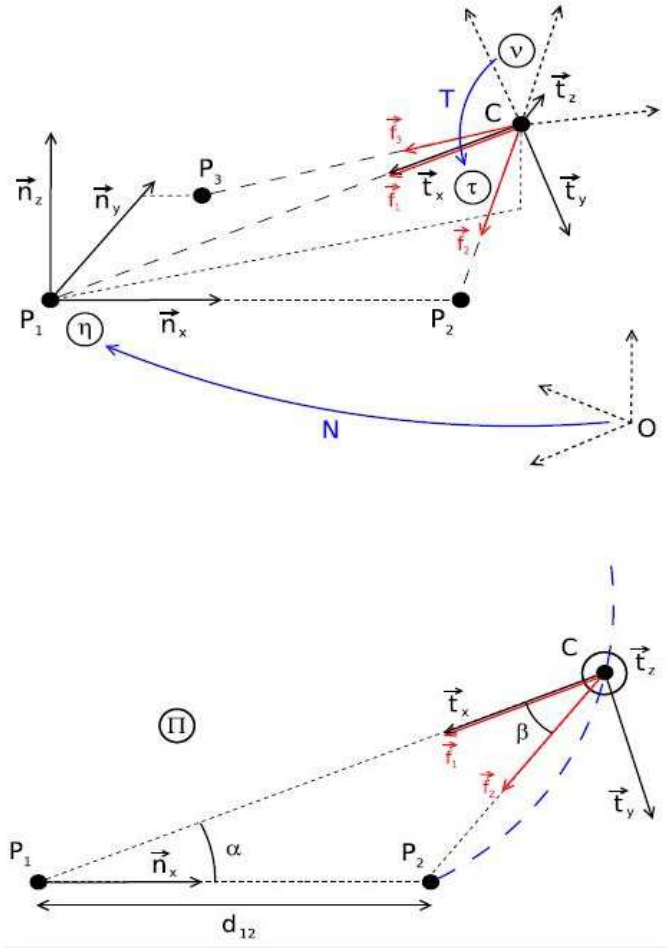

Figure 52 – Intermediate Camera Frame, Intermediate World Frame, Semiplane Π

By employing the sine-law the following equation can be written:

$$\frac{\| C\vec{P}_1 \|}{d_{12}} = \frac{\sin(\pi - \alpha - \beta)}{\sin\beta} \tag{27}$$

The position of the camera center C can therefore be expressed inside the semi-plane Π as a function of d_{12}, α and β.

Basis vectors of τ in Π are given by $\vec{t}_x^{\,\Pi} = (-\cos\alpha, -\sin\alpha, 0)^T$, $\vec{t}_y^{\,\Pi} = (\sin\alpha, -\cos\alpha, 0)^T$, $\vec{t}_z^{\,\Pi} = (0,0,1)^T$. In order to express them in η, the rotation θ of Π around $\vec{n}_x$ is given by the rotation matrix:

$$R_\theta = \begin{pmatrix} 1 & 0 & 0 \\ 0 & \cos\theta & -\sin\theta \\ 0 & \sin\theta & \cos\theta \end{pmatrix} \tag{28}$$

Therefore the camera center C^Π expressed in Π can be expressed in η through R_θ, and the transformation matrix from η to τ is given by $Q = \left[R_\theta \cdot \left(\vec{t}_x^{\,\Pi}, \vec{t}_y^{\,\Pi}, \vec{t}_z^{\,\Pi} \right) \right]^T$.

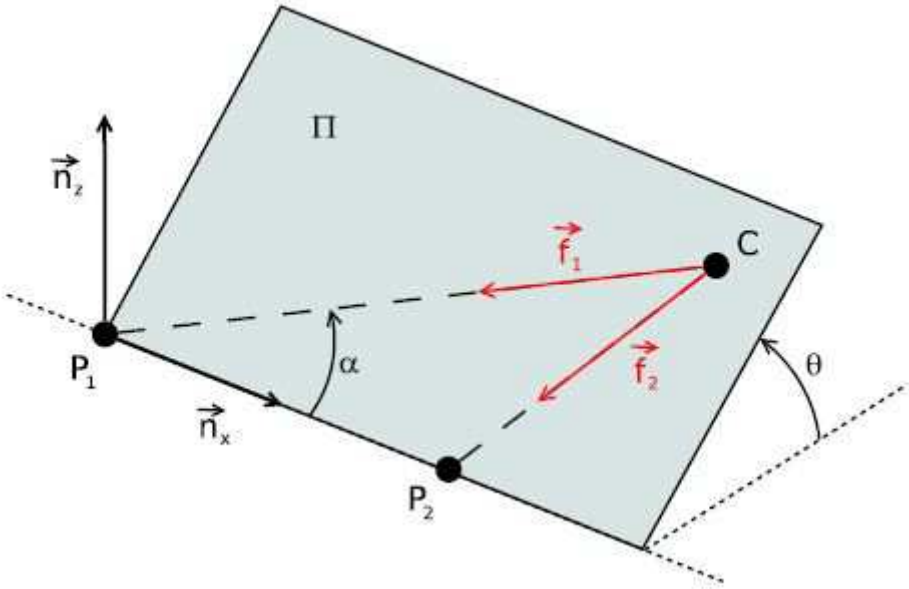

Figure 53 – Rotation of plane Π

In order to find the values of α and θ two conditions are imposed: P_3^η is expressed into τ, and its direction is equal to the one of $\vec{f}_3$. After a series of transformations a trigonometric equation with α and θ as unknown variables can be derived from these two conditions, and from a further substitution from the second condition, a fourth order polynomial equation is obtained with $\cos\theta$ as the only unknown variable (see [30] for the detailed passages). Through the application of Ferrari's closed form solution, this final equation can be solved obtaining up to four real solutions, through which the same number of corresponding values of $\cot\alpha$ can be found through the trigonometric equations with α and θ as unknown variables. Matrices C^η, Q can then be found through backsubstitution in the of the pair (α, θ) in the corresponding equations, and eventually the camera center and orientation wrt to the World Reference Frame can be determined respectively as:

$$C = P_1 + N^T \cdot C^{\eta} \tag{29}$$

$$R = N^T \cdot Q^T \cdot T \tag{30}$$

Extensive test sessions with this algorithm have shown that it presents accuracy and precision that are at the level of state-of-the-art approaches to the P3P problem, but at a much lower computational cost, i.e. approximately 15 times faster. Furthermore the algorithm has proven to be numerically stable, and to be poorly affected by degenerate configurations of the control points. Moreover its computational efficiency makes it suitable to be employed with the RANSAC outlier-rejection algorithm.

3.1.1.2 Measurement Algorithm

The first step of the measurement algorithm of the vision based navigation system consists in the detection, in each acquired image, of the projections ${}^C\boldsymbol{x}_i = \left[{}^C x_i, {}^C y_i, 1\right]^T$ of the 3D points ${}^S\boldsymbol{X}_i$ that are attached to the observed platform. The camera, through which the images of the test platform are acquired, is assumed to be optically calibrated, i.e. all its intrinsic parameters and optical distorsions are known, therefore the projected points can be expressed in an ideal camera having the same optical center as the real camera, but an ideal unitary focal length.
The matching phase consists then in associating each detected 2D point ${}^C\boldsymbol{x}_i$ with its corresponding 3D point. The 3D points are initially known only in the test platform frame of reference S. In order to minimize matching errors between the 3D points and their projections, opportune fiducial markers are employed. In this activity, markers with a square shape and a known number of internal dots inside the shape, have been employed. The square shape allows the detection of the four corners of each marker, in order to facilitate the determination of the marker's center, while the internal dots allow the identification of the marker, and therefore the retrieval of its position in the test platform frame of reference, in the phase of matching of the detected 2D points with the known 3D points. With the 3D points ${}^S\boldsymbol{X}_i$ and their corresponding projections ${}^C\boldsymbol{x}_i$ determined, the relative position and orientation between the camera and the platform can be determined through the explicit solution of the P3P problem presented in the previous section, inside a RANSAC scheme, and then with a non-linear optimization in order to refine the initial estimates.
For this particular problem, the output of the employed P3P algorithm consists in four rotation

matrices ${}^{C}_{S}\boldsymbol{R}_{j}$ from the test platform frame of reference S to the camera frame of reference C, and in four position vectors ${}^{C}\boldsymbol{X}_{S,j}$ of the platform frame of reference S expressed in the camera frame of reference C, witn $j=1,\ldots,4$. Subsequently a fourth point ${}^{S}\boldsymbol{X}_{4}$ is projected into the camera image as ${}^{C}\hat{\boldsymbol{x}}_{4,j}$ through the computed translations and rotations and at the same time measured as ${}^{C}\boldsymbol{x}_{4,j}$ in the camera image. Since only one of the four evaluated projections falls near the measured point, that projection provides the corresponding rotation matrix ${}^{C}_{S}\boldsymbol{R}$ and translation ${}^{C}_{S}\boldsymbol{X}$ as the correct solution.

This algorithm is applied not only for the estimation of the relative camera and test platform positions and orientations, but also for the estimation of the relative camera frame of reference and an external Global frame of reference defined by markers placed on the ground in the proximity of the test platform (Figure (54)). In this way also the trasnformation between the TM Body frame and the Global frame of reference can be derived.

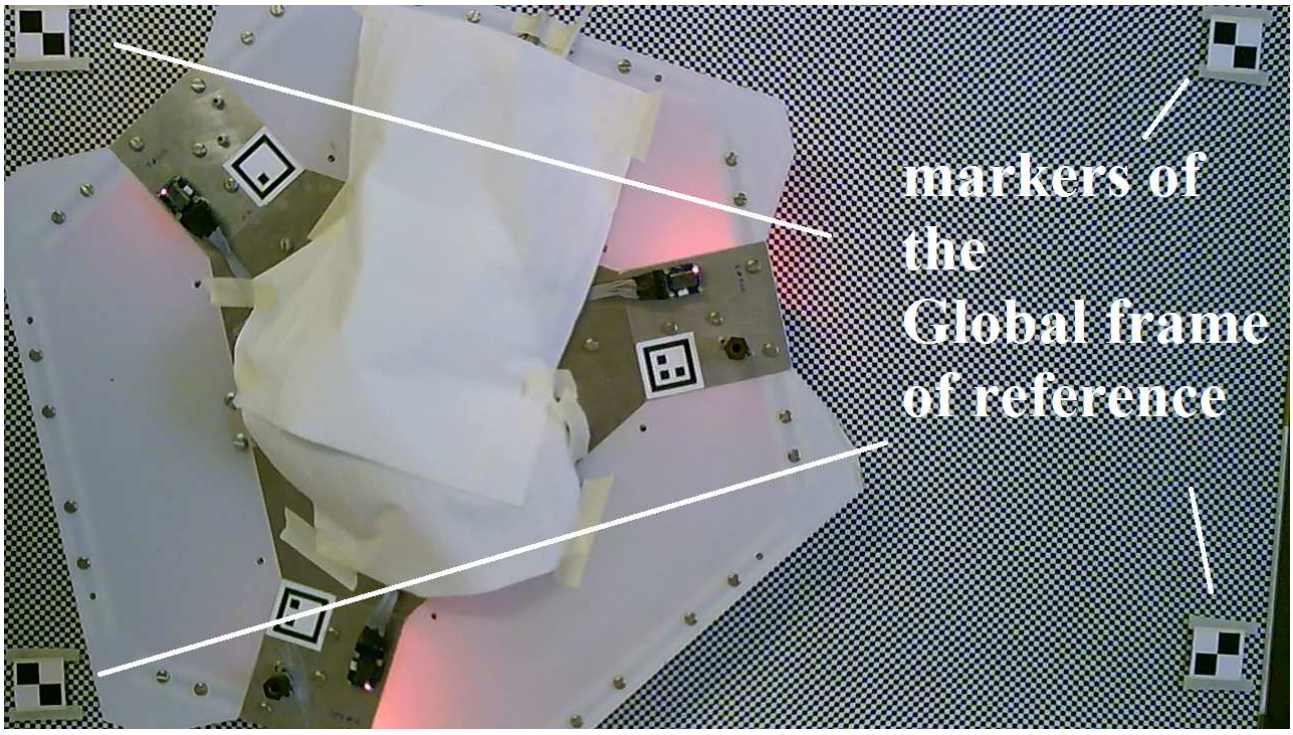

Figure 54 – Camera image withTM base and external markers defining the Global frame of reference

The proposed P3P solution is applied iteratively with a RANSAC approach that allows to discard uncorrect matches between 2D and 3D points. In each iteration of the RANSAC four points are randomly selected among all the available points, and with the rotation and translation evaluated through the solution of the P3P problem, the 2D projections ${}^{C}\hat{\boldsymbol{x}}_{i}$ are computed for all available

points $i=1,\ldots,N$. Subsequently, for all points the reprojection error is estimated through comparison of the computed 2D points ${}^{c}\hat{\boldsymbol{x}}_i$ with the measured 2D points ${}^{c}\boldsymbol{x}_i$, as $e_i=\|{}^{c}\hat{\boldsymbol{x}}_i-{}^{c}\boldsymbol{x}_i\|$. Each obtained error estimate e_i is then compared with a fixed threshold level, and if it results higher than the threshold it is considered an outlier for the pose evaluated in that RANSAC iteration and is therefore discarded. For each iteration the number of inliers in determined , and after a predetermined number of iterations, the solution is selected as the rototranslation presenting the maximum consensus, i.e. the highest number of inliers. The solution of the RANSAC can subsequently be refined through a non-linear optimization, which computes the parameters of the rototranslation as the arguments that minimize the cost function of the re-projection errors $g_{nl}=\sum_i\|{}^{c}\hat{\boldsymbol{x}}_i-{}^{c}\boldsymbol{x}_i\|^2$, computed only with the inliers selected by the RANSAC.

3.1.2 Results from the Experimental Setup

As already pointed out, an experimental setup has been assembled in the Measurement Laboratory for the execution of Azimuth and 2D translation maneuvers with simultaneous measurements with the OFS system and the Vision-based system.

The experimental setup consisted in the TM base with the OFS installed in the nominal configuration, with each optical sensor equipped with LEDs oriented in order to illuminate the chessboard pattern disposed at the nominal distance from the sensors lenses. An Arduino UNO microcontroller was employed to acquire the sensors measurements and save them in an external PC for the offline elaboration. The TM was installed on the assembly composed by the rotational motorized stage in the lower section, and by the 2-axes translational motorized stage in the upper section. The camera of the vision system was mounted on a horizontal profile beam supported by a tripod, such that the camera was pointed towards the TM from a vertical distance of approximately 1 m. The camera was then oriented as much as possible with its focal plane orthogonal to the vertical axis passing through the TM rotation center. The camera images were acquired in an external PC for the offline elaboration. On each acquired image, the features that had to be recognized by the vision system software were three markers applied on board the TM on the same plates supporting the OFS. The employed markers were squares with known dimensions with internal dots, and they were applied on known locations wrt to the Body frame of reference attached to the TM. Each marker was unequivocally recognized by the software through its distinctive

number of internal dots.

The elaboration of the measurements of the vision system provides as already pointed out the transformation matrix from the TM Body frame of reference to the camera frame of reference, and also the transformation matrix from the camera frame of reference to the World frame of reference, which is defined by markers applied along orthogonal directions on the floor near the test platform, in known locations amongst each other and wrt to the TM Body frame. In offline elaboration of the test sessions the position and Azimuth estimates obtained with the OFS and with the vision system were therefore both referred through the transformation matrix to the World frame of reference.

A series of tests was performed with the described setup, for translational, rotational and combined maneuvers. Tests performed with this setup showed a good correspondence between the results from the two navigation systems, with a concordance in the order of few mm in terms of position and comprised between ± 1° wrt to the Azimuthal rotation, as can be seen from results reported in Figures (55), (56) of a combined maneuver test with the sequence + 4° (counterclockwise) Azimuth rotation, + 2 cm along X axis of TM Body frame, - 4° (clockwise) Azimuth rotation, - 2 cm along X axis of TM Body frame.

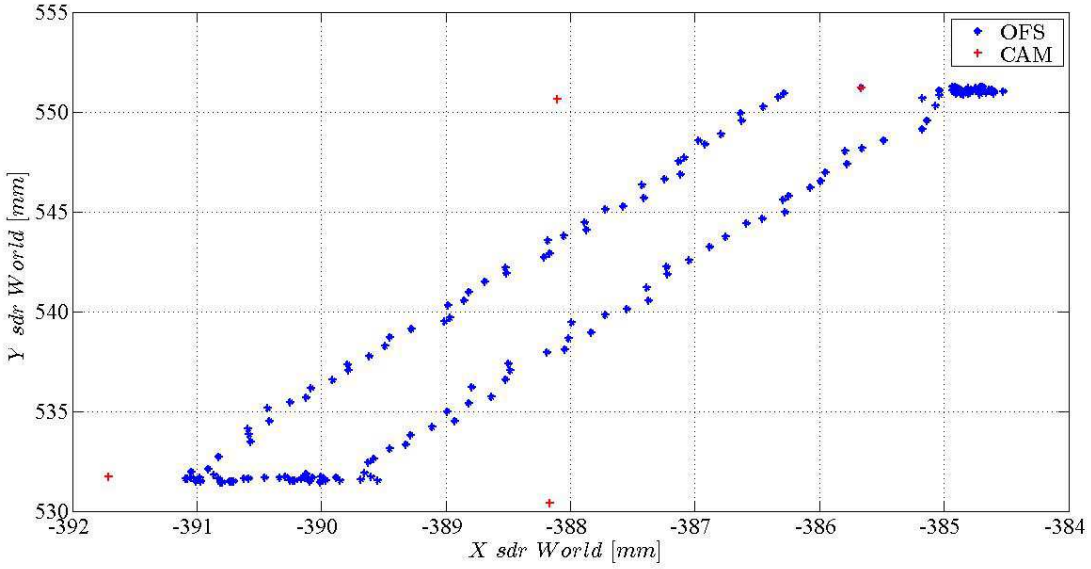

Figure 55 – Test results of combined maneuver with OFS system (blue) and vision system (red) solutions, position in World frame of reference

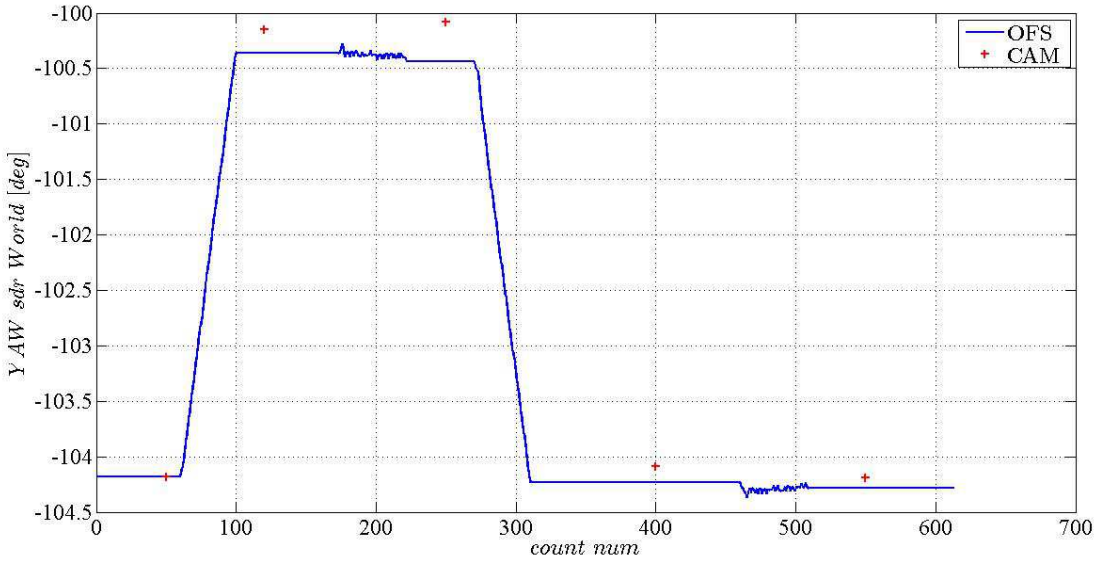

Figure 56 – Test results of combined maneuver with OFS system (blue) and vision system (red) solutions, Azimuth in World frame of reference

As in the case of the reconstruction manuevers with the OFS system only, also in this case the original test setup was modified in order to allow the execution of combined maneuvers with extended ranges in translation and rotation. In this case however, the motorized stages assembly was no longer employed, instead the TM base was disposed on a granite levelable table, (the same employed for the air skids tests) with a glass layer under which a A0 sheet with chessboard pattern was placed (Figure (54)). For these types of tests, the reference were Vision based position and Azimuth estimates, and OFS and vision system estimates were also combined through an Extended Kalman Filter (EKF). The TM platform was manually moved with no predetermined motion, but with an approximate idea of the position and rotation trajectory to be imposed to the platform. The camera was installed on a support appendix above the TM platform, in the same configuration as in the first version of the test setup. Figure (57) shows the results of one of this type of tests, comprising the EKF solution.

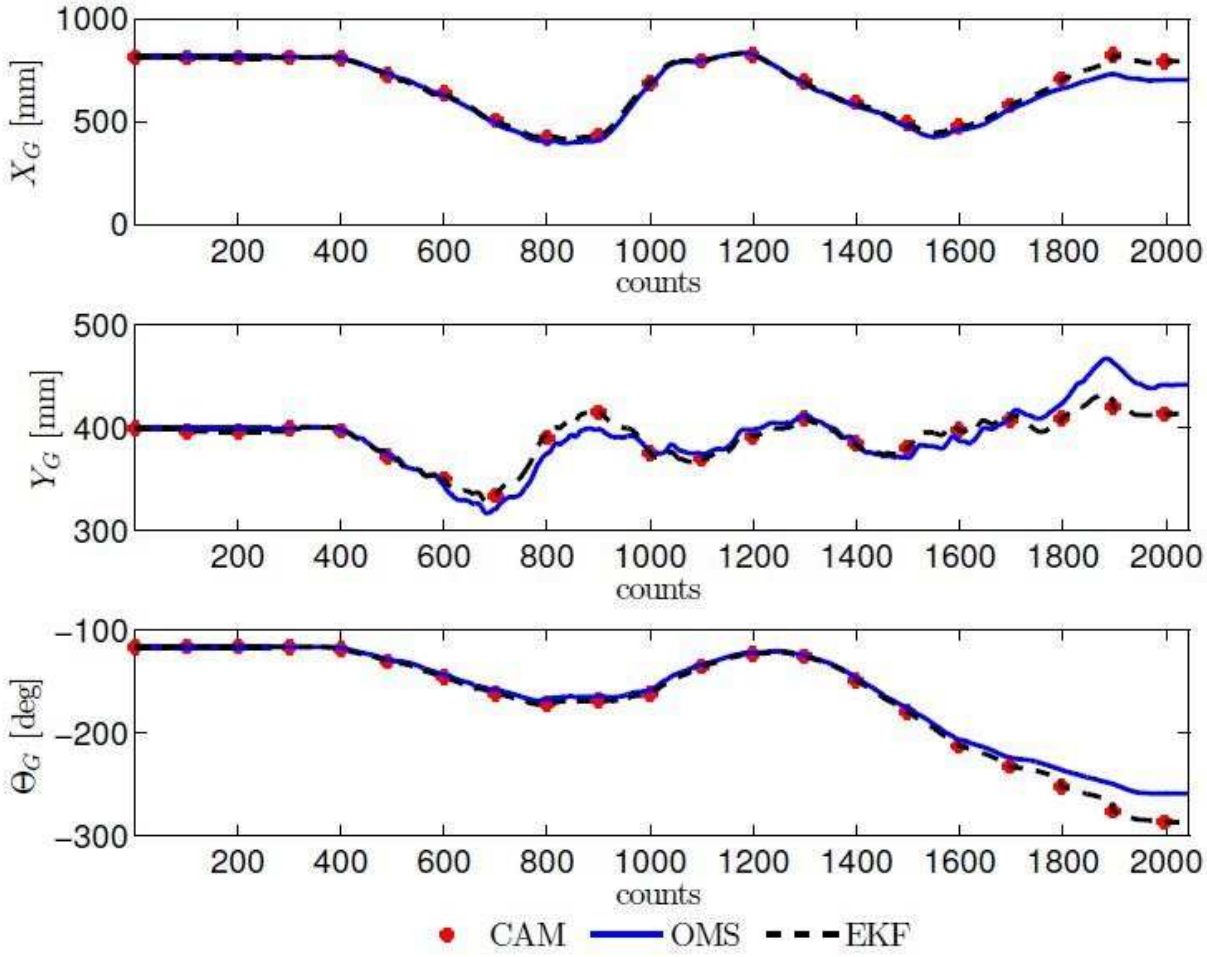

Figure 57 – Test results of manually imposed combined maneuver with OFS system solution (continuous blue line)), vision system solution (dotted red line), EKF solution (dashed black line)

As it can be seen from the results, there is a good concordance between the vision based and OFS system, until the range of combined maneuver is extended. After that, again the OFS system shows a drift trend, with at the beginning a drift visible only for position, and at the end of the test visible also for rotation, with final differences at the level of approximately 5 cm in position and of approximately 35° in Azimuth rotation. The EKF appears able to compensate the drift trend of the OFS system, since the vision system is considered as fiducial reference, with the EKF uncertainty output provides max vaules of $\left[\sigma_X, \sigma_Y, \sigma_\Theta\right] = \left[7.38\,mm, 7.38\,mm, 1.76\,deg\right]$.

4 GUIDANCE NAVIGATION AND CONTROL STRATEGIES FOR SATELLITE FORMATION FLYING AND PROXIMITY MANEUVERS

4.1 Relative Motion Models

Relative motion models are especially useful in the implementation of robust and optimal Guidance Navigation and Control (GNC) systems for SFF and ARPO applications, since they allow reference trajectories generation for the Guidance function, optimal state estimation for the Navigation function and optimal control law synthesis for the Control function. Moreover, by employing relative motion models different formation configurations can be implemented, according to the required application, and also the evolution and the effects of a certain configuration can be studied through the analysis of orbital disturbances. Also, the selection of appropriate initial conditions can be studied with the goal of mitigating disturbances that result in formation evaporation, i.e. secular drifts.

Spacecraft relative motion models can be categorized through the following characteristics: linearity, and non linearity, time invariance and time variance, and according to employed Coordinate system type, e.g. orbital elements differences or Cartesian relative coordinates. In particular, from a GNC design point of view, relative motion models can be divided in Linear Time-Invariant (LTI) models, Linear Time-Varying (LTV) models, and Non-Linear (NL) models, of which LTI models are the most simple. In the early 1960's Clohessy and Wiltshire published a work in which a Hill-like rotating Cartesian coordinate system was employed in order to derive the equations for the relative motion between two satellites, in the case of a rendez-vous problem [1]. In the Hill-Clohessy-Wiltshire (HCW) model the orbit of the target spacecraft is assumed to be circular, the distance between the target and the chaser is small wrt to the target's orbit radius, and no perturbations affect the orbital motions of the target and the chaser. Under the point of view of SFF, the HCW model describes the relative motion of a follower spacecraft wrt to a leader spacecraft in the Hill's Local-Vertical Local-Horizontal (LVLH) rotating Cartesian coordinate system with origin at the leader spacecraft position and orientation given by axes $\{x, y, z\}$, with x along the orbit radius direction, z parallel to the spacecraft angular momentum in the normal direction, and with y completing the righ-handed coordinate system. The relative state of the follower spacecraft is expressed in this frame of reference as the relative position $\rho=[x_f, y_f, z_f]^T$ and the relative velocity $\dot{\rho}=[\dot{x}_f, \dot{y}_f, \dot{z}_f]^T=[u_f, v_f, w_f]^T$

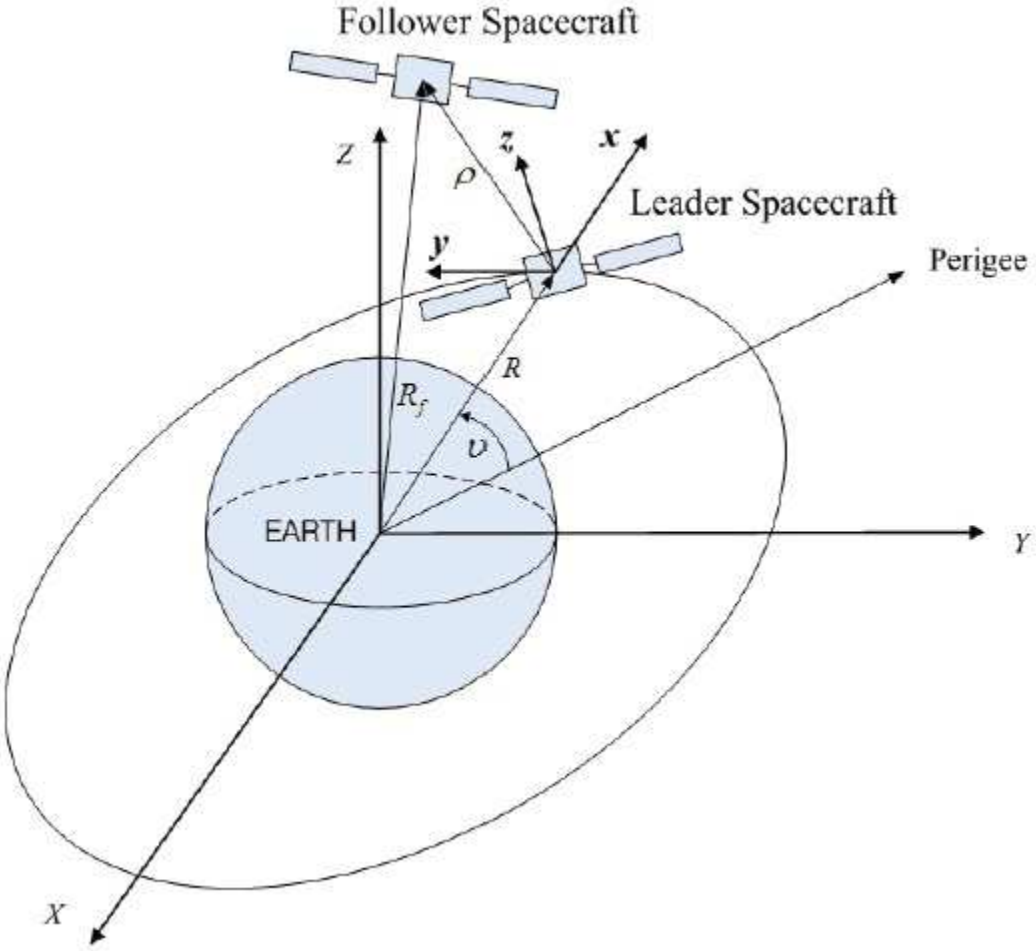

Figure 58 – Representation of the Local-Vertical Local-Horizontal (LVLH) Frame of Reference

The Hill's differential equations of the relative motion between the follower and the leader spacecraft can be therefore expressed as [17], [18]:

$$\ddot{x} - 3n^2 x - 2n\dot{y} = f_x \tag{31}$$

$$\ddot{y} + 2n\dot{x} = f_y \tag{32}$$

$$\ddot{z} + n^2 z = f_z \tag{33}$$

In the Hill's equations, the right side terms represent relative external accelerations which can be produced by perturbations and by the on board propulsion system.
By solving Hill's differential equations with no external accelerations applied, the HCW equations are obtained as:

$$x(t) = \frac{\dot{x}_0}{n}\sin nt - \left(3x_0 + 2\frac{y_0}{n}\right)\cos nt + 4x_0 + 2\frac{\dot{y}_0}{n} \tag{34}$$

$$y(t)=2\frac{\dot{x}_0}{n}\cos nt+(6x_0+4\frac{\dot{y}_0}{n})\sin nt-(6nx_0+3\dot{y}_0)t-2\frac{\dot{x}_0}{n}+y_0 \tag{35}$$

$$z(t)=\frac{\dot{z}_0}{n}\sin nt+z_0\cos nt \tag{36}$$

$$\dot{x}(t)=u(t)=\dot{x}_0\cos nt+(3nx_0+2\dot{y}_0)\sin nt \tag{37}$$

$$\dot{y}(t)=v(t)=(6nx_0+4\dot{y}_0)\cos nt-2\dot{x}_0\sin nt-(6nt+3\dot{y}_0) \tag{38}$$

$$\dot{z}(t)=w(t)=-z_0n\sin nt+\dot{z}_0\cos nt \tag{39}$$

A bounded relative motion to the first order is obtained from these equations if the following constraint is satisfied by the initial conditions:

$$\dot{y}_0+2nx_0=0 \tag{40}$$

if this constraint is satisfied then the secular term present in equation (35) is always zero. In this case the HWC equations can be expressed as:

$$x(t)=\rho_x\sin(nt+\rho_{xy}) \tag{41}$$

$$y(t)=2\rho_x\cos(nt+\rho_{xy})+\Delta y \tag{42}$$

$$z(t)=\rho_z\sin(nt+\rho_z) \tag{43}$$

The initial conditions of the relative motion allow the determination of parameters Δy , ρ_z , ρ_{xy} and ρ_z as follows:

$$\rho_x=\sqrt{x_0^2+\frac{\dot{x}_0^2}{n^2}} \tag{44}$$

$$\Delta y=y_0-2\frac{\dot{x}_0}{n} \tag{45}$$

$$\rho_z=\sqrt{z_0^2+\frac{\dot{z}_0^2}{n^2}} \tag{46}$$

$$\phi_{xy}=\tan^{-1}\left(\frac{nx_0}{\dot{x}_0}\right) \tag{47}$$

$$\phi_z=\tan^{-1}\left(\frac{nz_0}{\dot{z}_0}\right) \tag{48}$$

Equations (44) to (48) express an elliptic cylinder with a parametric rapresentation, in which the in-plane motion is an ellipse with semi-minor axis ρ_x in the radial direction, semi-major axis $\rho_y = 2\rho_x$ in the along-track direction, and eccentricity equal to $\sqrt{3}/2$. The motion center is located in the along-track direction with an offset of Δy from the origin. The out of plane motion consists in an oscillation with semiamplitude ρ_z , while ϕ_{xy} is the initial phase angle of the in-plane motion, and ϕ_z is the initial phase angle of the out of plane motion.
By selecting appropriate values for these parameters different formation geometries can be obtained in terms of the shape of the along track – radial plane and along track – cross track plane: in the LVLH frame of reference, the motion can describe an elliptical, circular or rectilinear trajectory.
The HCW equations can also be written in terms of differential orbital elements as follows:

$$x(f) = \delta a - a\delta e \cos f \tag{49}$$

$$y(f) = a(\delta\omega + \delta M + \delta\Omega\cos i) + 2a\delta e \sin f \tag{50}$$

$$z(f) = a\sqrt{\delta i^2 + \delta\Omega^2 \sin^2 i \cos(\theta - \theta_z)} \tag{51}$$

where f is the true anomaly, a is the semi-major axis, e is the eccentricity, ω is the argument of perigee, M is the mean anomaly, Ω is the longitude of the ascending node, i is the inclination, $\theta = \omega + f$ is the true latitude, θ_z is function of the initial conditions.
Several different configurations can be obtained through appropriate choices of the differential orbital elements, for instance in the fixed ground track formation systems, the satellites are on slightly different orbit with difference in the longitude of the ascending node that are chosen so the satellites pass on the same point on the ground after a certain time interval, while in circular formation satellite systems the satellites respect the condition of having a fixed distance between each other.

4.2 Guidance, Navigation and Control

Guidance, Navigation and Control (GNC) consist in the three functions that allow the estimation and control of the kinematic state of a vehicle. This involves the position and attitude of the vehicle and the related variational rates as the estimated and controlled variables.
The Navigation function is intended to allow the determination of the kinematic state of the vehicle at a certain time and in a chosen reference system. The Guidance function allows the determination

of a desired trajectory from the vehicle's current position and attitude to the intended target ones. The Control function is in charge of determining and applying the necessary forces and torques that allow to reach and maintain the desired state of the vehicle.

Amongst the three functions, Navigation and Control imply an interaction with the environment, in the case of Navigation by performing measurements through navigation sensors, in the case of Control by applying torques and/or forces through the on board actuators. Both functions are characterized by constraints of the employed hardware. In the case of the Guidance function, no interaction with the environment happens, however updates of the vehicle state and of the measured environmental conditions are most likely needed during the mission in order properly re-formulate the vehicle's trajectory. Hardware limitations for the Guidance function are related to the computational capability of the on board computer.

Two main Guidance Navigation and Control system types are possible: Open Loop GNC, and Closed Loop GNC. The Open Loop case occurs when the Guidance function is defined before the start of the mission, and it remains fixed throughout the whole mission duration, while the Control function follows a predetermined actuation sequence. On the contrary, in the Closed Loop case, deviations from the predicted enivironmental conditions are taken into account through sensors measurements and are employed to modify the Guidance and Control functions accordingly, which results in improved system performances. In most cases, to actually reach the desired vehicle's state a Closed Loop GNC system is required.

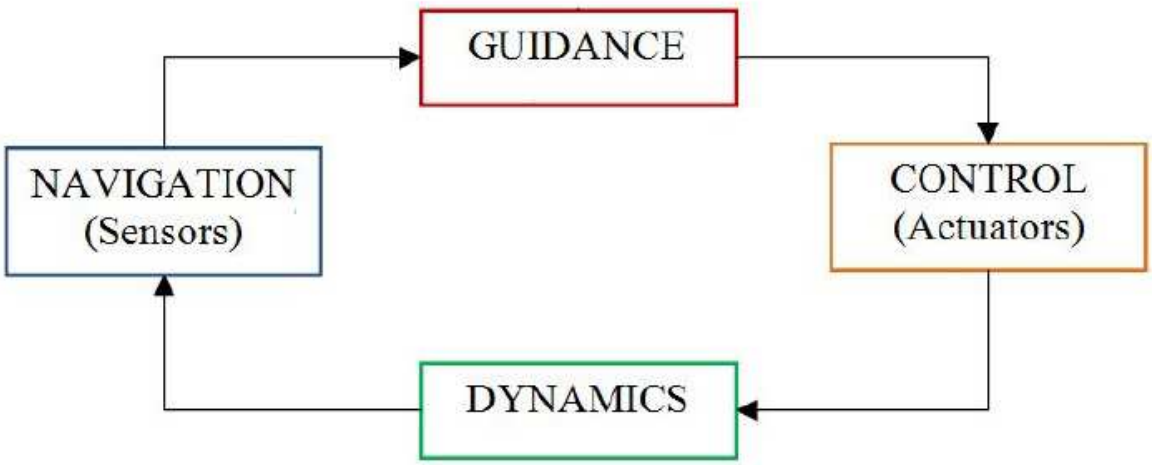

Figure 59 – The Guidance, Navigation and Control Loop

4.2.1 Guidance Function

In the problems of SFF, RVD, and proximity operations in general, the Guidance function is in charge of generating reference trajectories for the whole state of the vehicle (position and attitude), which are then used as input of the on board control system of the satellites. Satellite systems can be operative in two main different types of space environments, with the formulation of the Guidance function changing accordingly: Deep Space environments, and Planetary Orbital Environments. Satellites that operate in Deep Space environments experience generally very low levels of orbital disturbances. As a consequence, their relative dynamics can be reduced to the double integrator form, and a formation can be maintained with very low fuel consumption, or even without fuel consumption, if the formation geometry is properly planned.
On the other hand, satellites that carry out their tasks in Planetary Orbital Environments experience orbital disturbances with effects that are most likely not negligible. A typical way in SFF to avoid excessive fuel consumption in order to counterbalance the disturbances encountered in these environments, is the employment of Passive Relative Orbits, i.e. periodic relative trajectories that need limited position control actuations. With a certain Passive Relative Orbit chosen so that the formation evaporation is prevented in nominal conditions, the orbit robustness to disturbances must neverthless be evaluated, especially wrt gravity gradient, luni-solar perturbations, atmospheric drag, electric charges acting on the satellites. In order to evaluate the robustness of these orbits, the HCW equations have been modified with the inclusion of drag and J2 effects, however if the relative orbit presents an eccentricity of 0.005, the error induced by neglecting the eccentricity becomes higher that the error due to the neglect of J2. In order to incorporate both J2 and orbit eccentricity in the equations, the relative motion has to expressed in the LVLH frame as function of the solutions of the differential mean orbital elements.

4.2.2 Navigation Function

The Navigation function in the problems of SFF and proximity operations is in charge of providing estimates of the absolute and relative states of the involved satellites.
According to [20], there can be three fundamental state estimation schemes in SFF: Centralized, Decentralized and Hierarchic.
The case of the Centralized Architecture occurs when one satellite is designed as chief, while the other satellites are followers, with each follower sending its measurements to the chief satellite

which processes them through a Kalman filter, and can then broadcast the processed estimations to the followers.
In the Decentralized Architecture the state estimation effort is equally distributed over the satellites of the formation, which implies a higher autonomy for each satellite with reduced inter-communication links requirements. This architecture can be implemented in two different ways, in one case every spacecraft performs an estimation of the state of the entire formation, while in the other case each spacecraft estimates only its own state, which implies, wrt to the former solution, higher synchronization requirements between the satellites when carrying out GNC tasks.
Last, the Hierarchic Architecture foresees state estimation at first for reduced groups of satellites in the formation, with the results being subsequently gathered by the satellites that are designed with higher hierarchy. In this way each cluster of satellites performs the ranging and orientation estimations indipendently, with the expection of the chief of the cluster. Each chief of the cluster gathers then with each other to form the higher level cluster.
For relative state estimation in SFF, a widely employed solution is the GPS, which through differential navigation presents especiallu high accuracy in the position estimation, in the order of few centimeters. For RVD and proximity operations, vision systems, LIDARs, laser rangers, and infrared cameras are navigation systems that can be employed for relative state estimation in terms of relative range and bearing angles.

4.2.3 Control Function

In the case of SFF, but also in the general case of robotic formations for ground or underwater applications, the Control function has the goal of performing the coordination of multiple vehicles. To achieve this objective, a minimum of one spacecraft has to track a certain relative state reference wrt to another satellite, and the state of the latter has to be available to the former for the control law elaboration. This definition of control law for this specific problem is referred to as Formation Tracking Control Law. The general control architecture foresees three main levels. The first level is the Spacecraft Local Control. At this level, the system S_i is the i^{th} spacecraft which presents control input vector u_i, and measurable state output y_i. This level is therefore in charge of computing the actuator vector and a performance indicator for each spacecraft, from the measured spacecraft state output and the input reference state trajectory and commands. The second level is given by the Formation Control. This block has the task of elaborating and sending the outputs of

the reference trajectory and commands to all the satellites, and the outputs of the performance indicators of all satellites to the higher level, i.e. the Supervisor, which employs the measured Formation Control output to determine the input to be sent back to the Formation Control. Generally, the Formation Control is in charge of the absolute and relative attitude and position control of each spacecraft of the formation.

The problem of defining a control law in SFF has been studied in the context of Formation Flying Control (FCC) with the definition of five main architectures as proposed by [4].

The first one is the Leader/Follower Architecture (L/F). In the L/F architecture, one spacecraft is designed as leader, with a certain absolute reference state to be tracked with its own individual control, while the remaining satellites are designated as followers that track only the states of the other nearest follower satellites. In terms of navigation, the L/F architecture presents a Hierarchical organization with the formation reference state defined by the leader spacecraft.

Another FCC architecture is the Multiple-Input, Multiple-Output (MIMO) architecture: in this case, every spacecraft of the formation is treated as the element of a MIMO plant, to which therefore every method of modern control can be potentially be applied, e.g. Linear Quadratic Regulator (LQR), Model Predictive Control (MPC), etc., resulting in an optimal, stable control.

A FCC architecture that is essentialy an hybrid between L/F and MIMO is the Cyclic architecture. In the Cyclic architecture, the satellites of the formation have a more uniformly distributed control with a non-hierarchical structure.

The other two main FCC architectures defined by [4] are the Virtual Structure architecture, and the Behavioral architecture. The Virtual Structure architecture foresees the satellite formation as a unique system, which has a certain reference state trajectory defined in accordance to the mission target, with the actual motion and control for each satellite derived subsequently at an individual level. This architecture is especially indicated for cases such as interferometric missions, in which the spacecraft formation must be operative as the equivalent of a bigger satellite with a single payload resulting from all the payloads of the formation, and therefore the formation has to move as much as possible as a rigid body. In the Behavioral architecture, all satellites of the formation are set to cooperate with each other in order to reach the intended formation configuration, by following certain predetermined behavioral schemes that are implemented in for safety and stability reasons, i.e. collision avoidance schemes, obstacle avoidance schemes, formation keeping schemes, etc.

In the case of the Control function for automated RVD and proximity maneuvers between two satellites, the general architecture is considerably simplified. The position and attitude control is carried out at a relative level in order to perform the maneuver, with the management of reference trajectory and commands in charge of the on board computer of the spacecraft which actively

performs the maneuver. As in the case of SFF, certain behavioral schemes are implemented in order to carry out this type of maneuvers, for instance collision avoidance schemes are relevant in this case, since these maneuvers present an increased risk of impact between the satellites.
For the problems of SFF and proximity operations, four main types of controllers will be presented: Proportional – Integral – Derivative (PID), Linear Quadratic Regulator (LQR), Model Predictive Control (MPC).
The plant dynamics of the Linear Time Invariant (LTI) model employed in LQR and MPC control syntheses can be written in state-space form as follows:

$$\dot{x}(t) = A\,x(t) + B\,u(t) \tag{52}$$

$$y(t) = C\,x(t) \tag{53}$$

with $x(t)$ the state vector, $u(t)$ the control input vector, $y(t)$ the output, A the state matrix, B the control matrix, C the output matrix.

4.2.3.1 PID Control

The Proportional-Integral-Derivative (PID) controller is given by a control law consisting of three components. The first component, the proportional component $u_p(t)$, is proportional to the instantaneous control tracking error $e(t)$. The second component, the integral component $u_i(t)$, is proportional to the integral of $e(t)$. The third component, the derivative component $u_d(t)$, is proportional to the time derivative of $e(t)$. The complete formulation of the control law is given by:

$$u_{PID}(t) = u_p(t) + u_i(t) + u_d(t) = K_p e(t) + K_i \int_0^t e(\tau)\,d\tau + K_d \frac{d\,e(t)}{dt} \tag{54}$$

with $e(t) = r(t) - y(t)$ the control tracking error, $y(t)$ the controlled variable, $r(t)$ is the reference signal, K_p, K_i, K_d are respectively the proportional, integral and derivative gains. The proportional term has the effect of compensating large control errors by increasing the control action proportionally. The integral term introduces a pole at the origin of the complex plane, resulting in the reduction to zero of the steady-state error with a step reference signal applied to the

system. The derivative action follows the predicted future values of the control errors and therefore compensates for trends that are not predicted on part of the other two components. This basic formulation is however modified in practical applications on the basis of three main aspects: proportional and derivative kicks avoidance, saturation, low pass filtering of the derivative components.

With regards to the first aspect, the proportional and derivative kicks appear with controllers that have high gains which are set to produce fast disturbance rejection. This however results in oscillatory responses to step set points. To compensate for proportional and derivative kicks, set point weighting can be employed for both the derivative and proportional actions.

The problem of actuators saturation can be treated in PID controllers by employing a saturation model in an anti-reset windup feedback scheme, so that the nonlinear behaviors introduced by saturation are properly managed. Since in the occurence of saturation the system operates in open-loop, feedback can be reintroduced by feeding back to the controller the difference between the saturated and unsaturated control signal, so that the correct state of the controller is estimated.

With regards to the third aspect, a first-order low pass filter can be used in order to reduce the effects of measurement noise in the control action.

With the inclusion of proportional and derivative kick avoidance, anti-reset windup feedback scheme, and low pass filtering of the derivative component, the modified PID formulation can be written as:

$$u(t)=K_p\left\{\beta\, r(t)-\ y(t)+\frac{1}{T_i}\int_0^t\left[e(\tau)+\frac{T_i}{K_pT_t}(u'(t)-\ u(t))\right]d\tau+T_d\left[\frac{d(\gamma\, r(t)-\ y_f(t))}{dt}\right]\right\} \quad (55)$$

$$\frac{T_d}{N}\frac{dy_f(t)}{t}=y(t)-\ y_f(t) \quad (56)$$

with $u(t)$ the computed control variable, $u'(t)$ the process control input, $T_i=K_p/K_i$, $T_d=K_d/K_p$, β the proportional set-point weight, γ the derivative set-point weight, with $0\le\beta\le 1$, $0\le\gamma\le 1$ in general.

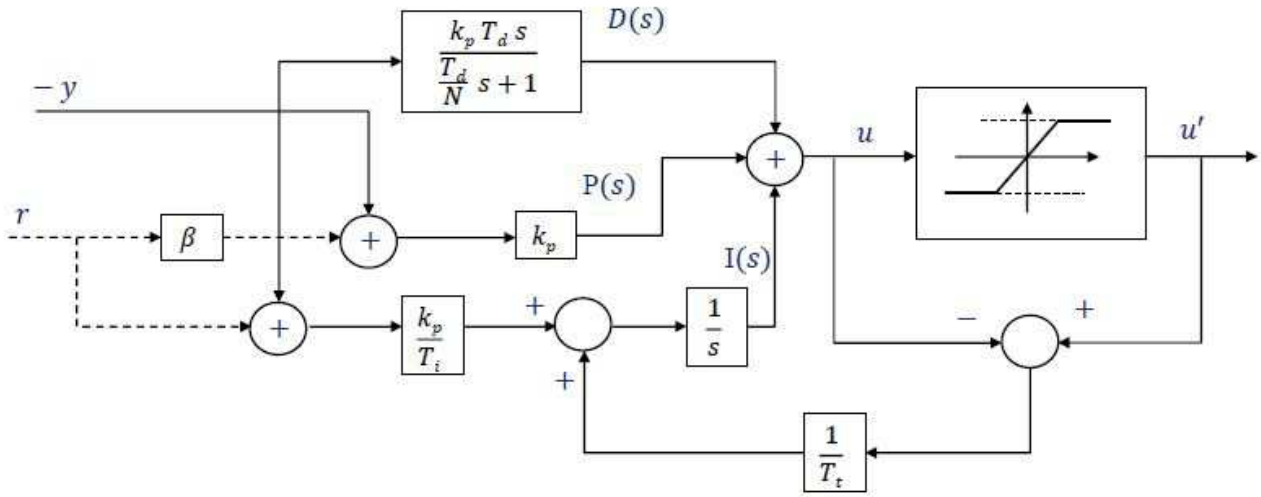

Figure 60 – Block Diagram of PID controller with proportional and derivative kick-avoidance and anti-reset wind up

4.2.3.2 Linear Quadratic Control

The Linear Quadratic Regulator (LQR) has the goal of finding, through the control synthesis, a state feedback control law of the type $u(t) = -K e(t)$, with K the gain matrix.
The control synthesis is accomplished through the minimization of a quadratic performance index with the following form:

$$J = \int_0^\infty \left[e^T(\tau) Q(\tau) e(\tau) + u^T(\tau) R(\tau) u(\tau) \right] d\tau \tag{57}$$

with Q the positive-definite state error weighting matrix, and R the positive-definite control weighting matrix. The index J represents the system's global energy resulting from the sum of the system error energy and the control energy. The conditions that the pair (A, B) is controllable and the pair (A, C) is observable imply the existince of a unique solution to the control synthesis, corresponding to the gain matrix having the following formulation:

$$K(t) = R^{-1}(t) B^T P(t) \tag{58}$$

with the matrix $P(t)$ the solution of the Algebraic Riccati Equation:

$$P(t)A+A^{T}P(t)-P(t)BR^{-1}(t)B^{T}P(t)+Q(t)=0 \tag{59}$$

Matrices Q and R are arbitrary parameters, with values that must be chosen in accordance to the characteristics of the system to be controlled, and to the desired performances in tracking the reference trajectories, considering also the overall amount of control action spent during the maneuver.

4.2.3.3 Model Predictive Control

Model Predictive Control (MPC) [22, 23, 24], also referred to as Receding Horizon Control (RHC), consists in a modern optimal control technique that has been widely employed in industry in order to solve multivariable constrained control problems [25, 26, 27]. In its basic formulation, MPC foresees the employment of an explicit model of the plant that has to be controlled, and a sample of the current state $\hat{x}_{t_k}$ in order to predict the future behavior of the output $y(t)$ over a finite horizon of length p, as function of a control sequence. In this prediction of the future behavior of the state, the control signal is assumed to be changing only in the interval $[t_k, t_{k+m}]$, while it remains constant for the subsequent $\{p-m\}$ control steps, with $\{m \leq p\}$, where p is the length in time steps of the prediction horizon, and m is the length of the control horizon. Through this prediction, the current control action to be applied is computed by solving an on-line finite horizon open-loop optimal control problem, obtaining the optimal control sequence $U'_k(\hat{x}_{t_k})=\{u'_{t_k}, u'_{t_{k+1}}, ..., u'_{t_{k+m}}\}$ that minimizes a certain system cost measure over the chosen prediction horizon. With the optimal control sequence available, the subsequent step foreseen in the MPC scheme, consists in applying only the first action of the sequence, and then solving back the optimal control problem with a new state estimate at the subsequent time instant. In this way feedback is introduced in the system, allowing compensation of possible modeling errors and/or disturbances.

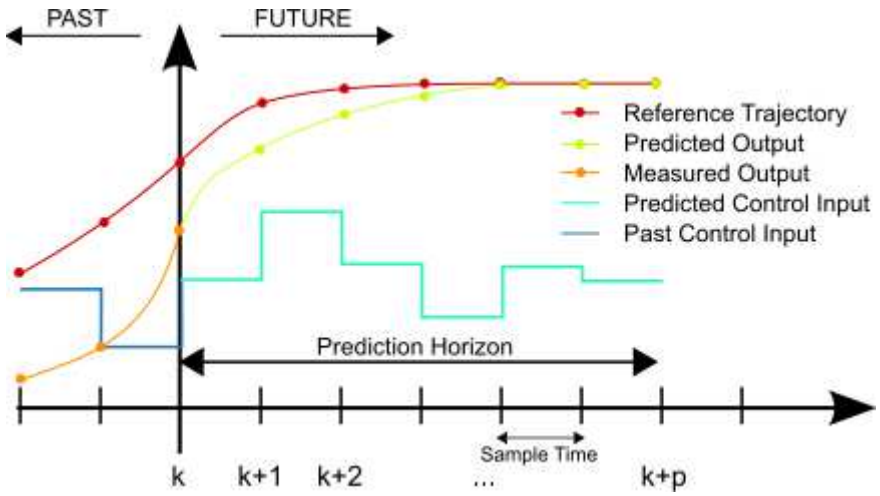

Figure 61 – Basic idea of Model Predictive Control

The basic formulation of MPC employs the linear time-invariant model of the system:

$$x_{k+1|k} = A\,x_{k|k} + B\,u_k \tag{60}$$

$$y_{k|k} = C\,x_{k|k} \tag{61}$$

The variable value $a_{k+j|k}$ denotes the value of a evaluated at time t_{k+j}, according to the information available at time t_k. Defining $\Delta u_{k+j|k} = u_{k+j|k} - u_{k+j-1|k}$ as the difference between two consecutive control sequences, $e_{y,k+j|k} = y_{k+j|k} - y_{r,k+j|k}$ as the output tracking error wrt to the reference output y_r, and $e_{u,k+j|k} = u_{k+j|k} - u_{r,k+j|k}$ as the difference between the input and the reference control, then for a given state sample $\hat{x}_k$ at time t_k, MPC solves the optimization problem:

$$V'(x_{k|k}) = \min_{\Delta U_k} e^T_{y,k+p|k} P\, e_{y,k+p|k} + \sum_{j=0}^{p-1} e^T_{y,k+j|k} Q_j e_{y,k+j|k} + e^T_{u,k+j|k} R_{u,j} e_{u,k+j|k} + \Delta u^T_{k+j|k} R_{\Delta u,j} \Delta u^T_{k+j|k} \tag{62}$$

in which, for $0 \le j \le p-1$, the following conditions apply:

$$x_{k+j+1|k} = A\,x_{k+j|k} + B\,\Delta u_{k+j|k} \tag{63}$$

$$y_{k+j|k} = C\,x_{k+j|k} \tag{64}$$

$$x_{k|k} = \hat{x}_k \tag{65}$$

$$[E\ G]\left[\begin{matrix} y_{k+j|k} \\ u_{k+j|k} \end{matrix}\right] \leq L \tag{66}$$

$$H\,\Delta u_{k+j|k} \leq M \tag{67}$$

$$\Delta u_{k+h} = 0, \forall\ h = m, \ldots., p-1 \tag{68}$$

with the optional terminal constraint $E_f\, y_{k+p|k} \leq L_f$.

The solution of the optimal control problem is given by the optimal control sequence:

$$\Delta U'_k = \{\Delta u'_{k|k}, \Delta u'_{k+1|k}, \ldots, \Delta u'_{k+m-1|k}\} \tag{69}$$

the MPC control law can therefore be written as:

$$u_k^{MPC} = \hat{u}_{k-1} + \Delta u'_{k|k} \tag{70}$$

Equation $[E\ G]\left[\begin{matrix} y_{k+j|k} \\ u_{k+j|k} \end{matrix}\right]^T \leq L$ expresses a polyhedral constraint which includes different types of constraints on the output and on the control input.

In the design of a MPC controller it has to be considered that a small prediction horizon p ,together with tight control constraints and high state error weight, implies a more aggressive control with finer tracking performances but with higher control action expense. On the other hand, a high control horizon m implies more optimality of the control, neverthless with higher computational effort. Therefore the choice of the prediction and control horizons values should result from a trade-off involving optimality, tracking performances, computational effort, and memory allocation in the on-board processors.

4.2.3.3.1 Explicit Model Predictive Control

An explicit solution to LTI MPC problems that are constrained can be obtained by solving off-line a multi-parametric Quadratic Program, as it has been shown by Bemporad et al. [28]. The explicit solution is ideal for the case of plants which present processing systems with limited availability of power and memory.

Considering the MPC problem:

$$\min_{U_k}\left\{x_{k+p|k}^T P\, x_{k+p|k}+\sum_{i=0}^{p-1} x_{k+i|k}^T Q\, x_{k+i|k}+u_{k+i}^T R\, u_{k+i}\right\} \tag{71}$$

$$y_{min}\le y_{k+i|k}\le y_{max}, i=1,\dots,p \tag{72}$$

$$u_{min}\le u_{k+i}\le u_{max}, i=1,\dots,m \tag{73}$$

$$x_{k|k}=x_k=\hat{x}(t_k) \tag{74}$$

$$x_{k+i+1|k}=A\,x_{k+i|k}+B\,u_{k+i}, i\ge 0 \tag{75}$$

$$y_{k+i|k}=C\,x_{k+i|k} \tag{76}$$

$$u_{k+i}=K\,x_{k+i|k}, m\le i\le p-1 \tag{77}$$

in which (A, B) is a stabilizable pair. Assuming non active constraints when $i\ge m$ and $i\ge p$, then when the final cost matrix P and gain matrix K are computed from the algebraic Riccati equation, the MPC problem solves exactly the constrained infinite horizon LQR problem. Treating x_k as a vector of parameters θ_k, Bemporad et al. showed that the MPC problem can be rewritten as a multi-parametric Quadratic Program. For this multi-parametric problem, the Karush-Kuhn-Tucker conditions are necessary and sufficient for optimality, which guarantees the existence of a unique solution.

The resulting control law $u^{MPC}=f(\theta_k)$ is continuous and Piece Wise Affine:

$$f(\theta_k)=F^i\theta_k+g^i, if\ H^i\theta_k\le k^i, i=1,\dots,N_{MPC} \tag{78}$$

with N_{MPC} standing for the number of neighbouring convex polytopes (or regions) in which the theta-space is divided. With the control synthesis performed offline, the MPC computational effort reduces eventually to a table lookup. In fact, when a given vector of parameters θ_k is known, the control gains F^i and g^i are automatically determined by the polyhedral region $H^i\theta_k\le k^i$ which contains the parameters vector.

The explicit MPC formulation makes this type of control algorithm especially attractive for plants that suffer from stringent on-line computational requirements. Deciding between an on-line MPC or an explicit MPC controller should in any case derive from the comparison between the computational effort required by the implicit solution and the memory allocation for the lookup table of the explicit solution.

4.3 Planning of Control Maneuvers tests with the Matlab Software Simulator

This section presents some examples of control maneuvers planned with the Matlab Software Simulator described in Section 2.5. The planned control maneuvers are of two main types, either 3 DOF maneuvers in position and Azimuth, in the case of the AM blocked through the additional interface, or 5 DOF maneuvers in position and 3 DOF Attitude, with Yaw, Pitch, Roll provided by the 3-axes joints structure of the AM.

4.3.1 Planning of 3 DOF Position and Azimuth Control Maneuvers

This section reports examples of control maneuvers performed with the Matlab Software Simulator for the 3 DOF configuration of the complete Unit (See Figure (16) in Section (2.4.1.1) for the 3D model representation). Two types of 2D position and Azimuth control maneuvers were planned through the simulator: control maneuvers in standard formulation through PID, and in optimal formulation through explicit MPC. The equations of motion integrated within the software simulator in order to evaluate the Unit state, are :

$$m\ddot{x} = F_{x,ctrl} + F_{x,d} \tag{79}$$

$$m\ddot{y} = F_{y,ctrl} + F_{y,d} \tag{80}$$

$$I_z\ddot{\Theta} = \tau_{\Theta,ctrl} + \tau_{\Theta,d} \tag{81}$$

with m the estimated mass of the complete Unit, $F_{i,ctrl}$ the position control force along the i^{th} axis, $F_{i,d}$ the disturbance force along the i^{th} axis, I_z the estimated moment of inertia about the Azimuth axis, $\tau_{\Theta,ctrl}$ the control torque about the Azimuth axis, $\tau_{\Theta,d}$ the disturbance torque about the Azimuth axis. The three equations are integrated in the software simulator through the Matlab ODE45 function.

4.3.1.1 Standard Control Maneuvers

The version of the Matlab Software Simulator allowing 2 translational and 1 rotational DOF (Azimuth) was firstly employed for the planning of a position and attitude control maneuver with PID position and attitude controllers. The PID controllers were implemented according to the

formulation provided in Section (4.2.3.1), i.e. the basic PID formulation with the addition of a low pass filter for the derivative component noise, an anti-reset wind-up feedback scheme to manage the acutator's saturation, with both attitude and position thrusters presenting a maximum force of approximately 0.38 N, resulting in a max control torque of approximately 0.216 Nm for Azimuth control. The activation sequence of each thruster is managed through a Pulse Width Modulation (PWM) scheme. Table (8) reports parameters and results of the control maneuver, and Figures (62) to (65) present position and position control forces profiles.

Initial Conditions	$X_0 = [0.5\,m, 0.6\,m, 20\,°]$
Reference	$X_r = [0\,m, 0\,m, 30\,°]$
Translation Controller Type	PID w/h low pass filter
Azimuth Controller Type	PID w/h low pass filter
Thrusters Activation Scheme	PWM
Disturbances included	No
Translation Control Settling Time (10%)	~ 75 s
Azimuth Control Settling Time (10 %)	~ 6 s
Final differences between State (ODE45) and Reference	$\delta X_f = [7\text{e-}4\,m, 9\text{e-}4\,m, -\,3\text{e-}5\,°]$

Table 8 – Matlab Software Simulator PID control maneuver in 3 DOF configuration

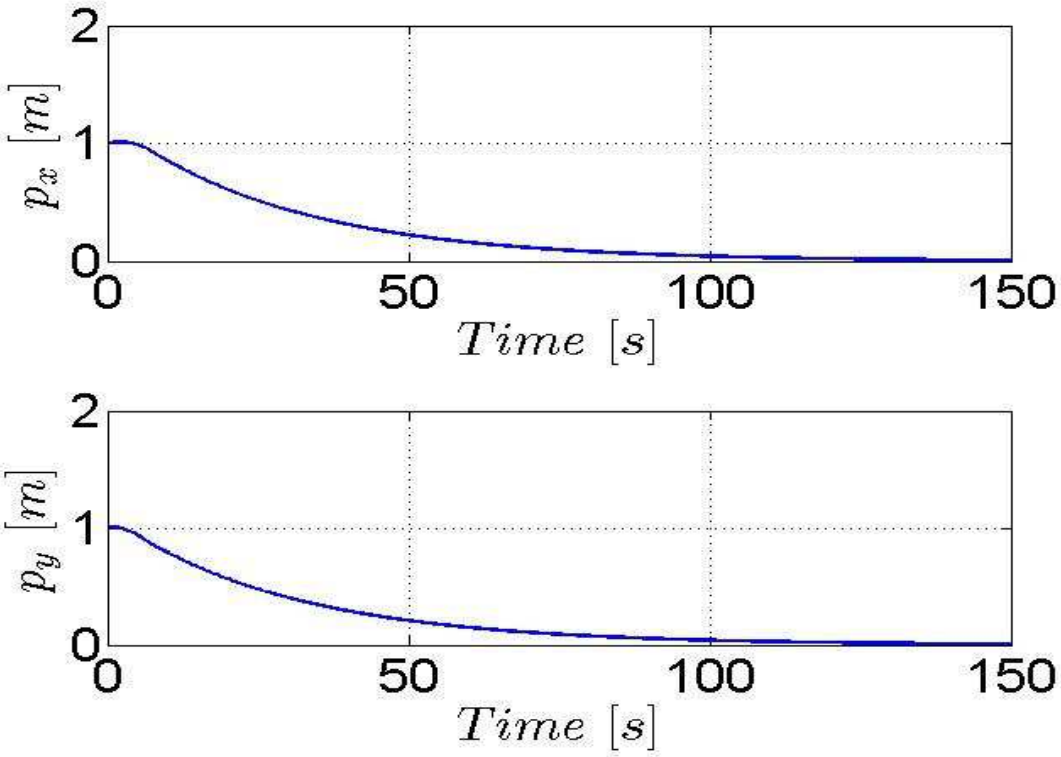

Figure 62 – Matlab Software Simulator 3 DOF PID control maneuver results, position

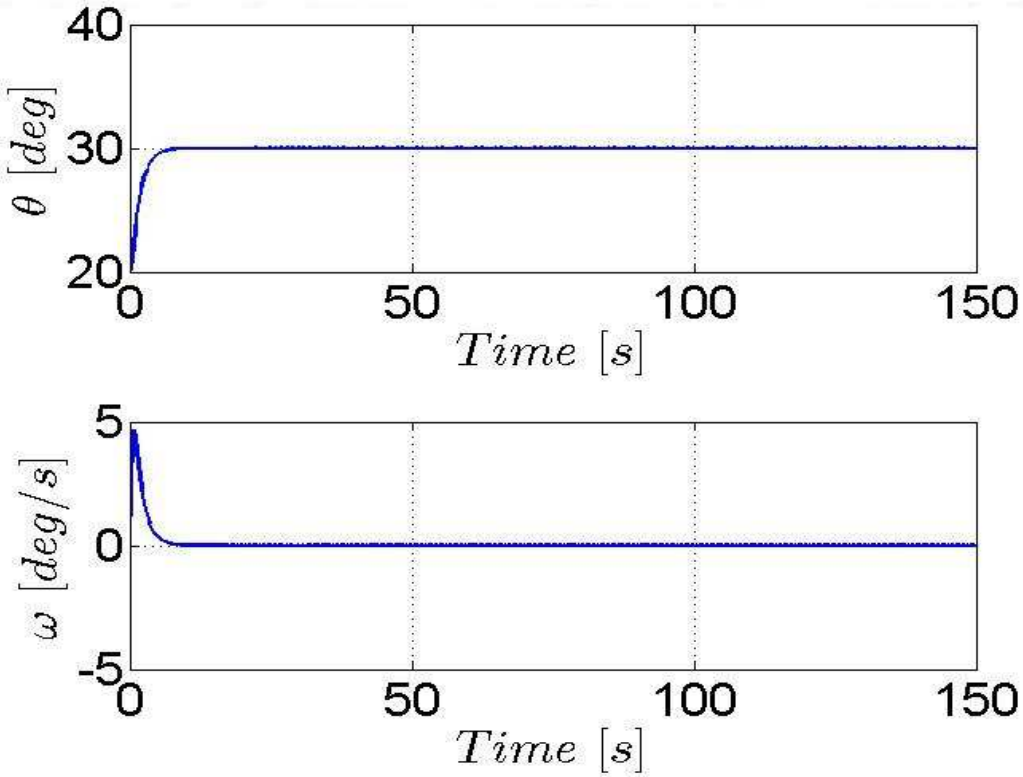

Figure 63 – Matlab Software Simulator 3 DOF PID control maneuver results, Azimuth with angular velocity

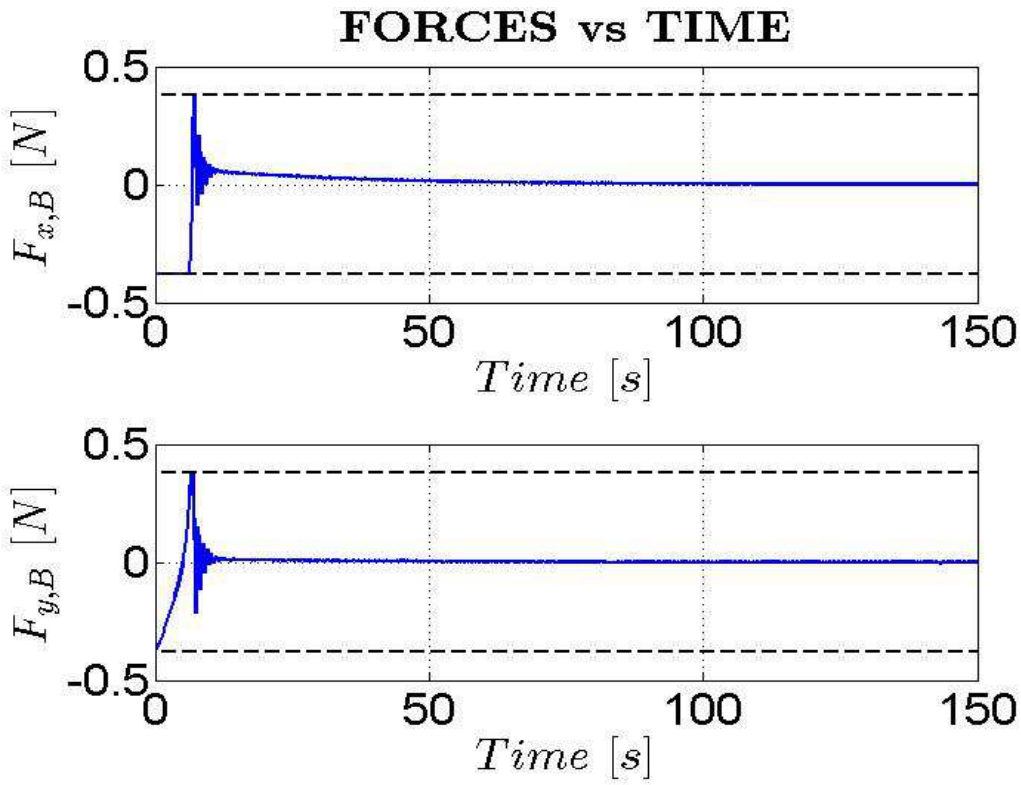

Figure 64 – Matlab Software Simulator 3 DOF PID control maneuver results, position control forces profiles

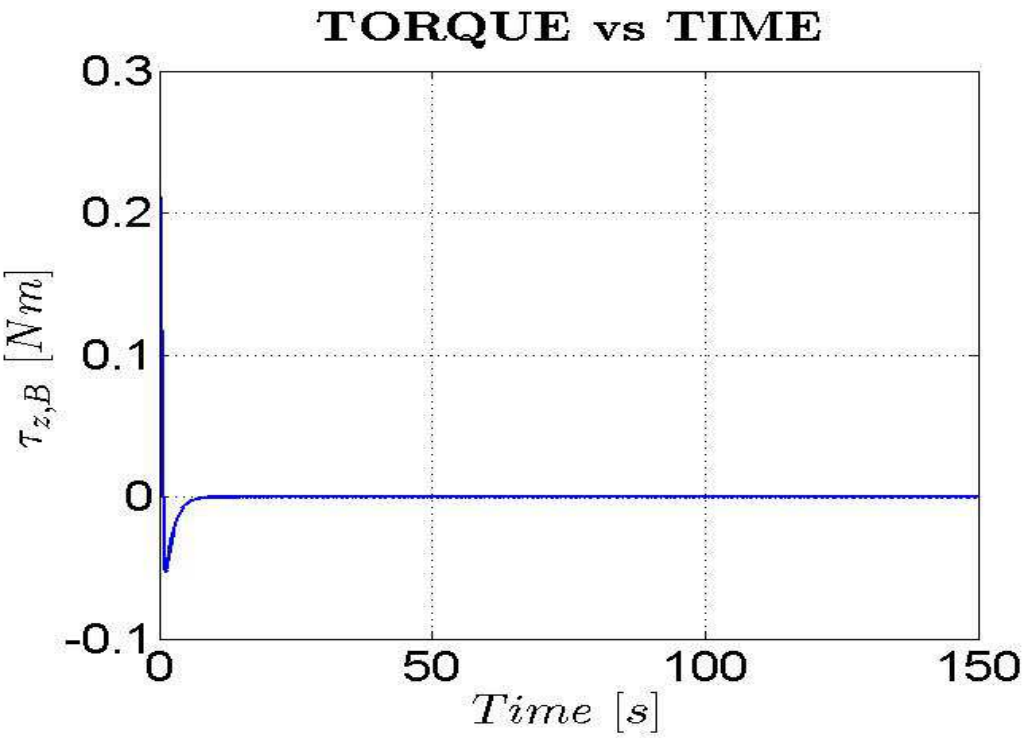

Figure 65 – Matlab Software Simulator 3 DOF PID control maneuver results, Azimith control torque profile

It can be seen from results that both position and azimuth control maneuvers are carried out by the respective PID controllers, with a settling time for position control that is approximately 12 times higher than azimuth control settling time. To make the simulation more realistic, the uncertainty associated to the employed measurement system for position and Azimuth estimation can be reproduced if the system has been characterized or its uncertainty level is known. Moreover disturbances at the predicted level can be introduced in the simulation loop.

4.3.1.2 Optimal Control Maneuvers

In the case of optimal control, an explicit MPC controller was employed in order to verify position and azimuth maneuvers. Tables (9), (10) reports the look-up list as the solution of the optimal control problem associated to the plant that is object of simulation, with prediction horizon $m=2$ and control horizon $p=2$ and default set values for state error and control action weighting matrices, as given by the Hybrid Control Toolbox developed by Bemporad et al.

Explicit MPC control synthesis, x,y translational axes control	
$if -0.8166(x,y)-1.75(\dot{x},\dot{y})\le 1$ $\wedge\ 0.8166(x,y)+1.75(\dot{x},\dot{y})\le 1$ $\wedge\ 0.6124(x,y)+0.4957(\dot{x},\dot{y})\le 1$ $\wedge\ -0.6124(x,y)-0.4957(\dot{x},\dot{y})\le 1$	$u=\left(-0.8166(x,y)-1.75(\dot{x},\dot{y})\right)0.38[N]$
$if\ 0.297(x,y)-0.9333(\dot{x},\dot{y})\le 1$ $\wedge\ -0.8166(x,y)-1.75(\dot{x},\dot{y})\le -1$ $\wedge\ -0.9712(x,y)-2.699(\dot{x},\dot{y})\le -1$	$u=-0.38[N]$
$if -0.3864(x,y)-1.074(\dot{x},\dot{y})\le -1$ $\wedge\ -0.297(x,y)-0.9333(\dot{x},\dot{y})\le -1$	$u=-0.38[N]$
$if\ 0.3864(x,y)+1.074(\dot{x},\dot{y})\le -1$ $\wedge\ 0.297(x,y)+0.9333(\dot{x},\dot{y})\le -1$	$u=0.38[N]$
$if -0.3864(x,y)-1.074(\dot{x},\dot{y})\le 1$ $\wedge\ 0.9712(x,y)+2.699(\dot{x},\dot{y})\le 1$ $\wedge\ -0.6124(x,y)-0.4957(\dot{x},\dot{y})\le -1$	$u=\left(-0.5528(x,y)-1.536(\dot{x},\dot{y})-0.4308\right)$ $0.38[N]$
$if -0.9712(x,y)-2.699(\dot{x},\dot{y})\le 1$ $\wedge\ 0.3864(x,y)+1.074(\dot{x},\dot{y})\le 1$ $\wedge\ 0.6124(x,y)+0.4957(\dot{x},\dot{y})\le -1$	$u=\left(-0.5528(x,y)-1.536(\dot{x},\dot{y})+0.4308\right)$ $0.38[N]$
$if -0.297(x,y)-0.9333(\dot{x},\dot{y})\le 1$ $\wedge\ 0.8166(x,y)+1.75(\dot{x},\dot{y})\le 1$ $\wedge\ 0.9712(x,y)+2.699(\dot{x},\dot{y})\le -1$	$u=0.38[N]$

Table 9 – Explicit MPC loop-up table for 3 DOF control maneuver, position

Explicit MPC control synthesis, Azimuth control	
$if -0.8166\Theta - 1.75\dot{\Theta} \leq 1$ $\wedge\ 0.8166\Theta + 1.75\dot{\Theta} \leq 1$ $\wedge\ 0.6124\Theta + 0.4957\dot{\Theta} \leq 1$ $\wedge\ -0.6124\Theta - 0.4957\dot{\Theta} \leq 1$	$u = \left(-0.8166\Theta - 1.75\dot{\Theta}\right) 0.216\left[Nm\right]$
$if\ 0.297\Theta - 0.9333\dot{\Theta} \leq 1$ $\wedge\ -0.8166\Theta - 1.75\dot{\Theta} \leq -1$ $\wedge\ -0.9712\Theta - 2.699\dot{\Theta} \leq -1$	$u = -0.216\left[Nm\right]$
$if -0.3864\Theta - 1.074\dot{\Theta} \leq -1$ $\wedge\ -0.297\Theta - 0.9333\dot{\Theta} \leq -1$	$u = -0.216\left[Nm\right]$
$if\ 0.3864\Theta + 1.074\dot{\Theta} \leq -1$ $\wedge\ 0.297\Theta + 0.9333\dot{\Theta} \leq -1$	$u = 0.216\left[Nm\right]$
$if -0.3864\Theta - 1.074\dot{\Theta} \leq 1$ $\wedge\ 0.9712\Theta + 2.699\dot{\Theta} \leq 1$ $\wedge\ -0.6124\Theta - 0.4957\dot{\Theta} \leq -1$	$u = \left(-0.5528\Theta - 1.536\dot{\Theta} - 0.4308\right) 0.216\left[Nm\right]$
$if -0.9712\Theta - 2.699\dot{\Theta} \leq 1$ $\wedge\ 0.3864\Theta + 1.074\dot{\Theta} \leq 1$ $\wedge\ 0.6124\Theta + 0.4957\dot{\Theta} \leq -1$	$u = \left(-0.5528\Theta - 1.536\dot{\Theta} + 0.4308\right) 0.216\left[Nm\right]$
$if -0.297\Theta - 0.9333\dot{\Theta} \leq 1$ $\wedge\ 0.8166\Theta + 1.75\dot{\Theta} \leq 1$ $\wedge\ 0.9712\Theta + 2.699\dot{\Theta} \leq -1$	$u = 0.216\left[Nm\right]$

Table 10 – Explicit MPC loop-up table for 3 DOF control maneuver, Azimuth

The look-up table is employed within the simulation loop in order to compute at each time step the required control action according to the current state of the plant. Wrt to the previously presented simulation, in this case an uncertainy model of the employed measurement system has been added to the state output by the ODE45 function, as a random measurement noise contained within a predetermined interval, according to the max uncertainty values obtained from the EKF output with integrated vision and OFS navigation systems (See Section (3.1.2)). Moreover a costant disturbance has been added to the translational axes at the level obtained from Finite Element Analysis on the 3D model of the test table (Section (2.6.2)), i.e. 0.001 N. Table (11) reports the parameters of the simulation. Simulation results are shown in Figures (66) to (69)

Initial Conditions	$X_0 = \left[0.3\,m, 0.3\,m, 10^\circ\right]$

Reference	$X_r = [0\,m, 0\,m, 0\,°]$
Translation Controller Type	Explicit MPC
Azimuth Controller Type	Explicit MPC
Thrusters Activation Scheme	PWM
Disturbances included	Yes
Translation Control Settling Time (10%)	~ 20 s
Azimuth Control Settling Time (10 %)	~ 13 s
Final differences between State (ODE45) and Reference	$\delta X_f = [0.01\,m, 0.011\,m, -1\,°]$

Table 11 – Matlab Software Simulator Explicit MPC control maneuver in 3 DOF configuration

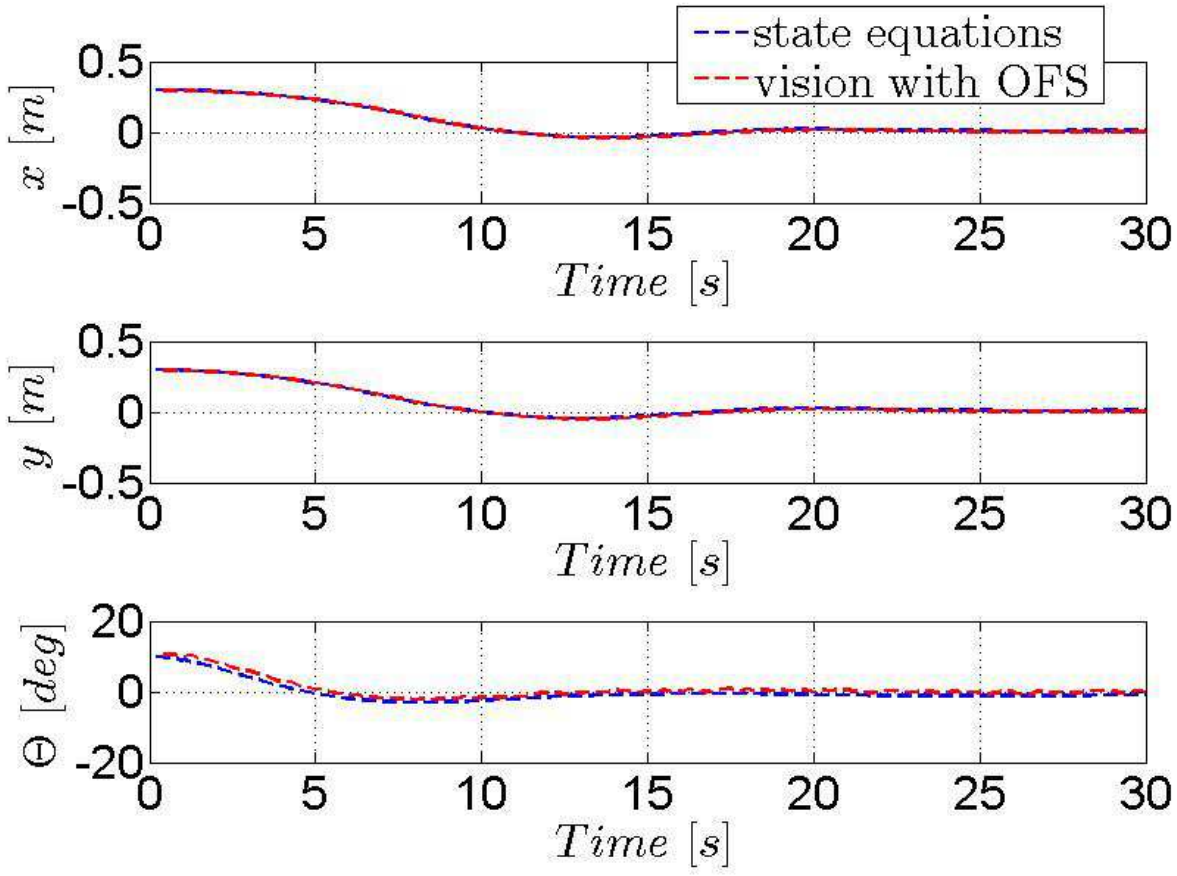

Figure 66 – Matlab Software Simulator 3 DOF explicit MPC control maneuver results, state (ODE45) and simulated measurement system estimates profiles

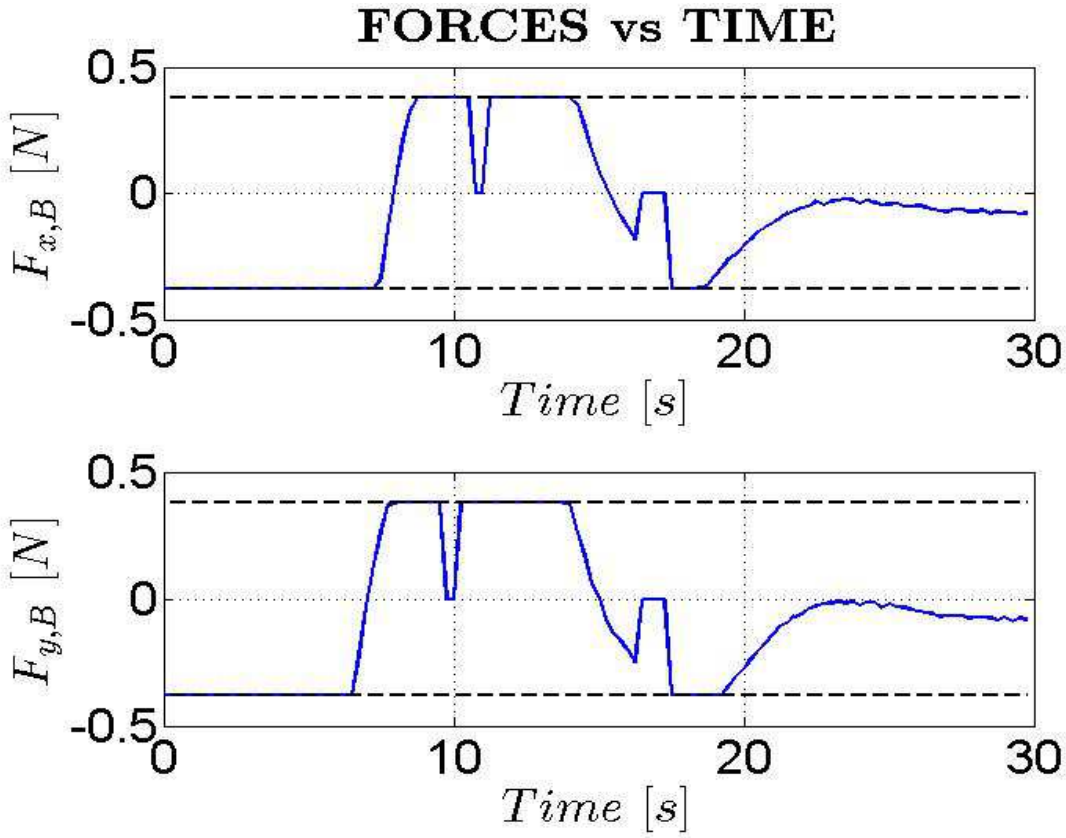

Figure 67 – Matlab Software Simulator 3 DOF explicit MPC control maneuver results, position control forces profiles

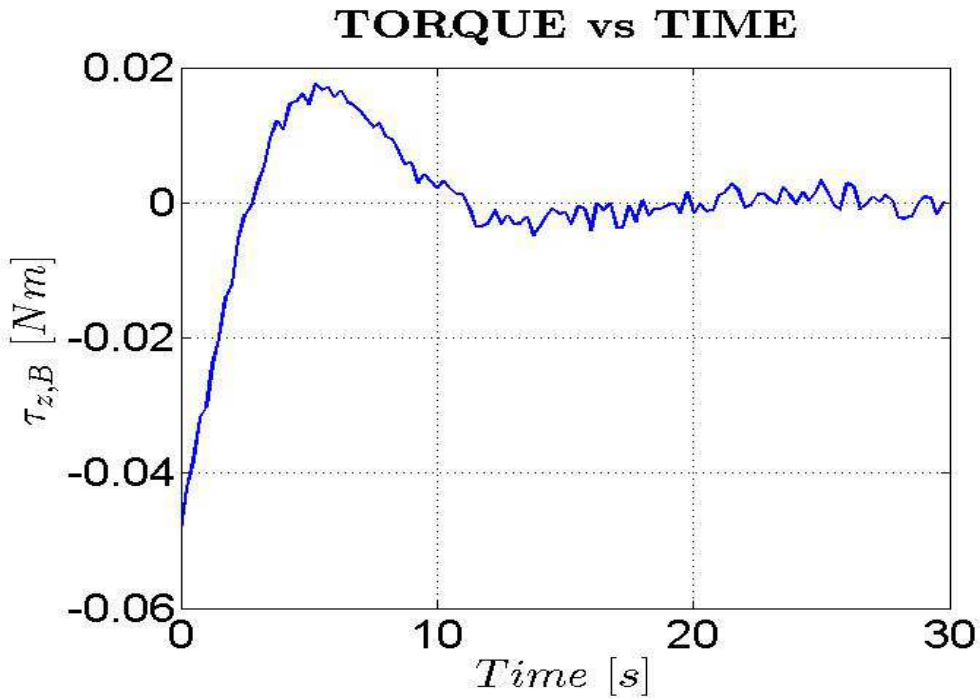

Figure 68 – Matlab Software Simulator 3 DOF explicit MPC control maneuver results, Azimuth control torque profile

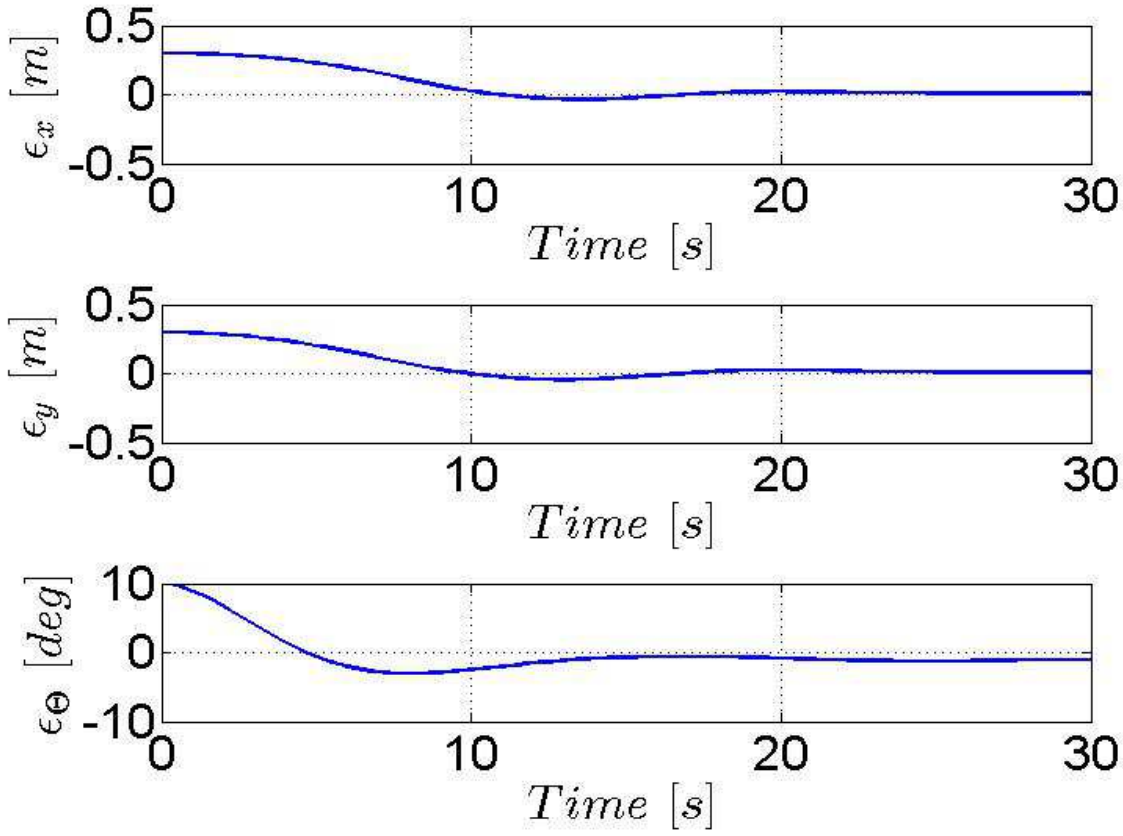

Figure 69 – Matlab Software Simulator 3 DOF explicit MPC control maneuver results, differences between state (ODE45) and references profiles

It can be seen from the results that the Explicit MPC controllers for position and Azimuth are able to track the state reference. However wrt to the previous case with PID controllers, the tracking accuracy is decreased to levels that are similar to the accuracy margins estimated for the measurement system with integrated vision and OFS systems.

4.3.2 Planning of 5 DOF Position and Azimuth Control Maneuvers

For the planning of control maneuvers with 2D translational and Yaw, Pitch, and Roll DOF, the same type of control algorithms, e.g. PID and Explicit MPC, employed for 3 DOF control maneuvers, can be implemented. However when performing control synthesis with a controller requiring a linear model such as explicit MPC, the applicability of the controller is limited by the fact taht the 3 DOF attitude non linear dynamics have to be linearized in the proximity of the state reference.

In 5 DOF maneuvers it is required that the position control actions are executed only when the Roll and Pitch DOF are near 0°, otherwise the control force provided by position control thrusters is lost through a not neglectable component along the vertical axis.

Figures (70), (71) present the results of a 3 DOF attitude control maneuver performed with the first protoype of the AM, an activity to which I could give a small support at the beginning of my PhD. The test consisted in a trajectory tracking repointing maneuver, in which the attitude trajectory was determined through pseudospectral methods with active constraints and the employment of attitude dynamics equations expressed through quaternions. In this test, the encoders on board the joints axes of the AM were employed as fiducial reference for Euler angles and angular velocity estimations through Kalman filtering. The trajectory tracking errors for Roll Pitch Yaw resulted in the tests always comprised between ± 0.5°

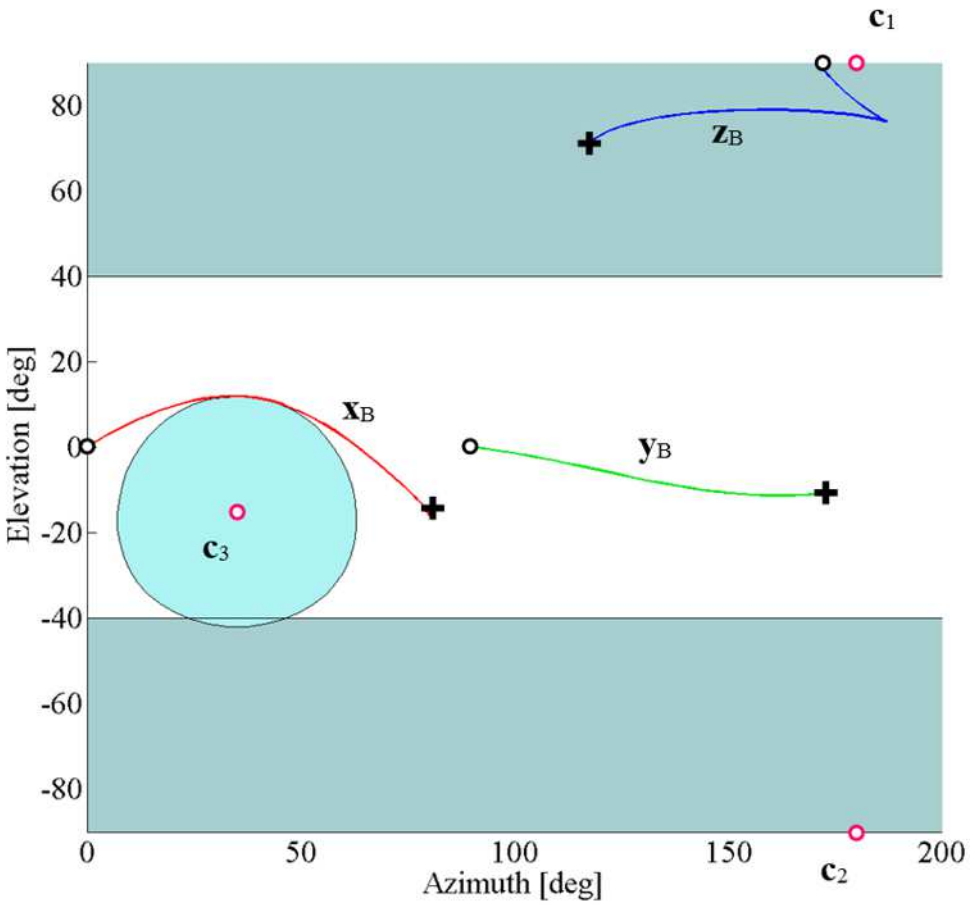

Figure 70 – Attitude Reference Trajectory from pseudospectral optimization, keep-out cones in cyan

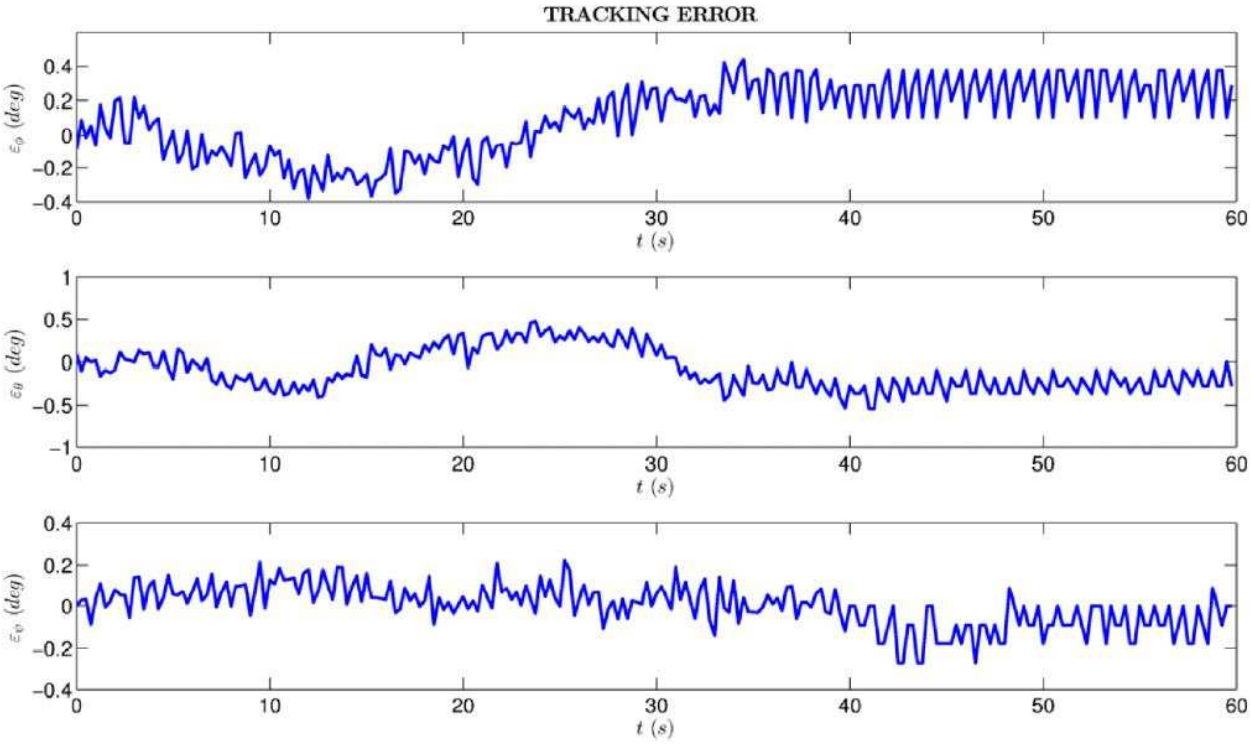

Figure 71 – Roll, Pitch, Yaw trajectory tracking errors

5 SCENARIO OF INSPECTION OF A NON COOPERATIVE TARGET SPACECRAFT IN LEO THROUGH PASSIVE RELATIVE ORBIT ACQUISITION

5.1 Inspection Scenario Overview

This chapter presents the results from the investigation of a scenario related to the employment of Passive Relative Orbits for the inspection of a non cooperative target spacecraft, as it is generally the case for no more functioning satellites that have not been removed from their orbits.
In particular, the study is focused on assessing the performances in the employment of relative circular orbits for inspection purposes, which implies the satisfaction of a predetermined set of initial conditions that allow the inspection spacecraft to maintain a fixed distance wrt to the non cooperative target satellite that must be inspected. One of the main goals of this analysis is the subsequent reproduction of the satellite relative dynamics in scale through the SPARTANS simulator.
In particular, a specific scenario has been considered of interest for this investigation, in terms of evaluating the performances of LQR and MPC controllers in the acquisition and mainteinance of a passive relative orbit of a generic spacecraft for the inspection of the Envisat satellite.
The Envisat (Environmental Satellite) satellite is an Earth-observation spacecraft which was operated by ESA and built by Airbus Defence and Space. It was launched in 2002 with 10 instruments on board, designed to acquire important information regarding Earth meteorology, climatology, environment, atmospheric chemestry, vegetation, hydrology, ocean and ice evolution. After launch, the spacecraft was inserted in a sun-synchronous orbit at approximately 790 km of altitude and an inclination of 98 °.
Compared to average satellites, the Envisat spacecraft presents very high dimensions, reaching 25 x 20 x 7 m in full deployment, with its solar panels occupying an area of 70 m^2.
After 10 years of operations in orbit, in April 2012 the ESA ground segment of Envisat lost contact with the satellite's communication system, and since then it was never more able to acquire it back. The presence of such a large, unmonitored spacecraft in its nominal orbit constitutes a serious threat in terms of collisions with other satellites, since at its nominal altitude and inclination there is a probability that every year at least two satellites could pass below a distance of 200 m from it.
A collision between a spacecraft and Envisat can produce a very large debris cloud, which in turn can trigger more and more collisions with other spacecraft with increasing rate and number of newly produced debris, resulting in what could become a chain reaction with catastrophic

consequences. Furthermore it is foreseen that passive atmospheric re-entry of Envisat due to drag forces would occur in approximately 150 years, leaving sufficient time for such collisions to be likely to happen.

Figure 72 – Envisat during integration in ESTEC in 2000 (ESA)

It is therefore currently being envisioned a mission for the removal of Envisat from its nominal orbit. The designed spacecraft would be approaching Envisat, monitoring it in a passive relative orbit in order to assess its overall conditions, and it would subsequently perform a capture maneuver at one of its appendices, in order to eventually drag it away from its orbit.
The analysis presented in this chapter is focused on the manuever for the acquisition and mainteinance of a passive relative orbit for the inspection of the target satellite. The analysis has been performed with the fundamental assumption that the relative state between the inspection and the target satellite is available below a sufficiently low distance between the two, through a relative measurement system that is assumed to be installed on board the inspection satellite. This assumption is primarily based on results from recent numerical investigations related to this subject. In particular, a recent study [35] considering a chaser and a target satellite, has shown that by employing a vision system based on a sparse stereovision algorithm on board the chaser satellite, the Body frame of the target spacecraft can be re-established by identifying its natural features, and subsequently its translational and rotational states can be estimated through Kalman filtering of the measurements. Numerical simulations for a target spacecraft in torque-free tumbling with maximum initial angular velocity component of 3 °/s have shown that the proposed system reaches accuracies in the order of 6 mm and 0.2 mm/s for the translational state estimation, and in the order of 0.1° and 0.03 °/s for the rotational state estimation, considering a target in the range of 10 m distance from the chaser, and with general dimensions that are approximately one order of magnitude lower than those of Envisat.

5.2 Definition of Relative Conditions and Disturbances

The fundamental condition in the proposed inspection scenario is related to the relative circular orbit. Without external disturbances on the satellites' motion, the satisfaction of a certain set of predetermined initial conditions produces a certain type of relative orbit that is maintained in time, unless for errors in the initial conditions.
In the case of the relative circular orbit, the inspection satellite motion has to satisfy the following relations between relative initial conditions, wrt to the target spacecraft:

$$\delta \dot{y}_0 = -2n\delta x_0 \tag{82}$$

$$\delta y_0 = 2\frac{\delta \dot{x}_0}{n} \tag{83}$$

$$\delta z_0 = \pm \sqrt{3}\, \delta x_0 \tag{84}$$

$$\delta \dot{z}_0 = \pm \sqrt{3}\, \delta \dot{x}_0 \tag{85}$$

These conditons are obtained by imposing that $\delta x^2 + \delta y^2 + \delta z^2 = r^2$ in the solution of the HCW equations, with r the radius of the formation. The first condition corresponds to the elimination of the secular term, while the other three derive from the circularity of the relative orbit, with the last two conditions to be taken with the same sign. The signs option implies that the relative orbit plane is inclined of ± 60° wrt to the x-y plane of the LVLH frame.

Given these constraints on initial relative conditions, in the presence of external disturbances in the satellites motions, and in presence of errors in the constraints satisfaction at the moment of acquisition of the relative circular orbit, there is a more or less rapid and dramatic modification in the initial geometry of the relative orbit.

With the inspection spacecraft motion initially taking place in a generic relative orbit wrt to the target satellite, the satisfaction of the constraints on initial conditions of the inspection relative orbit depends heavily on the precision with which the orbit acquisition maneuver is performed, and therefore on the employed controller. With regards to disturbances, they are treated by periodically activating the orbital control in order to re-establish the initial, desired value of the distance between the inspection and the target spacecraft, when the distance exceeds a certain threshold value.

In this investigation the only disturbances that are considered in software simulations are those related to differential drag forces, and those deriving from the J2 Earth gravitational potential term. The disturbances caused by the J3 Earth gravitational potential term have been neglected by virtue of the small eccentricity of the target and inspector orbits.

5.2.1 Relative Acceleration Disturbance due to J2

The relative effects caused by the J2 Earth gravity potential term are modeled through the gradient of the J2 potential field [36]. The linear relative J2 disturbance in the LVLH frame is given by multiplication of the relative position vector expressed in the LVLH frame by the J2 gradient matrix:

$$\delta \vec{a}_{J2} = \nabla\ J_2\, \delta \vec{x} \tag{86}$$

with the J2 gradient matrix given by:

$$\nabla J_2 = -6\mu_E J_2 \frac{R_e^2}{r_{ref}^5} \begin{bmatrix} 1-3\sin^2 i \sin^2\theta & \sin^2 i \sin 2\theta & \sin 2i \sin\theta \\ \sin^2 i \sin 2\theta & -\frac{1}{4}-\sin^2 i\left(\frac{1}{2}-\frac{7}{4}\sin^2\theta\right) & -\frac{\sin 2i \cos\theta}{4} \\ \sin 2i \sin\theta & -\frac{\sin 2i \cos\theta}{4} & -\frac{3}{4}+\sin^2 i\left(\frac{1}{2}+\frac{5}{4}\sin^2\theta\right) \end{bmatrix} \quad (87)$$

with r_{ref} the radius of the reference orbit, which in this case corresponds to the target orbit, and i , $\theta = \omega + f$ the inclination and true latitude of the reference satellite, respectively.

5.2.2 Relative Acceleration Disturbance due to Drag Force

For the relative acceleration disturbance due to the drag force, an orbit-averaged simplified formulation [37] is employed in this investigation, expressed in the LVLH frame as:

$$\delta\vec{a}_{drag} = -\frac{1}{2}\left(\frac{1}{\beta_I}-\frac{1}{\beta_T}\right) a n^2 \tilde{\sigma}_2 \begin{bmatrix} 0 \\ 1 \\ 0 \end{bmatrix} - \frac{1}{2}\frac{1}{\beta_I} n^2 \tilde{\sigma}_2 \begin{bmatrix} 0 & -1 & 0 \\ 2 & 0 & 0 \\ 0 & 0 & 0 \end{bmatrix} \begin{bmatrix} \delta x \\ \delta y \\ \delta z \end{bmatrix} - \frac{1}{2}\frac{1}{\beta_I} n \tilde{\sigma}_1 \begin{bmatrix} 1 & 0 & 0 \\ 0 & 2 & 0 \\ 0 & 0 & 1 \end{bmatrix} \begin{bmatrix} \delta \dot{x} \\ \delta \dot{y} \\ \delta \dot{z} \end{bmatrix} \quad (88)$$

with:

$$\tilde{\sigma}_1 = 1 - \hat{\omega}_e \cos i \quad (89)$$

$$\tilde{\sigma}_2 = 1 - 2\hat{\omega}_e \cos i \quad (90)$$

$$\hat{\omega}_e = \frac{\omega_e}{n} \quad (91)$$

with ω_e the Earth's rotation rate and mean motion n and inclination i referred to the reference orbit, i.e. the target spacecraft orbit.

Parameters β_I and β_T represent the dimensionless ballistic coefficient of the inspection and target spacecraft, respectively, defined as:

$$\beta = \left(\rho \frac{C_d A}{m} r\right)^{-1} \quad (92)$$

with ρ the local atmospheric density, C_d the drag coefficient of the spacecraft, A the cross sectional area of the spacecraft, m the mass of the spacecraft, r the radius of the spacecraft orbit.

5.3 Overview of the Formation Flight Software Simulator in Matlab

In order to test the aforementioned control techniques in the context of the proposed scenario, a software simulator in Matlab has been updated and employed. The simulator in its fundamental structure had already been developed in the context of the SPARTANS research team, with the goal of the testing and validating GNC strategies for general formation flying applications. The simulator presents a modular structure, allowing different elements of the software to be designed separately and to subsequently evaluate its efficiency and robustness.

The main modules of the software simulator consists in the Dynamic Propagator module, the Sensors module, the Navigation module, the Guidance module, the Control module, the Actuators module, the Environment module.

The Dynamic Propagator module is in charge of estimating the dynamic evolution of the plant, by integrating the system of differential equations that models the system dynamic behaviour, expressed in the form:

$$\dot{\vec{X}}(t)=\vec{F}\left(\vec{X}(t),t,\vec{U}_{comm}(t),\vec{U}_d(t)\right) \tag{93}$$

with $\vec{X}(t)$ the dynamic state of the plant, comprising environment, sensors, actuators, attitude and orbital states, both absolute and relative, for each satellite in the formation, $\vec{U_{comm}}(t)$ the control vector formed by position and attitude accelerations to be imposed to the system through the actuators, $U_d(t)$ the disturbance acceleration vector. The input of the Dynamic Propagator is given by the plant state $\vec{X}(t_k)$ at time step t_k, the computed control accelerations $\vec{U}_{comm}(t)$, the disturbance accelerations $\vec{U}_d(t)$. The output of the Dynamic Propagator is given by the plant state $\vec{X}(t_{k+1})$ at time step $t_{k+1}=t_k+\Delta T_S$, with ΔT_S the simulation time step. The Dynamic Propagator module performs motion propagation through fixed time step integration of the system of six differential equations that describe the satellites motion, expressed

in the cartesian Earth Centered Inertial frame of reference, with time as independent variable.
The Sensors module is intended, through a proper model of the employed sensors, to reproduce the measurements of the system dynamic state as they are most likely to result. The measurement model can comprise a bias and a white noise components to be added to the plant state.
The Navigation module is in charge of performing the estimation of the current state of the system by employing the measurements that are output by the Sensors module, and a set of equations describing the dynamic behaviour of the system and the behaviour of the sensors. Current state estimation can be performed by the module through different estimation techniques, e.g. Kalman filtering, Bayessian estimation.
The Guidance module is in charge of computing the desired trajectories as reference for the state for each spacecraft of the formation, considering disturbances acting on the system, the current estimated state of the system, the actuators characteristics.
The Control module has the function of computing the control actions $\vec{U}_{calc}(t)$ that have to be performed by the actuators with the purpose of making the current estimated system state $\vec{\hat{X}}(t)$ reach the reference state $\vec{X}(t)$. The input of the Control module is given by estimated system state $\vec{\hat{X}}(t)$ at time t_k , the reference trajectory $\vec{X}(t_k)$ at time t_k , the disturbances acting on the system, and the actuators constraints.
The Actuators module is in charge of determining the actual control action that is going to be executed within the simulation. This module takes as input the control action vector $\vec{U}_{calc}(t_k)$ output by the Control module at time step t_k , and the plant dynamic state $\vec{X}(t_k)$ at time t_k , in order to determine through the model equations of the actuators describing their behaviour, the control action vector $\vec{U}_{comm}(t_k)$ to be executed by the actuators at time step t_k .
The Environment module is in charge of computing the perturbative accelerations, acting on the satellites of the formation, caused by interaction with the environment.
The formation flight simulator has been developed in Matlab through Object Oriented Programming (OOP). Amongst the most important characteristics of OOP there is the concept of data encapsulation, which implies the presence of a close link between data items and methods. Objects of a given type are generally instances of a class, which is defined in order to provide internal definition as well as public interface of its objects. The OOP presents the following advantages wrt to procedural programming: reduced program complexity, modularity, increased ease in performing program modifications, extensibility, and re-usability of objects for different programs.

The formation flight simulator in Matlab is composed of three main sections. The first section has a pre-processing function, defining and initializing all objects, structures and variables of the scenario. The second section consists of the main loop with a sequence of update of all modules at each simulation time step. The third section consists of the post-processing with final computations, and the saving and visualization of results. For each class, the interface functions can be divided in setup functions, used to initialize the objects during pre-processing, update and data printing functions used in the main loop to update the objects and visualize data in the command window at the current simulation time step, and post-processing functions, which are used to save results and create plots. A Set-Up m-file is employed in order to define the parameters of the scenario, i.e. absolute and relative dynamic states of the satellites, type of sensors, actuators, GNC strategy, etc.

5.4 Matlab Simulations Results

This section reports the results from the simulations performed for the proposed inspection scenario. Three main types of simulations have been performed. The first type consisted in the inspection scenario of the Envisat satellite with the inspection passive relative orbit acquired through a pre-computed 2 impulses maneuver, and orbit correction maneuvers performed with LQR and MPC controllers. The second type of simulations consisted in both the inspection orbit acquisition and correction maneuvers performed with the LQR controller, and the third type of simulations consisted in both the inspection orbit acquisition and correction maneuvers performed with the MPC controller.

The three types of simulations were performed with the same set of initial relative conditions between the inspection and the target satellite, and the same set of final conditions at the acquisition of the relative orbit for the inspection. In all three cases the final inspection orbit is circular with a radius of approximately 40 m. For the estimation of the relative disturbance due to drag, in the case of Envisat its nominal data have been considered in order to determine its dimensionless ballistic coefficient, while in the case of the inspection satellite a hypotetic value has been taken, representative for a spacecraft with average size and mass.

In both types of simulations, the initial relative orbit consists in an ellipse with semi-major axis of approximately 120 m and semi-minor axis of approximately 60 m, i.e. a flyaround orbit acquired through a previous initial relative approach. From the flyaround orbit, the inspection satellite is then directly inserted in the inspection orbit (Figure (73)).

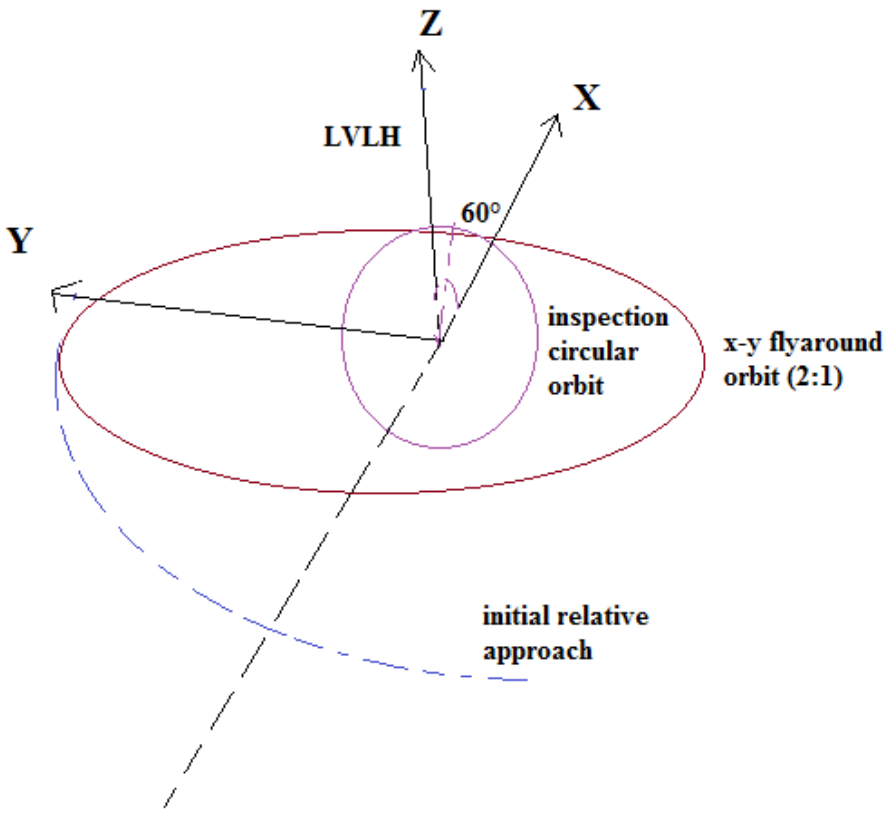

Figure 73 – inspection scenario

During the inspection phase, the radius of the passive relative orbit is intended to be maintained within approximately ± 2 meters apart from its nominal value. When a certain threshold value is exceeded, the controller is re-activated in order to reacquire the original relative orbit with a slight rephasing, with a set point correspondent to the the current relative value in the y axis of the LVLH frame, and δx and δz obtained consequently from the condition of circular orbit with the target radius.

Figure (74) shows in order 1) the initial relative orbit, 2) the first inspection circular relative orbit with plane at +60° wrt to the x-y plane of the LVLH frame, which has to be reached through the acquisition maneuver from the flyaround orbit, 3) the second inspection circular relative orbit, with plane at -60° wrt to the x-y plane of the LVLH frame, to be reached from the first inspection orbit.

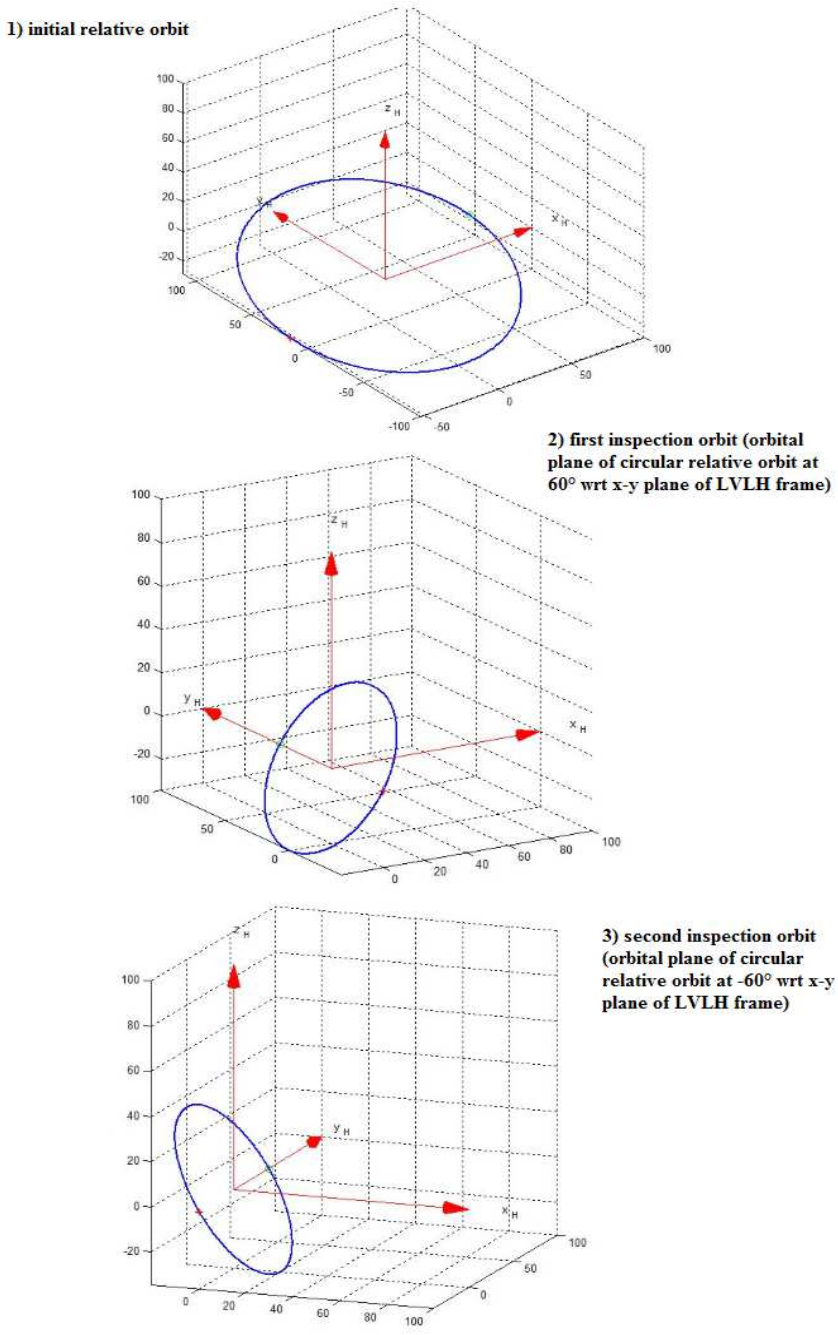

Figure 74 – initial and inspection relative orbits (meter as axes unit) in LVLH frame

For both simulations the state and output equations matrices, as defined in equations (52), (53) in Section (4.2.3), have been derived through finite differences discretization of the HCW equations, with sampling time $T_s = 1\,s$, resulting in:

$$A=\begin{bmatrix} 1 & 0 & 0 & 1 & 0 & 0 \\ 0 & 1 & 0 & 0 & 1 & 0 \\ 0 & 0 & 1 & 0 & 0 & 1 \\ 3n^2 & 0 & 0 & 1 & 2n & 0 \\ 0 & 0 & 0 & -2n & 1 & 0 \\ 0 & 0 & -n^2 & 0 & 0 & 1 \end{bmatrix} \tag{94}$$

$$B=\begin{bmatrix} 0 & 0 & 0 \\ 0 & 0 & 0 \\ 0 & 0 & 0 \\ 1 & 0 & 0 \\ 0 & 1 & 0 \\ 0 & 0 & 1 \end{bmatrix} \tag{95}$$

$$C=\begin{bmatrix} 1 & 0 & 0 & 0 & 0 & 0 \\ 0 & 1 & 0 & 0 & 0 & 0 \\ 0 & 0 & 1 & 0 & 0 & 0 \end{bmatrix} \tag{96}$$

with n the mean motion of the target orbit.

As arleady pointed out a control scheme has been introduced in the simulations in order to compensate relative orbit errors and put the inspector spacecraft back into the originally intended Passive Relative Orbit. Considering a reference radius of the relative circular orbit, when the current measured radius value exceeds a certain threshold, orbital control is reactivated with a reference position having the same y coordinate in the LVLH frame at the moment in which the trheshold is exceeded, and the coordinates in the x , z axes that are obtained from the condition of relative orbit radius being equal to the reference value R_{ref} . The new relative position reference can therefore be expressed as:

$$\delta p_{ref,curr}=\left[\delta x_{ref,curr}, \delta y_{TH}, \delta z_{ref,curr}\right]=\left[\delta x_{ref,curr}, \delta y_{TH}, \sqrt{3}\delta x_{ref,curr}\right] \tag{97}$$

with

$$\delta x_{ref,curr}=\frac{\sqrt{R_{ref}^2-\delta y_{TH}^2}}{2} \tag{98}$$

in which δy_{TH} is the value of the y coordinate at the time step of control activation for relative orbit correction.

5.4.1 Simulations Results for Inspection Orbit Acquisition through 2 Impulses Maneuver and Inspection Orbit Correction through LQR and MPC Control

This section reports the results for the simulation of the inspection orbit acquisition performed with a 2 impulses maneuver and the inspection orbit automatic correction maneuver executed with a LQR and with a MPC controller. Table (12) reports the set of relative conditions at the beginning of the simulation, the relative conditions at the beginning of the acquisition maneuver, and the relative conditions at the acquisition of the inspection relative orbit.

Initial conditions at the initial relative orbit	Initial conditions at the beginning of the acquisition maneuver	Initial conditions at the acquisition of the inspection orbit
$\delta x_0 = 52.7\,m$	$\delta x_0 = 52.3\,m$	$\delta x_0 = 20\,m$
$\delta y_0 = -\,6.4\,m$	$\delta y_0 = -\,12.1\,m$	$\delta y_0 = -\,7.1\,m$
$\delta z_0 = 28.1\,m$	$\delta z_0 = 28\,m$	$\delta z_0 = \sqrt{3}\,\delta x_0\,m$
$\delta \dot{x}_0 = -\,0.006\,m/s$	$\delta \dot{x}_0 = -\,0.009\,m/s$	$\delta \dot{x}_0 = \delta \dot{y}_0\,n/2\,m/s$
$\delta \dot{y}_0 = -\,2\,\delta x_0\,n\,m/s$	$\delta \dot{y}_0 = -\,0.109\,m/s$	$\delta \dot{y}_0 = -\,2\,\delta x_0\,n\,m/s$
$\delta \dot{z}_0 = -\,2e\text{-}4\,m/s$	$\delta \dot{z}_0 = -\,0.002\,m/s$	$\delta \dot{z}_0 = \sqrt{3}\,\delta \dot{x}_0\,m/s$

Table 12 – Initial conditions of simulation, orbit acquisition through 2 impulses maneuver

The 2 impulses manuever was planned with an iterative approach through the MATLAB software simulator in order to find the delta-v to be applied to the inspection satellite, at the beginning of the transfer maneuver, so that the transfer relative orbit brings it to the location of insertion in the inspection orbit. The disturbances inserted in the simulation consisted in those induced by differential drag and J2 with the formulations provided in the previous sections.
Results from the simulations are reported in Figures (75) to (78), in the alternate cases of orbit correction maneuver performed with the LQR controller and the MPC controller.
The synthesis of the LQR controller was performed with a preliminary manual tuning, with the goal of selecting convenient values for the error state and control action weighting matrix. The control synthesis with the selected Q and R matrices resulted in the following LQR feedback gain matrix:

$$K_{LQR}=\begin{bmatrix} 7.8921\text{e-}4 & -1.1608\text{e-}5 & 0 & 0.0401 & 1.214\text{e-}5 & 0 \\ 1.1608\text{e-}5 & 7.8894\text{e-}4 & 0 & -1.2045\text{e-}5 & 0.0401 & 0 \\ 0 & 0 & 7.8894\text{e-}4 & 0 & 0 & 0.0401 \end{bmatrix}$$

For the LQR controller, a maximum acceleration value of 0.1 m/s^2 per sampling time step was considered for the x, y, z actuations axes.

In order to select the parameters of the MPC controller, a preliminary analysis was conducted in order to perform a manual tuning, which was driven mostly by the minimization of the expended control action. Eventually, the analysis led to the selection of the default parameters assigned by the MPC function of the MATLAB optimal control toolbox which was employed in order to implement the controller. In particular, the MPC control synthesis was performed with a prediction horizon $p=10$ and a control horizon $m=2$. The constraint of maximum control action was imposed for all three LVLH axes with a value of 3e-2 m/s^2, since preliminary analyses showed that 0.1 m/s^2 led to a very high control action expense without significant improvement of tracking performances, and as for the simulations performed with the LQR controller, differential disturbances induced by J2 and drag were considered as acting on the satellites relative motion.

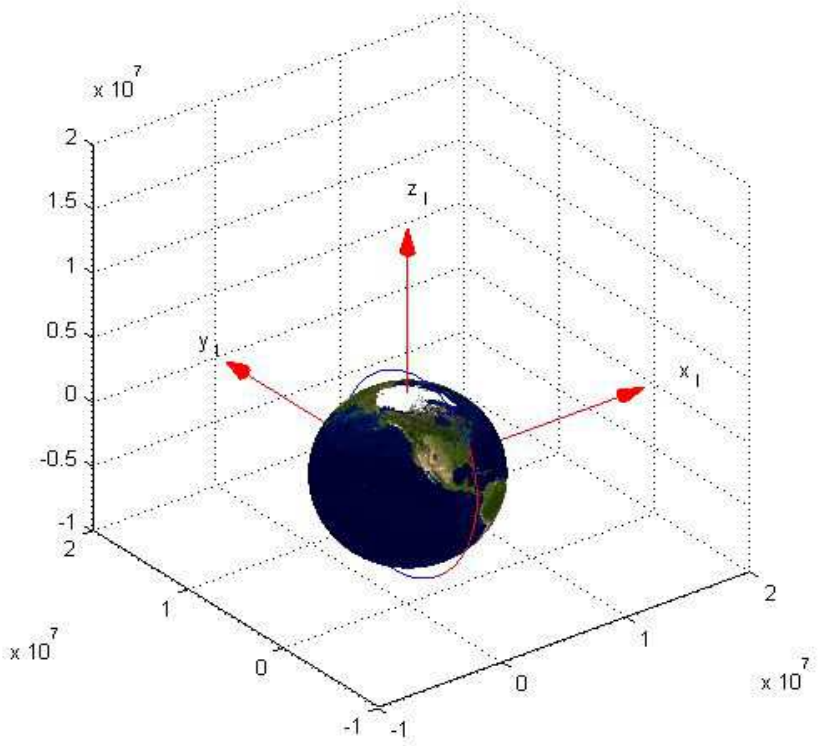

Figure 75 – Absolute orbit (meter as axes unit) of target satellite

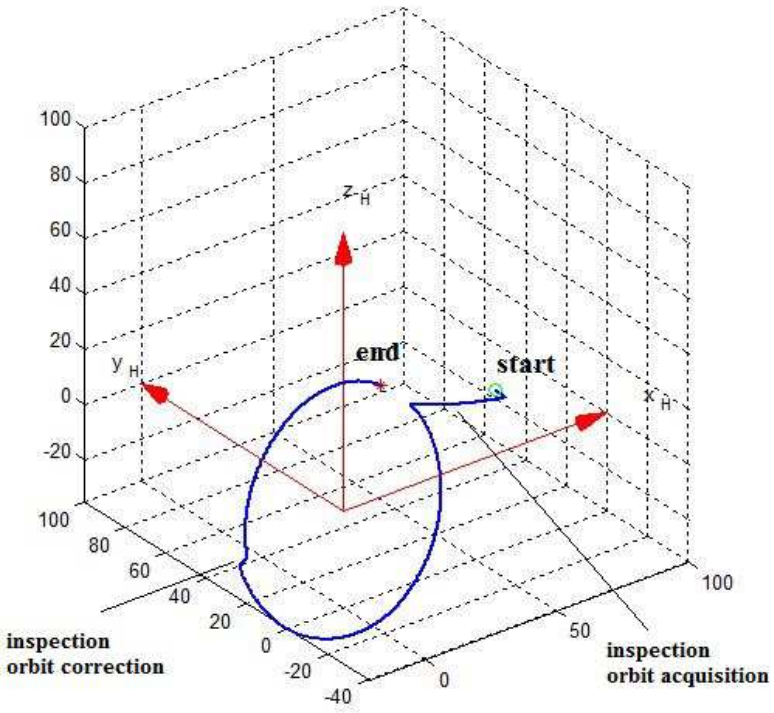

Figure 76 – relative orbit (meter as axes unit) in LVLH frame, inspection orbit acquisition through 2 impulses maneuver and correction through LQR control (green circle indicates start of simulation, red star indicates end)

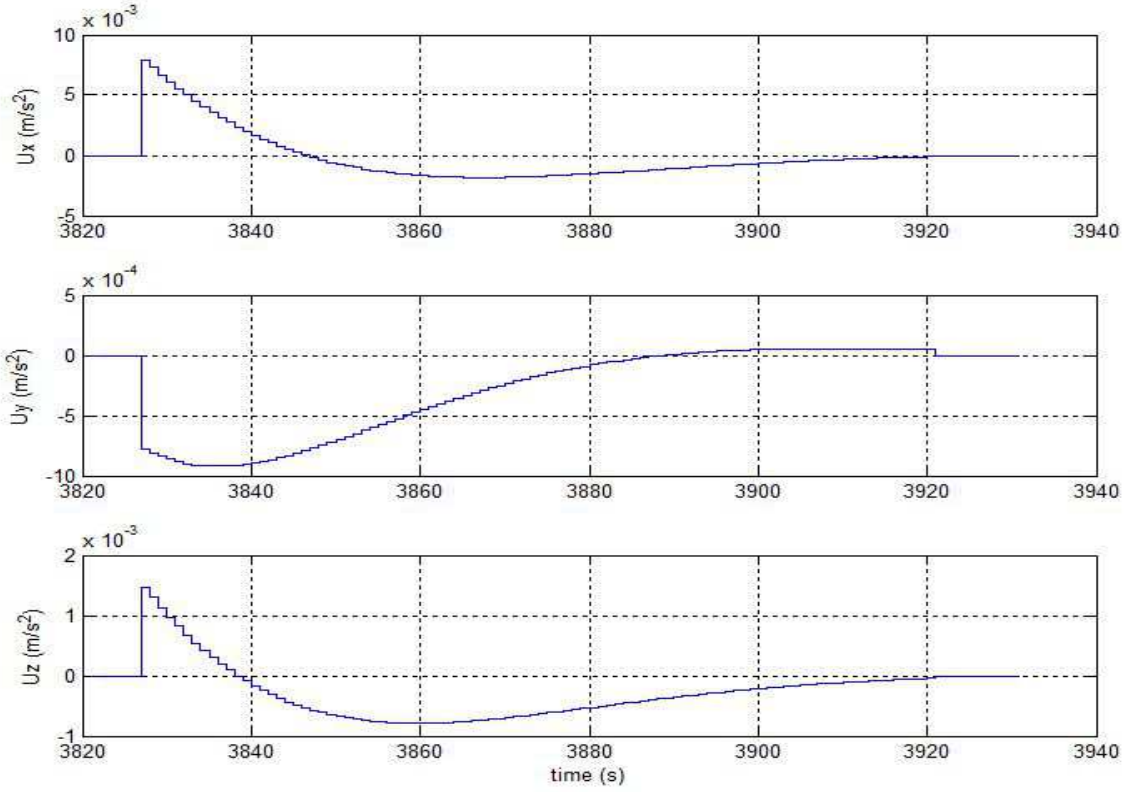

Figure 77 – LQR position control accelerations expressed in the LVLH frame for relative orbit correction

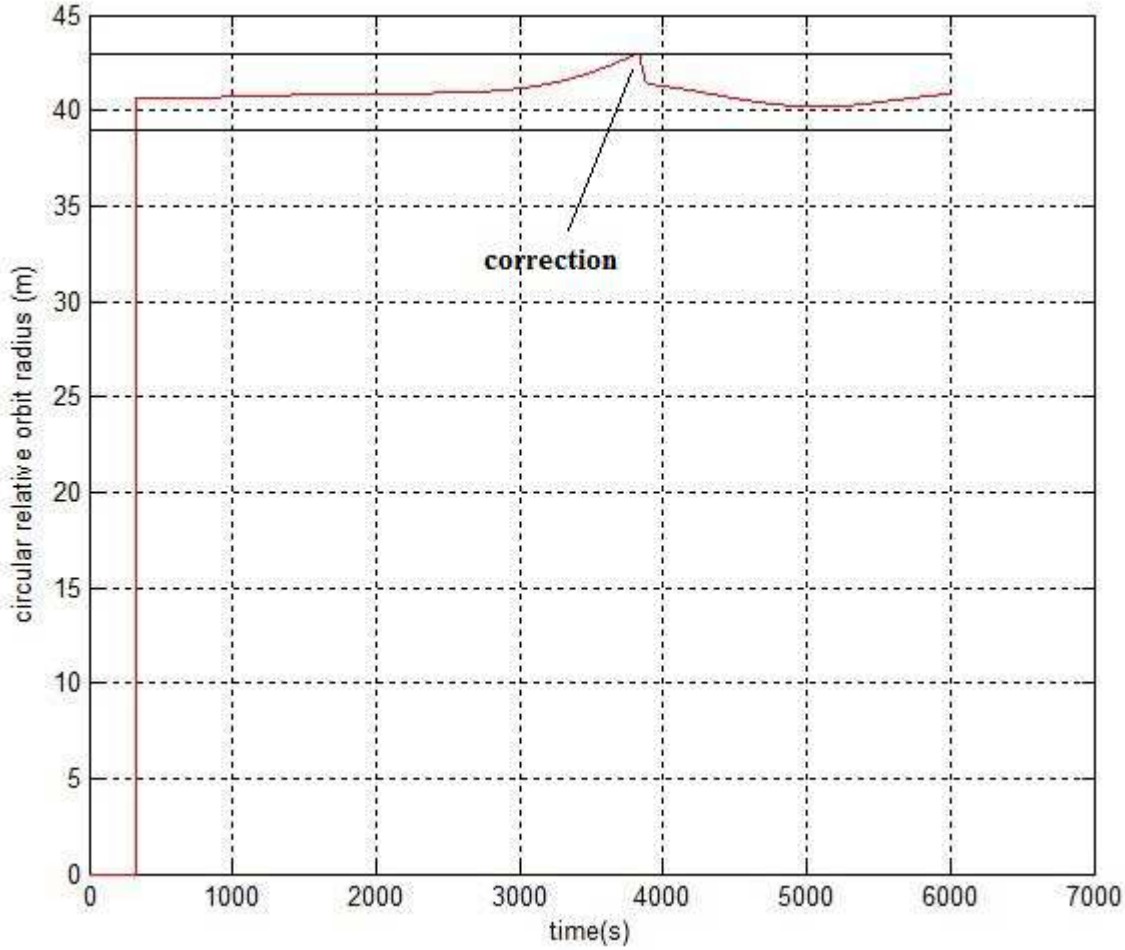

Figure 78 – circular relative orbit radius (red) with margins at 43 m and 39 m (black lines), correction through LQR control

Total delta-v requirement for inspection orbit acquisition through 2 impulses manuever	Total delta-v requirement for inspection orbit automatic correction through LQR controller
$\Delta v_x = 0.22\, m/s$ $\Delta v_y = 0.18\, m/s$ $\Delta v_z = 0.06\, m/s$	$\Delta v_x = 0.16\, m/s$ $\Delta v_y = 0.07\, m/s$ $\Delta v_z = 0.07\, m/s$

Table 13 – Delta-v requirement for orbit acquisition through 2 impulses manuever and orbit correction through LQR controller

2 impulses manuever tracking error at inspection orbit acquisition	LQR tracking error at inspection orbit correction
$\Delta\delta x = 0.005\,m$ $\Delta\delta y = -0.12\,m$ $\Delta\delta x = 0.007\,m$	$\Delta\delta x = 0.11\,m$ $\Delta\delta y = 0.69\,m$ $\Delta\delta z = -0.35\,m$

Table 14 – tracking errors at inspection orbit acquisition through 2 impulses maneuver and correction through LQR controller

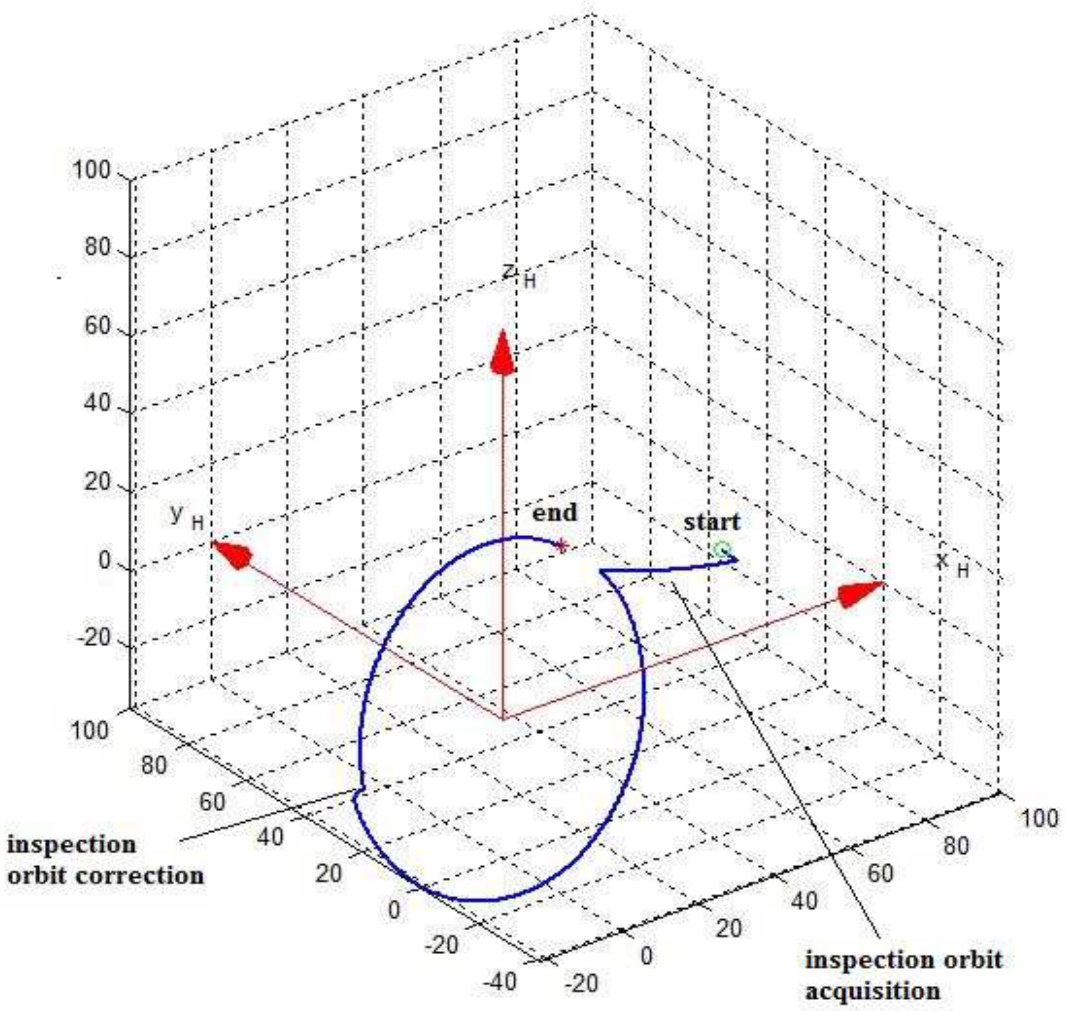

Figure 79 - relative orbit (meter as axes unit) in LVLH frame, inspection orbit acquisition through 2 impulses maneuver and correction through MPC control (green circle indicates start of simulation, red star indicates end)

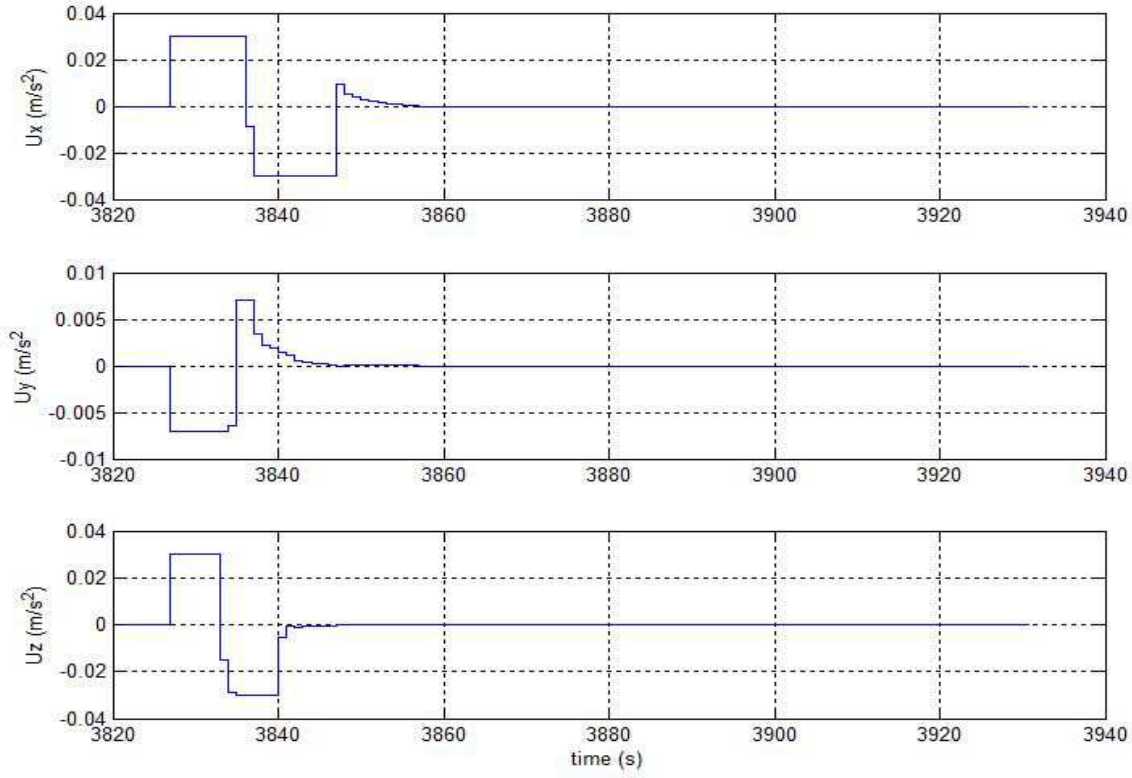

Figure 80 - MPC position control accelerations expressed in the LVLH frame for relative orbit correction

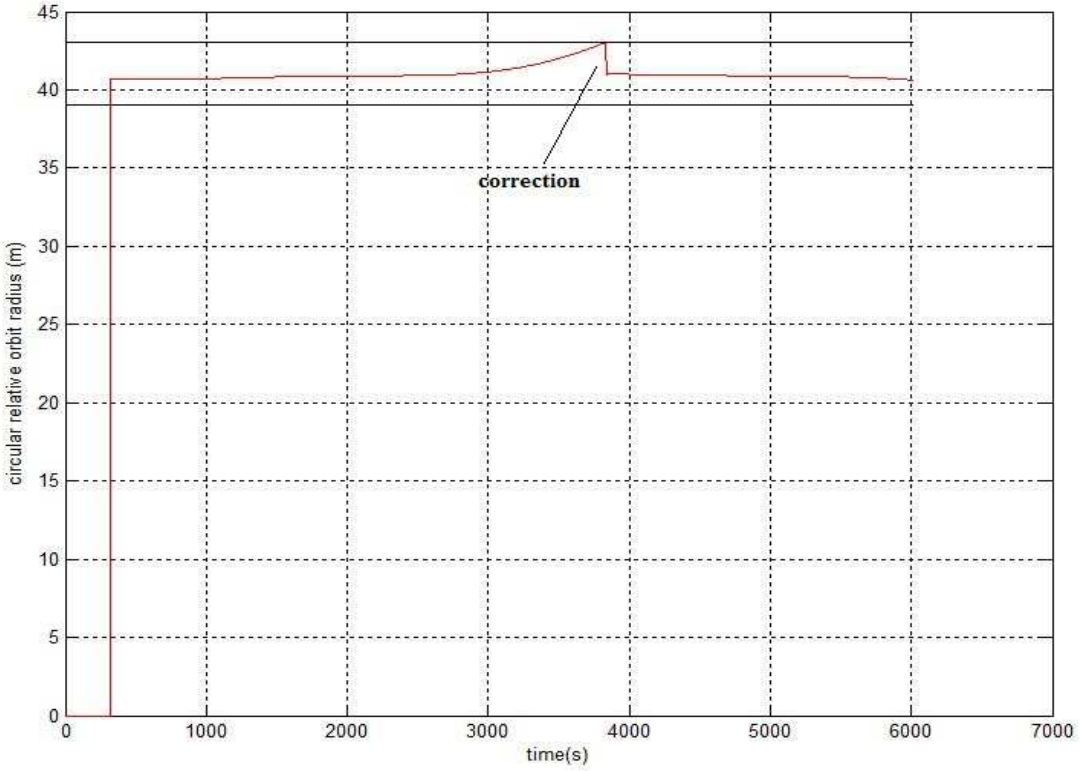

Figure 81 - circular relative orbit radius (red) with margins at 43 m and 39 m (black lines), correction through MPC control

Total delta-v requirement for inspection orbit acquisition through 2 impulses manuever	Total delta-v requirement for inspection orbit automatic correction through MPC controller
$\Delta v_x = 0.22\, m/s$ $\Delta v_y = 0.18\, m/s$ $\Delta v_z = 0.06\, m/s$	$\Delta v_x = 0.62\, m/s$ $\Delta v_y = 0.11\, m/s$ $\Delta v_z = 0.4\, m/s$

Table 15 - Delta-v requirement for orbit acquisition through 2 impulses manuever and orbit correction through MPC controller

2 impulses manuever tracking error at inspection orbit acquisition	MPC tracking error at inspection orbit correction
$\Delta \delta x = 0.005\, m$ $\Delta \delta y = -\ 0.12\, m$ $\Delta \delta x = 0.007\, m$	$\Delta \delta x = 0.003\, m$ $\Delta \delta y = 1e\text{-}5\, m$ $\Delta \delta z = -\ 7e\text{-}5\, m$

Table 16 – tracking errors for inspection orbit acquisition through 2 impulses maneuver and correction through MPC controller

As it can be seen from simulation results, in all cases the performed maneuvers bring the inspection spacecraft at the desired reference position, with more or less precision, and the inspection can take place along the selected circular relative orbit. The circular relative orbit acquired through the 2 impulses maneuver has a period of approximately 1.6 hours. For the maintainance of the relative orbit, a margin of ± 2 m from the reference radius value has been considered as trigger of the control reactivation, both for LQR and MPC controller.

In the case of the LQR control, the current relative orbit radius exceeds the threshold after approximately 58 minutes, therefore the controller is activated in a maneuver of 94 s of duration which brings the spacecraft in the new relative position reference. During the rest of the simulation, the relative orbit radius remains within the established margin.

In the case of MPC control, the current relative orbit radius exceeds the threshold after approximately 1 hour, therefore the controller is activated in a 30 s maneuver which brings the spacecraft to the new relative position reference. During the remaining time of simulation, the relative orbit radius remains within the established margin therefore the automatic control is not reactivated. It can be noticed from the results that the LQR controller brings the inspection

spacecraft to the desired reference with a lower delta-v wrt to the MPC controller, but the MPC controller presents a lower position reference tracking error.

A second set of simulations with the same type of maneuvers have been performed with the inclusion of a plane change at the ascending node of the relative circular orbit in order to put the inspection spacecraft in the relative circular orbit with opposite inclination. The plane change is performed with a single impulse delta-v, expressed in the LVLH frame, of [2.2e-4, 3.3e-4, 0.07] m/s in the case of the LQR controller, and of [2.4e-4, 3.4e-4, 0.07] m/s in the case of the MPC controller. Figures (82), (83) show the circular orbit radius profiles results of the simulations in the case of plane change.

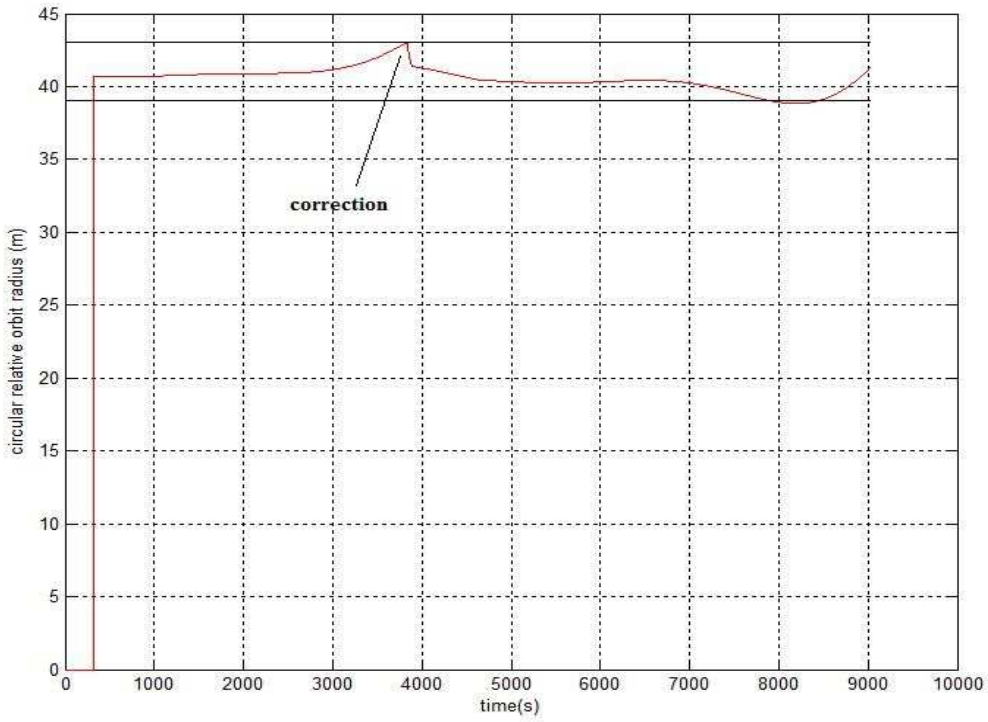

Figure 82 - circular relative orbit radius (red) with margins at 43 m and 39 m (black lines), correction through LQR control and relative orbit plane change

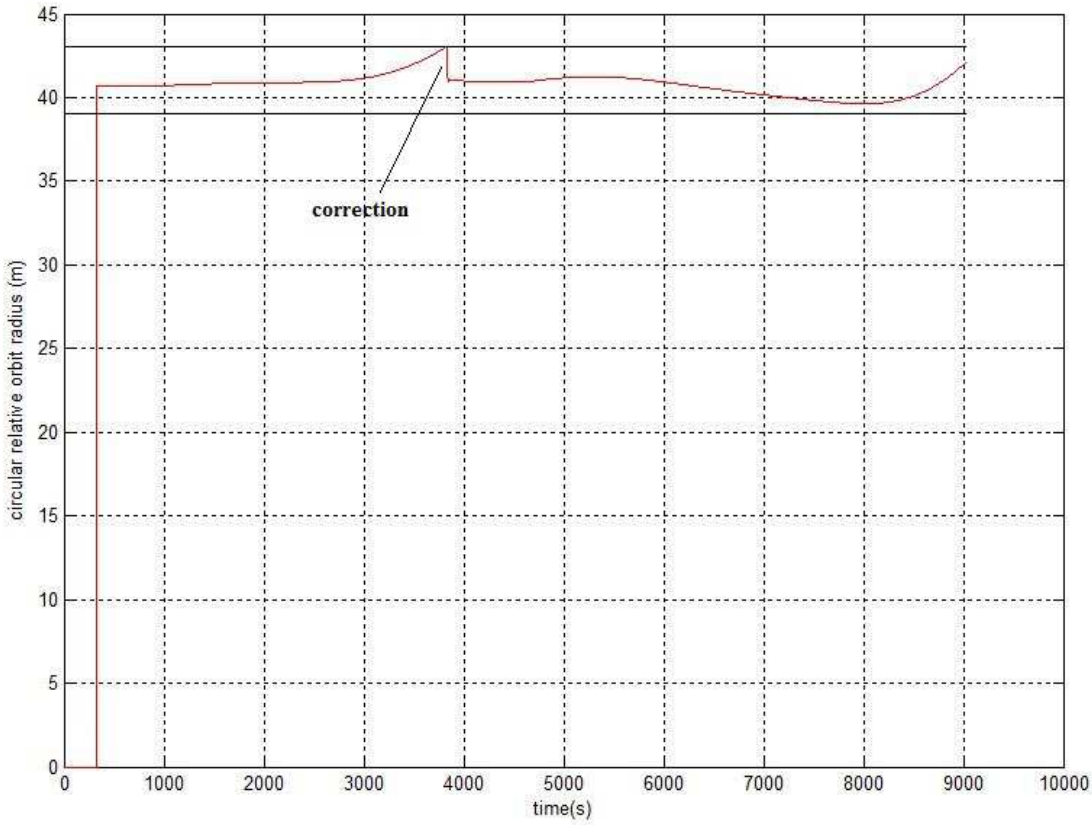

Figure 83 - circular relative orbit radius (red) with margins at 43 m and 39 m (black lines), correction through MPC control and relative orbit plane change

5.4.2 Simulations Results for Inspection Orbit Acquisition and Correction through LQR Control

This section reports the results for the simulation of the inspection orbit acquisition and correction maneuvers, performed both with the application of LQR control. Table (17) reports the set of relative conditions at the beginning of the simulation, the relative conditions at the beginning of the acquisition maneuver, and the relative conditions at the acquisition of the inspection relative orbit.

Initial conditions at the initial relative orbit	Initial conditions at the beginning of the acquisition maneuver	Initial conditions at the acquisition of the inspection orbit
$\delta x_0 = 52.7\,m$ $\delta y_0 = -6.4\,m$ $\delta z_0 = 28.1\,m$	$\delta x_0 = 52.3\,m$ $\delta y_0 = -12.1\,m$ $\delta z_0 = 28\,m$	$\delta x_0 = 20\,m$ $\delta y_0 = -7.1\,m$ $\delta z_0 = \sqrt{3}\,\delta x_0\,m$

$\delta \dot{x}_0 = -0.006\, m/s$	$\delta \dot{x}_0 = -0.009\, m/s$	$\delta \dot{x}_0 = \delta \dot{y}_0 n/2\, m/s$
$\delta \dot{y}_0 = -2\delta x_0 n\, m/s$	$\delta \dot{y}_0 = -0.109\, m/s$	$\delta \dot{y}_0 = -2\delta x_0 n\, m/s$
$\delta \dot{z}_0 = -2\text{e-}4\, m/s$	$\delta \dot{z}_0 = -0.002\, m/s$	$\delta \dot{z}_0 = \sqrt{3}\delta \dot{x}_0\, m/s$

Table 17 – Initial conditions of simulation, orbit acquisition through LQR controller

As in the previous set of simulations, the synthesis of the LQR controller was performed with a preliminary manual tuning in order to find convenient values for the error state and control action weighting matrix. The control synthesis with the selected Q and R matrices resulted with following LQR feedback gain matrix:

$$K_{LQR} = \begin{bmatrix} 7.8921\text{e-}4 & -1.1608\text{e-}5 & 0 & 0.0401 & 1.214\text{e-}5 & 0 \\ 1.1608\text{e-}5 & 7.8894\text{e-}4 & 0 & -1.2045\text{e-}5 & 0.0401 & 0 \\ 0 & 0 & 7.8894\text{e-}4 & 0 & 0 & 0.0401 \end{bmatrix}$$

i.e. the same feedback matrix which resulted from the control synthesis for automatic orbit correction only. For the x, y, z actuations axes a maximum control action value of 0.1 m/s^2 per sampling time step was considered. The disturbances inserted in the simulation consisted in those induced by differential drag and J2 with the formulations provided in the previous sections. Results from the simulations are reported in Figures (84) to (87) and in Tables (18), (19).

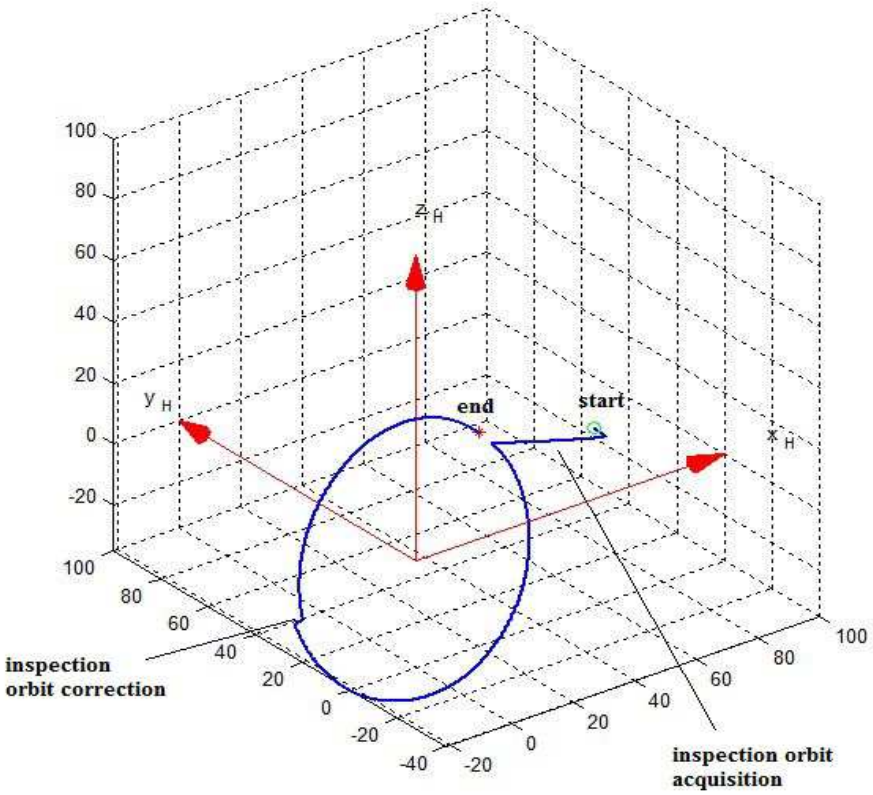

Figure 84 - relative orbit (meter as axes unit) in LVLH frame, inspection orbit acquisition and correction through LQR control (green circle indicates start of simulation, red star indicates end)

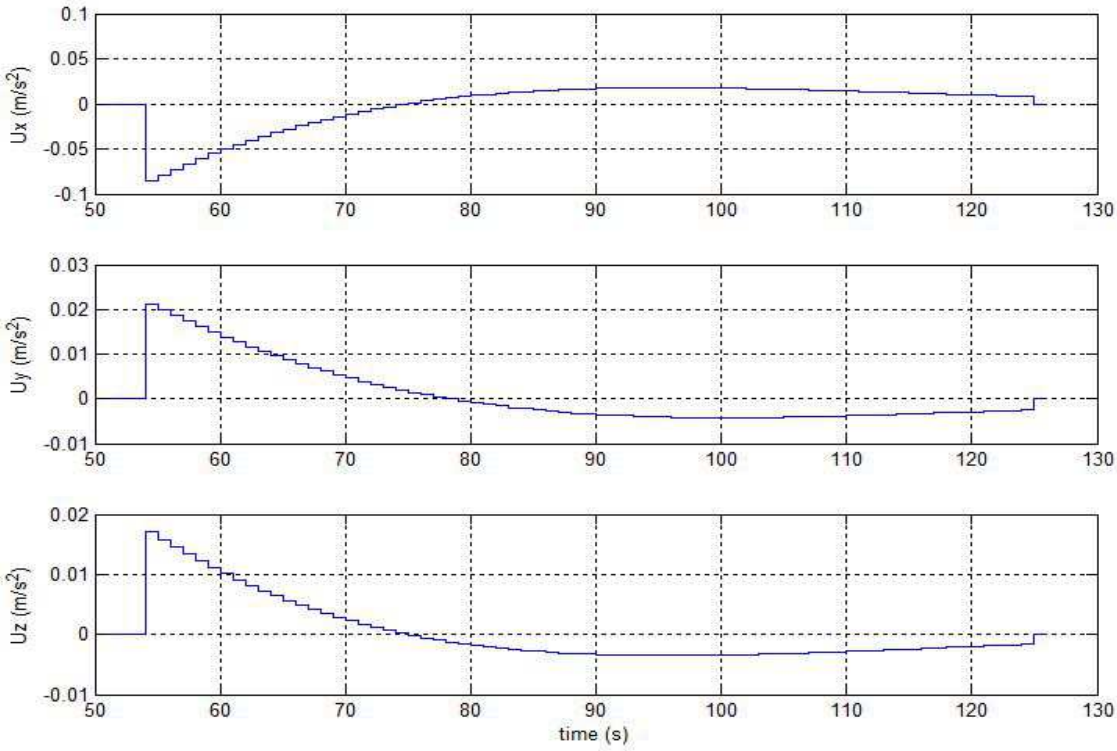

Figure 85 - LQR position control accelerations expressed in the LVLH frame for relative orbit acquisition

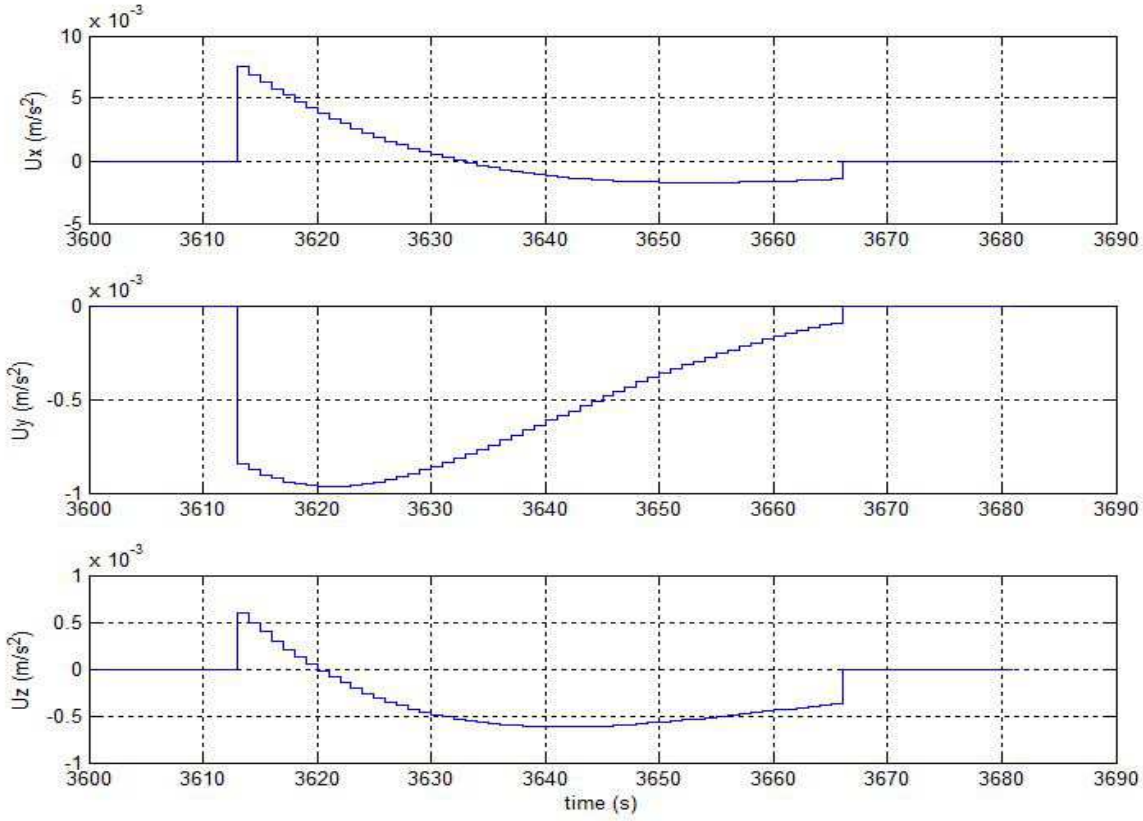

Figure 86 - LQR position control accelerations expressed in the LVLH frame for relative orbit correction

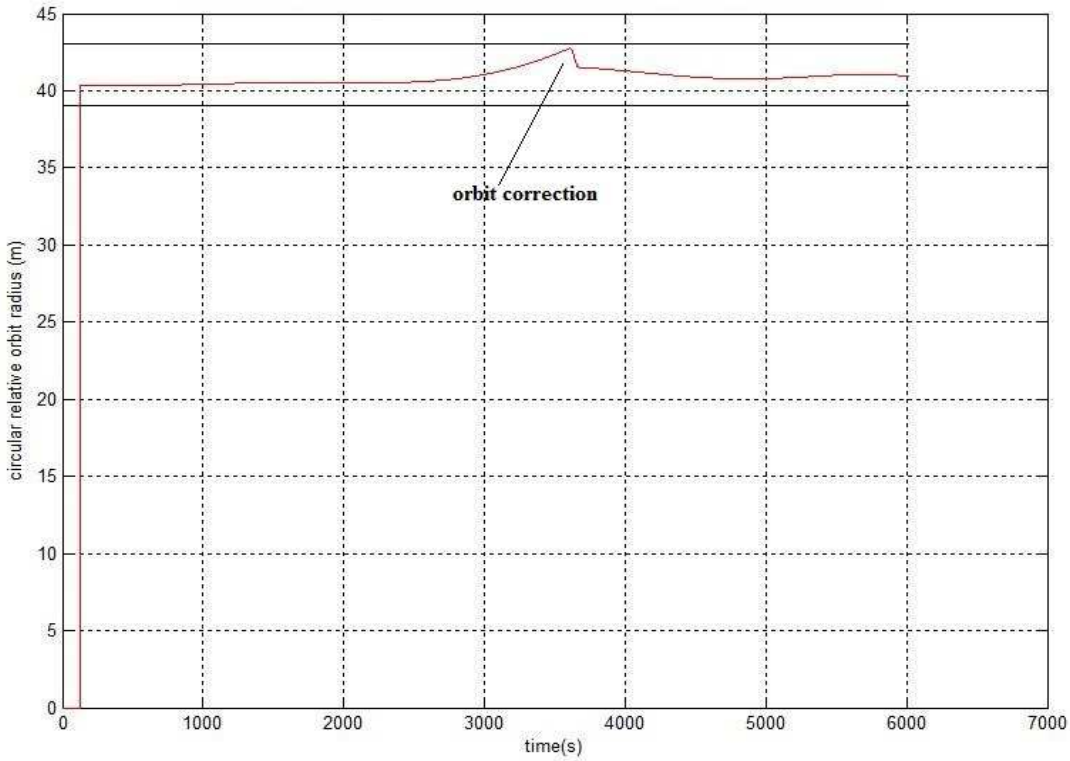

Figure 87 - circular relative orbit radius (red) with margins at 43 m and 39 m (black lines), correction

through LQR control

Total delta-v requirement for inspection orbit acquisition through LQR control	Total delta-v requirement for inspection orbit correction through LQR control
$\Delta v_x = 1.38\, m/s$ $\Delta v_y = 0.35\, m/s$ $\Delta v_z = 0.27\, m/s$	$\Delta v_x = 0.1\, m/s$ $\Delta v_y = 0.03\, m/s$ $\Delta v_z = 0.02\, m/s$

Table 18 - Delta-v requirement for orbit acquisition and correction through LQR controller

As it can be seen from the results, the LQR controller manages to put the spacecraft in the desidered passive relative orbit with a maneuver of approximately 70 s of duration. The acquired circular relative orbit has a period of approximately 1.6 hours. For the maintainance of the relative orbit, a margin of ± 2 m from the reference radius value has been considered as trigger of the control reactivation. In the simulation, approximately 58 minutes after the relative orbit acquisition the current radius value exceeds 43 m, therefore the orbital control through LQR is activated, resulting in a maneuver of 43 s of duration that brings the inspector spacecraft to the riacquisition of the reference relative orbit. During the rest of the simulation the relative orbit radius remains within the established margin.

LQR tracking error at inspection orbit acquisition	LQR tracking error at inspection orbit correction
$\Delta \delta x = 0.001\, m$ $\Delta \delta y = 0.69\, m$ $\Delta \delta x = -0.2\, m$	$\Delta \delta x = 0.29\, m$ $\Delta \delta y = 0.69\, m$ $\Delta \delta z = -0.29\, m$

Table 19 – tracking errors for inspection orbit acquisition and correction through LQR controller

After this preliminary analysis of the LQR controller performances in the inspection orbit acquisition and correction, a final type of simulation was performed consisting in a realistic inspection scenario with the inspection satellite making approximately two inspection orbit periods in the first inspection orbit at + 60° wrt to the x-y plane of the LVLH plane, and after that, approximately one and a quarter inspection orbit periods in the inspection orbit at – 60°, after the application an impulsive plane change. Table (20) reports the simulation parameters and the results

in terms of total expended delta-v for the inspection orbit radius correction, while Figures (88), (89) report the results.

Total simulation runtime	21675 s
Inspection duration	21551 s
Inspection duration in + 60° orbit plane	13361 s
Inspection duration in – 60° orbit plane	8190 s
Total delta-v for inspection orbit correction	$\Delta v = [0.685, 0.228, 0.303] m/s$

Table 20 – simulation parameters and total delta-v for LQR control for inspection orbit acquisition and correction

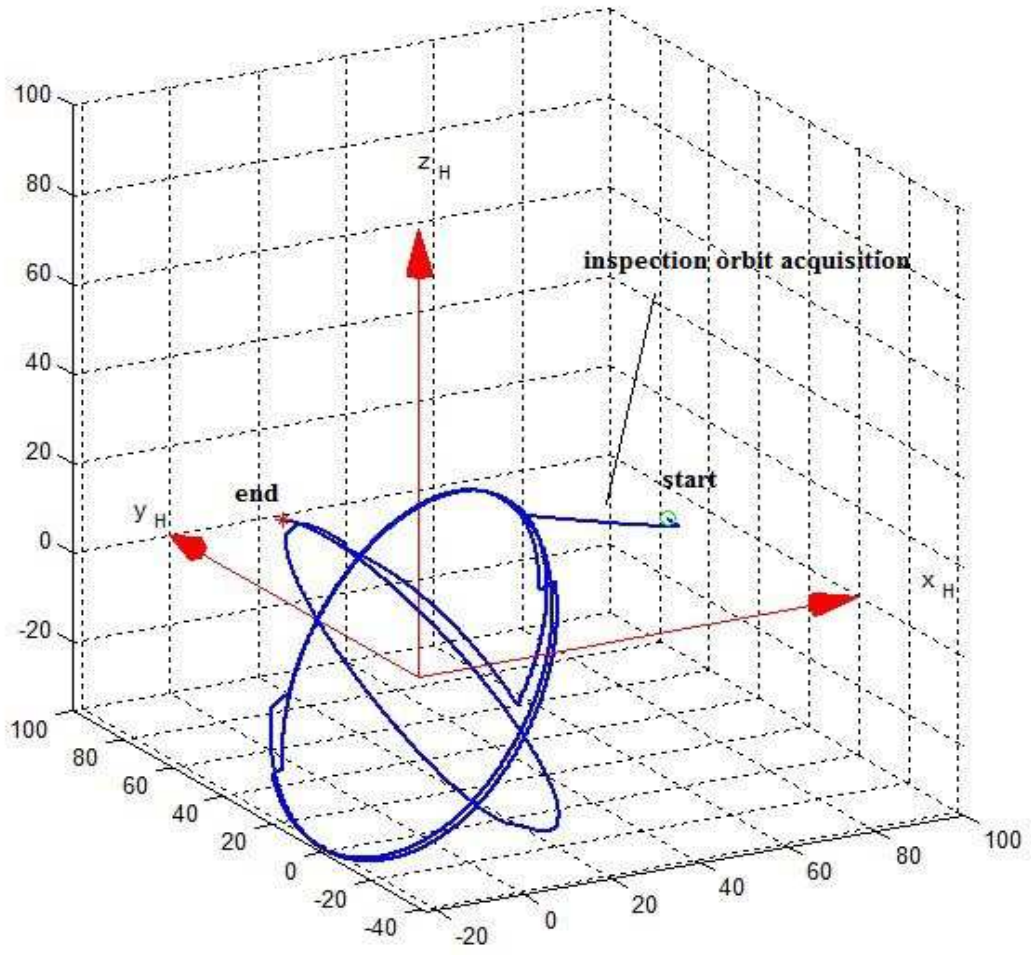

Figure 88 - relative orbit (meter as axes unit) in LVLH frame, inspection orbit acquisition and correction through LQR control, relative orbit plane change (green circle indicates start of simulation, red star

indicates end)

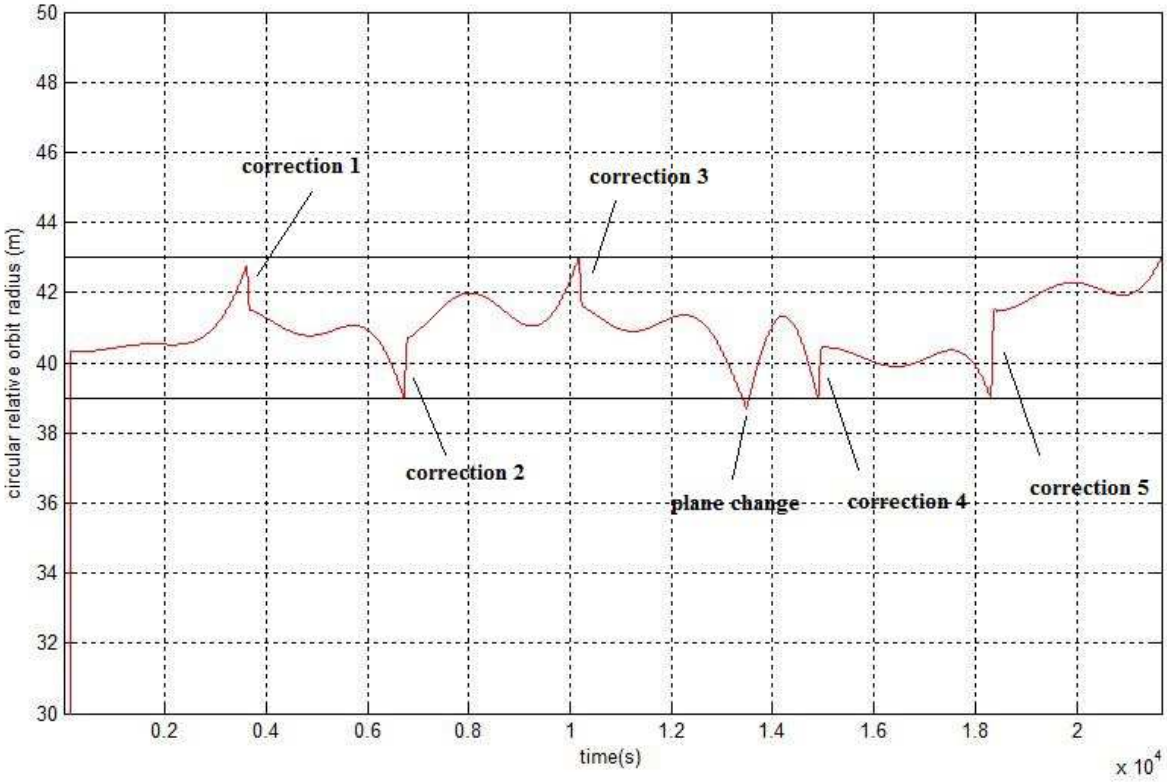

Figure 89 - circular relative orbit radius (red) with margins at 43 m and 39 m (black lines), correction through LQR control, relative orbit plane change

As visible from the graphic results, the inspection circular orbit radius is maintained within the desired margins through the application of a total of 5 orbital position control sequences. For each orbit correction control maneuver, tracking errors result on a similar level as those reported in Table (19), as obtained from the first orbit correction control sequence.

5.4.3 Simulations Results for Inspection Orbit Acquisition and Correction through MPC Control

This section reports the results for the simulation of the inspection orbit acquisition maneuver with the application of MPC implicit control. The set of relative conditions at the beginning of the simulation, of relative conditions at the beginning of the acquisition maneuver, and of relative conditions at the acquisition of the inspection relative orbit, is the same as for the LQR maneuver of the previous simulations set.

In order to select the parameters of the MPC controller, a preliminary analysis was performed with the goal of performing a manual tuning, which was driven mostly by the minimization of the expended control action. As for the first set of simulations, eventually the analysis led to the selection of the default parameters assigned by the MPC function of the MATLAB optimal control toolbox which was employed in order to implement the controller. The MPC control synthesis was therefore performed in the simulation with a prediction horizon $p=10$ and a control horizon $m=2$. The constraint of maximum control action was imposed for all three LVLH axes with a value of 3e-2 m/s^2, and as for the simulations performed with the LQR controller, differential disturbances induced by J2 and drag were considered as acting on the satellites relative motion. Results from the simulations are reported in Figures (90) to (93) and Tables (21), (22).

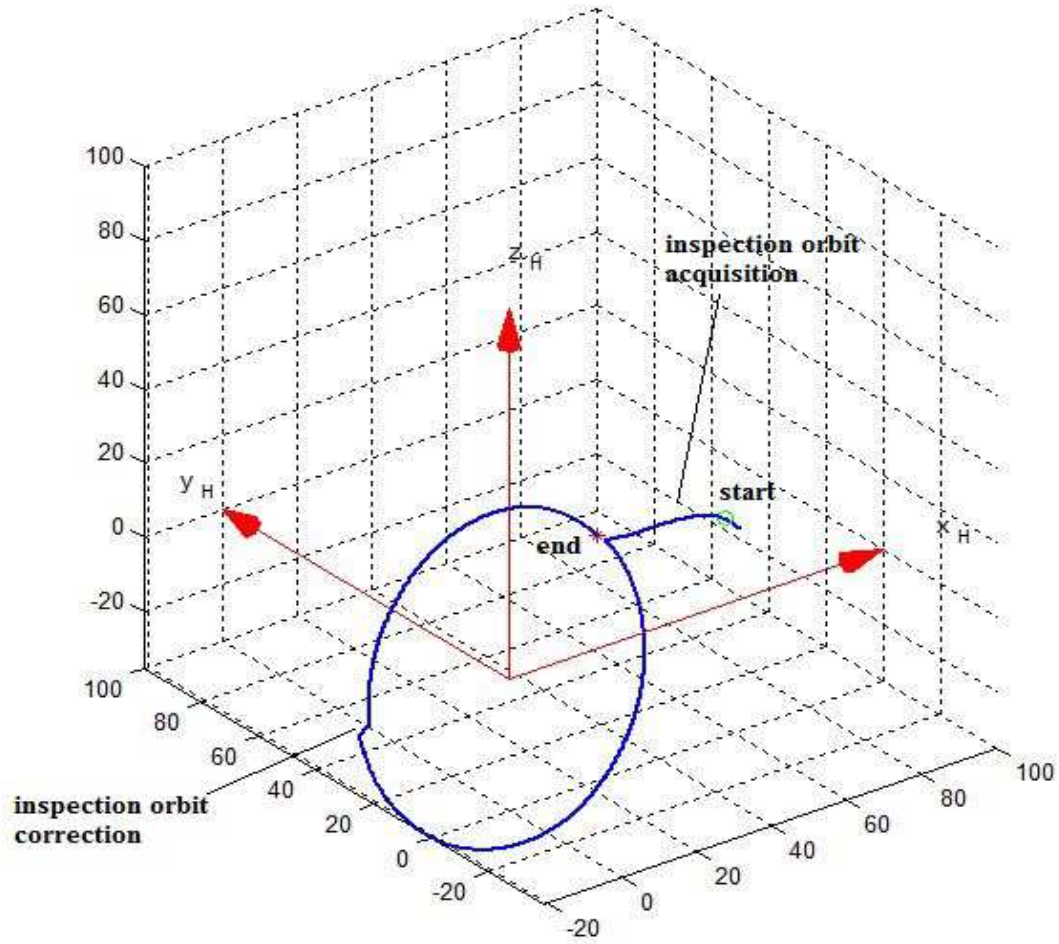

Figure 90 - relative orbit (meter as axes unit) in LVLH frame, inspection orbit acquisition and correction through MPC control (green circle indicates start of simulation, red star indicates end)

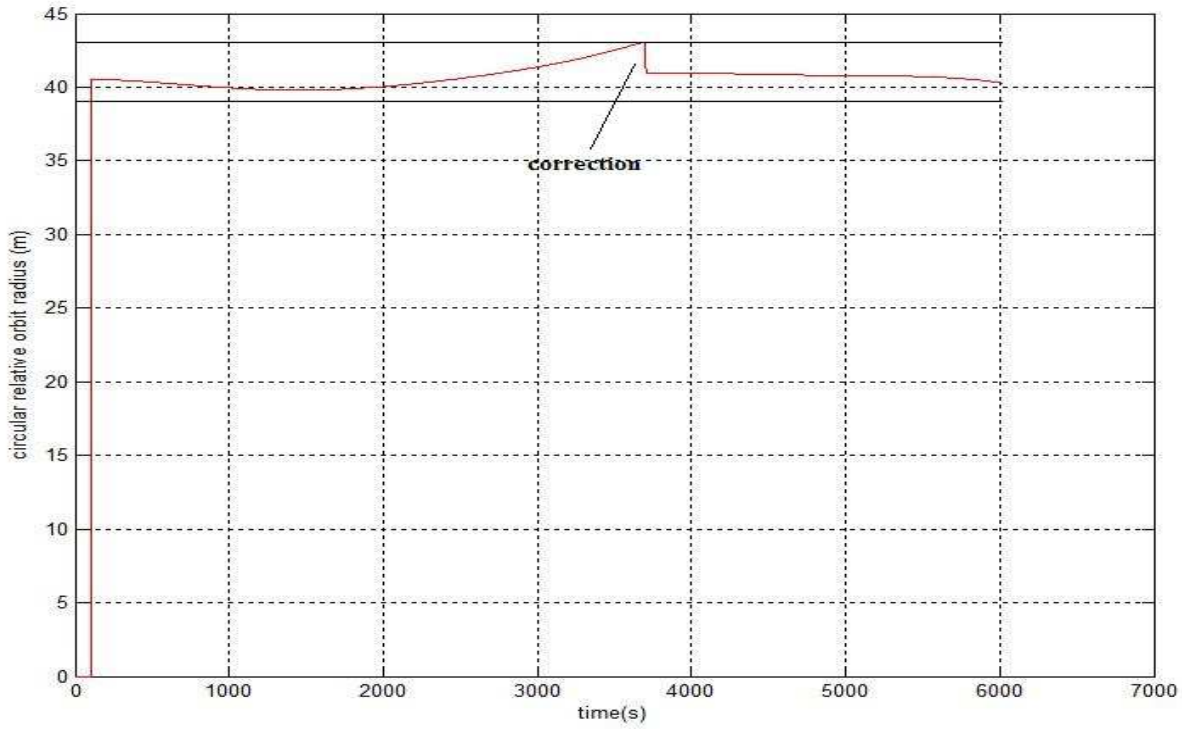

Figure 91 - circular relative orbit radius (red) with margins at 43 m and 39 m (black lines), correction through MPC control

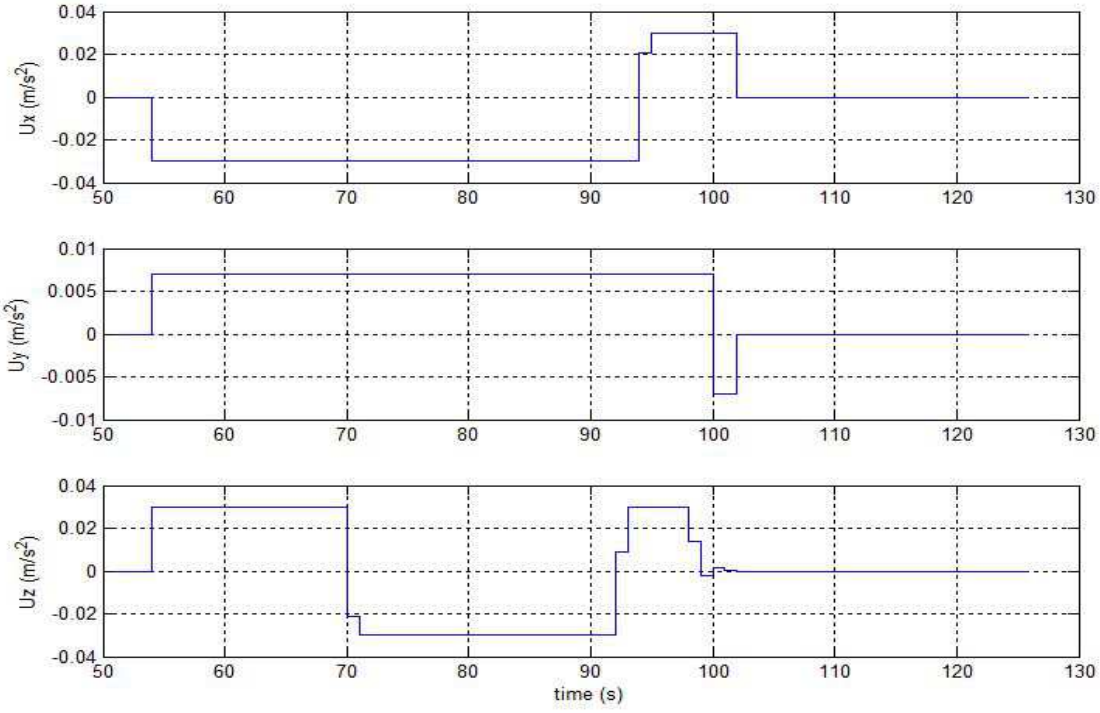

Figure 92 - MPC position control accelerations expressed in the LVLH frame for relative orbit acquisition

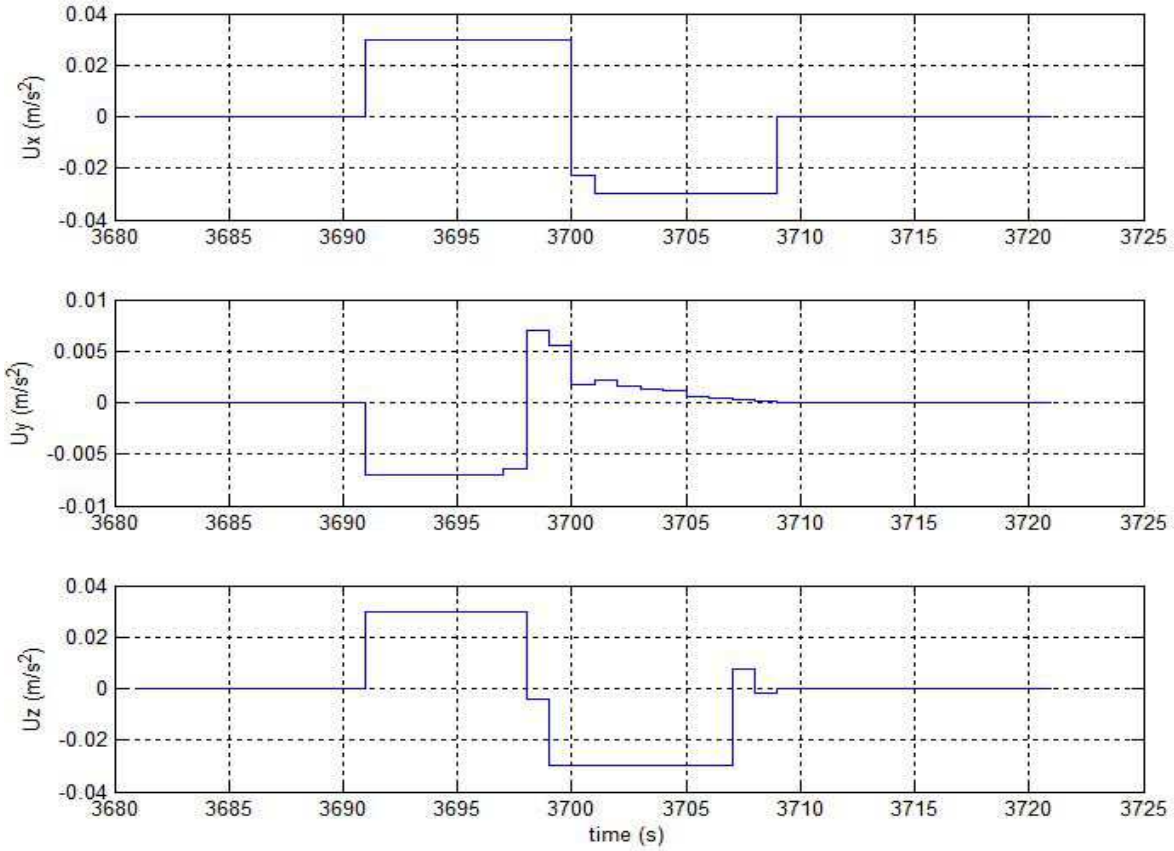

Figure 93 - MPC position control accelerations expressed in the LVLH frame for relative orbit correction

Total delta-v requirement for inspection orbit acquisition through MPC control	Total delta-v requirement for inspection orbit correction through MPC control
$\Delta v_x = 1.42\, m/s$ $\Delta v_y = 0.39\, m/s$ $\Delta v_z = 1.3\, m/s$	$\Delta v_x = 0.53\, m/s$ $\Delta v_y = 0.06\, m/s$ $\Delta v_z = 0.4\, m/s$

Table 21 - Delta-v requirement for orbit acquisition and correction through MPC controller

Results show that the MPC controller is able to send the inspector spacecraft at the desired location of acquisition of the Passive Relative Orbit, as in the case of the LQR controller. The acquisition maneuver has also an approximate duration of 70 s as resulted with the LQR control, with the acquired circular relative orbit having a period of approximately of 1.6 hours. As for the previous set of simulations, the control scheme for the relative orbit maintainance has been inserted in the

simulation loop, with thresholds at ± 2 m wrt to the reference value of the orbit radius. In this simulation set, after 1 hour of the relative orbit acquisition the current distance between the inspector and the target spacecraft exceeds the margin, therefore the control is reactivated, and orbit correction with the new relative position reference is executed in 15 s, with a better reference tracking wrt to the first acquisition, as it can be seen from Table (22), and moreover a better tracking wrt to the LQR controller, but with a higher control action expense as it can be seen from Table (21).

MPC tracking error at inspection orbit acquisition	MPC tracking error at inspection orbit correction
$\Delta\delta x = 0.3\,m$ $\Delta\delta y = 1.4\,m$ $\Delta\delta x = 0.006\,m$	$\Delta\delta x = 0.0072\,m$ $\Delta\delta y = 0.0012\,m$ $\Delta\delta z = 0.002\,m$

Table 22 – tracking errors for inspection orbit acquisition and correction through MPC controller

As in the previous case for the inspection scenario with the LQR controller, after this preliminary analysis of the MPC controller performances in the inspection orbit acquisition and correction, a final type of simulation was performed consisting in a realistic inspection scenario with the inspection satellite making approximately two inspection orbit periods in the first inspection orbit at + 60° wrt to the x-y plane of the LVLH plane, and after that, approximately one and a quarter inspection orbit periods in the inspection orbit at – 60°, after the application an impulsive plane change. Table (23) reports the simulation parameters and the results in terms of total expended delta-v for the inspection orbit radius correction, while Figures (94), (95) report the results.

Total simulation runtime	21675 s
Inspection duration	21575 s
Inspection duration in + 60° orbit plane	13383 s
Inspection duration in – 60° orbit plane	8192 s
Total delta-v for inspection orbit correction	$\Delta v = [3.345, 0.272, 3.203]\,m/s$

Table 23 – simulation parameters and total delta-v for MPC control for inspection orbit acquisition and correction

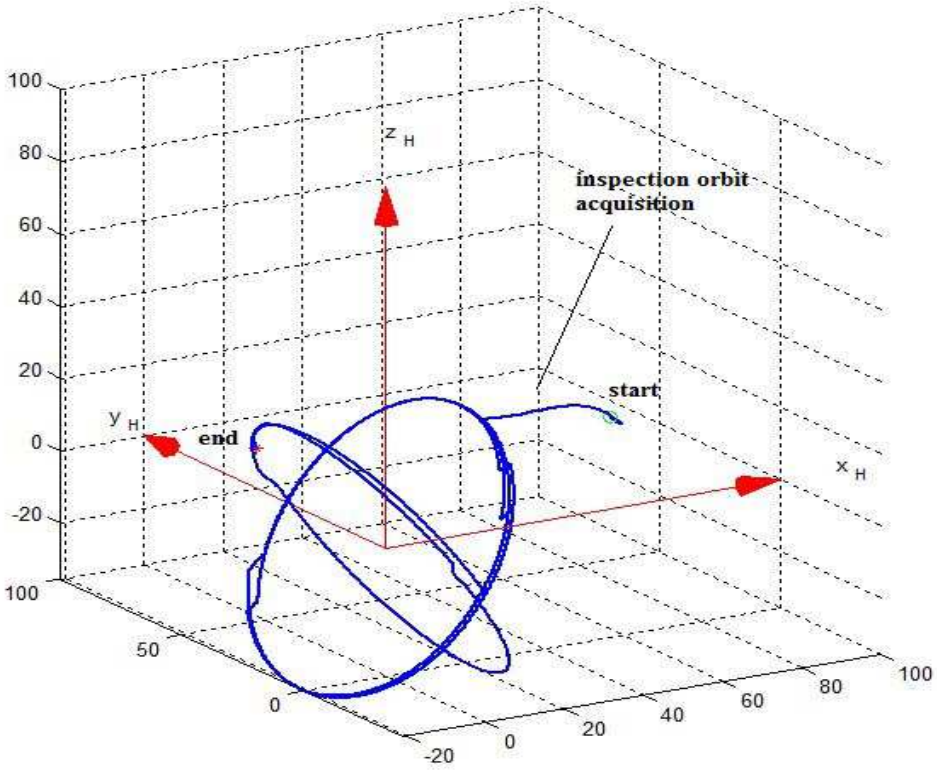

Figure 94 - relative orbit (meter as axes unit) in LVLH frame, inspection orbit acquisition and correction through MPC control, relative orbit plane change (green circle indicates start of simulation, red star indicates end)

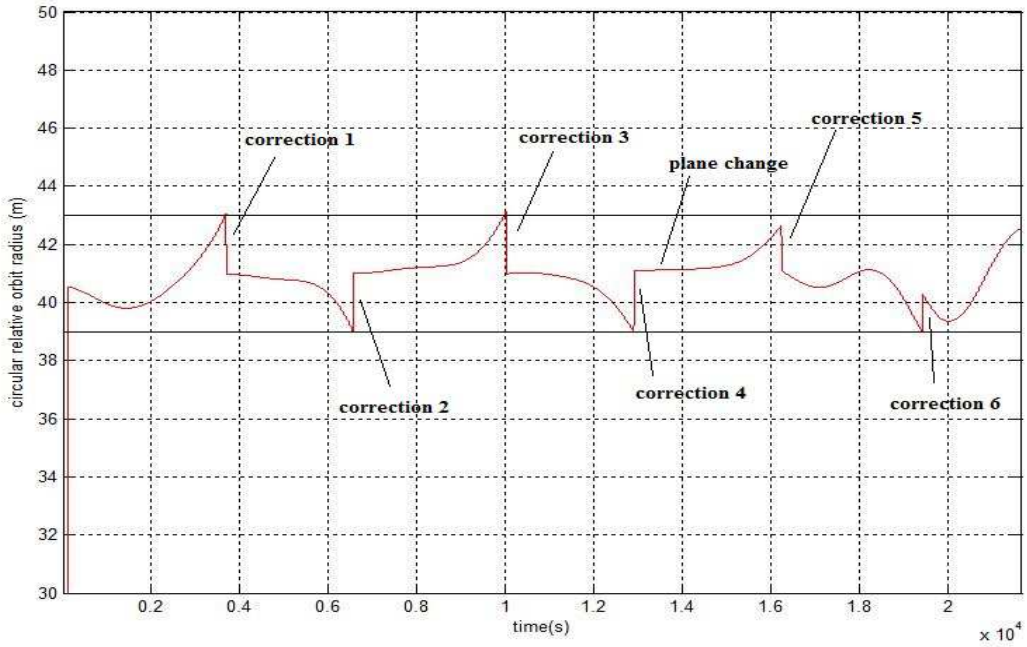

Figure 95 - circular relative orbit radius (red) with margins at 43 m and 39 m (black lines), correction through MPC control, relative plane change

As in the previous case, results show that the inspection circular orbit radius is maintained within the desired margins. In the case of the MPC controller, this is accomplished through the application of a total of 6 orbital position control sequences. For each orbit correction control maneuver, tracking errors result on a similar level as those reported in Table (22), as obtained from the first orbit correction control sequence. Result show that the delta-v for orbital correction is higher wrt to the LQR control case, however, the tracking error is lower (as in the previous simulation with only a single orbital correction), and the circular relative orbit radius value is kept longer in the proximity of the desired value of 41 m. This type of performance can be relevant wrt to the necessity of keeping the camera for the relative state estimation at a distance from the target that remains as more as possible fixed, so that there is as low as possible need to re-establish the camera focus.

6 CONCLUSIONS

The aim of my Ph.D. Activities has been focused on the development and testing of the cooperating SPAcecRaft Testbed for Autonomous proximity operatioNs experimentS (SPARTANS) hardware simulator, under development at the Center of Studies and Activities for Space (CISAS) of the University of Padova. This ground simulator is made up of robotic units which allow the reproduction in a controlled environment of the relative position and attitude motions of satellites in proximity or in formation, and can therefore be used in order to extensively study control algorithms and strategies for these types of applications, allowing the testing in a controlled environment of dedicated hardware in the loop. The Units of the simulator have 5 DOF each, 2 translational and 3 rotational, are equipped with a Guidance Navigation and Control (GNC) system which allows the execution of control maneuvers, and have a communication system which allows transmission and reception of data and commands between each other and an external control station consisting of a laptop. This type of testbed allows in particular a good reproduction of the relative motion of satellites in close proximity maneuvers at low position and attitude relative velocities, even though in the case of Rendez Vous and Docking or Capture maneuvers simulated with hardware interfaces the absolute contact forces can not be reproduced at their actual levels. For the case of proximity maneuvers at higher distances and Satellite Formation Flying the testbed can be employed for the study of relative maneuvers with scaled control accelerations profiles obtained from software simulation of the orbital maneuver.

Satellite Formation Flying and Proximity Operations are applications that have gained increasing interest, as they allow the substitution of a single spacecraft with a system made of multiple satellites, presenting higher accuracy of payload measurements, increased flexibility, redundancy, robustness, reduction of development costs, and they allow applications useful for several different purposes, such as Automated Rendez-Vous and Docking. These systems suffer however from a generally complicated design since position and attitude control presents both absolute and relative state requirements, which makes these systems liable to produce high control action expense, since the control must respond to both relative and absolute references. Moreover, applications like Automated Rendez-Vous and Docking and in general close proximity maneuvers present a high risk of impact between satellites. These aspects justify the development and employment of a ground hardware simulator which allows extensive test sessions with an easily accessible system.

At the beginning of my Ph.D., the testbed consisted in the first prototype of the Attitude Module (AM), a platform with three controllable DOF of Yaw, Pitch and Roll through a air-thrusters based control system. A small contribution was given as support to the execution of 3 DOF attitude

control maneuvers with the AM. After that, the first activity consisted in the design and development of the Air suspension system in order to allow the low friction translational motion of a whole Unit over a test table. Three air skids were tested in the Measurement Laboratory in the Department of Industrial Engineering, allowing the determination of the autonomy levels of the suspension system. After this activity, the Translation Module (TM) was designed and developed as a modular structure, as the lower section of the whole Unit of the testbed, which supports the air suspension system, the AM, and an on board localization system. The TM was designed in order to allow a 3 DOF configuration and a 5 DOF configuration. After this activity, a position and Azimuth localization system based on Optical Flow Sensors (OFS) was developed and tested through an experimental setup based on a prototype of the TM base. The system was calibrated with rotational and translational motorized stages mounted one on each other, with the imposition of known motions. A series of maneuvers were then performed with the same motorized stages assemby in order to assess the accuracy levels of the system. Purely translational and rotational maneuvers showed a good accuracy of the OFS system, with max deviations from the imposed trajectory of approximately 0.1° over an angular range of 40°, and of approximately 1 mm over a translational range of approximately 100 mm. Combined maneuvers, i.e. translational and rotational maneuvers in sequence, showed a drift behaviour, with a deviation of the level of 1 cm in planar position, when a rotation of 90° is imposed after a translation of 5 cm. After that, the OFS system, installed and calibrated in the TM, was integrated with an external vision system under development in parallel in the context of the SPARTANS project. Results from tests with the two systems and motions imposed on the TM through the motorized stages showed a good to fair concordance between the two navigation system (differences of few mm for position, ± 1° for Azimuth), whereas tests with manually imposed motions with the TM supported by the air suspension system presented again an evident drift behaviour both for position and rotation.

A parallel activity consisted in the development of the test table of the Units, designed with a modular structure, with separate sets of levelable legs sustaining the upper sections on which the Units can translate.

Another parallel activity consisted in the development of a Matlab Software simulator for the planning and preliminary verification of position and attitude control maneuvers with the Units of the testbed, and in the design and development of the Units test table. The simulator was employed for the preliminary planning of 3 DOF attitude and position control maneuvers with standard and optimal controllers.

The last activity of my Ph.D. consisted in the analysis of an inspection scenario with satellite removal purposes, with the goal of reproducing the relative dynamics in scale with the SPARTANS

simulator. The chosen scenario foresaw the inspection of the freely tumbling Envisat spacecraft in Low Earth Orbit (LEO). The analysis was focused on the acquisition and maintainance of a circular relative orbit for the inspection through a satellite, with an approximate range of 40 m, starting from a flyaround orbit. The analysis was performed with a Matlab orbital software simulator which integrates the Hill-Clohessy-Wiltshire equations, through the employment of Model Predictive Control (MPC) and Linear Quadratic Regulator (LQR) controllers for the acquisition and the maintainance of the inspection orbit, with the implementation of an automatic orbit correction scheme with triggering margins. Results showed that during all the inspection both LQR and MPC controllers are able to keep the relative orbit radius within the established margin of ± 2 m: this is done with lower control action spent by the LQR (max total delta-v component of 0.7 m/s for a total of 5 orbital correction sequences) wrt to the MPC, but with a higher tracking error, resulting in the circular orbit radius being more unstable and for less time close to the desired value, wrt to the MPC results, which in turn presented a max total delta-v component of 3.3 m/s for a total of 6 orbital correction sequences.

Activities in the immediate future will consist in the assembly of the Test Table, assembly of the second prototype of the AM and of the first complete Unit of the testbed, and development and testing of the vision-based navigation system for the estimation of the 5 DOF Unit dynamic state in an absolute external frame of reference. This will allow the execution of a first series of attitude and position control maneuvers with a single Unit, employing simulated virtual targets for the execution of coordinated control maneuvers. In its final form the SPARTANS simulator will present a minimum of two Units performing coordinated control maneuvers for the simulation of Satellite Formation Flying, Automated Rendez-Vous and Docking, and other proximity maneuvers with hardware in the loop.

Bibliography

[1] W. H. Clohessy and R. S. Wiltshire, "Terminal Guidance System for Satellite Rendez-Vous", Journal of the Aerospace Sciences, vol. 27, no. 1, pp. 653-658, 1960

[2] J. Leitner, "Formation Flying - The Future of Remote Sensing from Space", Proceedings of the 18th International Symposium on Space Flight Dynamics (ESA SP-548), 11-15 October 2004, Munich, Germany.

[3] D. Scharf, F. Hadaegh, and S. R. Ploen, "A Survey of Spacecraft Formation Flying Guidance and Control (Part I): Guidance," Proceedings of the American Control Conlerence, 4-6 June 2003, Denver, Colorado.

[4] D. P. Scharf, F. Y. Hadaegh, and S. Ploen,"A Survey of Spacecraft Formation Flying Guidance and Control (Part II): Control," Proceedings of 2004 the American Control Conlerence, June 30 - July 2 2004, Boston, Massachusetts.

[5] G. Krieger, M. Zink, M. Bachmann, B. Bräutigam, D. Schulze, M. Martone, P. Rizzoli, U. Steinbrecher, J. W. Antony, F. De Zan, I. Hajnsek, K. Papathanassiou, F. Kugler, M. R. Cassola, M. Younis, S. Baumgartner, P. Lopez-Dekker, P. Prats, and A. Moreira, "TanDEM-X: a radar interferometer with two formation-fying satellites", Acta Astronautica, vol. 89, no. 0, pp. 83 - 98, 2013.

[6] J. L. Schwartz, M. A. Peck, and C. D. Hall, "Historical Review of Air-Bearing Spacecraft Simulators," Journal of Guidance, Control and Dynamics, vol. 26, no. 4, pp. 513- 522, July-August 2003.

[7] J. P. M. O. Hilstad and A. G. Richards, The SPHERES Guest Scientist Program. Space Systems Laboratory, Massachusetts Institute of Technology, 2009.

[8] A. Valmorbida, F. Scarpa, M. Mazzucato, S. Tronco, S. Debei and E. C. Lorenzini, “Attitude Module Characterization of the Satellite Formation Flight Testbed”, Proceedings of the IEEE International Workshop on Metrology for Aerospace, May 29-30, 2014, Benevento, Italy

[9] A. Valmorbida, M. Mazzucato, A. Aboudan and S. Tronco, “Test of Attitude Control Maneuvers with a Satellite Formation Flight Testbed”, Proceedings of the IEEE International Workshop on Metrology for Aerospace, May 29-30, 2014, Benevento, Italy

[10] Valmorbida A., Mazzucato M., Tronco S., Debei S., Lorenzini E. C., “SPARTANS – a cooperating spacecraft testbed for autonomous proximity operations experiments”, Instrumentation and Measurement Technology Conference (I2MTC), 2015 IEEE International, Pisa, Italy

[11] Mazzucato M., Tronco S., Valmorbida A., Scibona F., Lorenzini E. C., “Development of a ground based cooperating spacecraft testbed for research and education”, 1st Symposium on Space Educational activities, December 9-11 2015, Padova, Italy

[12] Valmorbida A., Tronco S., Mazzucato M., Debei S., Lorenzini E. C., “Optical flow sensor based localization system for a cooperating spacecraft testbed”, IEEE Metrology for Aerospace 2015, Benevento, Italy

[13] A. Bonarini, M. Matteucci, and M. Restelli, "A Kinematic Independent Dead-reckoning Sensor for Indoor Mobile Robotics", Proceedings of the 2004 IEEE/RSJ Conference on Intelligent Robotics ans Systems, September 28 – October 2, 2004, Sendai, Japan.

[14] D. Miller, A. Saenz-Otero, J. Wertz, A. Chen, G. Berkowski, C. Brodel, S. Carlson, D. Carpenter, S. Chen, S. Cheng, D. Feller, S. Jackson, B. Pitts, F. Perez, J. Szuminski and S. Sell, “SPHERES: A Testbed for Long Duration Satellite Formation Flying In Micro-Gravity Conditions,” Proceedings of the AAS/AIAA Space Flight Mechanics Meeting, Clearwater, FL, USA, Jan. 23-26, 2000, AAS 00-110.

[15] M. Schlotterer and S. Theil, "Testbed for on-orbit servicing and formation flying dynamics emulation", AIAA Guidance, Navigation, and Control Conference, 2 - 5 August 2010, Toronto, Ontario, Canada.

[16] S. Bell, “High Precision Robot Odometry Using an Array of Optical Mouse”, Oklahoma Christian University colloquium paper, 2011. Available at: http://stanford.edu/~sebell/oc_projects.html.

[17] H. Schaub and J. L. Junkins, Analytical Mechanics of Space Systems. American Institute of Aeronautics and Astronautics Inc., 2003.

[18] K. T. Alfriend, S. R. Vadali, P. Gurl, J. P. How, and L. S. Breger, Spacecraft Formation Flying: Dynamics, control and navigation. Butterworth-Heinemann, 1st edition 2010.

[19] D. A. Vallado, Fundamentals of Astrodynamics and Applications. Microcosm Press/Springer, 3rd edition 2007.

[20] P. Ferguson and J. How, "Decentralized Estimation Algorithms for Formation Flying Spacecraft," in the AIAA Guidance, Navigation and Control Conference, pp. 2003- 5442, 2003.

[21] A. Visioli, Practical PID Control. Springer, 2006.

[22] J. M. Maciejowski, Predictive Control with Constraints. Prentice Hall, 2002.

[23] J. A. Rossiter, Model-Based Predictive Control - A Practical Approach. CRC Press, 2003.

[24] D. Q. Mayne, J. B. Rawlings, C. V. Rao, and P. O. M. Scokaert,"Constrained Model Predictive Control: Stability and optimality", Automatica, vol. 36, pp. 789-814, 2000.

[25] Y.-G. Xi, D.-W. LI, and S. LIN, "Model Predictive Control - Status and Challenges", Acta Automatica Sinica, vol. 39, no. 3, 2013.

[26] J. H. Lee, "Model Predictive Control: Review of the Three Decades of Development", International Journal of Control, Automation and Systems, vol. 9, no. 3, pp. 415 - 424, 2011.

[27] J. B. Rawlings, "Tutorial Overview of Model Predictive Control", IEEE Control System Magazine, pp. 38 - 52, June 2000.

[28] A. Bemporad, M. Morari, V. Dua, and E. N. Pistikopoulos, "The explicit linear quadratic regulator for constrained systems", Automatica, vol. 38, pp. 3 - 20, 2002.

[29] Mazzucato M., Valmorbida A., Tronco S., Costantini M., Debei S., Lorenzini E. C.,

“ Development of a camera-aided optical mouse sensors based localization system for a free floating planar robot”, IEEE Metrology for Aerospace 2016, Firenze, Italy

[30] L. Kneip, D. Scaramuzza, R. Siegwart, "A Novel Parametrization of the Perspective-Three-Point Problem for a Direct Computation of Absolute Camera Position and Orientation", Proc. IEEE Conf. on Computer Vision and Pattern Recognition, CVPR 2011.

[31] Pertile, M.; Mazzucato, M.; Bottaro, L.; Chiodini, S.; Debei, S.; Lorenzini, E., ”Uncertainty evaluation of a vision system for pose measurement of a spacecraft with fiducial markers,” in Metrology for Aerospace (MetroAeroSpace), 2015 IEEE , vol., no., pp.283-288, 4-5 June 2015

[32] M. A. Fischler and R. C. Bolles. Random sample consensus: a paradigm for model fitting with applications to image analysis and automated cartography. Commun. ACM, Vol. 24, Nr.6, pp.381 - 395, 1981.

[33] R. E. Kalman, "A New Approach to Linear Filtering and Prediction Problems," Transaction of the ASME - Journal of Basic Engineering, pp. 35 - 45, 1960.

[34] D. Sekimori and F. Miyazaki, ”Self-localization for indoor mobile robots based on optical mouse sensor values and simple global camera information,” 2005 IEEE International Conference on Robotics and Biomimetics - ROBIO, Shatin, 2005, pp. 605-610. doi: 10.1109/ROBIO.2005.246337.

[35] Feng Yu, Zhen He, Bing Qiao, Xiaoting Yu, "Stereo Vision Based Relative Pose Estimation for the Rendezvous and Docking of Noncooperative Satellites", Mathematical Problems in Engineering, Volume 2014 (2014), Article ID 461283

[36] Schweighart, S. A., & Sedwick, R. J. (2002). High-Fidelity Linearized J2 Model for Satellite Formation Flight. Journal of Guidance, Control and Dynamics,Vol. 25, No.6, pp. 1073-1080.

[37] Silva, E. D. (2008). A Formulation of the Clohessy-Wiltshire Equations to Include Dynamic Atmospheric Drag. Paper presented at the AIAA/AAS Astrodynamics Specialist Conference.

[38] Guangyan Xu, Tingting Yu, Jianchao Wang, Xia Chen, "Model Predictive Control of Passive

and Periodic Satellite Formation Based on Linear Programming Approach", Proceedings of 2014 IEEE Chinese Guidance, Navigation and Control Conference, August 8-10 2014, Yantai, China